DISSERTATION

PERFORMANCE ASSESSMENT OF SIMPLE BLAST WALL SYSTEMS

Submitted by

Assal Hussein

Department of Civil and Environmental Engineering

In partial fulfillment of the requirements

For the Degree of Doctor of Philosophy

Colorado State University

Fort Collins, Colorado

Spring 2019

Doctoral Committee:

Advisor: Hussam N. Mahmoud
Co-Advisor: Paul R. Heyliger

John W. van de Lindt
David I. McLean
Jennifer L. Mueller

ABSTRACT

PERFORMANCE ASSESSMENT OF SIMPLE BLAST WALL SYSTEMS

Numerous planned suicide attacks have been recorded since the beginning of the current century in several regions of the world. These attacks have impacted huge number of victims and have resulted in economic and psychological consequences on communities and nations, with complex global influences at times. In recent years, terrorist organizations have adopted new strategies that have made it difficult for security and intelligence operations to stop attacks. The main objectives of this dissertation are 1) draw the attention to the benefit of considering simple blast wall systems to mitigate the hazard of the suicide attacks, 2) determining the efficiency of readily available materials in dissipating the blast of shock wave energy, and 3) to investigate the performance of simple blast wall systems. This study discusses the threat of suicide attacks that are executed by bombers wearing vests and provides a general view of this type of man-made hazard and its consequences on the existence of communities and their future. The study clarified the impacts of suicide attacks in the Republic of Iraq, and the U.S. Muqdadiyah City was considered as a case study of these impacts in the Republic of Iraq. The results of the literature review highlighted the necessity to adopt a new approach to designing simple blast wall systems. Designing such systems made of low-tech materials can mitigate and reduce losses from such type of threat, make their implementation easier and more cost-effective, and potentially result in a reduction in death, injury, and damage.

Different engineering methods have been investigated and considered for civilian and military fields to mitigate blast shock wave effects. Standards and technical manuals have been published by federal agencies and research centers to set general safety precautions and/or structural design approaches, charts, and equations. However, many of these manuals are limited and not released to the public. In addition to a lack of funds, the technology of construction, and availability of high-tech materials, designing blast-resistant structures or high-tech blast wall systems are not an available option for designers in most developing countries. Design guidelines are sparse if not non-existent.

This research was focused on suggesting a new blast wall system using low-tech materials to mitigate the effect of a blast shock wave in free-air. The oriented stands board (OSB) and wood-sand-wood (WSaW) blast walls were considered in the current study as examples of blast walls made of readily available materials that can be installed with minimal effort. The response of these structural systems was investigated experimentally, and results verified with numerical analysis results. Moreover, distribution of free-air blast pressure was measured and compared with the Kingery-Bulmash reference measurements for a wide variety of explosive charges. A good agreement was noticed between the measured blast pressure and Kingery-Bulmash model. The numerical analysis was implemented using 3-D-dynamic finite element method (3-D-FEM). The commercial software ABAQUS/Explicit version 6.14 combined with ConWep blast loading model as inbuilt blast load function was considered to represent the interactions between blast wave and the wall. The numerical analysis results of a WSaW blast wall showed a good agreement with test results.

In addition to the focus on wall systems, initial efforts were made to measure damage to humans. Eardrum rupture is one of the main injuries due to blast shock wave and could lead to temporary and permanent hearing loss. In this study, the blast shock wave intensity on eardrum has been investigated experimentally. Due to the similarity between the sheep ear structure and human ear, five Rambouillet-Columbia sheep heads samples were subjected to blast shock wave. The measured blast pressure exceeded the threshold of eardrum rupture. This means that the threshold for eardrum rupture was already surpassed and a 50 percent probability of eardrum rupture is expected. The micro-CT images showed the structure of the eardrum is totally ruptured. Three eardrum samples on the right side were ruptured, while only two samples on the left side were ruptured. The probability of temporary hearing loss injury could take place at level of pressure less than the threshold which can be considered the starting point of eardrum rupture (UFC 3-340-02). These experiments are described in this dissertation.

Finally, a probabilistic analysis of an equivalent single-degree of freedom (SDOF) system was completed for WSaW blast wall to estimate the fragility curves (FCs) of the system under free-air blast load using direct Monte Carlo (MC) simulation method. The suggested framework of the probabilistic analysis was developed to study the performance of the proposed blast wall according to the uncertainties in the structural properties and blast load parameters. The FCs were also estimated based on the variability in the equivalent TNT weight of a suicide vest threat scenario.

This study recommends WSaW blast wall to reduce casualties and losses in properties in different scenarios. Furthermore, it is important to draw the attention of researchers and designer to start investigating the performance of simple blast walls made of other low-tech materials since it is an urgent need in most areas threatened by terrorism.

ACKNOWLEDGMENTS

All praise be to Allah for helping and supporting me to reach this far and make it all possible. I want first to express my sincere gratitude to my advisors, Professor Hussam Mahmoud and Professor Paul Heyliger for the advice, and support during my Ph.D. study at Colorado State University. Special thanks to Professor Hussam Mahmoud for funding the blast tests and to Professor Paul Heyliger to organize the blast tests. I would like to thank my doctoral committee, Professor David Mclean, Professor John van de Lindt, and Professor Jennifer Mueller for their contribution in my Ph.D. research. I also thank Mr. Karl Swenson and Mr. Christopher Giglio of the Environmental Health Services at Colorado State University for their efforts in providing, handling, placing and detonating explosive charges in all implemented blast tests. I thank Dr. Kevin Troyer, Mechanical Engineering Department, and Dr. Kirk McGilvray, Mechanical Engineering Assistant research of the Orthopaedic Bioengineering Research Laboratory (OBRL) for their help in providing, dissecting, and scanning the animal tissues. Thank you to Mr. Joel Vaad the manager of Maxwell Ranch site. I would like also to express my sincere gratitude to the Iraqi Government-Prime Minister office-The Higher Committee for Education Development in Iraq (HCED) for the financial support to finish my Ph.D. study at Colorado State University. Also, not to forget to thank wife, Intisar for taking care of the family, supporting, and encouraging me throughout my academic career. Thank you to my children, Haneen, Ali, and Maria for encouraging me to continue my study successfully. Last, but not least, I thank my mother and brothers for their support, to keep me working actively to get my goals.

DEDICATION

This work is dedicated to the spirit of my father Tehseen Hussein and my younger brother Ahmad. May God have mercy on them and place them in paradise.

TABLE OF CONTENTS

LIST OF TABLES

LIST OF FIGURES

Chapter 1. Introduction

1.1 Research Hypothesis

The occurrence of blasts around the world has resulted in devastating social and economic consequences. Numerous suicide attacks have been recorded in recent decades. These attacks were conducted at different scales and have targeted different locations including cities, malls, military and security facilities, airports, and metro stations, among others. Governments and communities have lost incalculable dollars in direct losses, not to mention the dire indirect social impacts. In these attacks, a large amount of energy is released rapidly from high explosive detonation, and once the blast wave reaches the targeted structure, partial or full damage and human casualties are inevitable. Government organizations and federal agencies have published several documents to clarify the consequences of explosions on infrastructure and have proposed various engineering recommendations to deal with this type of threat. This includes the utilization of advanced materials (Lee and Toole, 2004; Dharmasena, Wadley, Xue, & Hutchinson, 2008; Ha, Yi, Choi, & Kim, 2011; Yazici, Wright, Bertin, & Shukla, 2014), creative structural components and subassemblies (Dvorak and Bahei-El-Din, 2005; Ha et al., 2011; Yazici et al., 2014), as well innovative structural wall systems (Dvorak and Bahei-El-Din, 2005; Goel, Matsagar, & Gupta, 2014; Matsagar, 2016; Yazici et al., 2014). However, the behavior of simple blast walls under blast loading has not been investigated and literature of the environment behind blast walls are limited and rarely published (Crawford & Lan, 2006; Rose, Smith, & Mays, 1995).

The main advantage of using blast walls to mitigate blast impact is to keep safe distance between the source of explosion and the existing structures (Beyer,1986) since not all structures have been designed to resist blast loading (Remennikov & Rose, 2005). Undoubtedly, provisions can be devised to allow for designing an entire structure to resist blast loading. However, this is not economically feasible. Therefore, using blast walls to provide safe distance can be an economically attractive feature. This is particularly the case if low-cost simple blast walls can be utilized. Blast wall systems made of low-tech readily available materials, which is the focus of this study, could provide the required protection level and other design requirements in comparison to high-tech materials which are not cheap, require professional labor and not easy to maintain. Furthermore, it is not often required to design walls to resist blast loading without any visible damage since they could still exist after the blast wave has passed (Rose, Smith, & Mays, 1998).

1.2 Research Approach

Most recent suicide attacks have been implemented through innovative plans employing unconventional explosives and strategies to make the event more impactful – politically, economically, and socially. From an engineering perspective, while not all structures need to be designed to resist blast loadings, it is not clear how to do so to avoid partial or full collapse under detonation effect since threats can vary in terms of type and complexity. This study attempts to suggest an adequate simple blast wall to reduce losses resulting from terrorist attacks at relatively low cost of time, effort, and materials. Simple blast walls have been typically considered for military purposes and not generally used for civil applications. Design specifications for most blast-protective structures are limited and not released to the public. Different types of low-tech materials can be used to design simple blast walls such as wood and sand. These are almost always readily available in all countries. Several design parameters could be adopted to investigate the performance of the considered blast wall such as thickness of the wall, standoff distances, and explosive charge weight.

The goal of this study is to investigate the performance of a composite OSB and WSaW blast wall under free-air blast loading. The attack scenario considered in the present study was aimed at simulating suicide vest threat in an unconfined field since it is currently the most common scenario and the worst in terms of number of victims (Global Terrorism Database (GTD), 2016). The geometry of the considered blast wall is chosen according to residential buildings and fence dimensions in the Republic of Iraq. The materials selection and design considerations have been selected based on the availability of resources in the Middle East region. In addition, initial attempts to assess damage to the human ear are discussed. This work was described in more detail in another study (McCann, 2018), but the physical experiments were part of the same effort and used the same explosive charges and measurement equipment. Hence, they are described in this work also.

1.3 Research Framework

The efficiency of simple blast wall systems in mitigating blast hazard initiated from terrorist attack scenarios was investigated considering deterministic and probabilistic approaches. The framework of the current study is shown in Figure 1.1. The framework includes six main components; namely 1) open space blast pressure tests, 2) small and large-scale tests of OSB wall, 3) Animal tissue test 4) Large-scale test of WSaW wall, 5) 3D dynamic Finite element analysis, 6) probabilistic analysis of an equivalent SDOF system of WSaW blast wall. Furthermore, several trials and small-scale tests were to check the sensors connection and the distribution of the air-blast pressure around the source of the explosion.

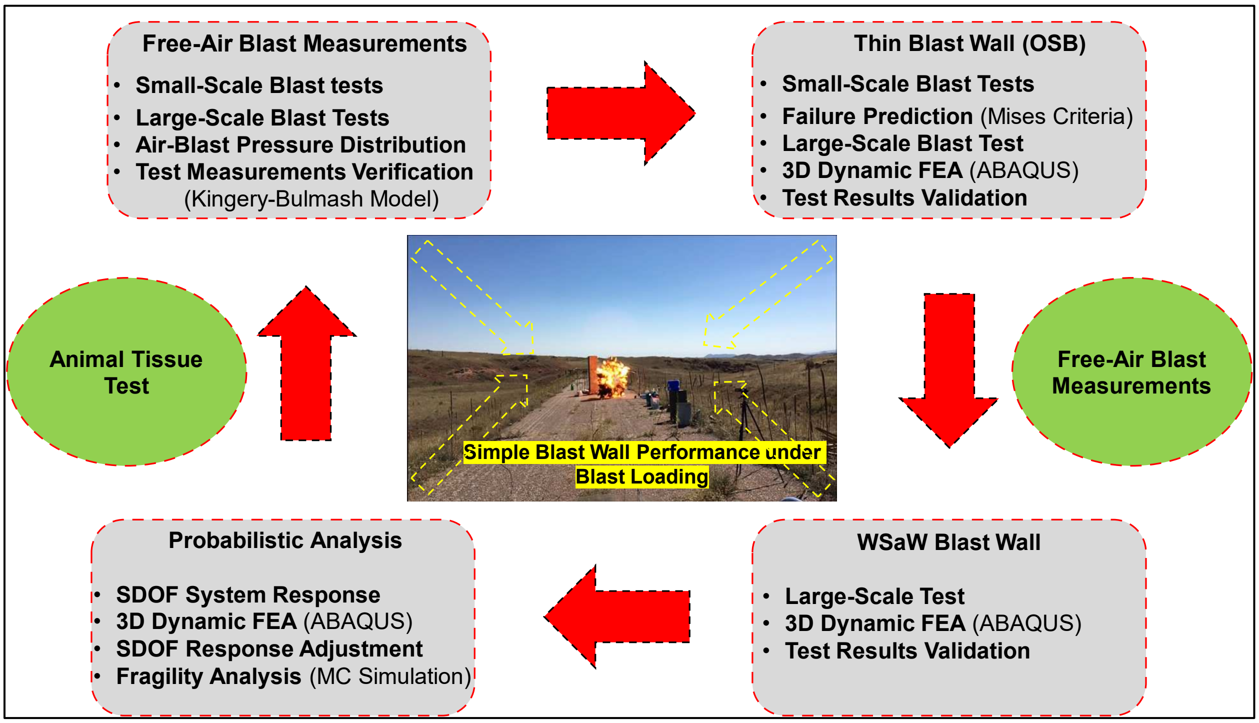

Figure 1.1 Current study framework.

The deterministic analysis was conducted using the finite element method to predict the response of 3-D structural system of blast wall. The response of the structural system provided from this analysis is based on structural and materials deterministic parameters. The outcomes of the deterministic analysis were compared with results from the open field blast test results.

The probabilistic analysis, presented in the form of fragility functions, was performed based on an adjusted equivalent SDOF system response of WSaW blast wall. The response of the spring-mass system is adjusted with the dynamic finite element analysis results of 3-D structural system. The FCs were estimated considering the uncertainty in the structural properties and the intensity of the blast loading. The conditional limit state in the probabilistic analysis framework was determined according to von Mises invariant failure criterion. Direct Monte Carlo simulation was used to predict the probability of failure. The probability of failure was established according to the structural system failure level.

1.4 Dissertation Outline

This dissertation is organized into seven chapters to support the research aims. Chapter two explains the characteristics of suicide attacks and why they present such an unusual challenge. This included presenting a list of some of the major suicide attacks in specified regions of the world and summarizing economic, health, and psychological impacts on communities. Then, demographic, economic, and psychological impacts of attacks in Muqdadiyah City, as a case study of one of the most troubled locations in the Republic of Iraq, are discussed.

Chapter three provides a historical perspective on using and classifying explosives including their applications. Next, blast loading categories based on confinement level are presented. Structural response and principles of blast loading are also explained. The behavior of materials under high strain-rate is explained through discussing some relevant material models. In this chapter computational approaches to quantify blast loading parameters and codes and standards for blast design are highlighted.

Chapter four focuses on security precautions and techniques to mitigate blast loading. The motivations behind considering the current approach to designing blast wall systems and research gap are also explained.

Chapter five includes test instrumentations and output of the OSB and WSaW blast wall tests. A Comparison between the measured free-air blast pressure and Kingery-Bulmash chart is performed. Additionally, all test results are compared and validated with the results of the numerical analysis.

Chapter six includes the probabilistic analysis of an equivalent SDOF system of WSaW blast wall. Fragility functions are developed to describe the probability of exceedance based on Monte Carlo simulation for an increased blast intensity level. Uncertainties in the structural properties and charge size are considered to estimate the probability of exceedance.

Chapter seven provides a summary and general conclusions of the current study. The major contributions of this study are highlighted and recommendations for future work are made.

Chapter 2. Suicide Bombing Attacks: An Overview

2.1 Terrorist Attacks Scenarios and Goals

Bombings have targeted centers of cities, airports, metro stations, military and security facilities around the world. There is uncertainty about the motivations behind the terrorist attacks and the adopted techniques by terrorists (Makhutov et al., 2009). These bombings, typically associated with terrorist attacks, have resulted in a variety of substantial losses due to complex in nature and dynamism of goals of these attacks (Makhutov et al., 2009). The attacks can be classified into two mains categories – 1) domestic, and 2) international (FEMA 453, 2006). The domestic and international attacks have different characteristics in terms of motivations, scenarios, and consequences. Attacks can be described based on types of weapons to 15 categories such as chemical, biological, radiological, nuclear, and high-explosive (FEMA 453,2006). They can also be categorized based on method of implementations to suicide vest/belt, improvised explosive devices (IEDs), vehicle-Born improvised explosive device (VBIED), and compound attacks (FEMA 453, 2006). Attack scenarios based on the technique used during the event are shown in Figure 2.1. These attacks have short and long-term impacts on the life of societies. Economically, negative impacts have been noticed on capital markets including insurance sectors and industries (Chesney, Reshetar, & Karaman, 2001). According to recent medical centers records, most people who are exposed to these attacks often suffer both psychological trauma and long-term disability as a result of their physical injuries. Several studies and a significant body of research have been conducted to study the psychosocial impacts, but such effects are outside the bounds of the present study.

Figure 2.1 Attacks scenarios based on the implementation methods (Photographers are unknown).

2.2 Suicide Attacks: The Challenge

In recent decades, nations have been experiencing significant suicide bombings, hindering their developments and in some cases threatening their existence. This threat is no longer a local problem but has become a global issue, which mandates collaboration between countries to overcome these threats. In recent years, significant increase in number of attacks has been recorded. Figure 2.2 shows the increase in worldwide number of attacks from 2011 to 2015 as an example of increased activity of this sort.

The Iraqi government has held number of security and military agreements with various countries for assistance, support, and exchange of information to face the challenges associated with these attacks. The United Nations and the Security Council have issued several orders and declarations to draw governments' attention while considering various practical joint actions with other organizations to rid the world from this threat.

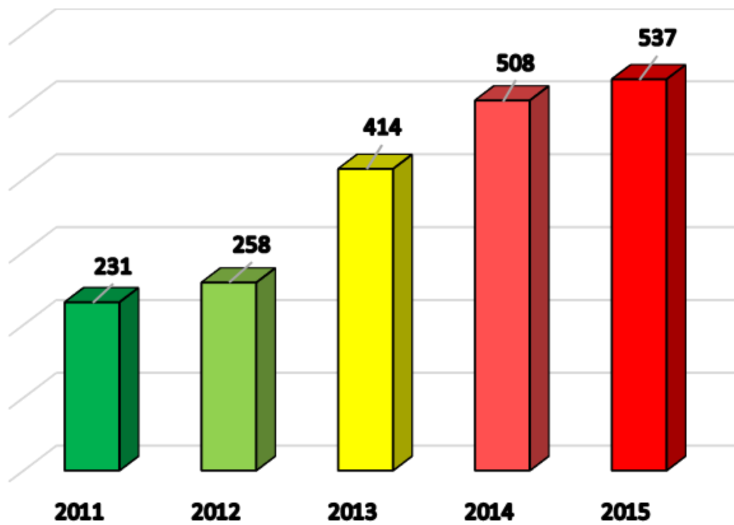

Figure 2.2 Number of worldwide attacks. (Chicago Project on Security and Threats, Chicago University, 2016, revised and reproduced by author).

There are some similarities between countries in terms of the type of threats, but there are also differences with respect to the volume of any individual attack. There are uncertainties about the origin of suicide attacks and factors that promote their spread them around the world (Makhutov et al., 2009). The question that needs to be answered, if this is even possible, is why those people are willing to die and kill others? Suicide attacks can occur anytime and anywhere based on the goals from these attacks. Everything is a goal to the terrorists such as cities, metro stations, airports, and military facilities. In the Middle East, the terrorism has focused on targeting the religious locations to initiate sectarian conflicts among community groups. Several mosques, churches have been destroyed in the Republic of Iraq and Syria in the last years. The characteristics of the suicide attacks are summarized in Figure 2.3.

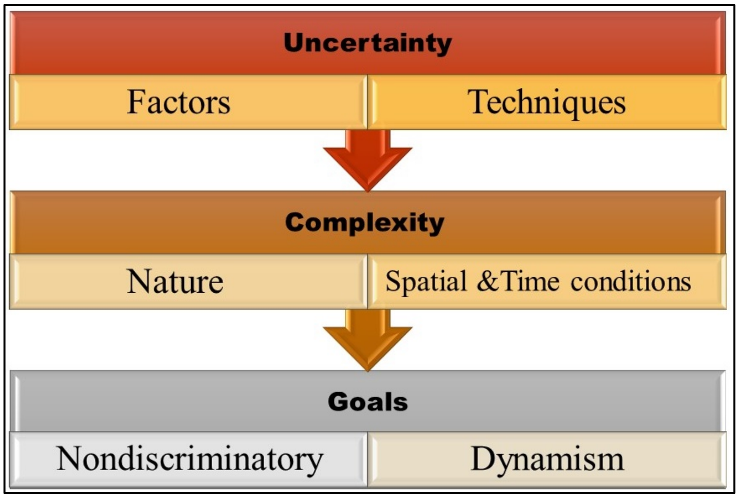

Figure 2.3 Characteristics of suicide attacks.

2.3 Bombing attacks: numbers and facts

Several attacks were recorded during the last decade in the Republic of Iraq and in the U.S. These attacks have emphasized the reality and seriousness of these threats. Figure 2.4 shows the total number in the world of the deaths and injuries from 2011 to 2015. An interactive map of the worldwide spatial distribution of attacks in 2013 is shown in Figure 2.5.

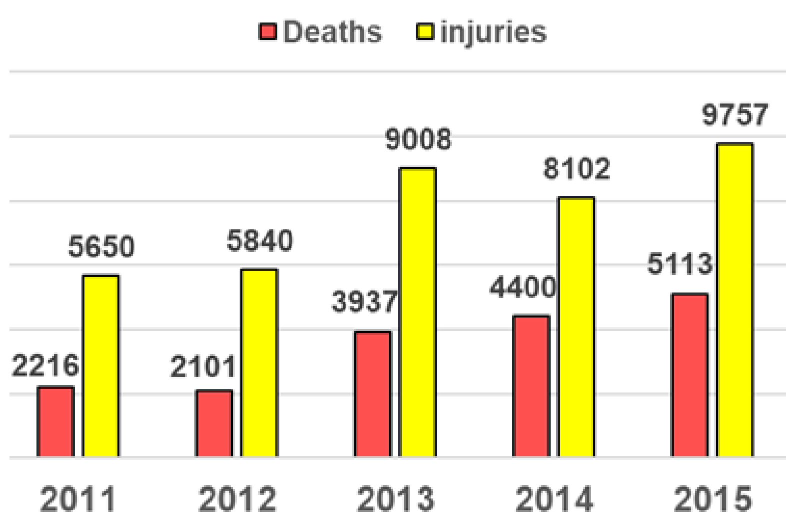

Figure 2.4 Total number of deaths and injuries from 2011-2015. (Chicago Project on Security and Threats, Chicago University, 2016, revised and reproduced by author).

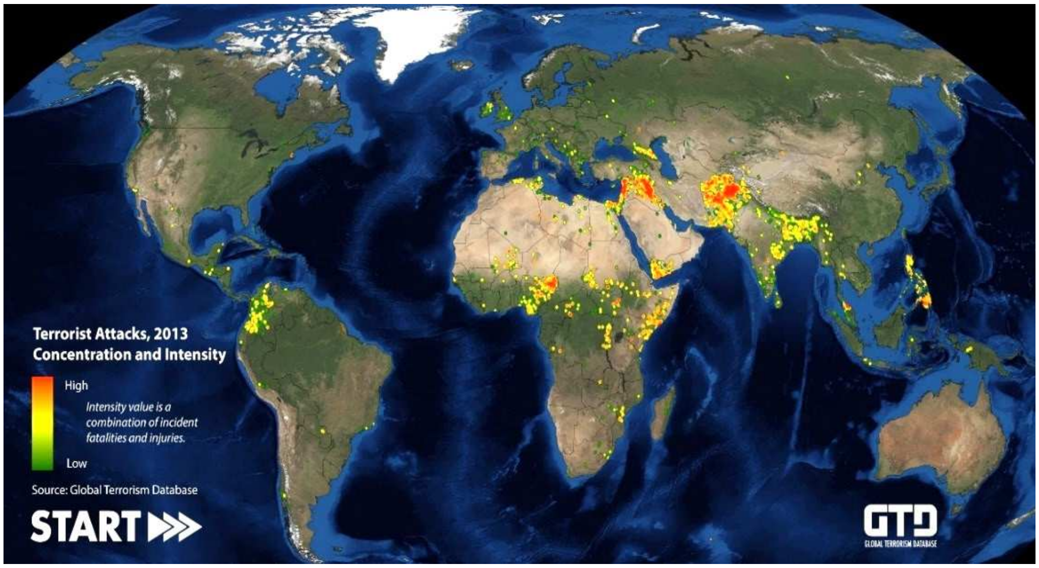

Figure 2.5 Worldwide number of attacks in 2013 (Global Terrorism DataBase, 2016).

What follows is a list of some of these attacks in some countries:

2.3.1 The United States of America

The United States has faced risk of suicide attacks since last decade. Most these attacks have targeted commercial, governmental, and public locations. The U.S. government allocated a large percentage of the budget to prevent or minimize the effects of these attacks and has adopted different strategies to protect the homeland by defeat terrorist groups abroad and stop or diminish their financial resources.

The U. S. has not only facing international terrorism, but several incidents have been recorded and classified as local terrorism. Not all of these events involved the use of explosives. For instance, several massive shootings targeted shopping centers, high schools, and university campuses. The terrorist attacks are dissimilar in terms of number and size every year. Figure 2.6 shows number of recorded attacks from 1970 to 2003 in the U. S. Numbers of terrorist attacks dropped significantly after the 9/11 events (Myre,2018). Examples of attacks targeting the U.S. locally and abroad are listed below.

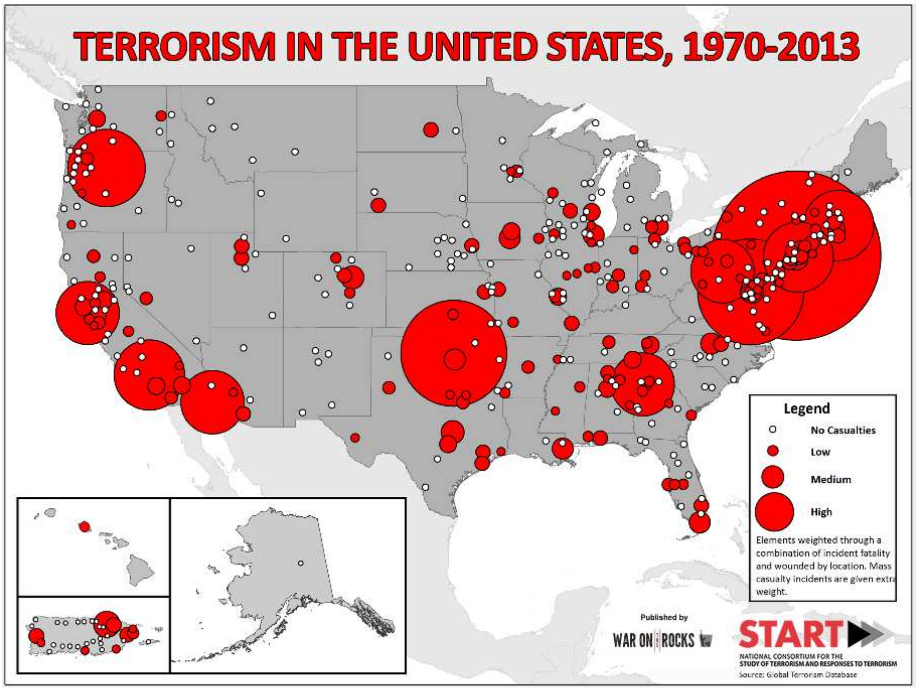

Figure 2.6 Terrorist attacks in the United States from 1970- 2003 (Global Terrorism DataBase, 2016).

WTC: September 11, 2001 - Four airplanes were used to execute suicide attacks in specified locations. Two of them hit the World Trade Center (WTC) in New York City (see Figure 2.7), the third hit Pentagon, while the fourth was destroyed near Pennsylvania. The total number of death and injuries in these attacks were 2,993 and 8,900, respectively (Johnston, 2017). The estimated economic losses after the events of 9/11 were $247.3 billion including site damage, economic losses, and insurance claims (cnn.com, 2016). This attack is considered the worst terrorist attack in the U. S. history due to the massive number of victims and economic losses in addition to other political and social consequences. This attack has not had an impact on the present and future of the U. S. only, but only several consequences were the result of this attack including the issuance of several legislations and orders to stop this risk.

Figure 2.7 World Trade Center attack (Reuters, Sean Adair, 2001).

Oklahoma City: April 19, 1995 – A truck packed with 2,200 kg of ammonium nitrate fertilizer, nitromethane, and diesel fuel mixture of explosives struck the Alfred P. Murrah Federal Building in Oklahoma City (see Figure 2.8). This attack left 168 dead and more than 650 injured. The explosion destroyed 300 buildings around the location in the worse domestic attack in the U. S. history before the 9/11 events.

Figure 2.8 Alfred P. Murrah Federal Building in Oklahoma City attack, 1995 (History.com, 2015).

World Trade Center Attack in New York City, February 26, 1993 - A parked car packed with explosives was left in the underground garage of the World Trade Center at noon on

Friday (see Figure 2.9). The weight of explosive charge was 606 kg of urea nitrate-hydrogen gas enhanced device placed inside a Ryder van. Six people were killed and more than 1,000 injured in this attack (Wikimedia Foundation, 2015).

Figure 2.9 World Trade Center attack in New York City, 1993(fbi.gov, 2008).

The U. S. Embassy Attack in Beirut, April 18, 1983 - A suicide car with 910 kg of explosives targeted the U.S. Embassy in Beirut (see Figure 2.10). The car was parked in front of the building and the explosion killed 63 people.

Figure 2.10 The United States Embassy attack in Beirut (Wikimedia Foundation, 2015).

2.3.2 Republic of Iraq

Since the end of the second Gulf War in 2003, the Republic of Iraq has faced a serious threat by suicide attacks and has ranked number one in the list in terms of number of attacks and victims since 2004 (Global Terrorism Index, 2014). Several victims have been killed and injured in these attacks in addition to billions of dollars' worth of losses. The number of bomb attacks resulting in more than 20 deaths is shown in Figure 2.11. Several attacks have been recorded in detail, some of which are summarized below:

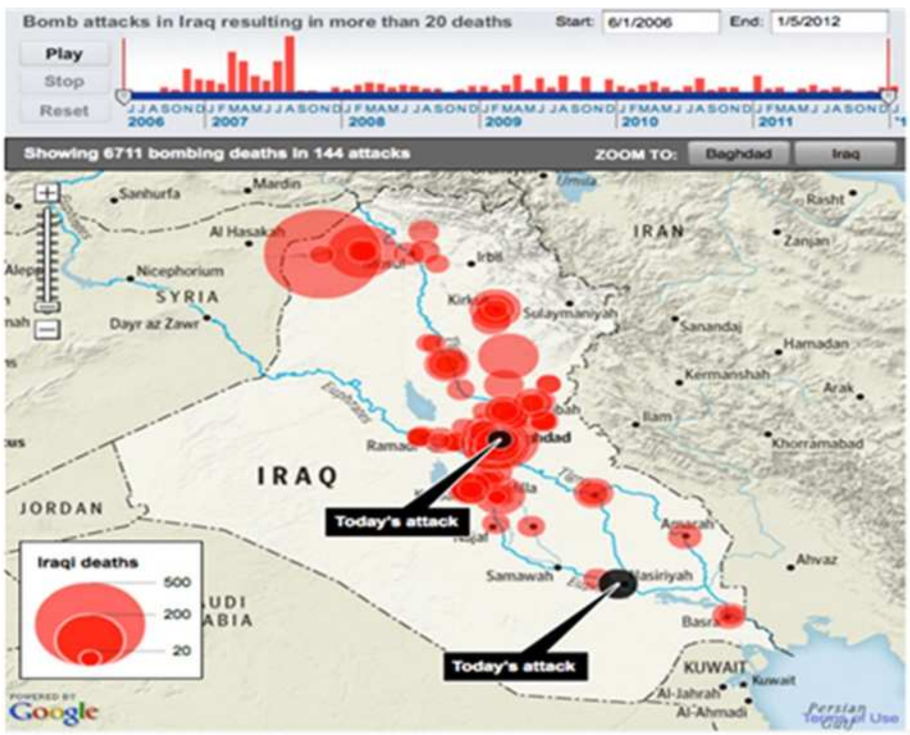

Figure 2. 11 Numbers of bomb attacks in Iraq resulting in more than 20 and more deaths (Thorp, 2013).

Baghdad: 27, May 2013 - Several attacks were executed in Baghdad City by suicide cars. These attacks targeted public places and markets centers and left 81 dead and about 246 injured (Griffis, 2013).

Baghdad Attacks, March 19, 2013 - Several attacks in central and northern Iraq were recorded. These attacks were implemented by car bombs and suicide bombings targeted public places and Iraqi security forces. The result of these attacks was 98 dead and about 240 injured (Muir, 2013).

Baghdad Attacks, April 15, 2013 - Several attacks occurred in different places of Baghdad City. The attacks were implemented by car bombs and suicide bombings targeted public places and Iraqi security forces. These attacks left 75 dead and 356 injured (Griffis, 2013).

Baqubah, Karbala, and Tikrit Attacks, March 20, 2011 - Several suicide attacks took place in Baghdad as well as other cities in Iraq. These attacks were implemented by car bombs and suicide bombings targeted Iraqi police centers, and governmental buildings in the capital. These attacks left 52 dead and about 250 injured (BBC News, 2011).

July Attacks-Iraq, July 23, 2012 **-** Series of suicide attacks targeted Iraqi security forces and governmental buildings. These attacks left 116 dead and 299 injured (Reuters, 2012).

August Attacks, August 16, 2012 - Several suicide attacks were recorded in the north and middle of Iraq. The attacks implemented by car bombs and suicide bombings targeted public places and market centers. These attacks left 128 dead and about 417 injured (Ghazi, 2012).

Jordanian Embassy Attack-Iraq, August 7, 2003 - A parked truck bomb exploded outside of the Jordanian embassy. Because of the concrete walls placed around the building, only some minor injuries were reported for the employees working in the embassy. However, substantially higher social losses were reported for those who were outside the embassy including 17 death and 40 injuries (Wilson, 2003).

United Nations Attack-Iraq, August 19, 2003 - A suicide truck targeted the United Nations Assistance Mission in the Republic of Iraq (cnn.com, 2003). The weight of the explosive charge was 227 kg. In this attack, 22 people were killed, and more than 100 people were injured (Kim, 2007).

2.3.3 Asia and the Middle East Countries

Marriott Hotel bombing- Pakistan, 2008 **-** On September 20, 2008, a suicide truck loaded with 590 kg of RDX mixed with TNT targeted Marriot Hotel in Pakistan. The attack resulted in 18-m deep hole outside of the Marriot Hotel and left 54 dead and 266 injured (Wikimedia Foundation, 2015).

Riyadh suicide Attack-Saudi Arabia, 2003 **-** On May 12, 2003, several suicide attacks by cars and armed teams targeted three residential buildings in Riyadh City. These attacks left 39 dead and 160 injured (Crime Scene.com, 2016).

Figure 2.12 Aftermath of Riyadh compound attacks (Academic, 2014).

Bali Bombings-Indonesia, 2002 - In October 12, 2002, three suicide cars loaded with 1020 kg of equivalent TNT targeted Bali Island in Indonesia. Two of these cars targeted nightclubs in Bali and the third detonated outside of the U.S. Consulate. These attacks left 202 dead and 209 injured (Wikimedia Foundation, 2015).

Shijiazhuang Bombings-China, 2001 **-** On March 16, 2001, Sequential explosions in Shijiazhuang City were orchestrated by four men. The total weight was 590 kg of domestic explosives. These attacks left 108 dead and 38 injured (Wikimedia Foundation, 2015).

Khobar Towers Attack-Saudi Arabia, 1996 **-** On June 25, 1996, a suicide tanker filled with 2268 kg of TNT targeted multistory residential building in Khobar City. These attacks left 20 dead and 372 injured (The Washington Times, 2011).

2.4 Economical, Demographic, and psychological Impacts of attacks in Republic of Iraq-Muqdadiyah City

Muqdadiyah City is located 80-kilometer northeast of Baghdad. It is one of main cities in Diyala governorate. This geographic location near the capital, Baghdad, and Iranian borders on the other hand gave the city economic, military, and political importance (Greenwald, 2010). It can be considered an agricultural town since most people work in farming. According to the latest statistics by the United Nations in 2003, the population of Muqdadiyah is 198,583. Muqdadiyah City can be considered a miniature Iraq because of the diversity of nationalisms, religions, and races of its population. The distribution of ethnicities is Arabic (80-90)%, 5% Kurd, and (3)% Turkmen (Diyala Government, 2014). Other cities in the Republic of Iraq also has faced massive suicide attacks with numerous victims and substantial losses. This study is focused on Muqdadiyah City due to its social characteristics and the familiarity of the author with the city as his hometown.

Figure 2.13 Muqdadiyah City location (Al Jazeera Media Network,2016).

2.4.1 The Impact of Suicide Attacks on Lifestyle in Muqdadiyah City, Iraq

Since the beginning of 2006, several bombing attacks targeted civilians, policemen, military people and government official, and commercial markets causing massive losses in lives and property. In 2004, the violence in Muqdadiyah City represented 0.83% of the total violence in Diyala governorate (Greenwald, 2010). Thereafter, the level of the attacks has increased significantly. There were 162 attacks in Muqdadiyah City from 2006 to 2014 at a rate of 1.5 attack per month as shown in Figure 2.14 (Global Terrorism Database, 2015).

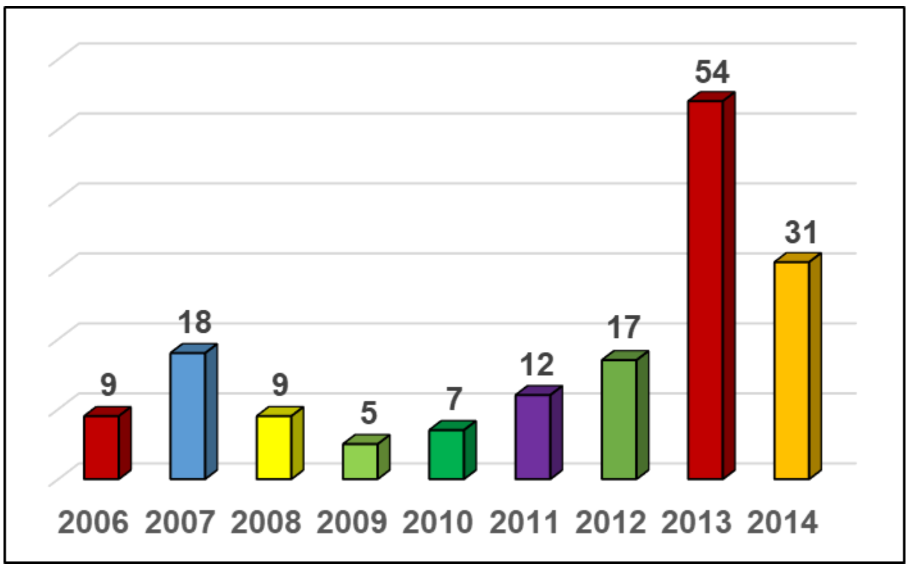

Figure 2.14 Number of attacks - Muqdadiyah City (Global Terrorism Database, 2015, revised and reproduced by author).

These attacks were varied in the way of implementation among VBIED, suicide vest/belt, and IED, which represent 67 percent of the total attacks as shown in Figure 2.15. These attacks targeted almost everything inside the city as shown in Figure 2.16. The main goal of these attacks was to create sectarian strife between residents and to destabilize security forces. Hundreds of dead among civilians and policemen in addition to thousands of orphans and widows were recorded. Furthermore, several families have migrated to another city of the country seeking safety. Social connections were significantly affected by these attacks and friction between various tribes became the norm. Economical activities have totally digressed, and most infrastructure projects have stopped.

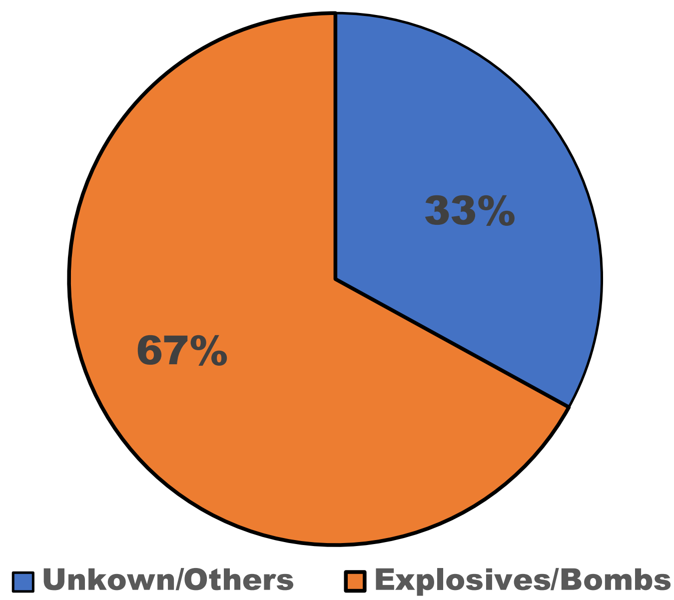

Figure 2.15 Weapons type - Muqdadiyah City (Global Terrorism Database, 2015, revised and reproduced by author).

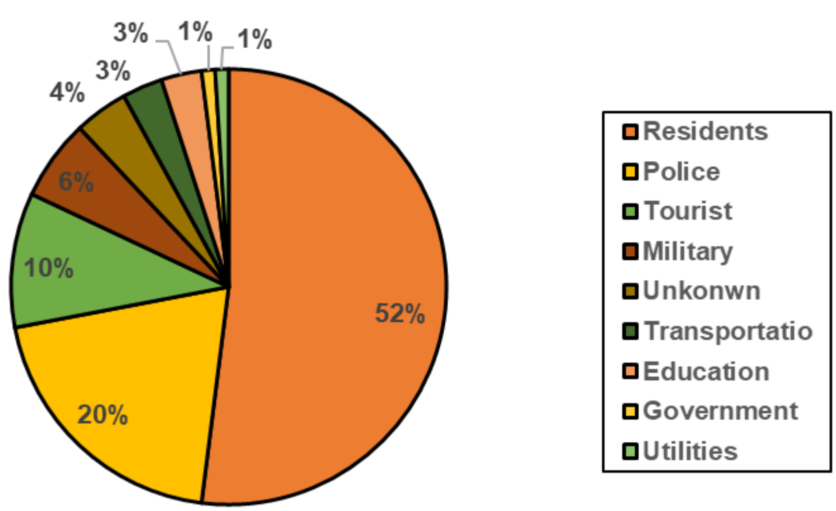

Figure 2.16 Type of targets - Muqdadiyah City (Global Terrorism Database, 2015, revised and reproduced by author).

2.4.2 Recent Suicide Attacks in Muqdadiyah City

From June 2014 to December 2016, Muqdadiyah City had experienced several massive suicide attacks. These attacks started after the Mosul City invasion of the Islamic State of Iraq and the Levant (ISIL), which are also known as the Islamic State in Iraq and Syria (ISIS). In July 2014, ISIL reached various cities in the north and north-west of Diyala Province, specifically, Jalawla, Al-Sadiyah, Qarataba, and Hemreen Hills. Muqdadiyah became the next target to ISIL due to the militarily and economic importance of the city. Sectarian congestion reached its peak in the city because of the suicide and armed attacks by ISIL. The Iraqi security forces, Peshmerga, and civilian volunteers started military operations against ISIL in the north and southwest to prevent ISIL from invading Baghdad and expanding their control the country. Following list of some of these attacks:

Muqdadiyah Café Attack, 01-11- 2016 - Several people were killed in a coffee shop in Al-Asri district in the center of Muqdadiyah city due to a car bomb followed by a suicide vest attack according to the witnesses and Iraqi security forces. This attack also left destructive damages to local shops (Al Jazeera Media Network, 2016; bbc news, 2016). In this attack, 42 people were killed as a result of the terrorist detonating another IED on medic crews and gathered civilians. The nature of the coffee shop location since it has one entrance and exist, and the frame of the building which is just made of aluminum sections and glass windows (see Figure 2.17), helped to increase the number of victims. Right after this attack, several attacks have targeted several mosques in the city, causing the Iraqi security forces to declare maximum alarm status and curfew inside the city. As a result, shortage in basic goods was noted including, for example, the availability of only few grocery stores, the lack of sufficient medicines in hospitals and pharmacies with some pharmacies staying closed for three days.

Figure 2.17 Al-Asri coffee shop attack-Muqdadiyah City, January 2016 (Photographer unknown).

Muqdadiyah Funeral Attack, 02-29-2016 - On February 29, 2016, a suicide bomber killed 40 people and wounded 58 inside a funeral hall (Reuters, 2016). This attack was also followed by a wave of violence as a reaction to this attack. This attack could be considered as the worse in terms of impact on Muqdadiyah. State of fear and expectation spread inside the city. Two days later, hundreds of protesters closed the main highway between the Republic of Iraq and the Islamic Republic of Iran for one week demanding the Iraqi government to take actions to mitigate the attacks before they can allow for the highway to be reopened. The Iraqi government later agreed to some of these demands. Figure 2.18 shows a scene from the attack. The attack resulted in substantial injuries to some people and death to those who were in close proximity to the suicide bomber. Those who sat far away from the bomber only suffered minor injuries. It is worth noting that some of those who were killed were sitting away from the bomber but were impacted by shrapnel from the unconventional nature of the explosive charge.

Figure 2.18 Muqdadiyah funeral attack, February 2016 (Photographer unknown).

Muqdadiyah Al-Molimen Street Attack,05-29-2016- According to the Iraqi press website, 2016, a suicide bomber killed and wounded 42 people on May 29, 2016. The terrorist was trying to enter a café but encountered an Iraqi policeman who tried to stop him. As a result, the bomber-initiated detonation just outside of the café. Prevention of the terrorist from entering the café helped to reduce the number of victims.

2.5 The Suicide Attacks in the Republic of Iraq and United States-Comparative Study

2.5.1 Number of Victims by Suicide Bombings

Stephanie Cutter, the spokesman for John Kerry who was the U.S. Secretary of States, said, “There was no terrorism in Iraq before we went to war”. Iraq did not have any terrorist attacks until 2003 while the first attack in the U. S. was on May 18, 1927, in Michigan, which is known as Bath School massacre. For instance, the number of dead from suicide bombings in 2014 in Iraq was 9,929 people and this number represents 30.4% of the total number of dead in the world (Global Terrorism Index, 2015). According to the Iraqi Group for Strategic Studies, 2017, there were more than 10,000 bombings attacks in Iraq from 2012 to 2017 (5.6 attacks per day). Out of the 10,000 attacks, Baghdad alone suffered 2,900 attacks (1.6 attack per day).

According to various non-governmental Iraqi organizations, the numbers declared are lower than the actual with 165,000 civilians being killed from 2003 to 2015 (1,145 victims per month). Most these attacks have targeted citizens and their property as shown in the Figure 2.19. In the U. S., number of victims from suicide attacks for the same period was 112 people (Global Terrorism database, 2016). Figure 2.20 shows the targeted categories locations in the United States.

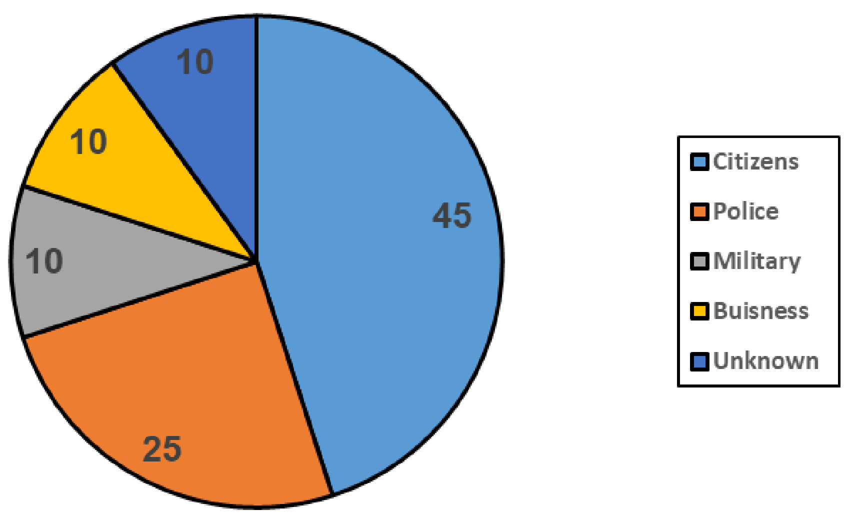

Figure 2.19 Distribution of attacks targets in Iraq in 2014 (Institution for Peace and Economics, 2015).

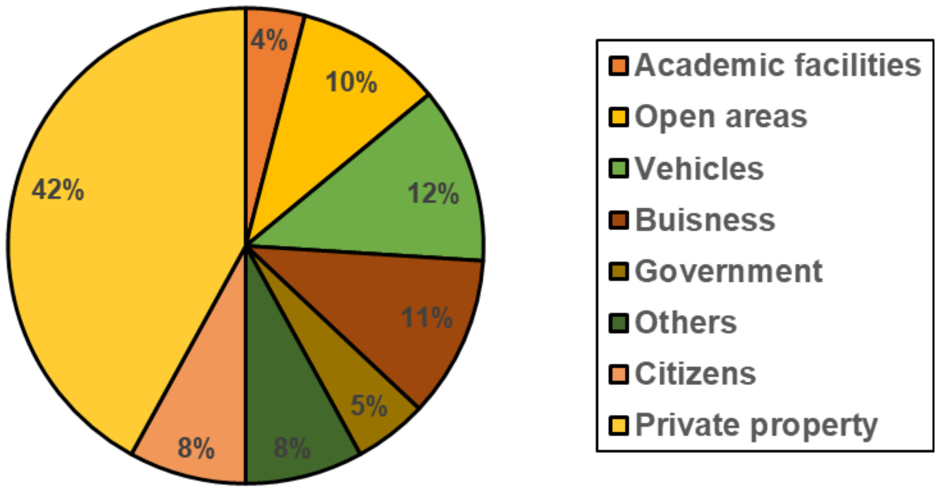

Figure 2.20 Targeted locations in the United States (Stewart, 2009).

2.5.2 Number and Nature of Suicide Bombings

According to the global terrorism index report (Institute for Economics and Peace, 2016), the Republic of Iraq has been ranked number one in the list of ten countries most impacted by terrorism with GTI score 10 out of 10, while the U.S. was ranked 32 with GTI score of 5.429 out of 10. Suicide bombings are the most followed strategy for terrorist attacks in Iraq, while in the U.S. suicide attacks have been implemented using different tactics. There were 3,370 suicide attacks in 2014 in Republic of Iraq, while there were 26 attacks in the U.S. for same period (Statista.com, 2016). Iraq has been entered to the top list of countries which they have facing numerous numbers of attacks annually since 2004 (Global Terrorism Index, 2015). Most suicide attacks in Iraq have been implemented inside cities and this is the reason that numerous victims are civilian. These attacks have not devoid of political allusions due to local and international political conflicts. In the U.S., local and international terrorism have been identified, but major attacks have been attributed to radical groups. The worst attacks in the history of the U.S. was on September 11, 2001 (9/11), nearly 3,000 people and thousands of injuries have been reported.

2.5.3 Economic Impacts of Suicide Bombings

Suicide attacks have had significant economic effects in the U. S. and the Republic of Iraq through direct and indirect losses. For example, in the U.S. the 9/11 attacks resulted in an estimated $247.8 billion in losses (cnn.com, 2017). Government spending on supporting security have increased, and reluctance from investors generally was recorded. The Republic of Iraq has lost billions of dollars since 2003 because of the instability of the security situation. For example, the economic growth index declined, and unemployment have increased significantly. Losses in human capital are impossible to measure accurately; therefore, all recorded statistics are not precise due to several factors and the variety in the methods adopted for estimating the values (Levy & Sidel, 2013). The market's movement was significantly impacted in Iraq after the invasion of the Islamic State in Iraq and Syria (ISIS) in June 2014 (Khan & Estrada, 2016).

These effects have coincided with the drop-in oil prices in the international markets since the Iraqi economy is unilateral and the public income is based on oil sales. According to the Iraqi Prime Minister Haider al-Abadi, 2016, losses due to ISIS invasion in Iraq could have reach $35 billion in addition to casualties. The U.S. government has exceeded the financial crisis due to the multi-income sources and the power of the American economy.

2.5.4 Psychological Impact of Suicide bombings

The main goal of suicide attacks is to create a feeling of fear among civilians and this represents a type of psychological war (Pedahzur, 2005). Figure 2.21 shows main consequences of suicide attacks. In both Iraq and the U.S., several cases of psychiatric comorbidities have been recorded. Moreover, some of unusual phenomena in the Iraqi community have been noted since 2003 such as increase in divorce cases, depression, and internal and external migrations, demographic changes, and lack of confidence in the future. The events of 9/11 in the U.S. have represented a turning point locally and internationally. Psychological effects have been recorded and analyzed from the human health agencies and can be summarized in feeling of fear, grief, confusion, and worry about the future, in addition to physical signs on the victims (Ritz, Hensley, & Witmire, 2004). In comparison, the situation in Iraq is the worst due to complications in the political and security situations, and instability in circumstances conditions.

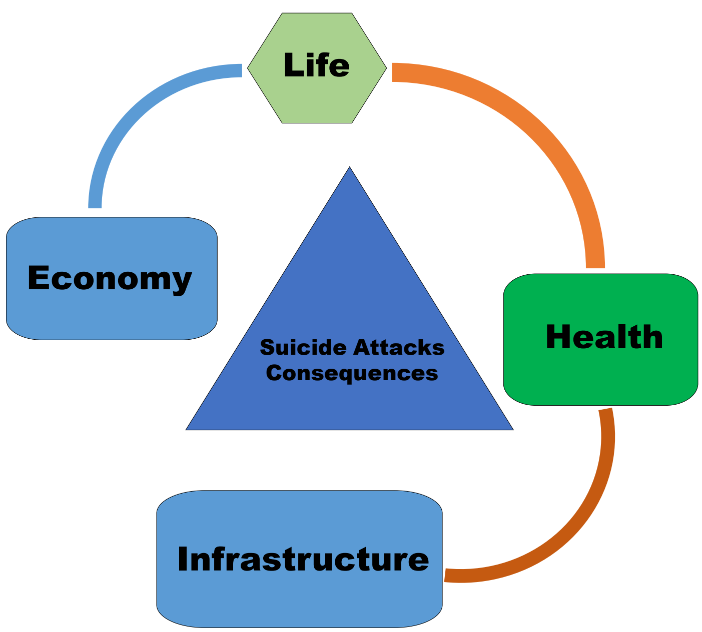

Figure 2.21 Consequences of suicide attacks.

2.6 Blast Injuries Categories

It is obvious that blasts are unique since each explosion has different characteristics based on several factors. In addition to the deadly and destructive effects of blasts, the survivors are often impacted by short and long-term health effects. The main factors affecting the level of threat is the period of exposure to blast and the amplitude of the shock wave. The short duration of the blast shock wave is typically between 1-50 milliseconds while the long duration is typically between 50-250 milliseconds (Bravo Zulu Services Inc., 2015). The shorter exposing to blast is the lowest impact. For example, at 34.5 kPa (5 psi) blast pressure could only cause hearing loss for short duration, while it could be deadly for long duration of blast. Blast shock wave is responsible for hard injuries to brain tissues, bleeding, chest and abdomen compressing (Bravo Zulu Services Inc., 2015). The blast shock wave pressure is the main phenomenon before any other blast wave phenomena can cause casualties. It's action like hammering the body hundreds time instantaneously. Figure 2.22 shows the categories of blast injuries. Table 2.1 shows the effect of short duration of blast shock wave on unprotected people (UFC 3-340-02, 2008).

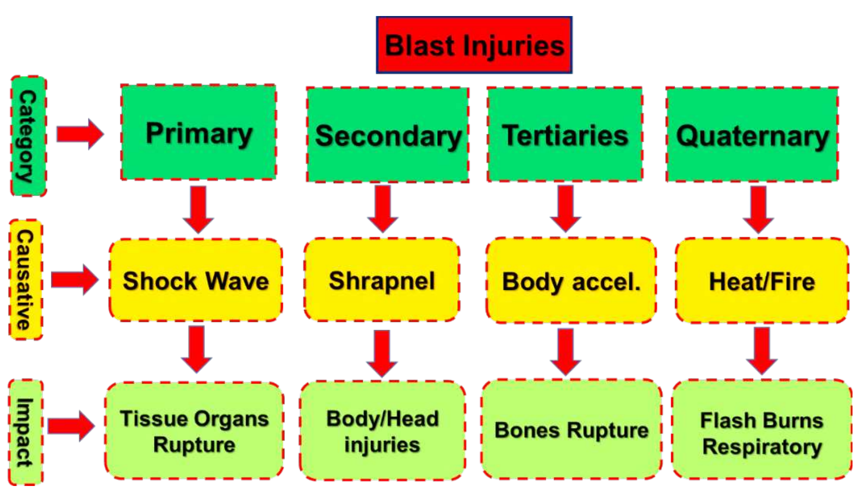

Figure 2.22 Blast injuries categories.

Table 2.1 Blast effects on Human body from short duration events (UFC 3-340-02, 2008).

Effect of blast shock wave	Maximum pressure (kPa)
eardrum rupture (Threshold-%50)	34.5-103
lung damage (Threshold-%50)	206-275
Chance of death (Threshold)	689.5
50% chance of death	896.3
death	1379.0

Another blast phenomenon that can threaten the lives of people is shrapnel impact. The fragments of the explosion and other flying objects from the center of the blast can hit the head passing the skull causing death. These fragments travel at high speed toward unprotected people and could lead to serious injuries. Table 2.2 shows the threshold of possible injuries to organs of the human body in terms of velocity and shrapnel weight (UFC3-340-02, 2008).

Table 2.2 Injuries to personnel from blast fragment impact (UFC 3-340-02, 2008).

Critical Organ	Weight (kg)	Fragment velocity (m/sec.)
Thorax	>1.13	3.05
	0.045	24.40
	0.0004	122.00
Abdomen and limbs	>2.72	3.05
	0.045	22.86
	0.0004	167.64
Head	3.63	3.05
	0.045	30.48
	0.0004	137.16

2.7 Blast effects on Health

Traumatic brain injury (TBI) is the most common injury induced by blast. It can cause death directly or can end with a permanent disability. Many blast injuries could lead to TBI (Bhattacharjee, 2008). There is complexity in diagnosing blast trauma since the trauma is not associated with any direct head injuries (Bhattacharjee, 2008). Even though the Department of Defense (DOD) has implemented extensive research to improve personal protective equipment (PPE) to minimize the possibility of body injuries (Curley et al., 2011), it is still a challenge to protect several parts of the body specially the head despite advancements in the field of high technology of helmets (Gupta & Przekwas, 2013). According to Cernak (2001 and 2008), shock waves pass to the brain through blood vessels causing long-term neurological problems which can stay for long periods of time without detection as illustrated in Figure 2.23. Cernak et al. (2001) noted that protecting the head from being in direct contact with the shock waves will not prevent damage of the cells.

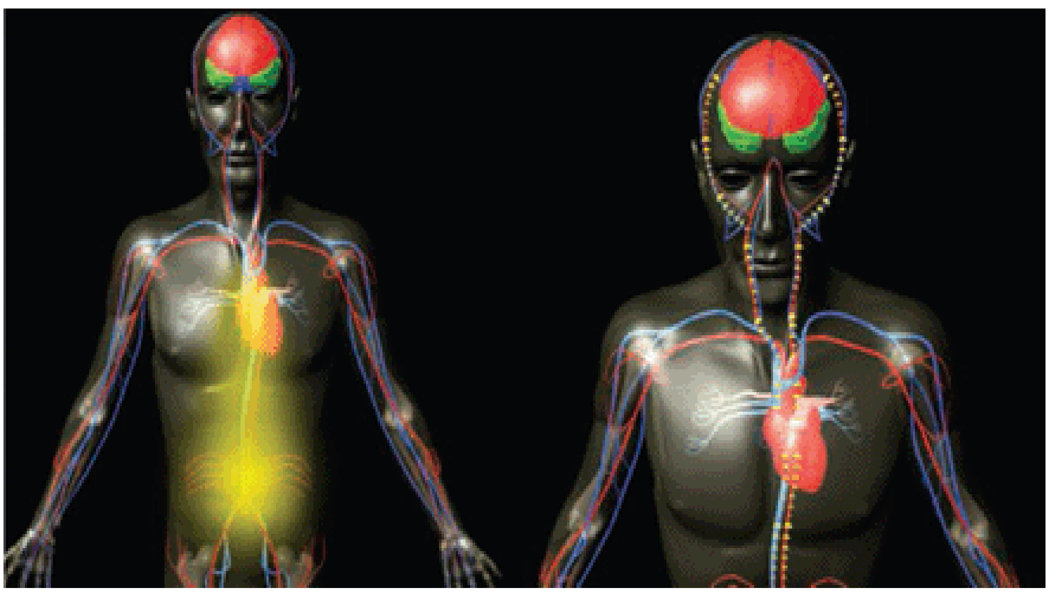

Figure 2.23 Shock wave passing to the brain through vessels (Cenrak, & ELBAZ, Johns Hopkins University, Applied physics Laboratory).

Other parts of the body can be also harmed or damaged by the blast shock wave. Most common are ear injuries which depend on the orientation of ear to the blast wave.

It can be recognized at the time of the blast event and can lead to hearing loss, canal bleeding, tinnitus, otalgia, and vertigo (Slotnic, 2010). For abdominal injuries, cut off bowel, abdominal pain, vomiting, and bleeding can be noticed (Slotnic, 2010). Eye injuries represent 10 percent of blast injuries for the survivors (Slotnic, 2010). Most eye injuries can result from the shock waves and/or flying shrapnel. Victims can suffer from rupture of the cornea, eye irritation, and blindness (U.S. Department of Health and Human Services, 2009). Many U.S army soldiers who returned from service in Iraq and Afghanistan have suffered from ear noise/ hearing loss due to exposure to blast shock waves (Geckle, & Lee, 2004). Figure 2.24 shows the complex blast environment injuries.

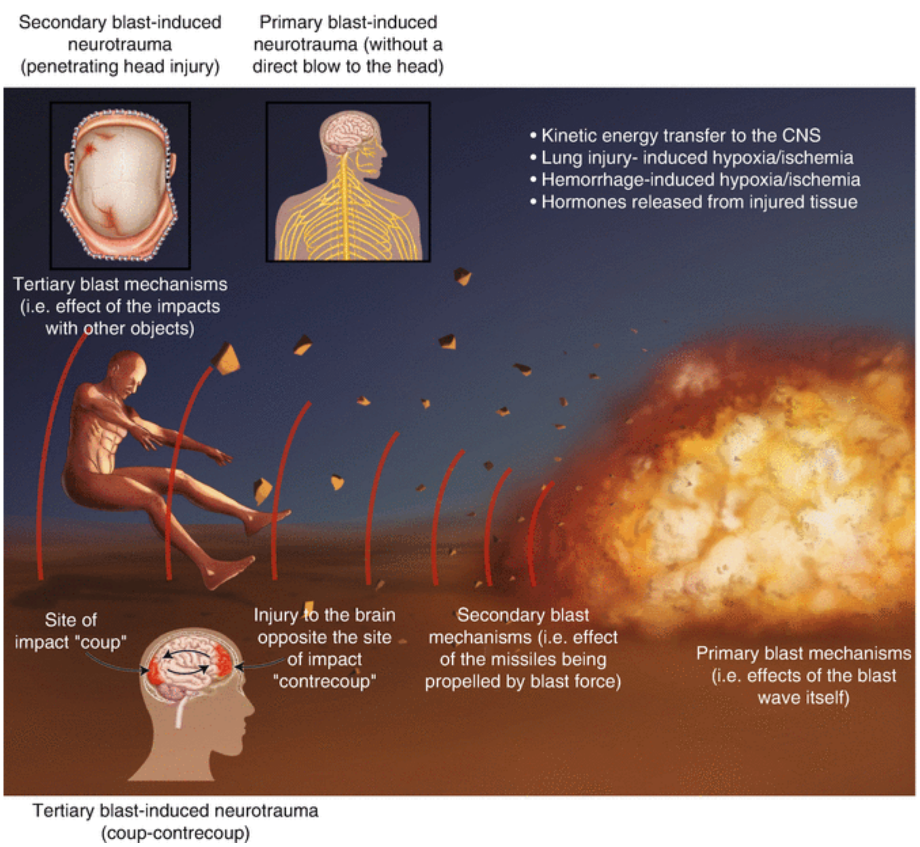

Figure 2.24 Complex blast environment injuries (Cenrak et al., 2010)

Chapter 3. Principles of Blast Loading

3.1 Introduction and Background

The first use of gunpowder explosive was in the 10th century in China (Buchanan, 2006). Thereafter it was used by different nations for burning because of its low-energy release characteristics. Industrially, the first use of explosions was in 1627 by Hungary in the fragmentation of mountain rocks (Henrych & Major, 1979). In 1863, nitroglycerin was developed in Italy by Ascanio Sobero. This new product could explode suddenly under heat effects and it is very unstable. Joseph Wilbrand invented trinitrotoluene (TNT) in 1863, which was the first-generation of high-power explosives (Siba, 2014). Alfred Nobel patented dynamite in 1867. This type of explosion has opened the door for more applications, most of them positive (Siba, 2014). In the following years, technology of explosives further developed and spread in all industrial and research fields such as welding technology, mechanical operations, nuclear energy generation, and other practical applications.

An explosion can be defined as an instantaneous released of energy due to physical and chemical variation in mass. The sudden release of energy quickly dissipates in different ways that can include blast shock wave and thermal radiation (Henrych & Major, 1979). The standard method for computing the magnitude of energy released from an explosion is to compare it to the energy of TNT as a reference explosive and such correlation is known as the relative effectiveness factor (RE). For example, RDX has a RE factor of 1.185: 100 kg of RDX is equivalent to 118.5 kg of TNT based on the specific energies ratio. This approach has been considered to obtain the scaled distance (Z), in terms of equivalent mass of TNT (Mays & Smith, 1995). The relative effectiveness factors for explosives have been published in several references (Baker et al., 2012). There are different ways to classify explosives. These can be adopted depending on purposes, forms, sensitivity, and released energy. In general, explosives can be divided based on the purpose of use into two categories: 1) commercial purposes, and 2) military purposes. Furthermore, explosives can take different forms such as nuclear, chemical, electrical, solar, and volcano explosions. The explosives can also be classified as primary or secondary explosives with respect to their sensitivity of ignition. Finally, explosives can be classified as high-power or low-power explosion (Bangash, 1993) as shown in Figure 3.1. In recent years, unconventional explosives have been used by terrorists. These explosives do not have standard chemical compositions. Therefore, they are not easy to define or be characterized by an equivalent factor. Several applications of using explosives have been considered as shown in Figure 3.2. In this dissertation, all explosive types and quantities will be referred to using the RE factor.

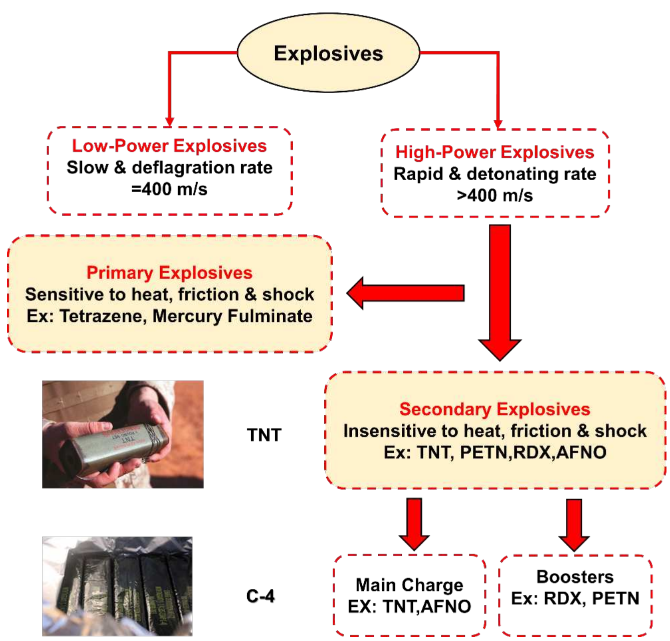

Figure 3.1 Classification of explosives.

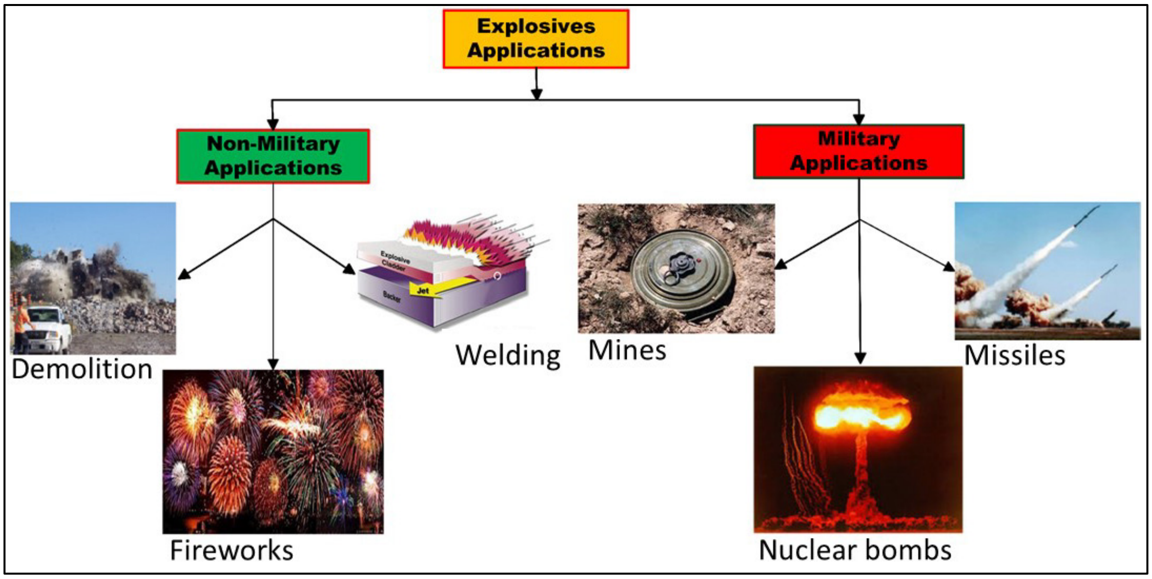

Figure 3.2 Applications of explosives.

3.2 Classification of Blast Loading

Blast loadings have been defined according to the surrounding environment such as air, water, and underground, etc., but the main classifications have been adopted based on the confinement type into two main categories: 1) unconfined burst and, 2) confined burst (UFC 3-340-02, 2008). The blast loading categories are shown in Figure 3.3.

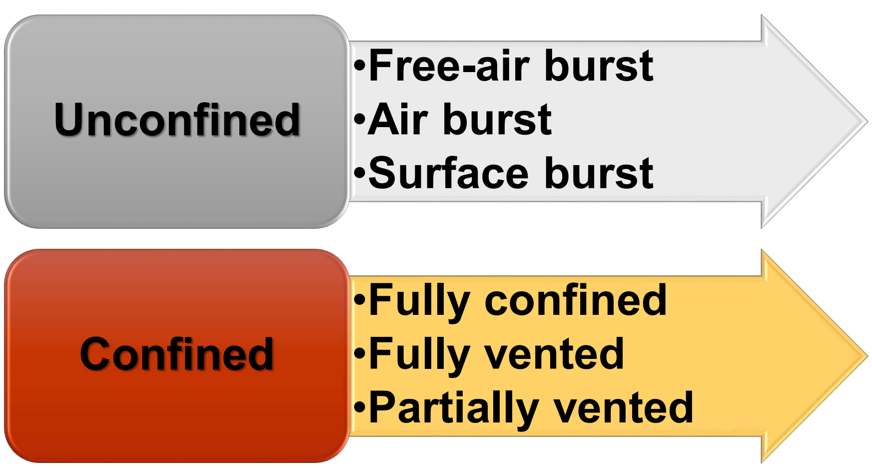

Figure 3.3 Blast loading categories.

Following the blast loading categories and subcategories based on confinement type:

Unconfined Burst - In this type of explosion, detonation occurs in the free-field without any restrictions of blast wave from traveling freely away from the center of the explosion (UFC 3-340-02, 2008). Reflections from the ground are the only factor can oppose the blast wave before reaching targeted structures. This category contains three types: free air burst, air burst, and surface burst.

Free Air Burst - In this explosion, shock wave travels from the center of blast towards the target without any changes in intensity magnitude since there is no reflection interaction before the blast wave reaches surface of the target (UFC 3-340-02,2008), as shown in Figure 3.4. This study considers normal incident wave traveling towards the structure directly without interruption with normal reflected pressure generated, and the surface of structure being rigid and perpendicular to the shock front.

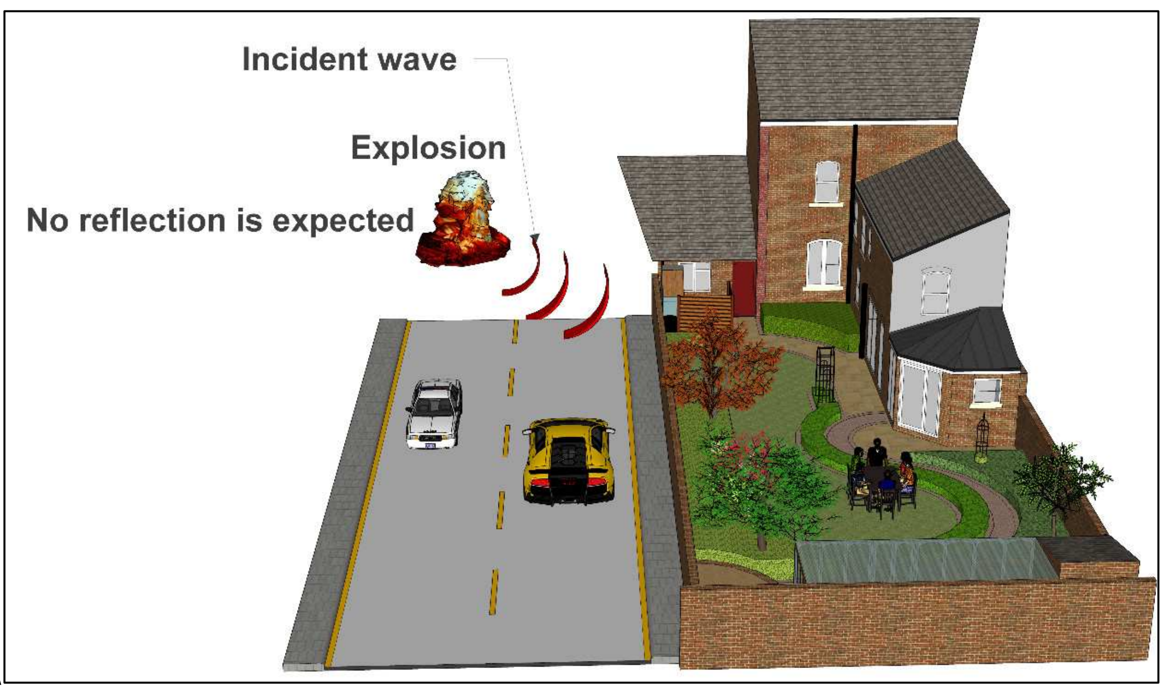

\

Figure 3.4 Free-air burst.

Air Burst - In this explosion, the point of detonation occurs at a distance above the ground as shown in Figure 3.5. The reflection from the ground occurs before the initial wave reaches and strikes targeted structure (UFC 3-340-02, 2008). The amplification of the initial shock wave is expected. The interaction (merge) between the incident wave and reflected wave generates what is known as Mach stem (front) with the magnitude of the reflected wave pressure being higher than the incident wave pressure.

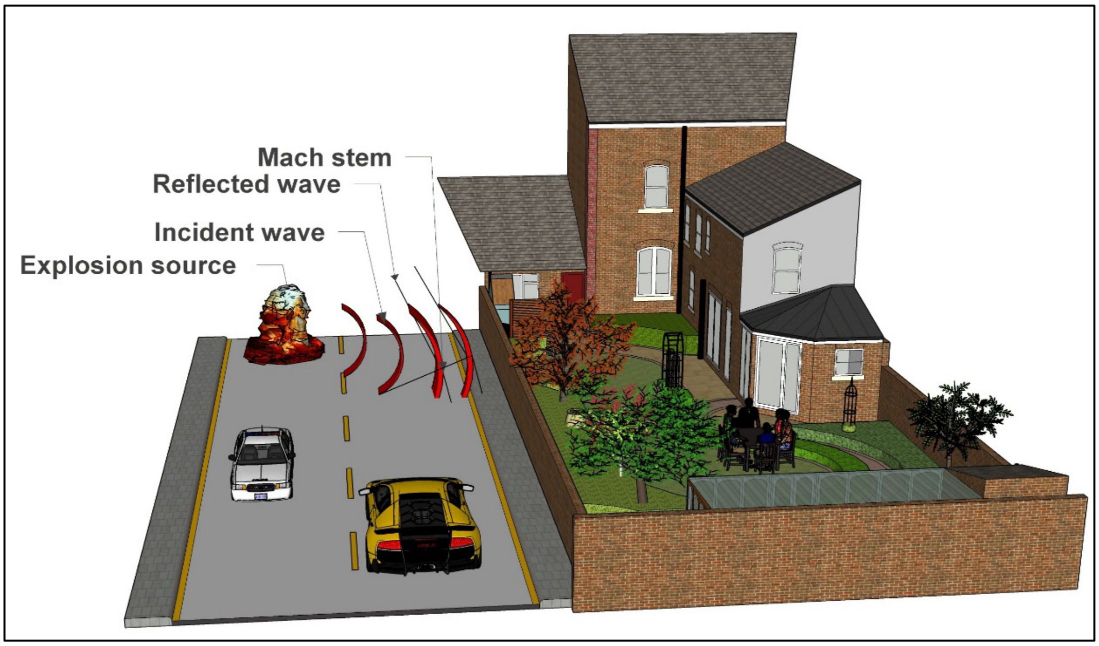

Figure 3.5 Air-blast burst.

Surface Burst **-** In this explosion, the point of detonation is placed on or very close to the ground (UFC 3-340-02, 2008). The reflection from ground initiates the primary shock wave as shown in Figure 3.6. The interaction between the incident and reflected waves will be at the detonation point, then both will merge to form one wave moves towards the target in hemispherical shape (UFC 3-340-02, 2008). Numerically, all blast wave parameters values are larger than free-air blast parameters for specified scaled distances. Mach stem phenomenon is generating at the detonation point, unlike the air bust type.

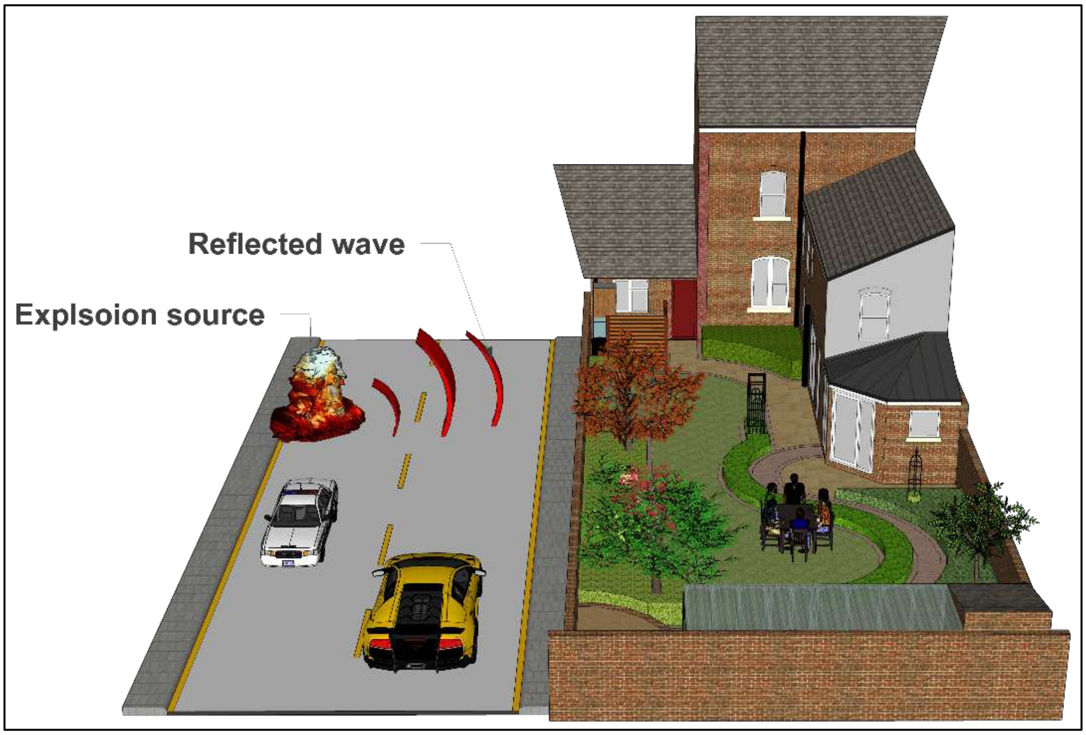

Figure 3.6 Surface blast burst.

In all unconfined explosion categories, blast wave parameters are calculated in terms of scaled distance $Z = R/\sqrt[3]{W}$ where, R is the standoff distance from the source of detonation to the target (m), and W is the weight of the explosive (kg). An empirical approach can be considered to calculate the blast wave parameters in many cases since there is no need to model the blast field or explosive material, (Hryciów et al., 2014). The input parameters for this approach are: 1) TNT equivalent charge weight .2) the distance between the blast source and the targeted structure (Goel, 2015). This method does not have capability to simulate the reflections between obstacles, therefore, it is not a precise choice for presenting blast phenomena in crowded areas when reflection is most common and expected (Goel,2015). In addition, there is some question about accuracy of empirical formulas for small scaled distances.

The most common empirical blast model is the Kingery-Bulmash model (Kingery and Bulmash, 1984). The Kingery-Bulmash was discussed in more details in section 3.12. In recent adopted strategies of implementing attacks, explosion event could be consisting of more than scenarios. In this case, the classifications and analysis of the blast will be different and needs to be considered accurately to get the blast load parameters precisely.

Confined Burst - This category has three types: fully vented explosion, partially vented explosion, and fully confined explosion. Figure 3.7 shows the three types of confined explosions. The main difference between unconfined and confined explosions is in the peak pressure due to the reflections phenomenon. The level of confinement and pressure venting determine the intensity of the blast shock wave pressure (UFC 3-340-02, 2008).

Fully Vented Explosion - The explosion takes place inside structures or box-form structures against one or more sides (faces) facing the field. The initiated shock wave volume doubles by the non-damaged parts of the structure and the output of this detonation is fully vented to the surrounding field (UFC 3-340-02, 2008).

Partially Vented Explosion - The explosion takes place inside box-form structures with small-size holes. The initiated shock wave passes through these openings fast to the surrounding environment (atmosphere). The intensity of the shock wave pressure is low if compared to the blast shock in free-field (UFC 3-340-02, 2008).

Fully Confined Explosion - The explosion takes place inside box-form structures without venting of pressure. The vented pressure is very low, and the impact only can affect structures in close-range based on the confinement level (UFC 3-340-02, 2008).

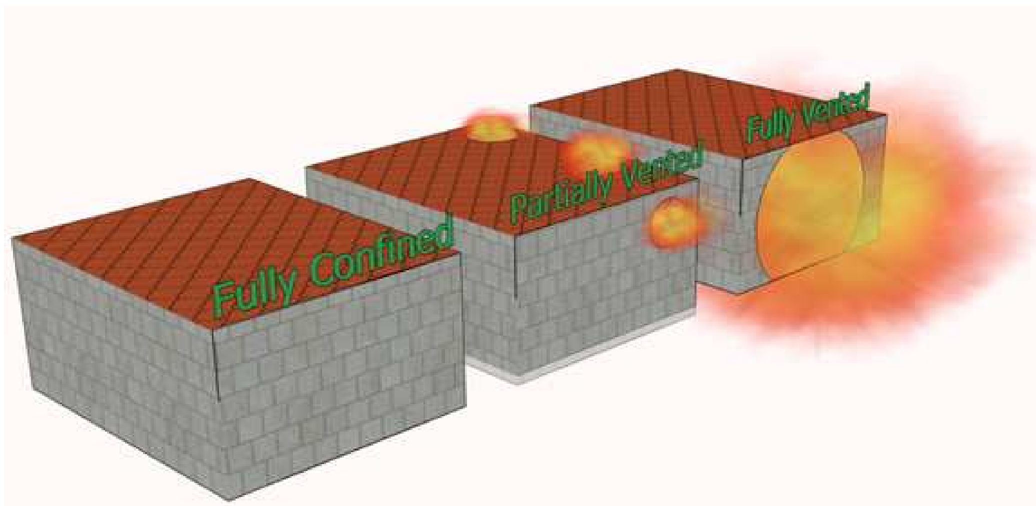

Figure 3.7 Confined explosion categories.

3.3 Blast Shock Wave Pressure Generating in Air

The most important quantity controlling the magnitude of the blast pressure is the volume of energy released (Bangash, 1993). At the onset of the explosion, air strongly shifts backward generating the blast wave. The explosive material is converted to hot gas due to the high chemical reactions, and a high-speed shock wave is generated moving radially away towards the target (Brown & Loewe, 2003). A fireball is also generated, and its volume increases and the air circumference temperature decreases. Only 33 percent of the explosion chemical energy is utilized effectively in the explosion process, and the rest mix and burn in air (UFC 3-340-02, 2008). Forces act on a nearby structure due to an explosion because of the difference in air pressure on various faces of the structure (Bangash, 1993). The shock wave passes through the structure and may reflect from it (Cullis, 2001). The detonation speed is almost 20 times larger than the speed of sound, and the shock wave moves faster than the speed of sound in air (supersonic) (Cullis, 2001). Typically, shock waves have a higher capability to destroy and harm than the blast pressure waves (Dusenberry, 2010). The shock wave in air is known as “blast shock wave” due to the sudden impact (Mniszewski, Longinow, & Kenner, 2009).

3.4 Typical Pressure-Time Curve in Free Field

Blast wave characteristics change according to the type of explosives, surrounding environment, wave-wave, and wave-structure interactions, but the general profile is usually the same for detonation in free field. Due to high energy release, the pressure rapidly increases to a certain value above the atmospheric pressure, which is known as side-on overpressure or peak overpressure at the shock front (Ngo et al., 2007). As the shock wave propagates, the pressure decays exponentially and becomes less than the atmospheric pressure and this is known as the negative phase (Cullis, 2001). The negative phase is longer, but less in magnitude in comparison to the positive phase (Ngo et al., 2007; Dusenberry, 2010). The negative phase is mostly negligible since it has small effect in comparison with the positive phase (Goel, 2015). This phase is responsible for carrying shrapnel away from explosion source (Ngo et al., 2007). Finally, at the conclusion of the negative phase, the pressure is restored to the atmospheric value while the blast wave is moving away from the source (Mays & Smith, 1995). Figure 3.8 shows typical pressure-time history of a blast wave in free homogenous field from symmetric spherical charge. The blast wave in free air is described by Friedlander's equation as shown in Equation 3.1 (Goel, 2015).

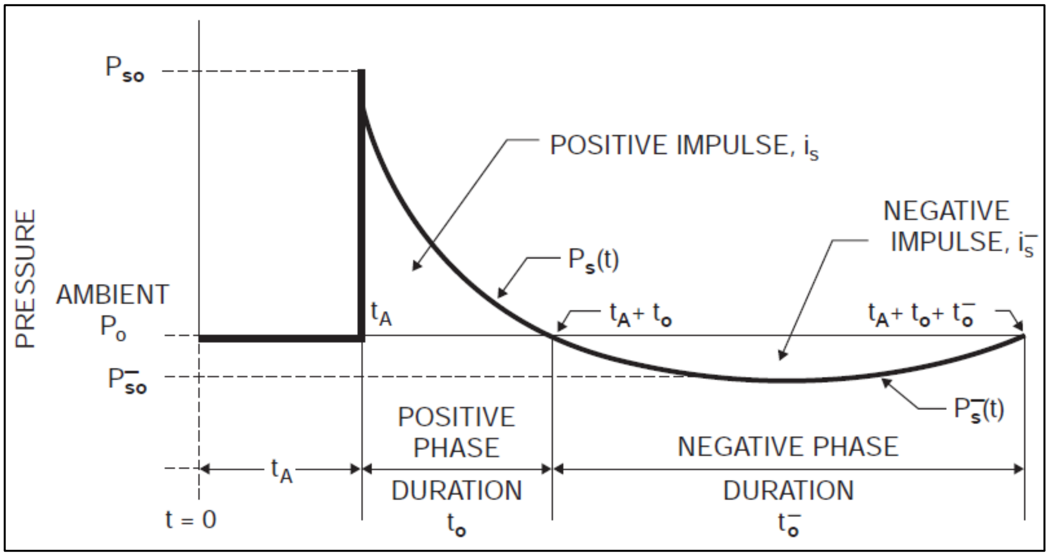

Figure 3.8 Typical pressure-time curve in free field (UFC 3-340-02, 2008).

$$P(t) = P_{so}[1 - \frac{t}{t_0}]e^{[\frac{-\alpha*(t-t_A)}{t_0}]} \qquad (3.1)$$

Where: $P(t)$ is the pressure at a certain time (N/m^2); P_{so} is the peak incident pressure (N/m^2); t_0 is the positive phase duration; t_A is the arrival time, and α is the wave decay factor which can be found in blast standards and manuals. The same equation can be used to calculate the blast wave pressure for surface blast (hemispherical wave) by multiplying it by 1.8, to consider the reflection from the ground (Smith & Hetherington, 1994). Another important parameter is the positive impulse, is^+, which is equal to the area under the blast pressure curve of positive phase as shown in Equation 3.2. This blast wave parameter can provide an estimate on the expected level of structural damage.

$$i_s^+ = \int_{t_a}^{t_A+t_o} P(t)dt \qquad (3.2)$$

3.5 Scaling Law of Blast Loading

Three factors quantify explosions intensity - 1) amount of released energy, 2) distance from explosion source, and 3) nature of the medium (Goel, 2012). Scaled parameters have been specified through experiments using different scaling laws. Scaling can be used to determine various blast wave parameters under the same conditions using reference values from controlled tests. The most common used scaling law is called the cubic root law, which was formulated independently by Hopkinson (1915) and Cranz (1926) (Goel, 2015). The principles of Hopkinson-Cranz blast scaling law can be summarized as follows: If two masses of the same explosive charges W_1 and W_2, have similar geometry detonated at distance R, in a specific field, but their diameters are different, d1 and d2 and the blast wave parameters of explosive charge W_1, are P_{so}, t_{01}, t_{A1}, and i_s. Then, the blast wave parameters of explosive charge W_2 are scaled with length factor (λ): λR_1, λi_s, λt_{A1}, and λ_{d1}. The only parameters are not subjected to scale are pressure, density, velocity, and temperature (Baker et al, 1981). The scaling law can be expressed in terms of a scaled distance as cube-root scaling law, Z ($m/kg^{1/3}$), as

$$Z = R/\sqrt[3]{W} \qquad (3.3)$$

Where, R is the distance from the source of detonation (standoff distance) in meters, and W is the charge mass of TNT in kilograms. This concept is presented in Figure 3.9. Table 3.1 shows the scale factors of the blast shock wave parameters. Hopkinson-Granz scaling law only predicts the blast wave parameters and is not applicable to scaled structural response. This scaling law is also not appropriate for small standoff distances due to the effect of blast wave interactions (Hammond & Sunders, 1997).

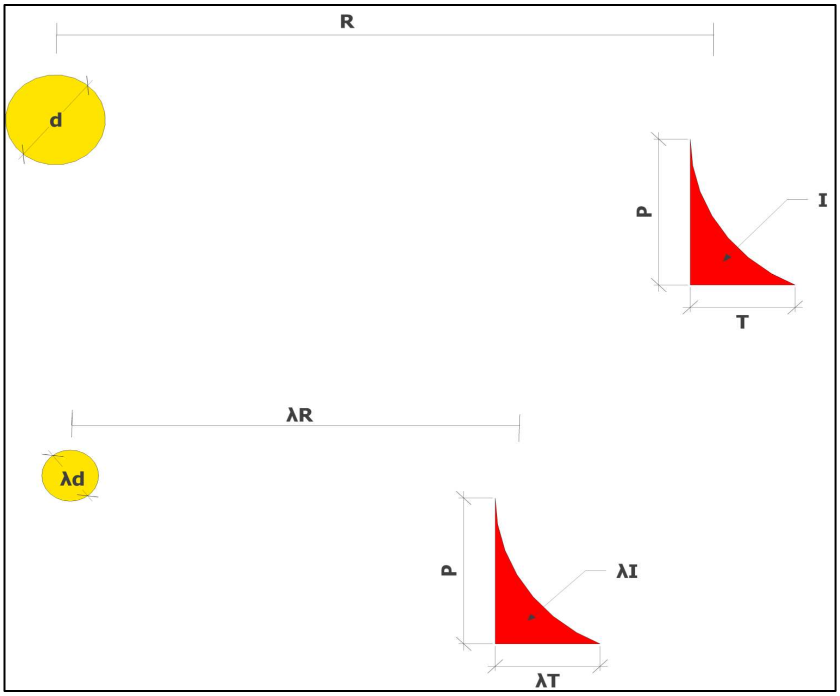

Figure 3.9 Hopkinson-Cranz blast wave scaling law (Baker et al., 1981).

Table 3.1 Blast shock wave parameters scaling factor according to Hopkinson-Granz scaling law (Hammond & Sunders, 1997).

Parameter	Charge	
	W1	W2
Standoff distance	R	λR
Characteristics length	L	λL
Charge Size (diameter)	d	λd
Peak overpressure	P	P
Pulse time	t	λt
Impulse	I	λI
Density	ρ	ρ
Velocity	V	V
Temperature	T	T

3.6 TNT Equivalency

The energy released from a specific TNT mass is usually used as a reference value (Goel, 2015). If there is a blast wave generated from another explosive material, the mass of the charge should be converted to an equivalent weight of TNT (Iqbal, 2008). Equivalency of explosive materials to TNT can be impacted by the energy released, material form, and confinement conditions (TM 5-1300, 1969). The output energy of a specified shape of explosive material to released energy of TNT can be expressed in terms of heat of detonation of different materials by multiplying the mass of the explosive material by conversion factor of heat detonation ratio. The equivalent mass of TNT can be calculated based on the heat released of blast detonation of different explosive materials as shown in Equation 3.4 (UFC 3-340-02, 2008). Conversion factors of some common explosive materials are listed in Table 3.2.

$$TNT_E = \frac{H_{EXP}}{H_{TNT}} W_{EXP} \qquad (3.4)$$

Where, TNT_E, equivalent TNT mass; H_{EXP}, heat detonation of an explosive; H_{TNT}, heat detonation of TNT; W_{EXP}, mass of an explosive.

Table 3.2 TNT equivalent mass factors (Mays & Smith, 1995).

Explosive Type	Mass specific energy Q_x(KJ/kg)	TNT equivalent (Q_x/Q_{TNT})
Compound B (60% RDX 40% TNT)	5190	1.148
RDX (Cyclonite)	5360	1.185
HMX	5680	1.256
Nitroglycerin (liquid)	6700	1.481
TNT	4520	1.00
Blasting Gelatin (91% nitroglycerin, 7.9% nitrocellulose, 0.9% antacid,0.2% water)	4520	1.00
60% Nitroglycerin dynamite	2710	0.60

3.7 Structural Response to Blast Loading

Engineers have focused on understanding the behavior of structures under blast loading by analyzing the applied pressure from the blast shock wave and associated level of damage that resulted from this pressure (Ngo et al., 2007). However, it is not clear if such simple representations are accurately capturing the physics of the blast wave in such cases, but it is possible if simplified equivalent SDOF systems (Ngo et al., 2007). Blast loading from an explosion can have simple or severe effect on structures, depending on several different factors. Of primary interests are deflections and the stresses within the structure, which can be associated with levels that will cause minor or major damage as well as partial or complete structural collapse (Kinney et al., 1962).

Dynamic analysis of structures subjected to blast loading can be complex, and this complication is associated with estimating the blast load, material inelasticity, and geometric nonlinearity (Ngo et al., 2007). Mathematically, structural response is controlled by impulse and mass inertia if the response time is longer than the loading time, while peak overpressure and targeted surface area “loaded area” control the behavior if the response time is shorter than the total time of loading (Baker et al., 1981). Having full knowledge and understanding of the characteristics of the blast wave, time scale, material response, and interaction of shock waves with structure is necessary to develop an appropriate design approach.

3.8 Prediction of Peak Overpressure of Blast Loading

Several analytic equations can be considered to calculate the generated pressure from a specific mass of explosive charge and standoff distance. The most used equation of peak overpressure (P_{so}) was developed by Kinney and Graham (1985). This equation is adopted by most studies (Karlos, and Solomos,2013) as shown in Equation 3.5.

$$P_{so} = P_o \frac{808[1+(\frac{Z}{4.5})^2]}{\left\{1+\left[(\frac{Z}{0.048})^2\right][1+(\frac{Z}{0.32})^2][1+(\frac{Z}{1.35})^2]\right\}^{0.5}} \qquad (3.5)$$

Where, Z is the scaled distance, P_o is the atmospheric pressure.

Another equation to calculate the peak overpressure from a spherical charge derived by Brode (1955). The derived equation has two forms: 1) for close-in burst when the peak overpressure is larger than 1 MPa as shown in Equation 3.6 a; and 2) for large scaled distances, when the peak overpressure ranges between (0.01 MPa< P_{so} <1.0 MPa), as shown in Equation 3.6b. These equations were derived for nuclear explosions and not for representing peak overpressure from conventional explosives (Karlos and Solomos, 2013). Hence, they are of almost no use in this study.

$$P_{so} = \frac{6.7}{Z^3} + 1 \qquad (P_{so} > 1.0 \quad \text{MPa}) \qquad (3.6a)$$

$$P_{so} = \frac{0.975}{Z} + \frac{1.455}{Z^2} + \frac{5.85}{Z^3} - 0.019 \qquad (0.01\ \text{MPa} < P_{so} < 0.1\ \text{MPa}) \qquad (3.6b)$$

3.9 Blast Shock Wave Versus Natural Hazards

Comparing the effect of blast to those of natural hazards can give a clear idea about the characteristics of the blast shock wave. In the case of an explosion, the frequency, intensity, and preventative measure are unknown. There is no set standard relating the characteristics and the impact of the blast and seismic loading. In recent decades, earthquake engineering and seismic design have been investigated theoretically and experimentally (Sammarco et al., 2014). Currently, advanced technologies implemented and considered to mitigate ground motion effects on structures (Sammarco et al., 2014). But very limited means of protection or threat reduction exist for explosives, although there has been some movement in this direction. In recent years, due to increase in number of international and domestic terrorism, government and federal agencies have focused on security status of buildings and infrastructure. Several standards, technical manuals, documents have been published offering blast-restraint design specifications.

There are important differences between the two hazards in load demands, system and components response. Even though each has different characteristics, structure response, and load effects, at the same time there is an overlapping in structural integrity measures that could be considered (Hinman, 2011). However, the two sources of force excitation are dramatically different. For instance, the blast loading is applied to the external faces of the structures, while seismic load is applied to the base of the buildings. Furthermore, blast is applied high pressure in seconds, while seismic load acting could last from seconds to minutes. The response attenuates when the mass of inertia increases in case of the blast, while it increases in case of the seismic loading. These dissimilarities and similarities can be summarized in Table 3.3 and Figures 3.10, and 3.11, respectively.

Table 3.3 Blast loading versus seismic loading.

Blast Loading	Seismic Loading
Applied to external faces of structures	Applied to base faces of structures
Interested in out-of-plane response	Interested in-plane response
High pressure in short period (msecond)	Acts in long period (seconds)
Local response is important	Global response is important
Mass inertia can help to mitigate	Mass Inertia can increase the hazard

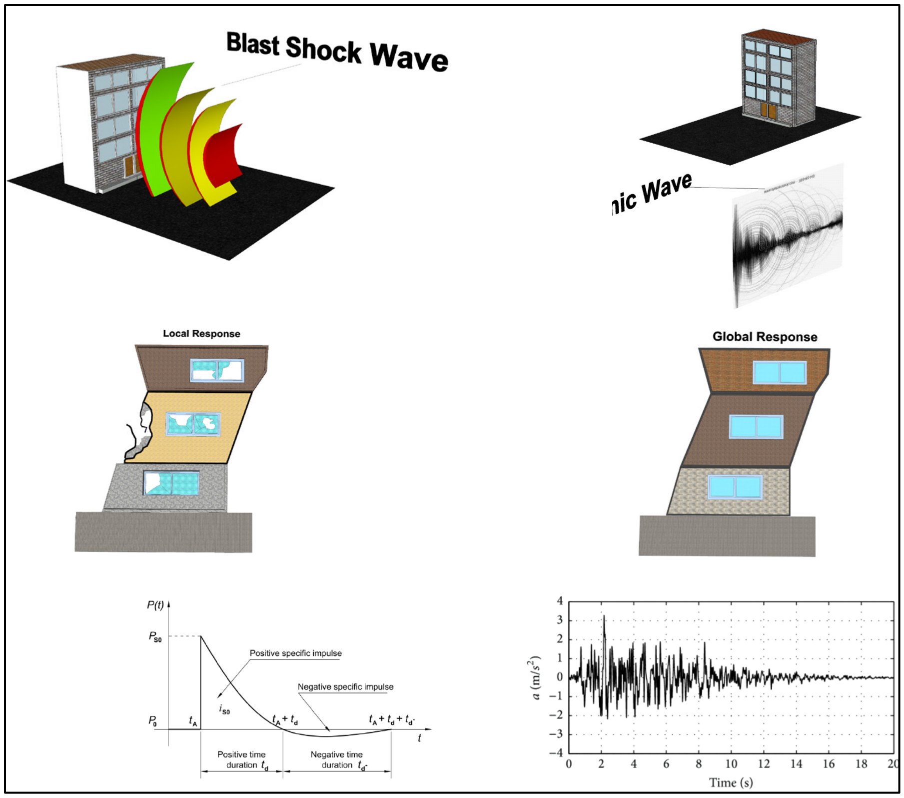

Figure 3.10 Comparison between seismic and blast loadings.

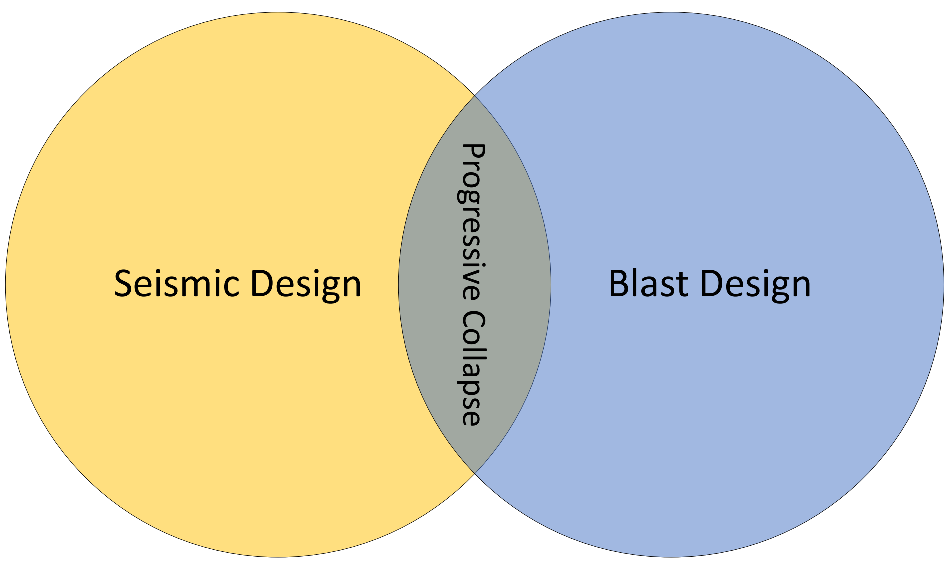

Figure 3.11 Overlap between blast and seismic loadings (Hinman, 2011).

Hurricanes events are somewhat similar to blast events in that they have left numerous victims and massive destruction to infrastructure, comparing the effects of blast shock wave to hurricanes can also give a clear view of the characteristics of blast shock wave. For example, comparison with hurricane IRMA which swept Florida State in the U.S. on September 10, 2017, is shown in Table 3.4 (National Hurricane Center, 2018). It is noted that Hurricane IRMA generated 93.2 kPa pressure but with very large impulse.

Table 3.4 Comparison between blast shockwave and Hurricane IRMA.

Parameter	Blast shock wave	IRMA Hurricane
Wind speed (m/s)	400	82-18
Pressure (kPa)	138[1]	93.20
Duration (msec)	(50-250)[1]	Relatively moving slowly
Zone of effect	Specified local area	vast areas

3.10 Behavior of Materials under Blast Loading

Constitutive models have been considered to represent the materials under blast loading (Johnson & Cook, 1983; Drucker & Prager, 1952; Karlsson & Sorensen, 2001). The most common model for metallic and non-metallic materials is the Johnson-Cook (J-C) model (Johnson & Cook, 1983). This constitutive model considers the plastic behavior of materials under strain-rate, strain hardening, and temperature (Johnson & Cook, 1983). The mathematical expression can be written as in Equation (3.7). This computational model considered the von Mises flow stress (σ).

[1] Could be different values based on generated blast wave energy.

$$\sigma_y = (A + B\varepsilon^n)(1 + Cln\dot{\varepsilon}^*)(1 - T^{*m}) \qquad (3.7)$$

Where, *A*, *B*, *C*, *m*, and n are material constants; $\dot{\varepsilon}^*$ is the plastic strain rate (dimensionless); and *T** is the homogenous temperature. The homogenous temperature defined as

$$T^* = \frac{T - \quad T_r}{T_m - T_r} \qquad (3.8)$$

Here T_r, is the temperature room, and T_m, is the melting temperature of the material.

For sand, the Drucker-Prager plasticity model (Drucker & Prager, 1952) represents the frictional relation between shear and normal stresses using the Coulomb friction model. This model is often used to simulate sliding motions between sand grains. Tensile and shear tests are required to calculate the Drucker-Prager parameters. This model can be expressed as shown in Equation 3.9 (Drucker & Prager, 1952).

$$F = \frac{q}{2}\left[1 + \frac{1}{K} - (1 - \frac{1}{K})(\frac{r}{q})^3\right] - \acute{p}tan\beta - d \qquad (3.9)$$

Where,

q = $1.225\sqrt{S_{ij}\colon S_{ij}}$;Sij: the deviatoric stress tensor; K is the yield surface shape parameter β is a parameter to calculate the angle of internal friction(ϕ); r is the third invariant of deviatoric stress; $\acute{p}$ = $\frac{1}{3}(\acute{\sigma_1} + \acute{\sigma_2} \dot{+} \acute{\sigma_3})$; d is the hardening parameter.

For concrete, concrete damage plasticity model (CDP) is used to consider the degradation of the elastic stiffness induced by plastic straining (Karlsson & Sorensen, 2001). This constitutive model accounts for failure under both compression and tension.

This model assumes that strain hardening is followed by strain softening, which describes the compressive behavior (Karlsson & Sorensen, 2001). This model can be written in the following format as shown in Equation 3.10 (Jankowiak & Lodygowski, 2005). The simplified form of CDP model can be written as in Equation 3.11.

$$\sigma = (1-d)D_0^{el}:(\varepsilon - \varepsilon^{pl}) = D^{el}:(\varepsilon - \varepsilon^{pl}) \qquad (3.10)$$

$$\sigma = (1-d)\bar{\sigma} \qquad (3.11)$$

Where, σ is the Cauchy stress; ϵ is the strain tensor; *d* is the scalar stiffness degradation D_0^{el} is initial elastic stiffness;D^{el}, is the damaged elastic stiffness; $D_0^{el}:(\varepsilon - \varepsilon^{pl})$is called the "effective stress" tensor.

Wood is unusual and shows ductile behavior in compression and brittle behavior in tension and shear (Tsai & Edward, 1970; Sandhaas et al., 2012). For wood-based structures, several failure criteria have been examined using 3-D continuum damage models, and in-plane stress failure theories (Quadratischer et al., 2001; Zhu et al., 2005; Sandhaas et al., 2012; & Cabrero et al., 2012). It has been found OSB behaved linearly until failure point in tension, while in compression it showed plasticity behavior (Zhu et al., 2005). Four failure criteria have been studied and verified with experimental data (Quadratischer et al., 2001). These damage models are linear, quadratic, Tsai-Hill, Tsai-Wu tensor polynomial, and von Mises invariant criteria and predict failure based on an interaction equation, developed using biaxial state stress. The von Mises invariant showed a good agreement with experimental data even though it has not been considered for structural wood before (Quadratischer et al., 2001). The interaction equation for the von Mises invariant failure criterion can be written as:

$$\left(\frac{\sigma_x}{f_x}\right)^2 - \frac{\sigma_x \sigma_y}{f_x f_y} + \left(\frac{\sigma_y}{f_y}\right)^2 + 3\left(\frac{\tau_{xy}}{f_v}\right)^2 = 1.0 \qquad (3.12)$$

Where, σ_x, σ_y, and τ_{xy} are on-axis stresses; f_x and f_y: are on-axis normal strengths; f_v: is on-axis shear strength. This failure criterion is used in this study to predict the failure surface of the OSB and WSaW walls.

3.11 Blast Loading Calculation Methods

Due to the difficulty in conducting blast tests (Goel, 2015; Courtney et al., 2015), three computational approaches have been considered to calculate the blast loading parameters and structural response: 1) empirical; 2) semi-empirical; and 3) numerical (Goel, 2015). The accuracy of empirical methods is based on the size of the test data from which the empirical equations were developed (Razaqpur & Campidelli, 2012), and are only applicable to cases that resemble the tests from which the data were collected (Mlakar & Bounds, 2010). Semi-empirical methods were developed based on experimental data and simplified physical models for specific case studies (Razaqpur & Campidelli, 2012). It is the first type of method that is of most interest in the present study. Software packages can use either coupled and uncoupled analyses (Ngo et al., 2007), the uncoupled analysis considers blast pressure applied to a rigid surface, while coupled procedures consider load applied to the deformable structure (Ngo et al., 2007). Several finite element software packages have been developed to capture the response of material under high strain rate (e.g. BlastX, ABAQUS, Air3D, ConWep, Air3D, SHOCK, and DYN3D). Figure 3.12 summarizes the computational methods used in blast loading analysis.

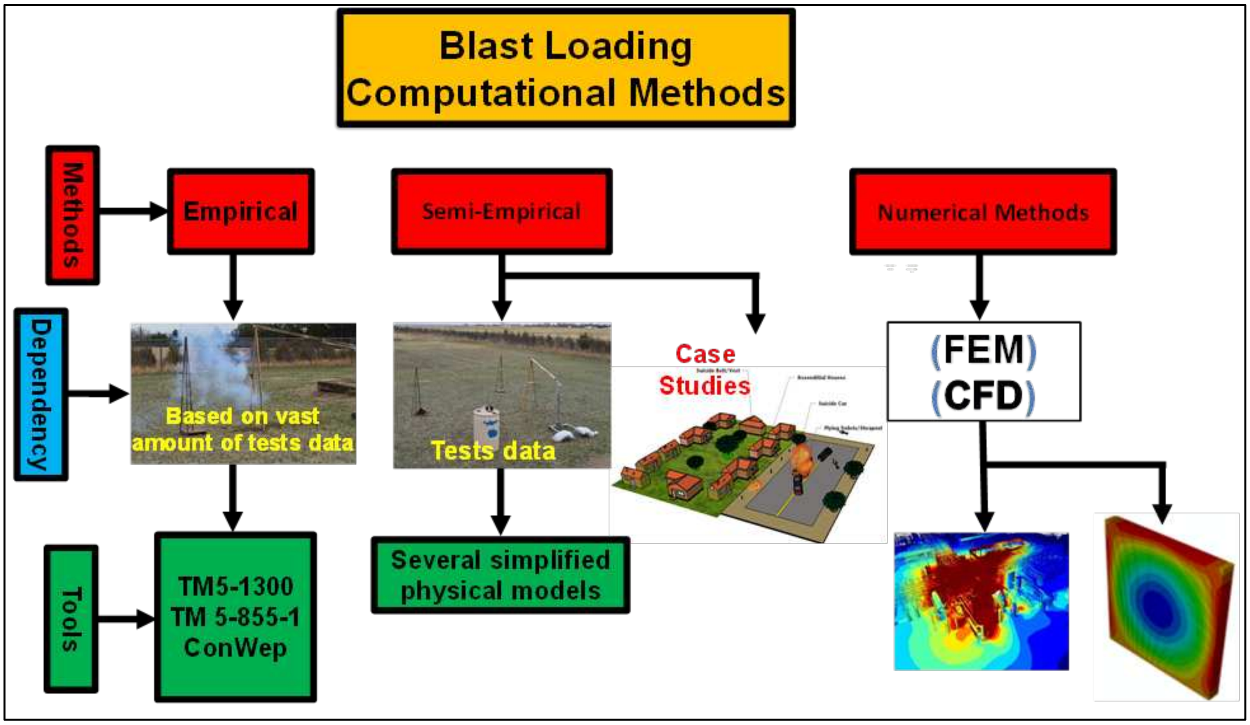

Figure 3.12 Computational method of blast loading.

3.12 Kingery-Bulmash Equations-principles and limitations

3.12.1 Introduction and Background

Kingery and Pannill (1964), conducted experimental tests to estimate the incident overpressure from surface bursts of hemispherical charges of TNT at Suffield Experimental Station, Alberta Canada (Shin, 2014). There is not much information about the instrumentations and direct methods of calculating the incident peak overpressure. Rankine and Hugoniot (1870, 1887) computed the incident overpressure from shock front velocity. The study derived high-order polynomial governing the relationship between the incident overpressure and the scaled distance. For near-field detonations ($Z < 0.4$ $m/kg^{1/3}$), the Rankine-Hugoniot equation is not valid since the shock front velocity is not stable and changes instantaneously (Karlos et al., 2016). In 1966, Kingery estimated and added positive phase duration and impulse to the previous blast wave parameters which were calculated from a 500-ton of surface detonation test by Kingery and Pannill (1964). The outcomes of this study were presented in hand-drawn diagrams with scaled distances in the abscissa versus time, incident peak overpressure, impulse, and positive phase duration in the y-axis. In 1984, Kingery and Bulmash published blast wave parameters in free air for spherical and surface detonations in TM5-1300 manual (Department of the Army, the Navy, and the Air Force). The air blast wave parameters were expressed in terms of scaled distance through high order polynomials (9^{th} order polynomial). These parameters have been published in graphical forms in many technical manuals, books, and official documents. The Kingery and Bulmash equations are valid for scaled distances range of $Z > 0.053\ m/kg^{1/3}$ and $Z > 0.067\ m/kg^{1/3}$ for spherical and hemispherical blast, respectively (Karlos et al., 2016). The experimental data of near-field detonations are not available due the possibility of damaging test sensors from thermal effect of high-intensity blast shock wave, non-ideal pressure-time curve which is already assumed by Ferdinand's equation and multi-peak of pressure could generate till the arrival time (Guzas & Earls, 2010). Several approaches and methods have been used to simulate blast phenomena for different scenarios and environment conditions. The Kingery and Bulmash (1984) equations showed good agreement with experimental data for free-air blast tests and are widely used to predict pressure levels.

The Kingery-Bulmash charts of positive phase for spherical and hemispherical detonations in free air are shown in Figure 3.13 and 3.14, respectively, for range of scaled distances ($0.0531\ m/kg^{1/3} \leq Z \leq 40\ m/kg^{1/3}$), (UFC 3-340-02,2008). Negative phase parameters were included in the Kingery-Bulmash equation but were later presented graphically in TM5-1300 (later known as UFC 3-340-02) manual without providing any information about their accuracy (Bogosian et al., 2002).

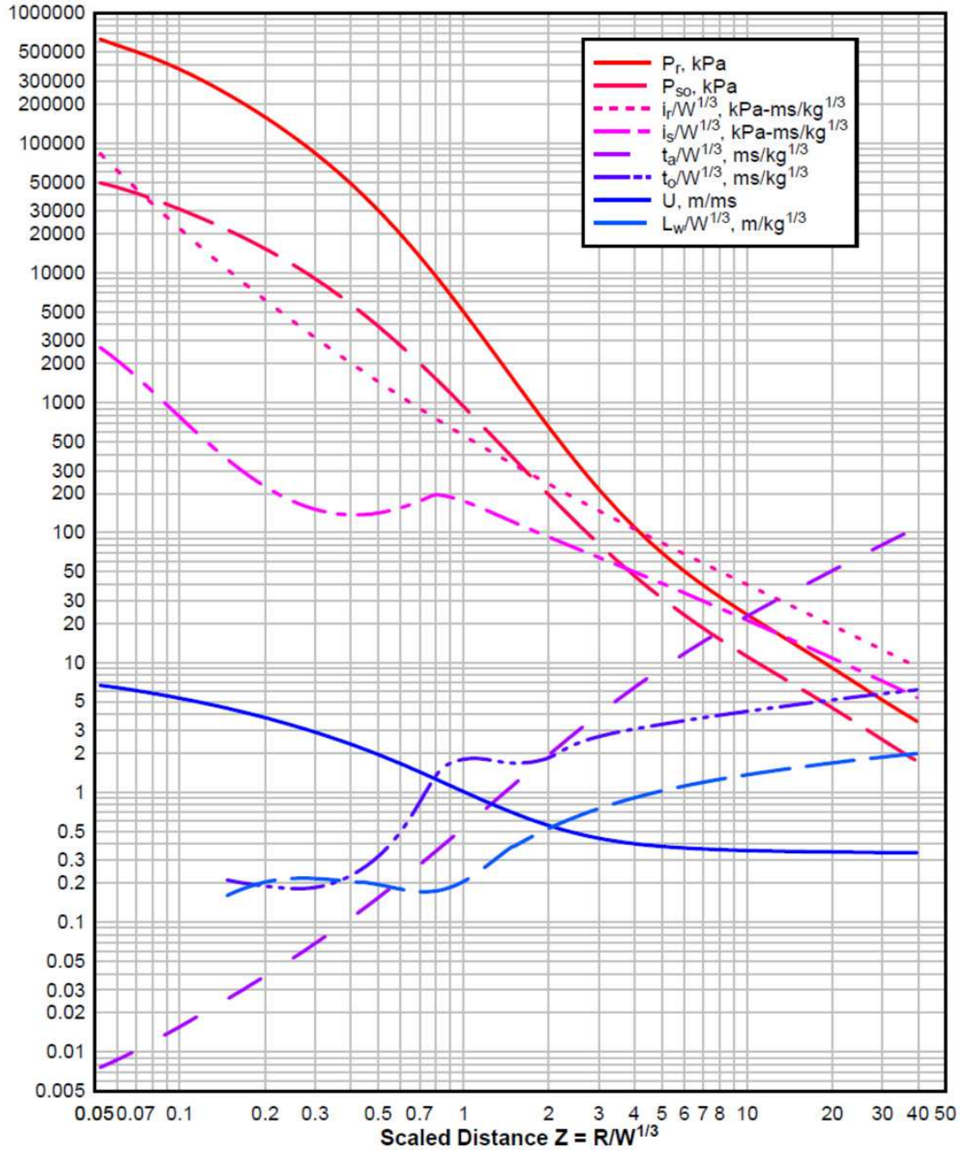

Figure 3.13 Blast wave parameters of positive phase of spherical free-air detonation of TNT charges (UFC 3-340-02, 2008).

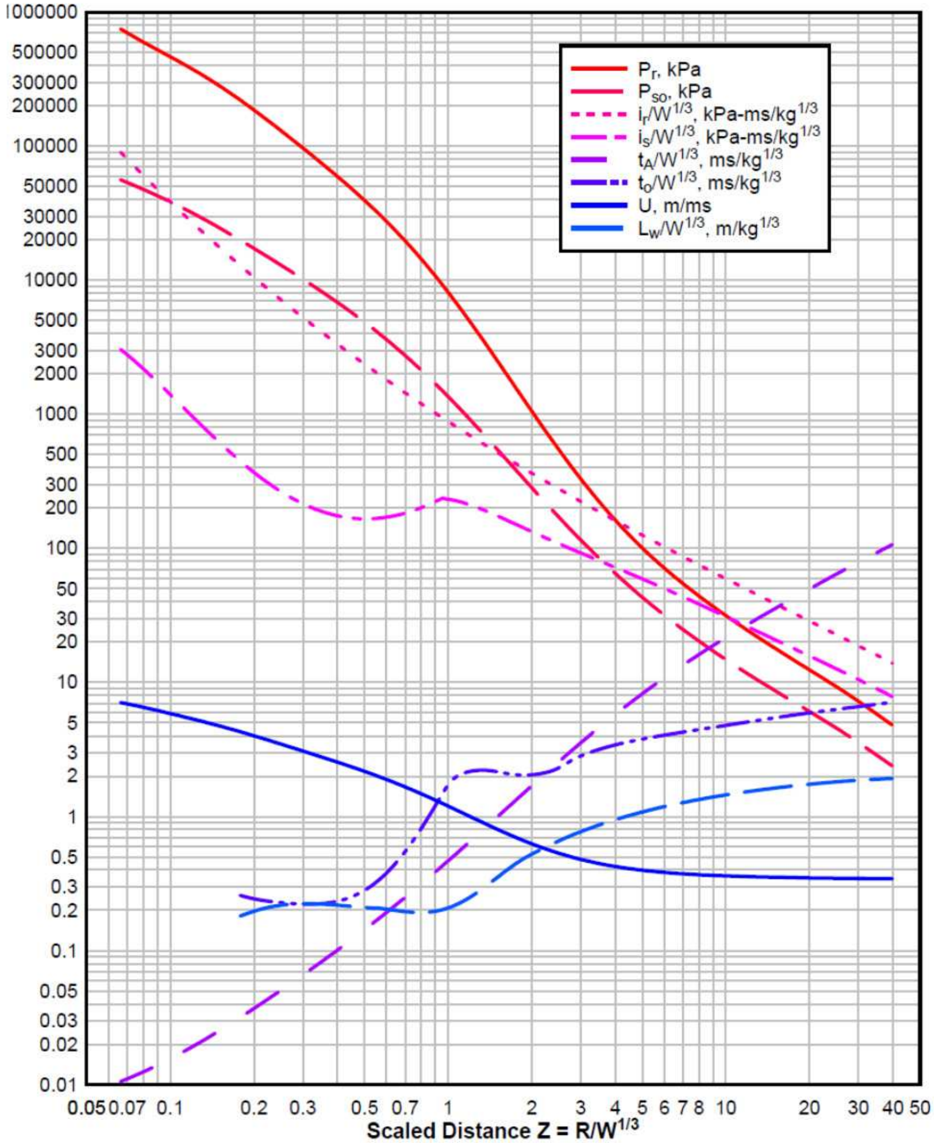

Figure 3.14 Blast wave parameters of positive phase of hemispherical free-air detonation of TNT charges (UFC 3-340-02, 2008).

3.12.2 Kingery and Bulmash Equations: Mathematical Format

Kingery and Bulmash (1984), developed a high order polynomial equation based on vast number of tests data with range of scaled distances from 0.0531-40.0 m/kg$^{1/3}$ (Guzas & Earls, 2010; Shin,2014). The output of the equation was modified using a fitting technique and presented on a log-log scale (Guzas & Earls, 2010). The mathematical expression is shown in Equation 3.13.

$$Y = C_0 + C_1 U + C_2 U^2 + \cdots + C_N U_N \qquad (3.13)$$

Where,

$U = K_0 + K_1 . T,\ T = log(R)$,

Y is the required blast wave parameter in base 10 logarithms such as log (P_r), log (P_s),

N is the order of fit

C, and *K* are constants computed by the least-square method to fit the calculated decay parameter (b) and order of the polynomial.

The decay coefficients of the Kingery-Bulmash equation *(C_0, C_1, …, C_n, K_0, and K_1)* were determined for spherical and hemispherical waves for specified range of scaled distances (Karlos et al., 2016). The current study was focused on free-air blast and decay coefficients of spherical wave. Only positive phase of the blast wave time history has been presented in these charts (Karlos et al., 2016). The Kingery-Bulmash measurements are not allowed to be used outside of the military and government offices (Guzas & Earls, 2010; Smith & Hetherington, 1994).

3.13 Conventional Weapons (ConWep) Blast loading Model

The ConWep model is one of the most widely used blast loading models and it is intended to simulate ideal blast wave in unconfined environment (Jablonski et al., 2013; Lahiri et al., 2011). It has been developed based on high degree polynomial equation derived by Kingery and Bulmash (1984), to fit the graphical experimental data in TM5-855-1 with mass range between (1-4,000) kilogram using curve fitting technique. ConWep code assumes normal reflection from a rigid surface and pressure is applied to the surface manually. Therefore, blast wave-structure interaction is neglected (Razaqpur & Campidelli, 2012). Blast-structure interaction in the ConWep code is uncoupled (Wadley et al., 2010). The design producers, analysis, and blast loading effects on structures published in the technical manual TM-5-855-1 (US Department of the Army 1986 (limited access)), currently replaced by UFC 3-340-01 (USACE (limited access)), (Razaqpur & Campidelli, 2012). The input data are TNT mass and, standoff distance, and the output includes peak overpressure, arrival time, impulse, and positive phase duration. ConWep does not require modeling of the flow of explosive material in the field since the event of the blast is short and the interaction between the blast wave and the air is weak (Budziak & Garbowski, 2014). Regarding the applied loads on structure, two configurations are considered 1) a vertical configuration: when spherical charge placed at a specified height from the ground act on a rigid flat surface; and (2) a horizontal configuration where a hemispherical charge is placed at or close to the ground. In both configurations, the surface was meshed to 64x64 grid of the ConWep Code. (Razaqpur & Campidelli, 2012). Generally, ConWep model can provide good accuracy in case of simple geometries. The main advantage of considering empirical methods is to avoid the complexity in modeling blast wave-field interactions. Therefore, these methods are not good to simulate the interactions of blast wave while traveling inside the detonating field (Lahiri et al., 2011; Remennikov & Rose, 2005). In this study, the detonation is happing in the free air and the interaction with air is not, therefore considering ConWep blast loading model is suitable to simulate the blast loading.

3.14 Codes and Standards Blast Design Manuals

There are several approaches documented to design structures exposed to blast loads. Currently, several standards, technical manuals, handbooks, and documents have been published which comprised principles of blast loading, design methods, design tables, and charts. Below is a list of some of the main codes and standards for mitigating blast loading:

Structures to Resist the Effects of Accidental Explosions - TM 5-1300

This manual was established by the U.S. Departments of the Army, Navy, and Air Force (U.S. Department of the Army, 1969). The goal was to derive blast wave parameters to design structures to resist blast loading. The design procedures, constructions details, and principles of dynamic theories to estimate the response of steel and concrete structures were included. This document contains blast load design parameters, design steps, calculation methods of structural elements response, and design curves of blast wave parameters of free-air explosion, air explosion, and surface explosion (U.S. Department of the Army, 1969). Four protection categories were considered including 1) personal protection against hazardous materials; 2) equipment's protection from direct and indirect effects of explosion; 3) prevent detonations communication, 4) prevent mass detonation of explosives (U.S. Department of the Army, 1969).

Fundamentals of Protective Design for Conventional Weapons - TM 5-855-1

This manual was published by the U.S. Department of the Army (1986). It had reviewed and revised several times. Modern conventional weapons characteristics were updated to include penetration and slenderness ratio of structural elements. Air blast pressure-time history was estimated based on empirical equations of free-air and surface burst configurations. This manual neglected wave-structure interaction which is the main limitation in this code. There is a lack in simulation of blast wave for near-field blast due to complication in getting the measurements from the blast tests (Goel, 2015). This manual is limited in scope, and circulation is not permitted outside of government agencies. The author has not viewed a copy of this manual.

Design and Analysis of Hardened Structures to Conventional Weapons Effects-UFC 3-340-01

This manual is a recent modified version of TM 5-855-1, and it is also limited due to the sensitivity of the materials (Razaqpur & Campidelli, 2012). This manual considered design based on simplified spring-mass systems (single-degree-of-freedom). Design and analysis methods of structures to maintain the demand of the conventional weapons were explained, furthermore, characteristics of conventional weapon data, design of hardened protective structures were also clarified (Deschambault & Zehrt, 2010). Blast wave parameters for two scenarios as in the TM 5-855-1 manual were presented. The distribution of this manual is limited due to criticality and sensitivity of the information and data it contains. The author has not viewed a copy of this manual.

Structures to resist the effects of accidental explosions-UFC 3-340-02

This manual was published by the Department of Defense, U.S., and it is a modified version of TM 5-1300. This manual was approved for a tri-service manual (Naval Facilities Engineering Command, U.S. Army Corps of Engineers, Air Force Civil Engineering Support Agency), and has all design methods of protective structures (DoD, 2008). In addition to design steps and construction techniques of blast wave propagation in confined and unconfined bursts, detailed examples, figures, tables, and equations were included to be used by engineers (Goel, 2015). Design and analysis procedures were included in the appendixes of this manual. This code has unlimited distribution and can be considered the main cited manual by other blast design chapters/codes.

Design of Blast Resistant Buildings for Petrochemical Facilities

This design guidance was published by ASCE first in 1997 by Task Committee on *Blast-Resistant Design of the Petrochemical Committee of the Energy Division of ASCE* without details as in TM 5-1300. Types of construction, dynamic material strengths, allowable response criteria, analysis methods, and design procedures were discussed. This code considered three levels of damages of low explosives materials (Dusenberry, 2010). The response was provided in terms of ductility ratio and/or support rotation for each level of response, and combination response was provided in the new version of this manual (Dusenberry, 2010).

Single Degree of Freedom Blast Design Spreadsheets (SBEDS)

The Single degree of freedom Blast. Effects Design Spreadsheets (SBEDS) computer spreadsheets were used by U.S. Army Corps Protective Design Center to satisfy the requirements of Department of Defense (DOD) of designing structures to resist explosions (Polcyn & Myers, 2010). It has been developed by BakerRisk® to design and analyze structures subjected to blast loading considering equivalent single-degree-of-freedom (SDOF). The user should define the resistance function of the material and run single-degree-of-freedom analyses. A variety of structural systems can design and analyze such as steel, concrete, and wood structures (Deschambault & Zehrt, 2010). The above-mentioned blast design codes and manuals were summarized in Table 3.5.

Table 3.5 Summary of blast codes

Code	Publisher	Purpose	Restriction
TM5-1300	U.S. Department of Army	Blast wave parameters, structural response, & Protection categories	No
TM5-855-1	U.S. Department of Army	Design & analysis fortified structures to resist conventional weapons	Yes
UFC3-340-01	DOD, U.S (updated ver. of TM5-855-1)	Design & analysis fortified structures to resist conventional weapons; blast load parameters	Yes
UFC3-340-02	U.S. Department of Army (updated ver. of TM5-1300)	Blast wave parameters, structural response, &Protection categories	No
SBEDS	U.S. Army Corps	Design and analysis structural components considering SDOF	No

Chapter 4. Mitigation of Blast loading

4.1 Security Precautions-Methods and Techniques

Since the beginning of life on the earth, humans have considered primitive protection systems to guard from surrounding risks, whether natural or man-made. Thereafter, with evolution and complexity of life, the need to use effective methods to reduce losses resulting from these risks have appeared. Different mitigation strategies have been considered to minimize the effects of explosions in general and suicide attacks specifically. These strategies include for example perimeter protection, façade protection, and curtain wall protection systems (Smilowitz, 2008). Figure 4.1 shows the main considered strategies of mitigating blast impact.

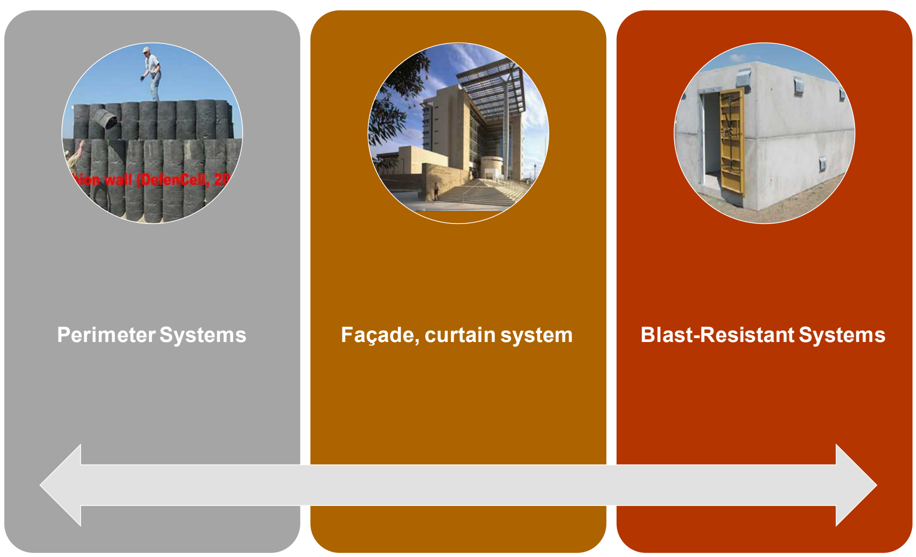

Figure 4.1 Blast mitigating strategies.

4.1.1 Perimeter Protection Systems

The main objective of this technique is to increase the standoff distance between occupants and assets, and explosion source (Smilowitz, 2008). This strategy is considered for structures that do not have the capability to resist the blast loading (FEMA 459, 2008). In case of a car bombing threat scenario, several methods can be used to ensure maximum distance between the targeted structure and location of explosion such as anti-ram decks, speed reducing bumpers, traffic control techniques, and walls. It is not practical to use wall blast systems in crowded areas, cities centers, and malls (PCI Northeast, 2016). Safe standoff distance can be determined based on the size of the explosive charge and threat scenario.

According to FEMA 453 (2006), the U.S. Department of Defense (DOD) lists safe evacuation distances for unreinforced concrete structures in free space as shown in Table 4.1. Examples of perimeter systems are shown in Figure 4.2. The current study aim is to suggest applicable blast walls to be used in different site conditions after considering some architecture design modifications. Explosion generated from suicide vest attack is considered in this study since it is the most considered by terrorists and the worse scenario in terms of victims.

Table 4.1 Safe evacuation distances of different attack scenarios (FEMA 453, 2006).

Attack scenario	TNT equivalent mass (kg)	Building evacuation distance (m)	Outdoor evacuation distance (m)
Belt	4.5	27	330
Suicide vest	9	34	415
Suitcase bomb	23	46	564
Compact car	227	98	457
Water truck	13608	375	1982
Semi-trailer	27216	475	2134

Figure 4.2 Examples of perimeter protection systems.

4.1.2 Façade Protection

Exterior elements can play a substantial role in improving the response of structures to blast loading (Smilowitz, 2008). These elements improve the post-damage of the system and protection level of occupants from flying debris (PCI Northeast, 2016). The function of façade systems is to resist and absorb shock wave energy (FEMA 453, 2006). However, they require significant changes to the architecture appearance of the structure ((Koccaz et al., 2008; Smilowitz, 2008). The materials of façade systems should exhibit ductile behavior under blast loading. An example of this type of facades materials is laminated glass as shown in Figure 4.3.

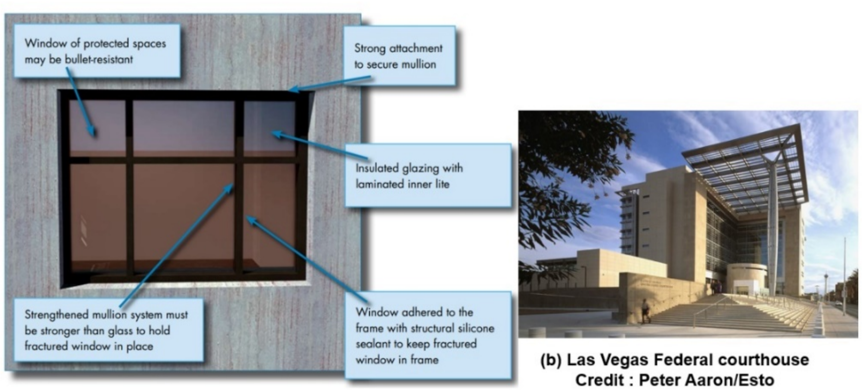

(b) Las Vegas Federal courthouse
Credit : Peter Aaron/Esto

(a) Protective façade design (FEMA 453,2006)

Figure 4.3 a. Protective façade design. b. An example of using laminated glass (FEMA 453,2006).

4.1.3 Curtain Wall Protection

Curtain walls are non-structural outer coverings of building linked to the interior frame of the building. These systems are supported by structural frames, have higher flexibility, and lighter than other window systems (Smilowitz, 2008). The main objective of this system is to minimize the number of injuries due to glass fragments (FEMA 459, 2008). Since curtain wall will be the first part of the building exposed to blast load, it should resist blast wave without separation. The curtains are the major components in this system, and it can be designed for different applications (FEMA 459, 2008). Figure 4.4 shows a typical blast curtain system.

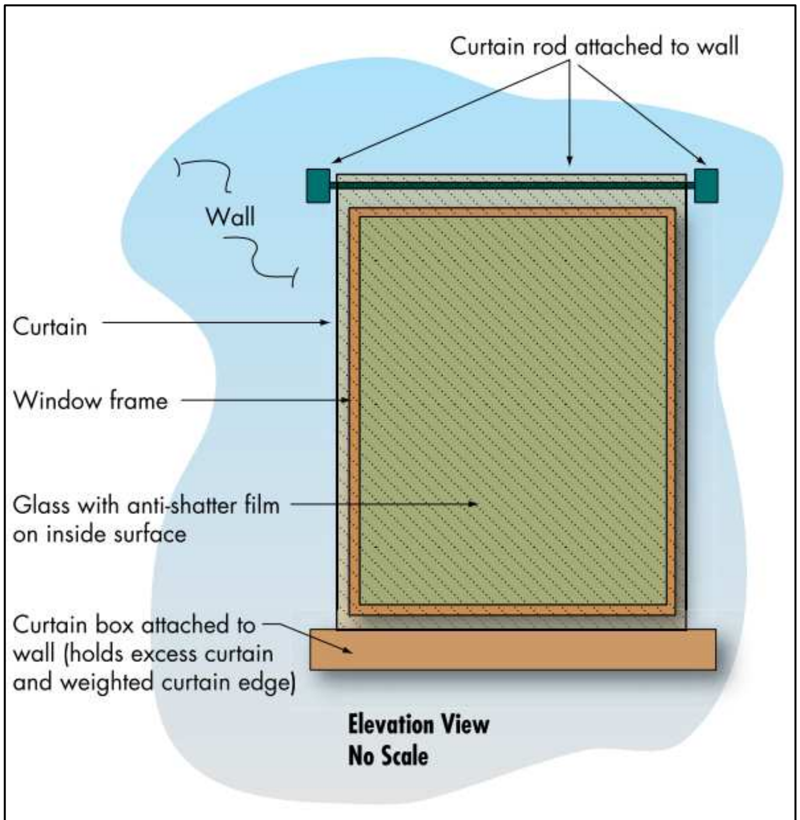

Blast curtain system(FEMA 453,2006)

Figure 4.4 Blast curtains (FEMA 453, 2006).

4.2 Layered Sand/Soil in Protective Systems-Historical Perspective

Historically, natural materials have been used for different purposes and goals. Sand is used as a protection material from numerous threats such as floods, and fires in addition to wide range of civil and military applications. In the middle ages, sand was used to fortify forts and cities since it provides a good level of protection from catapult strikes and exploded projectiles. An example of this application was the Douaumont Fort in north-eastern France as shown in Figure 4.5. Thereafter, during World War II, sandbags were used in different applications of protection, such as shielding windows, ballast, non-permanent fortifications, soft armor for vehicle, and blast walls. Sandbags have also been used to control floods and stabilize soil. Figure 4.6 shows some of these applications. Recent applications of using sand in protection from suicide/bomb attacks were noted in the U.S. at different events by the security agencies and local police departments.

Sand is a granular material formed by rock breaking and mineral particles. Classification of sand is based on the size of these particles. Mechanically, It has high compressive strength and low shear strength (Andrew, 2017). The main advantage of using soil/sand as a core material in blast wall systems is the high capability of sand to dissipate the kinetic energy of the blast wave even for large-scale of explosive charges (Crawford & Lan, 2006). The attenuation level of sand is function of the thickness and density (UFC 3-340-02,2008). The response of structure under blast load is mitigated significantly by the mass of the structure since the blast load will be passed fast while the mass has not been mobilized yet (FEMA 426,2004). Moreover, sand does not produce any debris, therefore would be no injuries from flying fragments.

Figure 4.5 Fort Douaumont (Verdun Fort Douaumont, 2007).

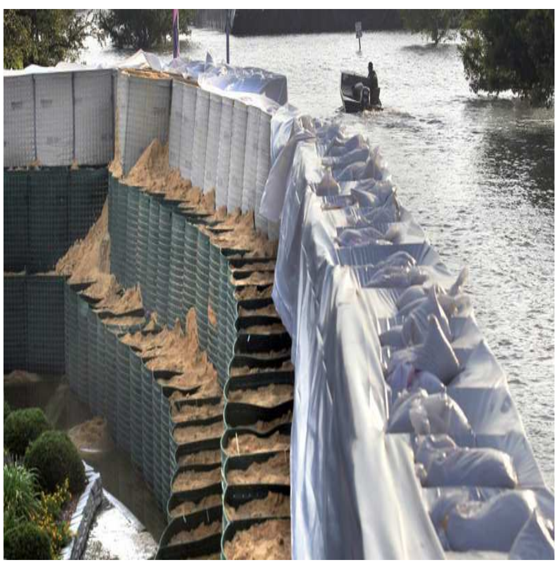

Figure 4.6 Applications of sand to mitigate hazard impacts (Credit, Waitt, 2017, and Farmer, 2011).

4.3 Recent Attempts of using Sand in Protection

Sand is a cheap and safe material to use to mitigate blast shock wave (Golub et al., 2005). Recently, several trials have been noticed to use sand in urban areas for protection from planed explosions. For instance, The New York City Police Department (NYPD) used 82 Sand-filled trucks to protect Macy's Thanksgiving Parade on November 23, 2016 (Associated Press, 2016) as shown in Figure 4.7.

Figure 4.7 Dump truck in New York Thanksgiving Parade (Joe Levin, 2016).

These trucks were placed to create a 2.5-mile of blast walls to protect the parade (Associated Press, 2016). They loaded with sand to mitigate the effects of any attacks (weight about 30 tones with sand). Another example of using sand to protect from bombings is when the New York City Police Department (NYPD) used trucks filled with sand on November 8, 2016, around Trump Tower in Manhattan to mitigate any expected attacks (see Figure 4.8). Similarly, a number of trucks distributed around three hotels as people gathered on election night in New York City (Levin, 2016). Also, dump trucks filled with sand put around the Javits Center, New York’s Peninsula Hotel, Hilton Hotel where

Hillary Clinton, a presidential nominee, held the election events on the election night (The Washington Post, 2016).

Figure 4.8 Sand trucks outside of Trump Tower (Andrew Kelly, 2016).

Sand has been used before in the U.S. for protection from expected attacks. The first time was in 1983 when security forces placed trucks loaded with sand around the White House to protect from unknown threats after U.S. campground attacks in Beirut (The New York Times, 1983). The second time was in 2015 during the Pope Francis visit to the U. S. (US TODAY, 2015). Some other examples of using sand-filled trucks have been recorded inside the U.S. as an effective strategy to protect VIP, government buildings, and security facilities.

4.4 The behavior of Composite Panels Subjected to Blast Loading-Review of Literature

The blast-resistant systems have been designed considering sophisticated, high-tech systems. These systems are composed of two face-sheets made of high ductile materials to resist/reflect the incident blast shock wave. the core structure is made of high compressible (low density) materials such as foams to absorb the blast shock wave. Figure 4.9 illustrates the main components of these systems.

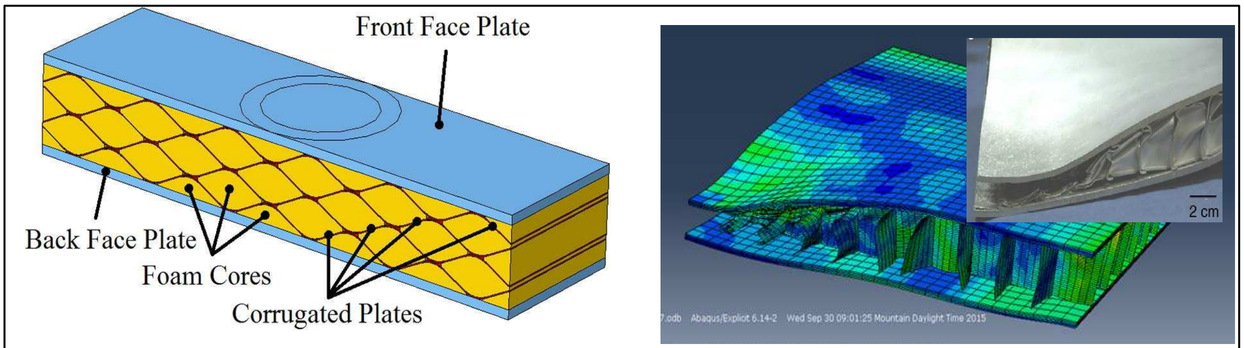

(Karen et al.,2016)

Dharmasena et al.,2008)

Figure 4.9 Blast-resistant sandwich panel components.

Lee and Toole (2004), examined numerically the energy absorbed by flat sandwich panels made of Aluminum 5456-H116 with honeycomb foam as a core material. The study considered different types of honeycomb panel simulated using LS-DYNA software. The study highlighted the importance of adding cover plates in absorbing energy in the plastic zone of deformation. It was also shown that if the cover plate thickness is not designed properly, non-uniform permanent deformation in the foam material will occur and in this case part of the load will be carried by the panel itself. Several parameters were analyzed to optimize absorbing energy of square-cell shape of honeycomb under blast loading such as cover plate thickness, number of cells, height of the core, and number of horizontal layers in the core.

Dvorak and Bahei-El-Din (2005) conducted a comparison between three new design models of sandwich panels with conventional model of a sandwich panel under blast loading. The interlayers made of stiff Isoplast polyurethane and elastomeric foam. The response was examined using finite element method utilizing LS-DYNA. The new design changes were implemented to prevent foam core crashing, local failure of the cover plate, and failure at interface surfaces. Extremely ductile "interlayers" between the inner foam core and outer surface were used in the study. Polyurethane interlayer was connected to elastomeric foam and this merge helped to protect the outer surface and inner foam core by reducing maximum kinetic energy. The study found that using interlayers of the core is beneficial to increase the performance of sandwich panels under blast loading. The use of ductile interlayers between the foam and outer face plate can help to protect the inner foam from crushing and increase the resistance of the outer surface to blast loading.

Trasborg et al. (2008), mentioned to a new approach which is adopted by most the U.S. government agencies in addition to some other countries to fulfill requirements of environment protection and blast resistance performance of sandwich panels. The study explained the construction and economic benefits from using precast panels rather than in site-cast panels. The article stated the need for using shear stiffeners to connect concrete layers with inner layers to work as a composite system. The authors mentioned that under "close-in" detonation, non-uniform pressure and local deformation are generated and shear mode controls while in case of “far-field” detonation, the pressure is uniform and flexural mode is governed. The test results have illustrated crucial relation between increasing ductility, resistance, and local un-bonding length.

Langdon et al. (2010), studied the effect of steel cover plate thickness on aluminum foam fracture, which is used as a core sacrificial cladding under air-blast loading. The authors considered different thicknesses of steel cover plate with various aluminum foam density to check the response of sacrificial cladding. The experimental results were analyzed and validated with finite element model using ABAQUS/Explicit software. The results clarified the effect of steel cover plate thickness on cracking level of foam, distribution of stress, and interface interaction between plate and foam. The study indicated that less cracking is expected when the cover plate is bonded to the foam and that the foam absorbed most of the blast energy. Fracture initiated in the foam during unloading because of the low tensile strength of the foam and kinetic energy stored in the cover plate. The plate thickness should select carefully to prevent permanent deformation in the foam.

Retrofitting RC structures by using fiber reinforced polymer (FRP) to resist blast loading have been investigated (Ha et al., 2011). The authors showed that the performance of RC elements could be increased through using a new composite material system. The new composite material is fiber reinforced polymer (CFRP) combined with Polyurea (PU). CFRP has high stiffness while PU has high ductility. Several tests were conducted to examine the blast resistance of the hybrid composite system. Various parameters were investigated such as reflected blast pressures, maximum and residual displacements, steel and concrete strains failure mode, and crack patterns.

Liu et al. (2012), evaluated the response of sandwich-walled hollow cylinders with graded aluminum foam as the core of panels under air blast loading. The authors conducted a comparison between graded and ungraded foam using 3-D finite element models. Three layers of foam core and two covers of steel plate were considered in addition to steel base plate. It was stated that the use of functionally graded core caused a reduction in the maximum strain elimination of crash collapse. In addition, the use of different arrangements of layers with different densities was evaluated experimentally. The contribution of the cover plate thickness of cylindrical panels was also investigated.

Fatt et al. (2013), conducted a comparison between the theoretical solution of elastic-plastic model of the curved sandwich panel and finite element solution results. The curved sandwich panel was modeled with a single radius of curvature, fixed in the x-direction with zero curvature. Core compressibility and transverse shear were assumed to be linear through the thickness. It was noted that design of the sandwich panel with thick face-sheet and less density foam core will increase the resistance to blast loading since the foam will have an acceptable limit of plastic deformation and prevent the local buckling and fracture of the face-sheet.

Yuen and Nurick (2014), conducted experimental tests to examine the performance of composite sandwich structures under quasi-static compression load with hollow tubes as an energy absorbing device. The authors mentioned several applications of using energy absorbing devices such as in cladding structures and in crashworthiness design of cars. The authors showed the role of the shape/topography of thin composite walls in changing the resulting deformation mode of the walls. Several parameters such as peak load, absorb crash energy, specific energy absorption, and crush force energy were considered as performance parameters. A relationship between the primary progressive collapse mode and the absorbing energy (dissipated energy) of the sandwich structures were found.

Hua et al. (2014), explained literature were done in benefits of using sandwich panels to mitigate blast loading because of the capability of absorbing energy. According to these studies, deflection at the back face of sandwich panels is much less than in case of using conventional plates. If core foam does not crush, sandwich panel efficiency to resist blast loading is still in effect (Dharmasena et al., 2008). According to the article, different parametric studies have been considered to investigate the performance of sandwich panels such as core material type, boundary conditions, and the effect of plastic deformation. This study focused on understanding the behavior of carbon fiber sandwich panels under blast loading analytically and experimentally. The results of this study presented incident peak overpressure and maximum impulse are increased with close-in field or strong explosion and these values are much higher for reflected wave. The authors found sandwich panel can be a good choice to resist and mitigate blast loading. The article illustrated core thickness, size of cover sheet are the most important design parameters to enhance sandwich panel design to resist blast loading.

Yazici et al. (2014), studied the behavior of sandwich panels with metallic rippled core under blast loading. The study included experimental and numerical analysis, and several parametric studies were considered. It was shown that sandwich panels with foam core can absorb most blast wave energy since it can experience large deformation at approximately constant pressure “high ductility” due to the nature of their cellular microstructure. Different conditions of rippled core were examined analytically such as solid, soft, medium, and hard for empty and filled panels. The authors alluded to the recent research trend on developing and using foam core in sandwich panels to mitigate blast loading. As a result, various new geometric shapes of core materials like “pyramidal cores”, “diamond celled lattice cores”, “corrugated core”, “hexagonal honeycomb cores”, “foam cores” and “square honeycomb cores” were investigated in various studies. These studies have found metallic rippled core has high efficiency to absorb energy in different ways “mechanisms”. Furthermore, sandwich panel with soft core structures can reduce the effect of impulse momentum of the shock wave and prevent isolation of face-sheets. The main findings of this research illustrated face-sheet thickness and boundary conditions role are more important than core thickness in decreasing panel deflection.

Goel et al. (2014), analyzed the response of stiffened sandwich panels with metallic foam core numerically. The effect of stiffeners configuration, foam thickness, foam density, and standoff distance on blast response of panel was investigated. The focus was on measuring the deformation at the center of back face-sheet of sandwich panels. It was found that sandwich panels with cross stiffeners configurations, higher relative density, and maximum thickness of foam have higher capability to mitigate blast loading. Type of foam core is an important factor to control sandwich panel behavior under blast loading. The authors stated that the total energy in case of unstiffened panels is higher than in stiffened panels configuration.

Matsagar (2016), compared the behavior of different types of plates, and sandwich panels. The research examined the dynamic response by considering 3-D finite element models of stiffened and unstiffened steel plates, plain concrete, reinforced concrete, steel fiber reinforced concrete slabs (SFRC), stiffened and unstiffened steel-foam-steel, and steel-sand-steel sandwich panels. Different materials were considered to perform the analysis like steel polyurethane foam-steel (SPS), steel-dytherm foam-steel (SDS), steel-cenosphere aluminum alloy syntactic foam with average size of cenosphere 90 lm (AlFoam90)-steel (SAS90), steel cenosphere aluminum alloy syntactic foam (AlFoam200)-steel (SAS200), and steel-sand-steel (SSS) panels. Moreover, different parameters such as foam and sand layer thickness, stiffeners arrangements, panel thickness, and materials properties of the sandwich panel, were altered to examine the behavior under blast loading.

Yazici et al. (2015), conducted experiments to study the performance of trapezoidal rippled core sandwich panels under air-blast loading. The research examined the behavior of two face-sheets (back and front) welded by laser with trapezoidal rippled core. The study found that increase the thickness of the front face is more important from increasing the thickness of the back cover sheet of panels with respect to deflection. In addition, increase the thickness of the core web and angle of rippled core improves the crush resistance. The height of the core can impact negatively the local stiffness behavior of the face-sheet despite improving the stiffness of panels.

4.5 The efficiency of Blast Wall Systems in Mitigating Blast Loading

Blast phenomena behind blast walls due to blast loading were investigated experimentally (Beyer, 1986). Blast wave parameters such as peak overpressure, impulse, and duration were measured. The study showed that the size and type of charge, standoff distance, and geometry of the wall are the main factors to identify the intensity of blast pressure at a specific location (Beyer, 1986). Rose et al. (1997), experimentally investigated the effect of blast loading parameters behind one-tenth scale of a rigid steel wall. The dimensions of the model were 300-millimeter height, 2100-millimeter width, 20-millimeter thick. The study found that blast loading pressure behind the wall at range of 3 to 6 wall height were reduced by 60% to 80% due to the presence of the blast wall. The authors extended the study by considering different heights of the wall and standoff distances to examine the performance of the walls (Rose et al., 1998). The main conclusion of this study is that the level of protection increased as the distance between the wall and the protected structure increased. Different materials were used such as concrete, wood, sand, and foam. The study found that this type of blast walls could mitigate the blast loading effects behind the wall.

Crawford and Lan (2006), studied the performance of steel-concrete-steel (RSA) and metal-sand-metal (CMI) walls experimentally. For RSA wall, the thickness was 30--60 cm, metal faceplates thickness is from 0.64 -2.5 cm and thickness of the core (RC) was from 1.2-4.9 m. For CMI wall, sand is used to increase the capability of absorbing the energy of blast wave. Several configurations have been considered and Dynamic finite element is used to simulate blast event and results compared with tests data.

These studies have either measured the blast wave pressure behind the wall or focused on the structural response. The current study has measured the blast wave pressure and the OSB and WSaW walls response.

4.6 Lessons from Invasion of Republic of Iraq

In 2004, several suicide attacks have been recorded in Iraq targeted international coalition forces and Iraqi security forces in addition to civilians. Consequently, huge concrete blocks, with an approximate mass of 5000 kg (11000 lbs.), were placed around military and security bases, government and other important buildings, and airports. This protective strategy (see Figure 4.10) left significant effects on community life in Iraq including losses in the cultural and architectural identities of Iraqi cities and have left many of the inhabitants of these communities in a state of depression. Mobility within and between cities has become difficult and requires relatively long time and effort since only specific entries and exits points can be used. The cost associated with constructing these walls adds another burden to the communities. For example, cost of manufacturing each block is $3000-$5,000 and as a result, to construct 21-kilometers (13.0 miles) of T-wall would require 4000 unit for a total cost of $12.5 million (Shachtman, 2007).

In 2006, the author started thinking of ways to replace this type of blast protection system with a reliable, economic, and suitable system to be used inside cities. The idea is to use readily-available materials to construct simple protection system which could be effective in reducing impacts of suicide attacks. In the Middle East, most residential houses, and most government and security facilities are constructed using either reinforced concrete and/or brick without any design consideration to resist abnormal loads. The fences of these houses have been built using clay brick or concrete blocks as shown in Figure 4.11. Several attacks were carried out inside residential complexes resulting in numerous casualties and major losses in residents' properties. Currently, it is not required to design residential buildings to resist blast loading in the Republic of Iraq. Therefore, developing new simple wall systems to be used is required.

Figure 4.10 Classical blast wall system as used in Iraq (Cathy Breen, 2012).

Figure 4.11 Typical houses fences in Iraq (Photographer: Mauricio Lima, 2004).

4.7 Blast Wall Systems-Research Gap

The current research trend is to design composite sandwich panels to resist blast loading. Several studies have been conducted to examine different types of high-tech blast wall systems to mitigate blast loading. Most studies focused on using sophisticated systems, and high-tech materials. While evaluating different types of systems using high-tech material is reasonable, since the objective is to mitigate the impact of the blast, the use of such materials might be hindered by its lack of availability in developing countries. The studies focused on evaluating blast wall systems, which can be part of structures as a structural element to mitigate blast loading. Some studies were conducted on simple blast wall systems such as special reinforced concrete walls, high strength steel walls, steel-concrete-steel (SCS), and concrete-sand-concrete (CSC) walls in addition to earth-filled walls for military purposes (Rose et al.,1997; Rose et al.,1998; & Crawford & Lan ,2006). Figure 4.12 summarizes the current approach of blast wall-resistant systems. The current study is intended to develop a new simple blast wall system that is capable of resisting blast loading at an appropriate standoff distance. The main advantages of considering this new blast wall system are cost, ease, and speed of construction, the lack of required skilled labors, and being environmentally friendly.

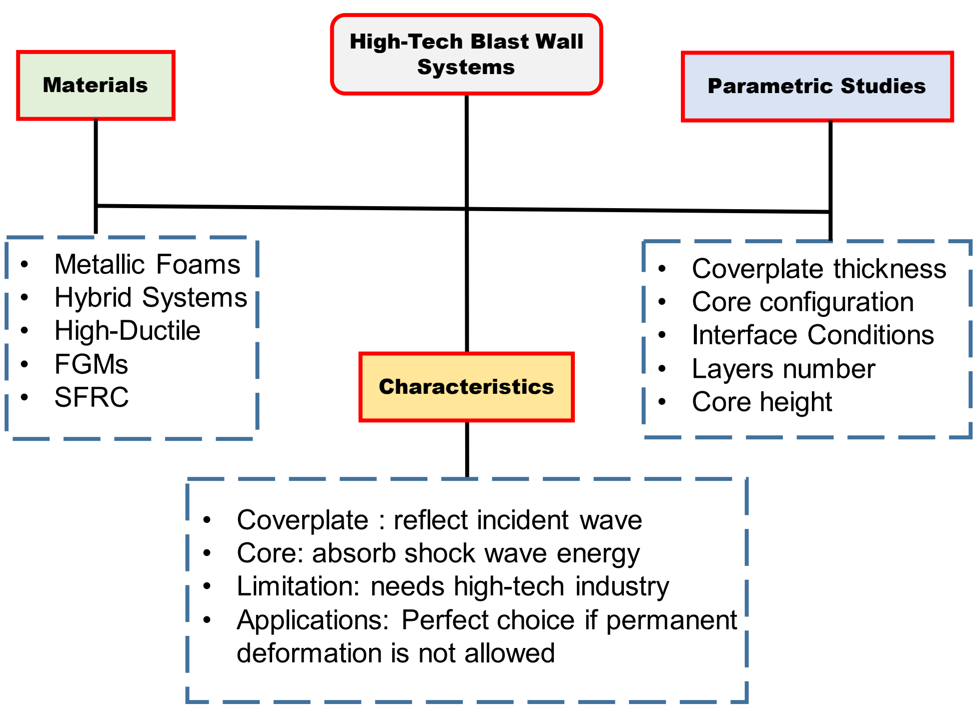

Figure 4.12 Current approach of blast wall systems.

Chapter 5. Numerical Verification and Tests validation of Simple Blast Walls

5.1 Introduction and Background

Suicide vests/belts attacks scenario are currently the most common and the worst in terms of number of victims based on the official records (GTD,2016). Discovering and identifying suicide attackers is no easy mission among people due to the complex tactics often followed by terrorists (Koccaz et al., 2008). Designing residential and commercial structures to resist blast loading is not required in design specifications and construction codes in most countries/cities. Furthermore, strengthening existing structures is not only very expensive but has negative impacts on the architecture appearance of structures (Koccaz et al., 2008; Smilowitz, 2008). Therefore, constructing blast walls at an appropriate distance (safe zone) from the structure can provide the required level of safety for occupants and property behind and around the blast wall (Rose et al., 1998). Blast walls have been primarily used for protecting military facilities, but with increase in the number of attacks inside cities, developing blast design specifications for typical non-military structures is ever pressing.

Temporary walls could be partially or completely damaged from interacting with blast loading; however, it can still provide the required level of protection/safety for occupants or property behind it. The main objectives of considering temporary walls to mitigate blast loading are ease of construction and maintenance in addition to the low cost of materials and labor (Rose et al., 1998). The literature on the distribution of air pressure behind/around and the response of simple blast walls is limited and rarely published (Crawford & Lan, 2006; Rose, Smith, & Mays, 1995).

This study is suggesting a new blast wall which can be used in different site conditions. The OSB and WSaW blast wall tests in free-air conducted to measure air-blast pressure distribution and the response of the system under blast shock wave. Due to limitation in the availability of instruments and explosive charges as well as blast field location restrictions, the number of attempted tests and the distance of interest behind/around the wall were limited to a specific range. The test results were validated with the analytical solution of 3-D dynamic finite element analysis.

5.2 Overview of the Finite Element Model

Three-dimensional dynamic finite element models are devised and used to evaluate the response of the walls to blast loading. The model is developed using the dynamic explicit procedure in the commercial package of ABAQUS software ver. 6.14 (Simulia, 2014). In addition to modeling the wall geometry, materials properties, boundary conditions, and structure-structure interaction, blast shock wave-wall interaction are modeled using a built-in blast load model (ConWep) to represent the interaction in free-air. Kingery and Bulmash (1984), derived closed-form equation to predict air-blast wave parameters of spherical and hemispherical bursts. Those equations were used to build the computer program ConWep (Hyde, 1991). The ConWep code considered the Friedlander's wave equation (see Equation 3.1), to calculate pressure time history of the blast load. The input parameters are the blast type (surface, air), standoff distance, and equivalent TNT mass. ConWep is commonly used to simulate blast in a free field. Dassault Systems Simulia Corp in 2010, considers this model as a built-in function in ABAQUS/Explicit ver.6.10 to simulate blast loading in free field (Lahiri & Ho, 2011). The only limitation for this model is in representing the physical structure-wave interaction. Accordingly, The ConWep model will not be a good choice to simulate blast phenomenon in crowded areas where reflections of waves between bodies/objects are expected (Razaqpur & Campidelli, 2012).

Eight-node linear brick elements with reduced integration (C3D8R) and hourglass control were used to model the geometry of the blast wall. A mesh size study was conducted to examine the convergence and stability of the solution. The materials behavior was modeled and defined in the elastic zone, except for sand, Drucker-Prager plasticity model was used, and only mechanical properties are defined in the software code while thermal effects are neglected. The default numeric values of linear and quadratic bulk viscosity parameters (0.06, and 1.2, respectively) were defined to represent the propagation of compressive blast shock wave. The boundary conditions of the wall were assumed to be fixed to the ground.

5.3 Failure Prediction and Structural Response of OSB Wall

A standard OSB panel is modeled using ABAQUS/Explicit software ver. 6.14. Geometrical dimensions of the panel are 2.44-meter (8-feet) height, 1.22-meter (4-feet) width, and the thickness is equal to 1.0-centimeters as shown in Figure 5.1. The mechanical properties of a typical OSB sheet are listed in Table 5.1, and It is modeled as an orthotropic material.

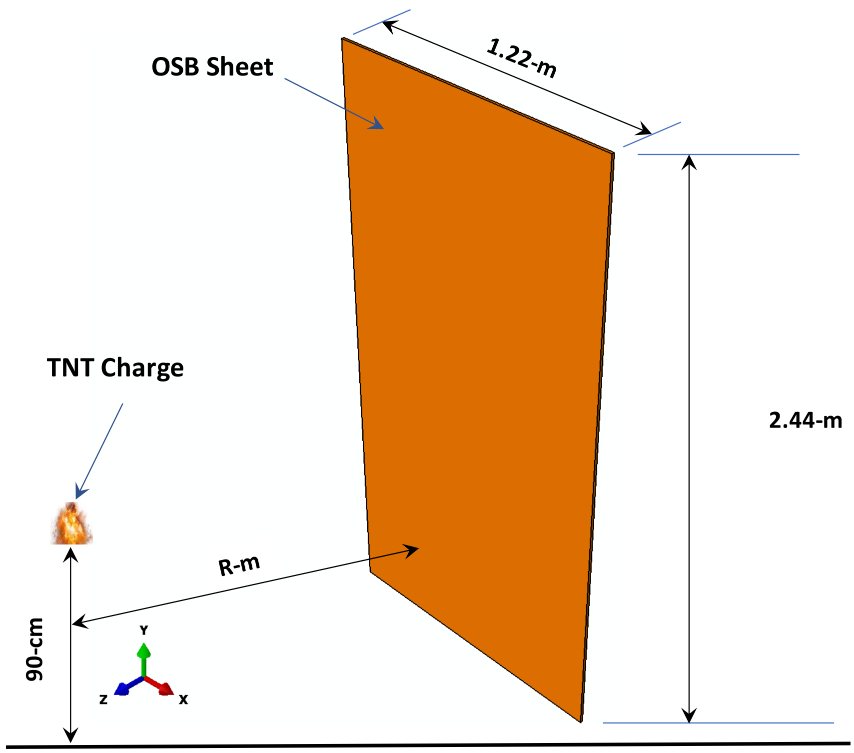

Figure 5.1 Geometry of OSB blast wall and TNT charge setting.

Table 5.1 Mechanical properties of OSB (Zhang et al., 2005).

Quantity	Values
ρ (Kg/m^3)	700
E_1 (GPa)	5.839
E_2(GPa)	5.827
E_3(GPa)	0.13
G_{12}(GPa)	2.33
G_{13}(GPa)	0.26
G_{23}(GPa)	0.12
V_{12}	0.219
V_{13}	1.70
V_{23}	1.02

The TNT charge is placed 90 cm above the ground level (exactly in front of the wall center), and different scaled distances considered to examine the performance of the wall. The reason for selecting 90 cm is because the source of the explosion is assumed to represent the suicide vest attacks scenario. In-plane stresses (σ_x, σ_y, and σ_{xy}) of the OSB model are computed numerically. The interaction equation of von Mises invariant failure criterion was used to predict the failure index (Quadratischer et al., 2001). The calculated failure index (I_F) versus the scaled distance (Z) index were listed in Table 5.2. Results of the analysis showed that the OSB wall can resist blast shock generated from high-explosive charges without fracture if the scaled distance Z ≥ 1.5 m/kg$^{1/3}$, any scaled distance less than this range leads to failure of the structure.

Table 5.2 Failure index of the OSB panel.

Z (m/kg$^{\wedge 1/3}$)	Failure Index (I_F)
0.5	10.46
0.75	5.34
1.0	2.43
1.5	0.67
1.75	0.427
2.0	0.25
2.5	0.09
3.0	0.045

The relationship between the failure index versus the scaled distance is shown in Figure 5.2. Peak out-of-plane deformation of OSB wall was measured at back-face of wall center. The deformation is reduced when scaled distance increased. For instance, peak of deformation reduced by 76 percent when scaled distance increased from 1.0 to 2.0 m/kg$^{1/3}$ as shown in Figure 5.3. The peak incident surface shock wave pressure decreased by 53 percent for the same increase range of scaled distance as shown in Figure 5.4. Time history of incident shock wave pressure was calculated from finite element analysis as shown in Figure 5.5.

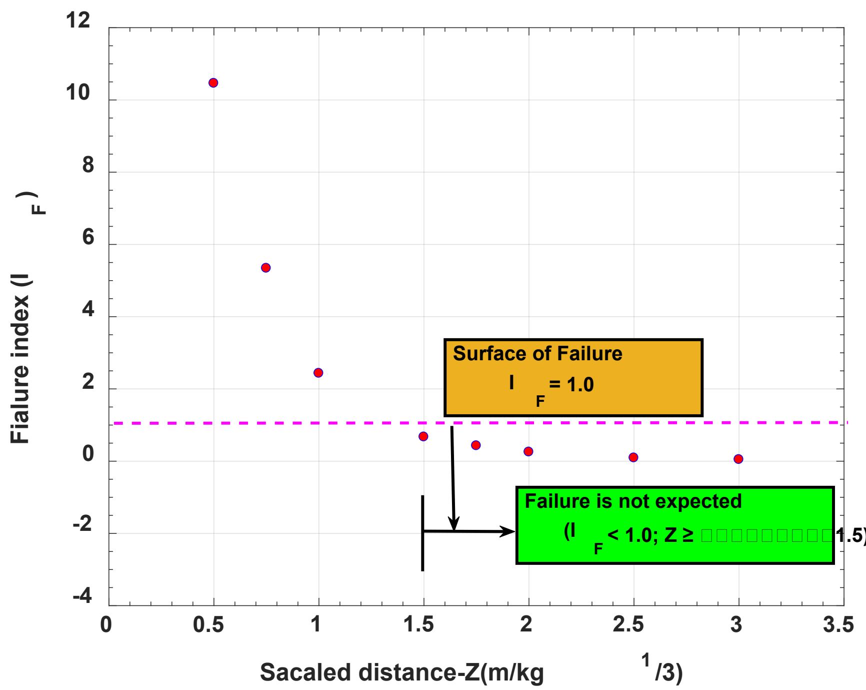

Figure 5.2 Failure surface versus scaled distance of OSB wall.

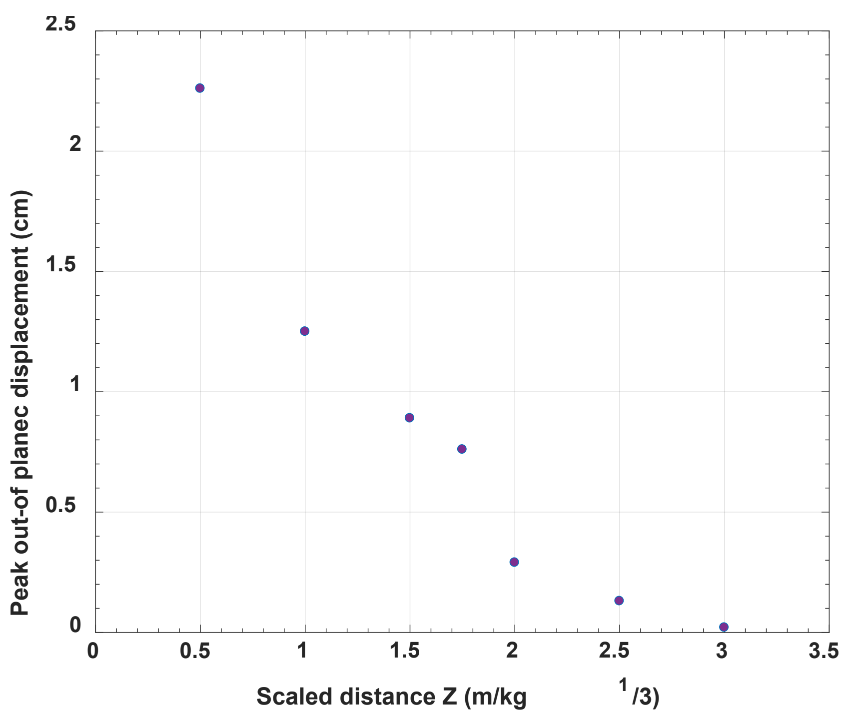

Figure 5.3 Peak out-of-plane displacement of OSB wall.

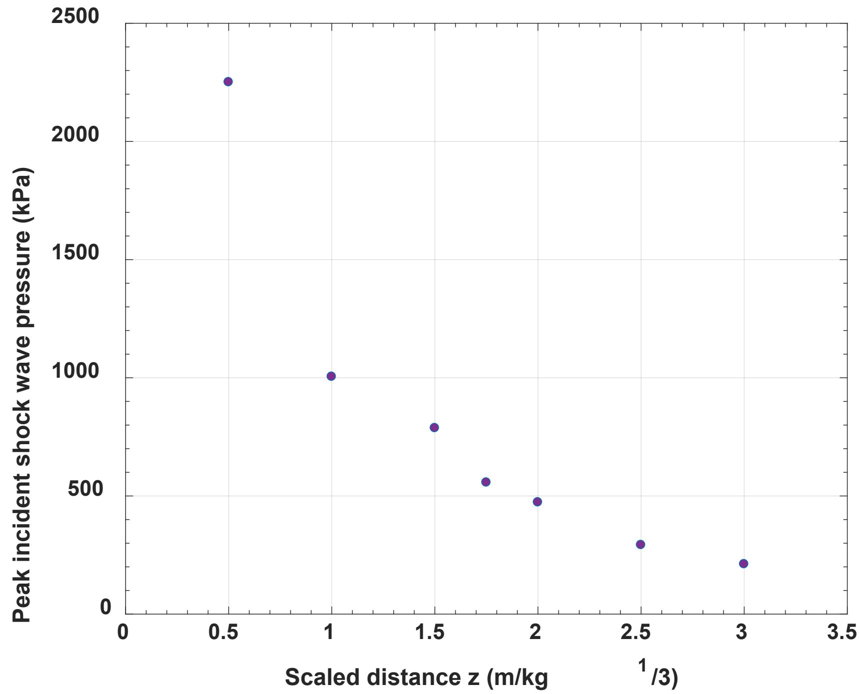

Figure 5.4 Peak incident shock wave pressure of OSB wall.

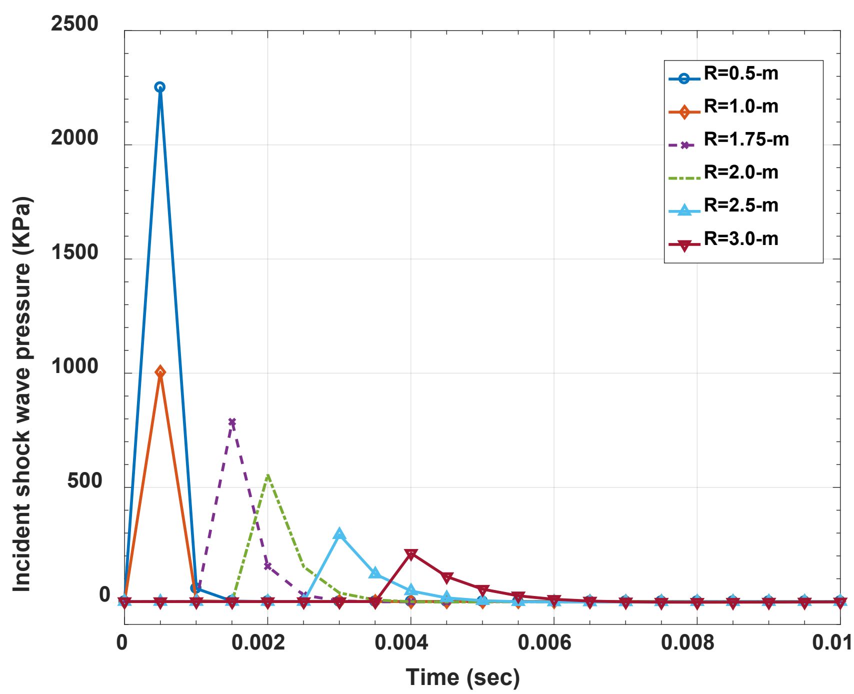

Figure 5.5 Incident shock wave pressure time histories of OSB wall.

5.4 Experimental Program

5.4.1 Introduction and Summary

Due to lack of data of simple blast walls behavior, running such type of tests is necessary to establish database of system response under free-air blast loading. In this study, free-air blast tests were conducted at the Colorado State University (CSU) Blast Field-Laporte site and Maxwell Ranch site. The purpose of these tests is to understand the behavior of simple blast walls under free-air blast loading, and level of protection around the wall. The experimental tests matrix, the tests were implemented in three stages 1) trial and blast pressure small-tests, 2) small and large-scale OSB test, 3) Animal tissue and WSaW wall tests.

Preliminary, two tests of small-scale charges of M-80, and detonation cord (0.82 grain/cm.) were conducted. The purpose from these two tests was to check the setting of instruments and the configuration of the high-speed data acquisition system (NI-PXIe-1082) through measuring peak overpressure (P_{so}) as it is the only blast wave parameter that could be measured using the existing instruments. Following the initial tests, a small-scale and large-scale tests of OSB wall were conducted to measure the response and the air-blast pressure distribution. Moreover, animal tissue was subjected to blast shock wave to measure the level of eardrum rupture. The experimental program was concluded by conducting a large-scale WSaW blast wall test. The response of the blasted walls was computed and verified with finite element results using ABAQUS/Explicit software.

5.4.2 Instrumentations

Free-field blast pressure (unconfined burst) was measured from high-explosive detonation. Two Piezoelectric sensors, ICP®, in some tests two, three and four sensors were used. This sensor is a registered trademark of PCB group. The ICP® sensor has the capability to measure dynamic pressure, strain, and acceleration in microseconds since it has a sensing element made of a piezoelectric material. The sensor converts mechanical strain to an electrical signal, then this signal is simplified and transmitted to a data acquisition system (DAQ) (PCB Piezotronics Inc.,2015). The pressure pencil probe model is 137B23B with maximum pressure of 6,895 kPa (1kpsi) as shown in Figure 5.6. The specifications at room temperature are shown in Table 5.3. The pressure probe is designed to measure very fast transient response in microseconds. It was connected to high-speed data acquisition (DAQ) system model NI PXIe-1082(see Figure 5.6).

Table 5.3 Specification of 137B23 PCB probe (PCB Piezotronics Inc., 2015).

Performance	Range
Measurement Range (for ±5V output)	345 kPa
Useful Overrange (for ± 10V output)	690 kPa
Sensitivity (± 15 %)	0.145 mV kPa
Maximum Pressure	6895 kPa
Resolution	0.069 kPa
Rise Time (Incident)	≤ 6.5 μ sec
Temperature (Operating)	-73 to 135°C
Sensing Element	Quartz
Housing Material	Aluminum
Diaphragm	Invar
Electrical Connector	BNC Jack

The chassis of the NI PXIe-1082 has eight slots for PXI (PCI eXtensions for Instrumentation) and PXI Express modules. In the current test configuration, the NI- PXIe 4492 card was used due to high-accuracy to measure shock wave, vibration, and sound waves applications. These probes provided a good understanding of air blast pressure distribution around the location of the explosion source. Shock acceleration was measured using two piezoelectric ICP® single axis shock accelerometers model 350C23 as shown in Figure 5.6, with a maximum measurement range of 98,000 m/s^2 (10,000g). The specifications of ICP® accelerometers are shown in Table 5.4. The Tests matrix of the current study is shown in Figure 5.7.

Table 5.4 Specification of 350C23 PCB accelerometers (PCB Piezotronics Inc., 2015).

Performance	Range
Measurement Range	± 98,000 m/s² pk
Sensitivity (± 30 %)	0.05 mV/(m/s²)
Frequency Range (± 1 dB)	0.4 to 10,000 Hz
Frequency Range (-3 dB)	0.2 to 25,000 Hz
Resonant Frequency	≥ 100 kHz
Overload Limit (Shock)	± 490,000 m/s² pk
Temperature (Operating)	-18 to +66 °C
Sensing Element	Ceramic
Housing Material	Diaphragm

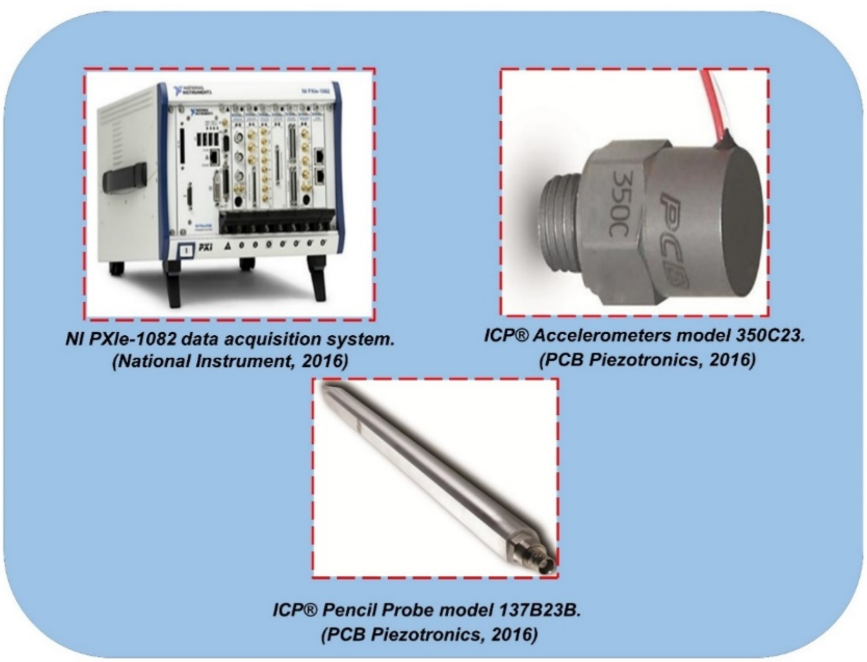

Figure 5.6 NI PXIe-1082 DAQ system, ICP® pencil probe 137B23B, and ICP® 350C23 shock accelerometers.

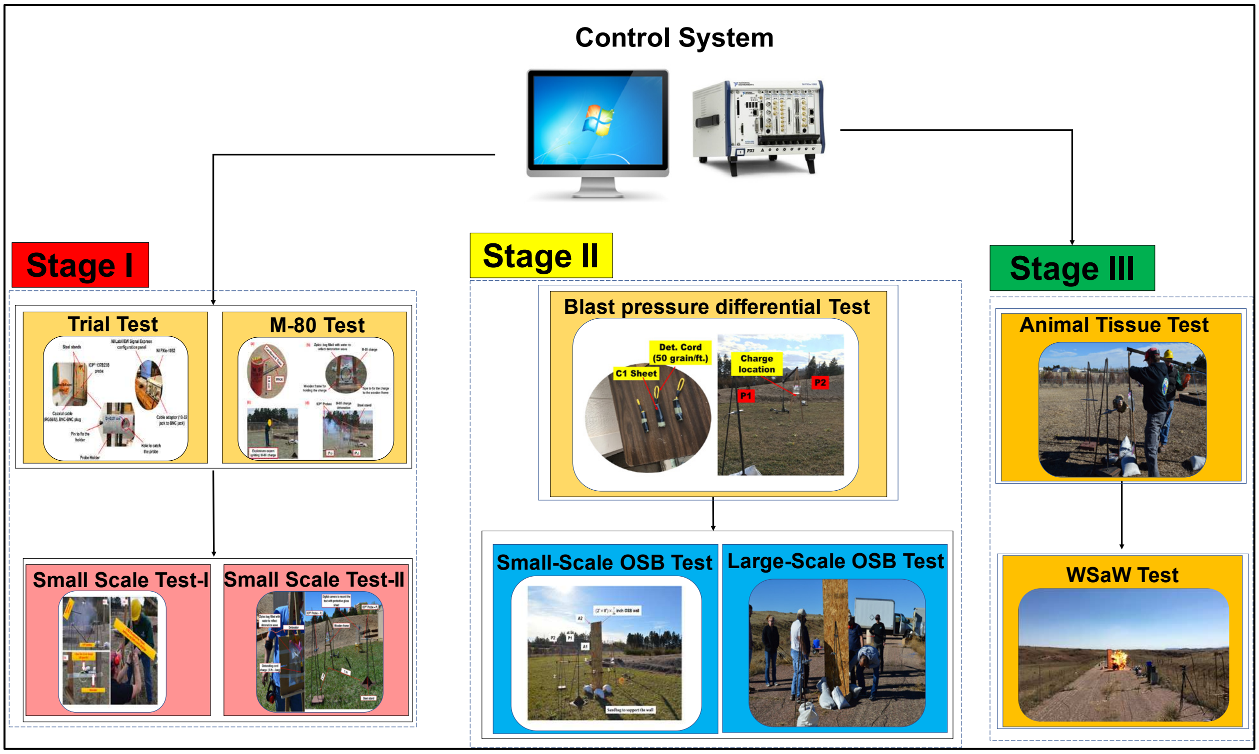

Figure 5.7 Tests Matrix of the current Study.

5.4.3 Free-Air Blast Pressure-Trial Test

A trial test was performed at the Structural Laboratory-Engineering Research Center (ERC) - Colorado State University (CSU) using Latex Balloons size 30-cm. The test setup is shown in Figure 5.8. Different configurations are realized to check probes connection and record the signal from the DAQ system based on the specifications of the ICP® probe. In this test, timing set, and current excitation were adjusted to measure low-level of air-pressure from blowing-up balloon.

The aim from this test was to measure peak pressure and get a good resolution for the pressure-time profile. The following conclusions were made from measuring air-pressure from blowing up a balloon:

- Generated pressure from blowing-up balloons is low and cannot be felt.

- Pressure profile is typical as blast wave from high explosive detonation in free air (since the balloon was placed very close to the sensor), but the characteristics are different. The measured air-pressure is presented graphically in Figure 5.9.
- Peak overpressure is 0.34 Pa, at 30-centimeter from the probe tip.
- Positive impulse is 0.017 Pa-sec.
- Rise time was 0.01 second, and positive and negative phases duration were 0.11, and 0.19 second, respectively.
- Pressure dropped by 88 percent for 0 < R ≤ 30 cm, and by 100 percent for 30 cm < R ≤ 90 cm. This means that the wave energy is low and attenuated quickly at only 30 cm from the ballon.

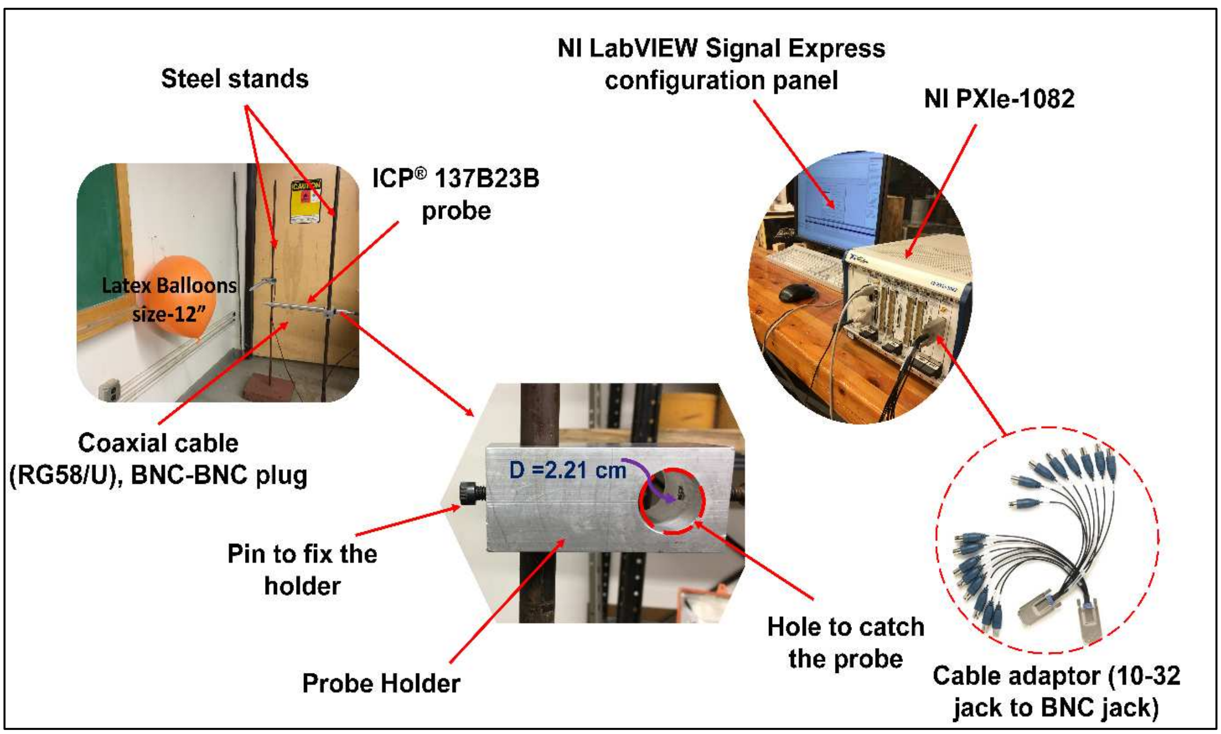

Figure 5.8 Balloon test setup.

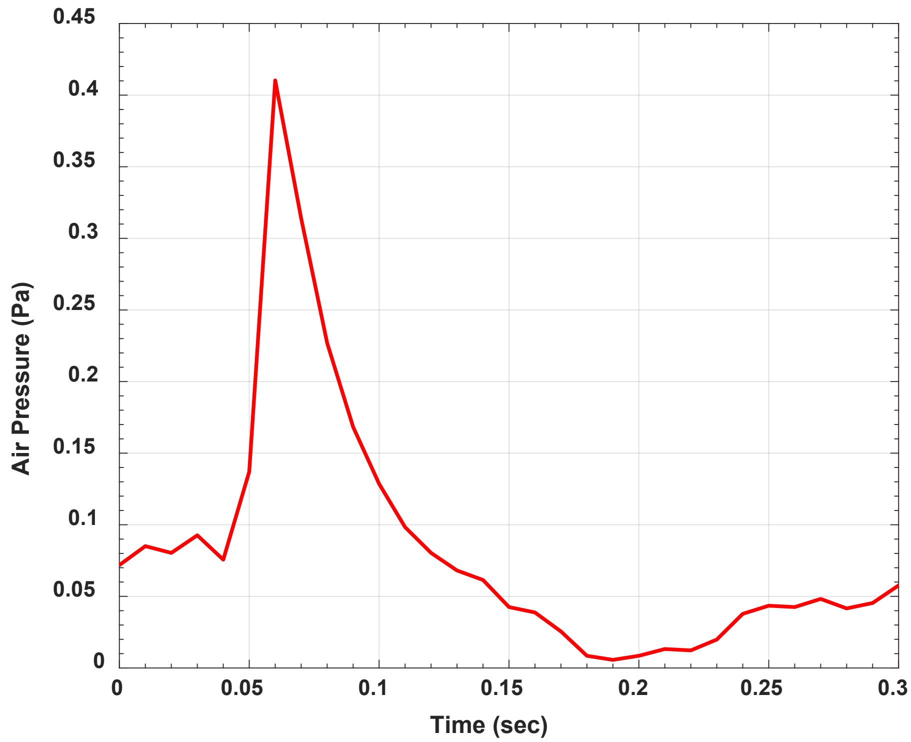

Figure 5.9 Pressure-time profile from blowing up balloon.

5.5 Free-Air Blast Pressure Tests-I

Two tests were conducted to measure peak overpressure at Colorado State University (CSU) blast field-Laporte site in March 2017. Range of M-80 and detonation cord (0.82 grain/cm.) charges detonated by CSU explosive team. According to the Bureau of Alcohol and Tobacco Firearms and Explosives (ATF), 2016, M-80 charge is prohibited from being used in fireworks since it could lead to serious injuries and property damages. In comparison to TNT detonation, however, M-80 detonation speed never exceeds local sound speed. It is composed of 3.8-centimeter long, and 1.4-centimeter inner diameter cardboard tube, with fuse going outside. Normally, the tube can carry between (2.5-3.0) grams of flash powder. The M-80 charge installed on a wooden frame and Ziploc bag filled with water fixed behind the charge to reflect the detonation wave toward the probe as shown in Figure 5.10 (a). The generated wave did not have the same characteristics of high-explosives charges due to the shape and low amount of explosive charge. Figure 5.10 (b), and (c) shows the ignition of the charge by a CSU explosive expert and the smoke of charge detonation, respectively.

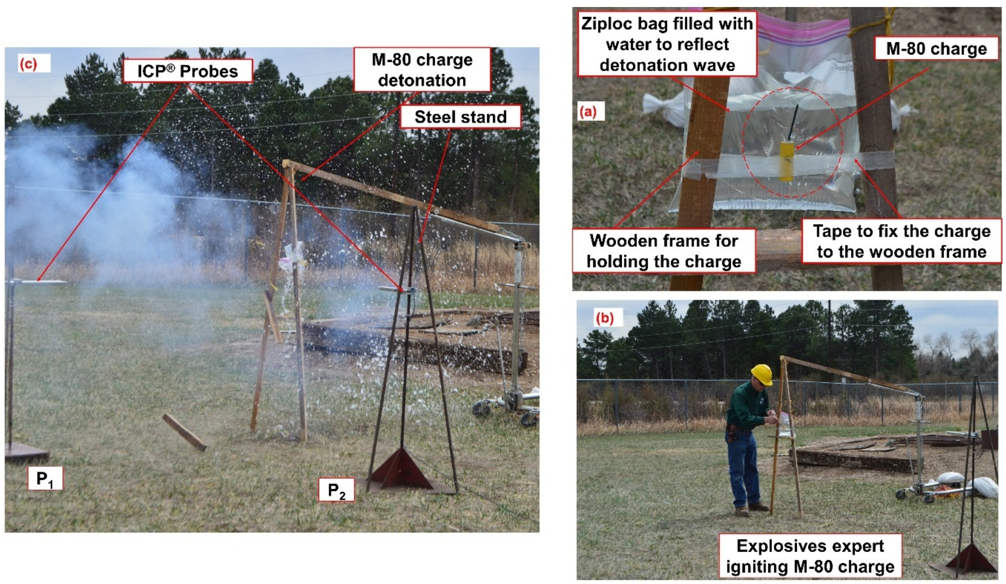

Figure 5.10 a. M-80 charge setting b. charge ignition c. charge detonation.

Peak overpressure versus standoff distance of M-80 charge measured by the probe, P_1, is shown in Figure 5.11(a). The equation of the measured pressure can be written in terms of peak pressure and standoff distance (R) as in Equation 5.1.

$$P_{so} = aR^b \quad (5.1)$$

Where, a, and b, are the constants of the model equation and their numerical values for the current test are, a = 49.75; and b= -0.803. Peak pressure versus standoff distances of the probe, P_2, is shown in Figure 5.11 (b). The equation of measured pressure can be expressed as in Equation 5.2.

$$P = aR^b \quad (5.2)$$

Where, a, and b, are the constants of the model equation and their numerical values for the current test are, a = 23.54; b= -0.1381. In general, generated air-blast pressure was in low-range, due to a small amount of explosive charge, also, the generated shock wave is asymmetric due to the shape of the charge.

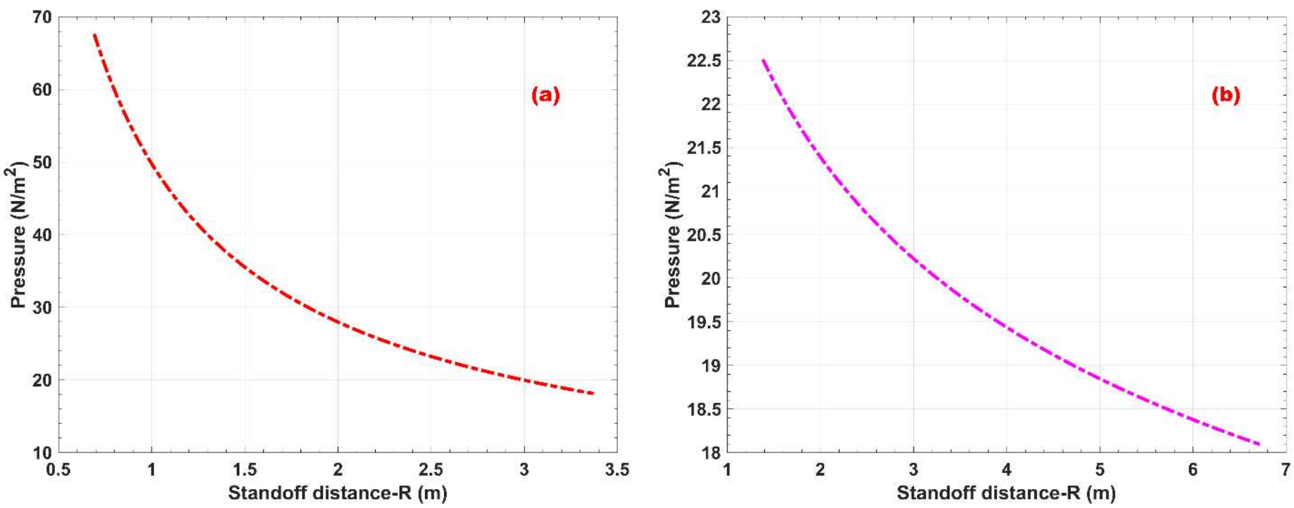

Figure 5.11 M-80 charge peak overpressure, a. probe P1, b. probe P2.

Detonating cord (Det. Cord.) is a flexible thin cord has a core of pentaerythritol tetranitrate (PETN) explosive. It has been used for different applications such as mining, drilling, cutting, and construction. Detonating speed of detonating cord is about 5000-7000 meters per second. There are several brands of detonating cord based on the amount of PETN and the applications as shown in Table 5.5. The same set up for the M-80 charge test was used for detonating cord charge test, and 30.5-cm of detonating cord (0.82 grain/cm.) was installed as shown in Figure 5.12(a), and b. All instruments settings were configured in accordance with recommendations provided by engineers from PCB Piezotronics, Inc.

Table 5.5 Technical information of detonating cord PRIMACORD trademark (PRIMACORD, 2016).

Det. Cord types	PETN core load		Outside Diameter	
	g/m	grain/ft.	mm	in
PRIMACORD 1	1.5	7.5	3.18	0.13
PRIMACORD 3	3.2	15	3.66	0.14
PRIMACORD 4Y	3.6	18	3.61	0.14
PRIMACORD 4R	3.6	18	3.61	0.14
PRIMACORD 5	5.3	25	3.99	0.16
PRIMACORD 8	8.5	40	4.47	0.18
PRIMACORD 10	10.8	50	4.70	0.19

Figure 5.12 a. Setting up the charge, b. Detonating cord charge test-I setting c. charge detonation.

The peak overpressure versus standoff distances of detonating cord charge measured by the probe, P_1, is shown in Figure 5.13 (a). The equation of the measured pressure can be expressed as in Equation, 5.3.

$$P_{so} = aR^b \qquad (5.3)$$

Where, a, and b, are the constants of the equation and their numerical values for the current test are, a = 193.4; and b = -0.9607. The peak pressure versus standoff distance of probe, P_2, is shown in Figure 5.13 (b). The equation of measured pressure can be expressed as in Equation, 5.4.

$$P_{so} = aR^b \qquad (5.4)$$

Where, a, and b, are the constants of the equation and their numerical values for the current test are, a = 357.6; and b= -1.559.

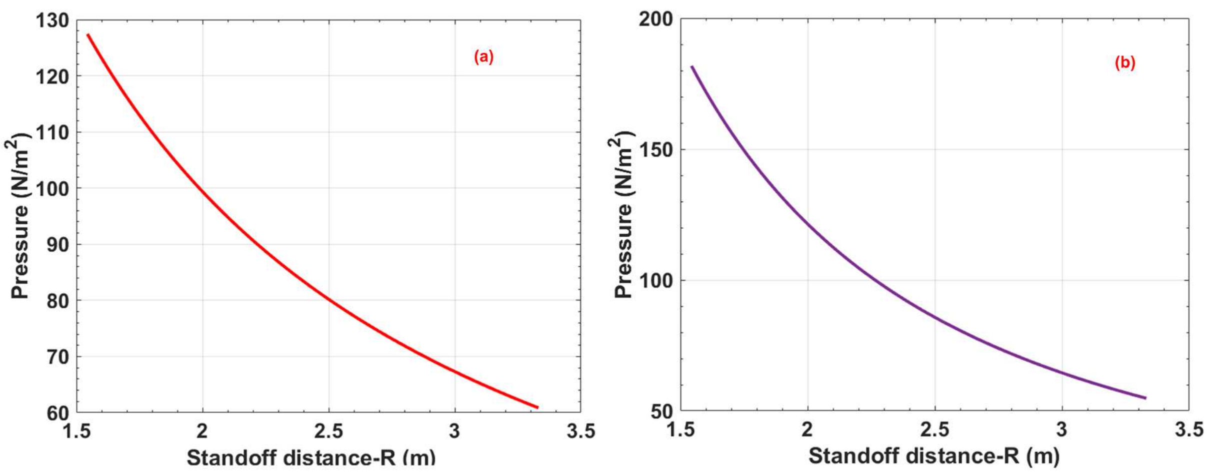

Figure 5.13 Peak overpressure of detonating cord charge, a. probe P1, b. probe P2.

In general, generated blast shock pressure is also in low-range, due to the small amount of explosive charge, and the shape of the charge. There is variation in probes readings for the same standoff distance, R, which could have resulted from the angle of incidents since the probes were not put on a straight line towards the charge. This study is the first work to measure blast shock pressure generated from low-explosive detonation since all previous work has been done on high-explosive bursts. The low-explosive charges could be used when testing small-scale systems to comply with site restrictions on using high-explosive charges.

5.6 Free-Air Blast Pressure Tests-II

The second free-air blast test was performed at Colorado State University blast field-Laporte site in May 2017. In this test, detonating cord charge was used due to a limitation in using high-explosive charge at the test site. The idea behind running this test is to check the maximum dynamic pressure input range in the configuration panel of the DAQ system since no exact/recommended value was available and sound pressure channel was used to measure the blast shock wave pressure. Three-time settings were also considered to ensure record that the peak overpressure since blast wave, could pass the probe sensing element in a very short time. The default value of the maximum dynamic pressure is (100 dB), but according to NI application engineers, it should be higher for the current application. Table 5.6 shows measurements matrix of the test. Three values of maximum dynamic pressure with two different internal excitations (Iex) versus three rate values were considered.

Table 5.6 Measurements matrix of detonating cord test II.

Parameters / Rate (Hz)	Max. dyn. Pressure = 100 Pa Iex = 4 (mA)	Max. dyn. Pressure = 160 Pa Iex = 6 (mA)	Max. dyn. Pressure = 200 Pa Iex = 6 (mA)
10k	✓	✓	✓
25k	✓	✓	✓
51k	✓	✓	✓

Theoretically, the maximum dynamic pressure of the shock wave can be calculated using the following expression:

$$dB = 20 \times log \frac{P}{P_O} \qquad (5.5)$$

where, P, is equal to 6,895 kPa for ICP® pencil probe model 137B23B.

The maximum dynamic pressure can be calculated from Equation 5.5, as follows:

$$dB = 20 \times log \frac{6895}{0.00002} = 230.75 \text{ Pa} \qquad (5.6)$$

In this test, CSU explosive experts increased the charge size, by using 1.52-m long of detonating cord just to generate higher intensity shock wave. The test was performed nine times for the considered parameters. The probes, P_1, and P_2 were placed at a fixed location (1-meter from the explosion source) and 90-centimeters above the ground as shown in Figure 5.14. Peak overpressure values were presented graphically versus the number of trials as shown in Figure 5.15 a, and b.

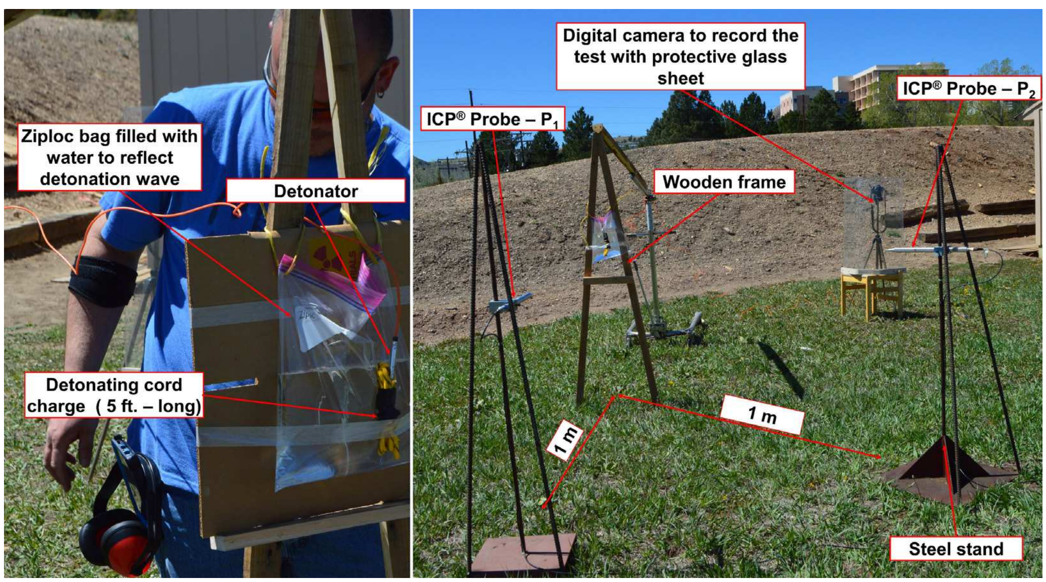

Figure 5.14 Detonating cord charge test-I.

The following conclusions were drawn from the test results:

- The generated blast shock wave did not propagate evenly in all direction.

- As compared to test I, the resultant air blast pressure was higher since larger charge size was used.
- A larger sampling rate (Hz) is preferred to measure the peak overpressure since the blast shock wave could pass the probe sensor in microseconds.
- For a recent application, setting maximum dynamic pressure to be between (160 –200) dB based on the ICP® pencil probe specifications are required for getting precise measurements.

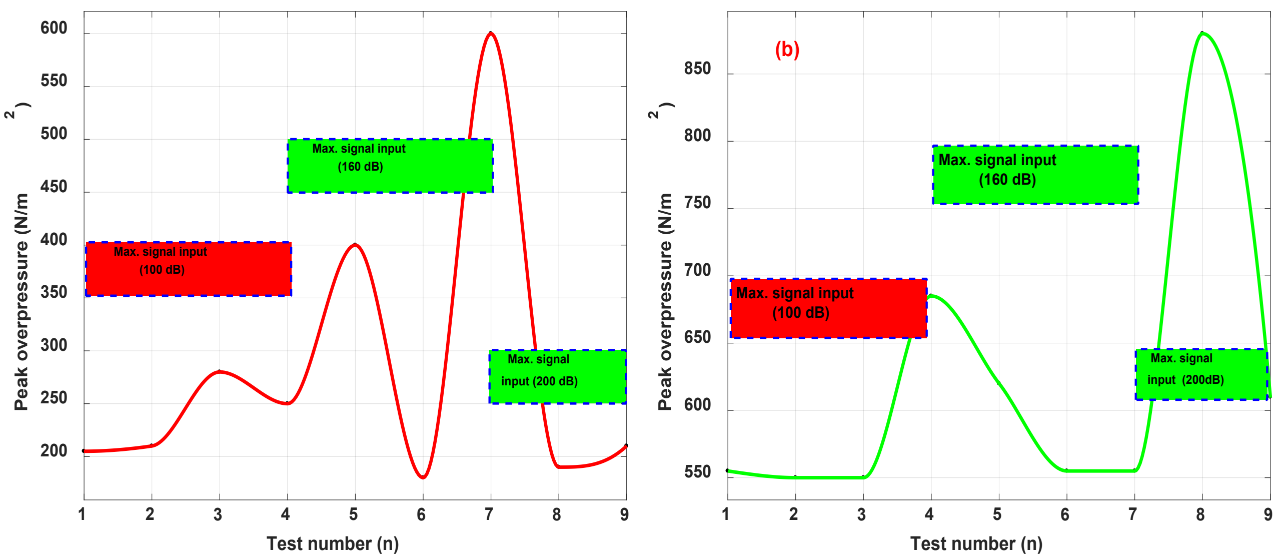

Figure 5.15 Peak overpressure versus test attempt of detonation cord charge. a. probe P1, b. probe P2.

5.7 Small-Scale Test of Oriented Strand Board (OSB) Wall

5.7.1 Test Setup and Results

A thin sheet of OSB wall was tested at Colorado State University (CSU) blast field-Laporte site in October 2017. The geometry of the OSB wall is 60-centimeter wide, 2.44-meter height, and 1.0-centimeter thick. The wall was connected to a wooden frame due to site limitations in constructing a foundation system (see Figure 5.16). Fabrication of the specimens was made at the Structural Laboratory-Engineering Research Center (ERC) of Colorado State University. The wall was fixed to the ground by using two rebars (# 4) anchored to the ground and four 14"x26" sandbags, capacity, 23-kilograms, which are designed for flood control, and military fortification as shown in Figure 5.16. The DETASHEET® flexible explosive charge of C1 (5-cm x 7.6-cm) used, and 60-cm of detonating cord. The equivalent TNT mass of this charge is equal to 9.96-grams. All handling and set up of explosive charge were done by the CSU explosives team. In addition to Piezoelectric ICP® pencil pressure probe model 137B23B, two Piezoelectric ICP® shock accelerometers model 350C23 were used to measure the wall response. This accelerometer was designed to measure the acceleration from high-frequency events such as blast shock wave. There were five trials of the tests in total. Some studies have focused on measuring acceleration from blast event due to complication in measuring the response of structures under high-intensity dynamic loading (Boyd, 2000). Measuring acceleration can provide a clear idea about the ductility of the structure (Yusof et al., 2011). High acceleration range was recorded from blast test of mild steel plate and steel fiber reinforced concrete (SFRC) (Yusof et al.,2011; Boyd, 2000). Table 5.7 shows measured peak acceleration of these tests. Furthermore, application engineers of PCB Piezotronics, Inc., clarified that acceleration from high-frequency loading could be 10x-to-1000x larger than the response from low-frequency applications.

Table 5.7 Peak acceleration from Blast tests (Yusof et al., 2011*; Boyd, 2000**).

Structure	R(m)	W (kg)	Peak of acceleration (g)
NRC*	0.3	1.0-PE4 (C-4)	774.98
SFRC*	0.3	1.0-PE4 (C-4)	520.05
Mild steel plate**	0.5	250 gm.- Spherical Pentolite	14657.00

In the current test, pencil probes were fixed on two steel stands and the accelerometers were mounted on aluminum plates as shown in Figure 5.16. This type of mounting is recommended for permanent use since it is providing a high level of safety to the sensor itself, and it is a perfect choice for high-frequency applications when the surface is flat (PCB Piezotronics,2016). The setting of the high-speed data acquisition system (DAQ) was done based on trial tests output. All sensor configurations and setting were based on the standard manuals and PCB Piezotronics, Inc., application engineers' recommendations. The probe, P1, placed at 2.44-meter from the charge,1.3-meter, behind the OSB wall, while probe, P2, fixed at 2.44-meter to the side of the wall. The standoff distance from the charge to the wall is 1.5-meter.

The time histories of the recorded accelerations from accelerometers A1 and A2 were presented graphically in Figures 5.17 and, 5.18, respectively. There was some variation in the recorded acceleration and free-air blast pressure because of the effect of the unsymmetrical generated shock wave. However, generally, all plots are consistent with typical standards charts for this type of application. The pressure-time profile of blast wave in the free air of probes P1 and P2 are shown in Figures 5.19, and 5.20, respectively. The peak shock acceleration at mid-wall is larger than its value at the top corner because of the high-intensity shock wave (see Figure 5.21). The air-blast pressure decreased when the wall presented and with increasing distance from the blast. This is can be seen clearly in Figures 5.22. The reduction in pressure was 18.24 percent for probes positioned 2.44-m behind the wall as shown in Table 5.8.

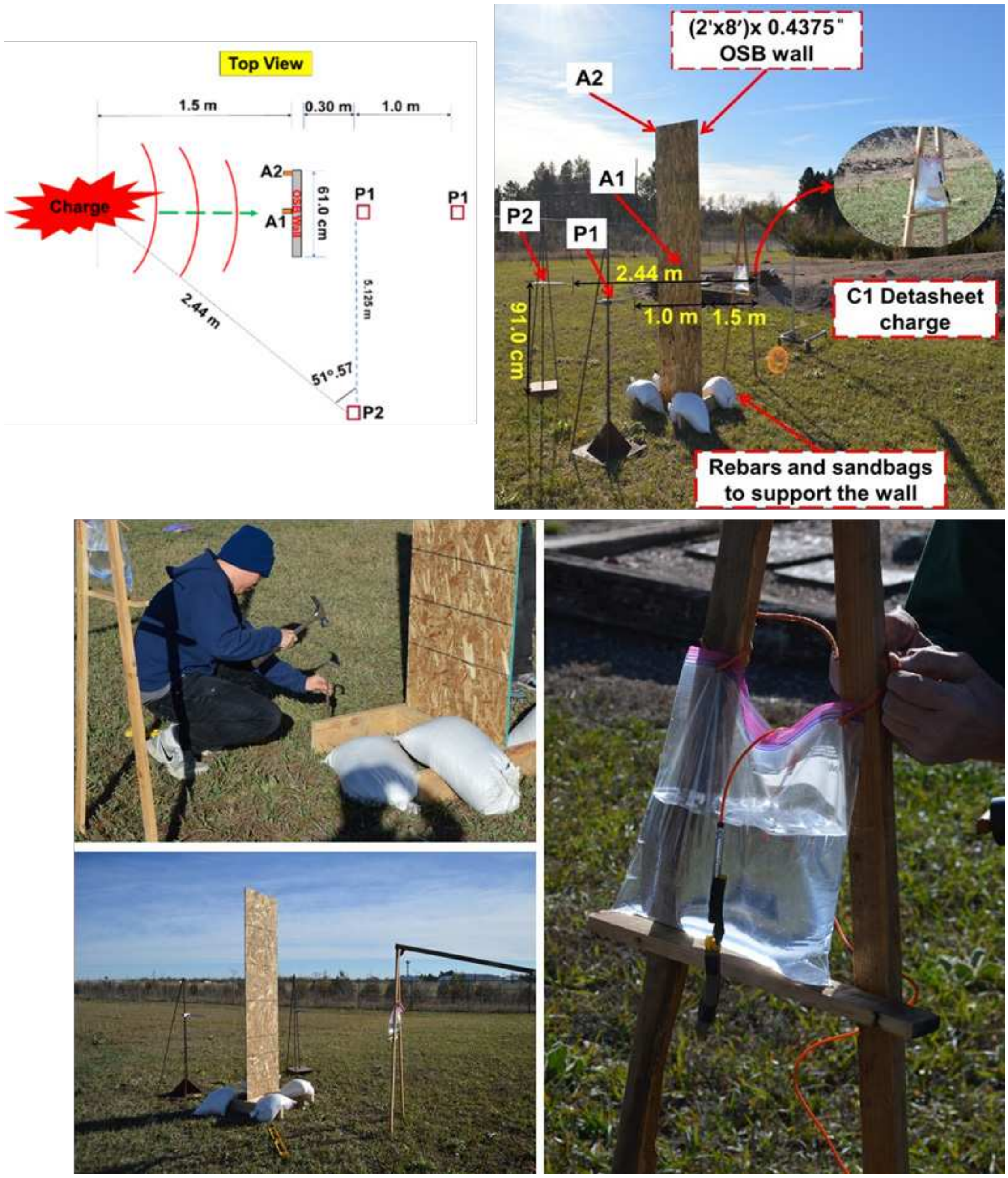

Figure 5.16 Small-scale oriented strand board (OSB) blast wall test setup.

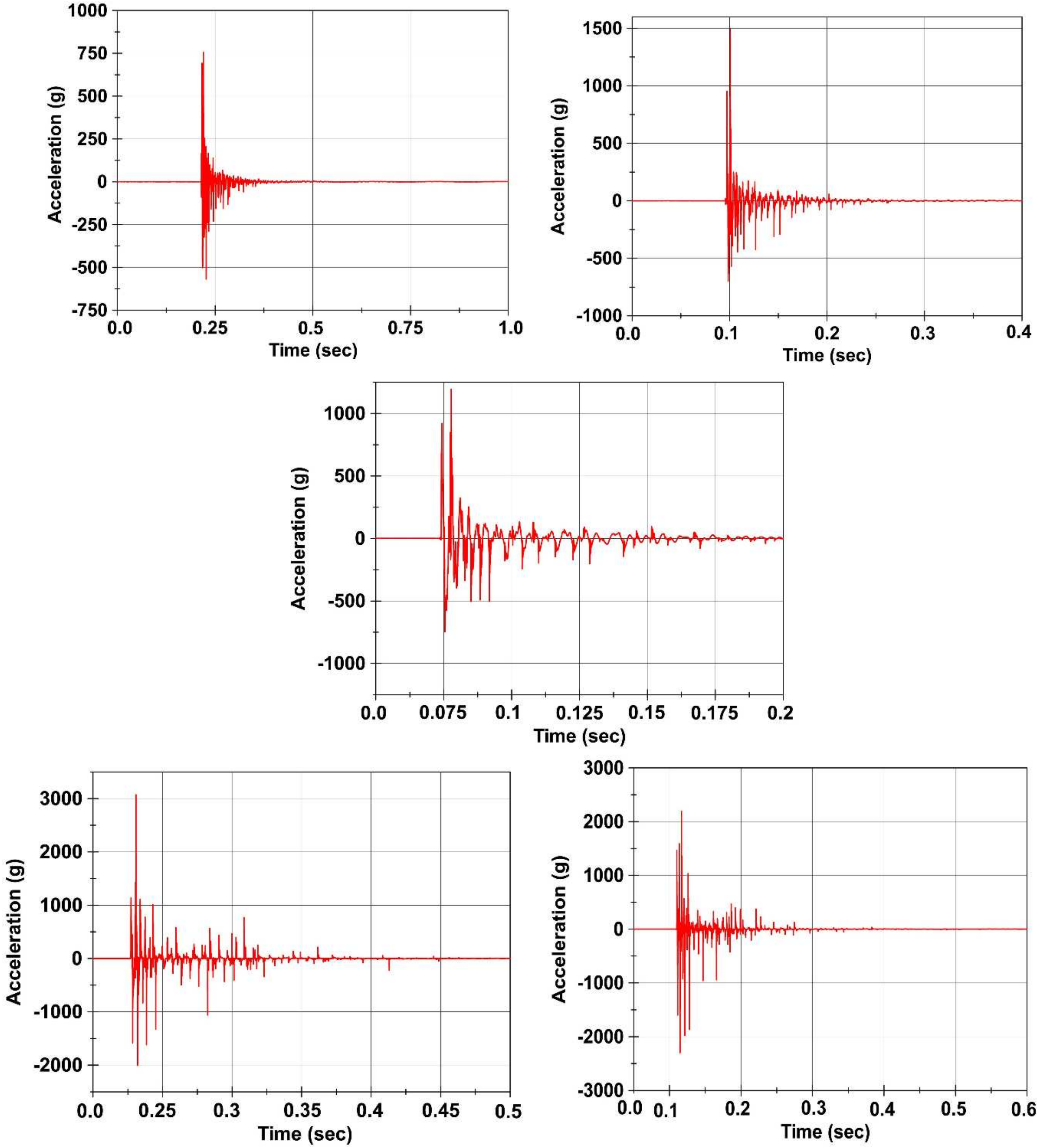

Figure 5.17 Out-of-plane acceleration at the center of OSB wall.

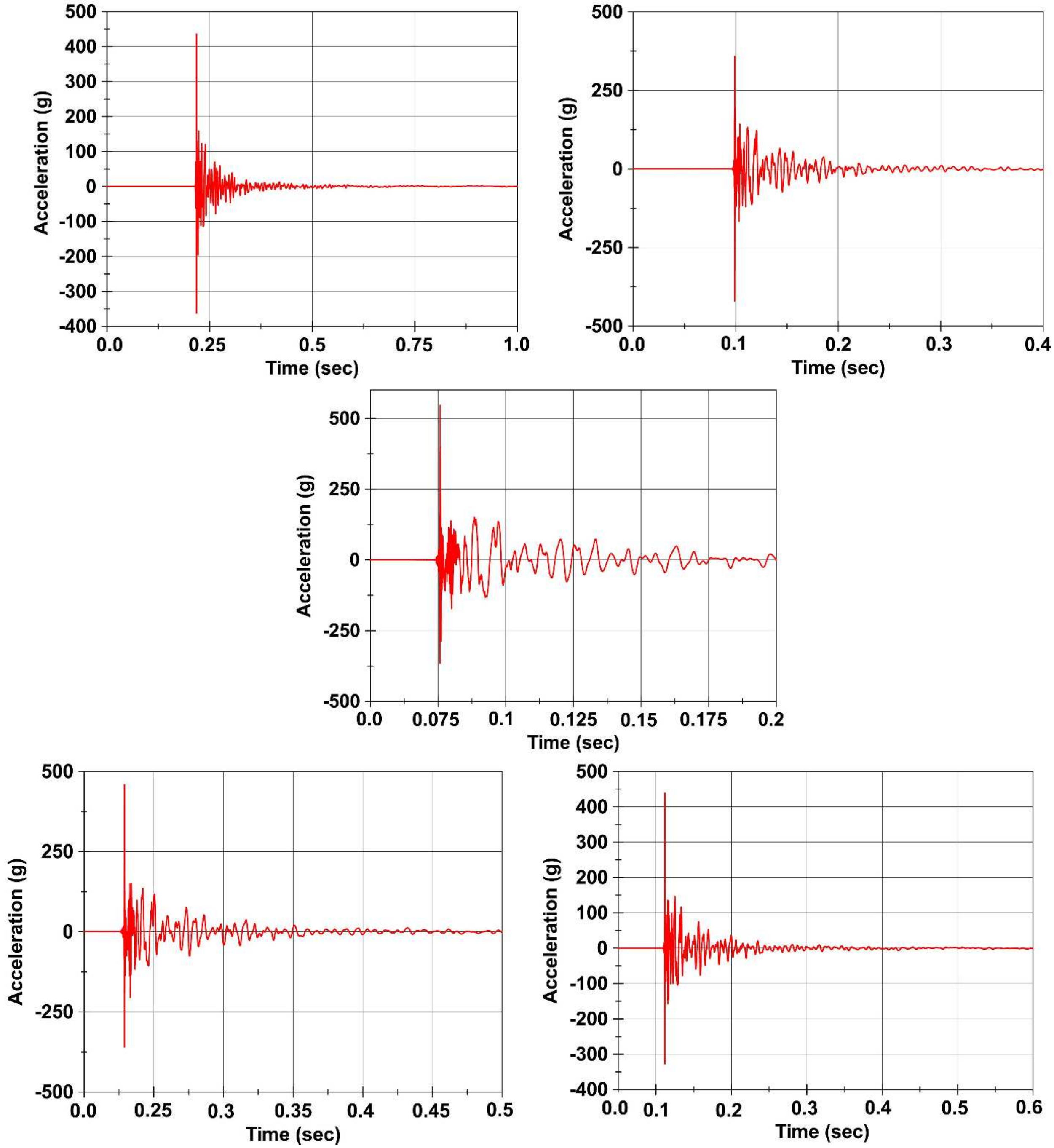

Figure 5.18 Out-of-plane acceleration at the top corner of OSB wall.

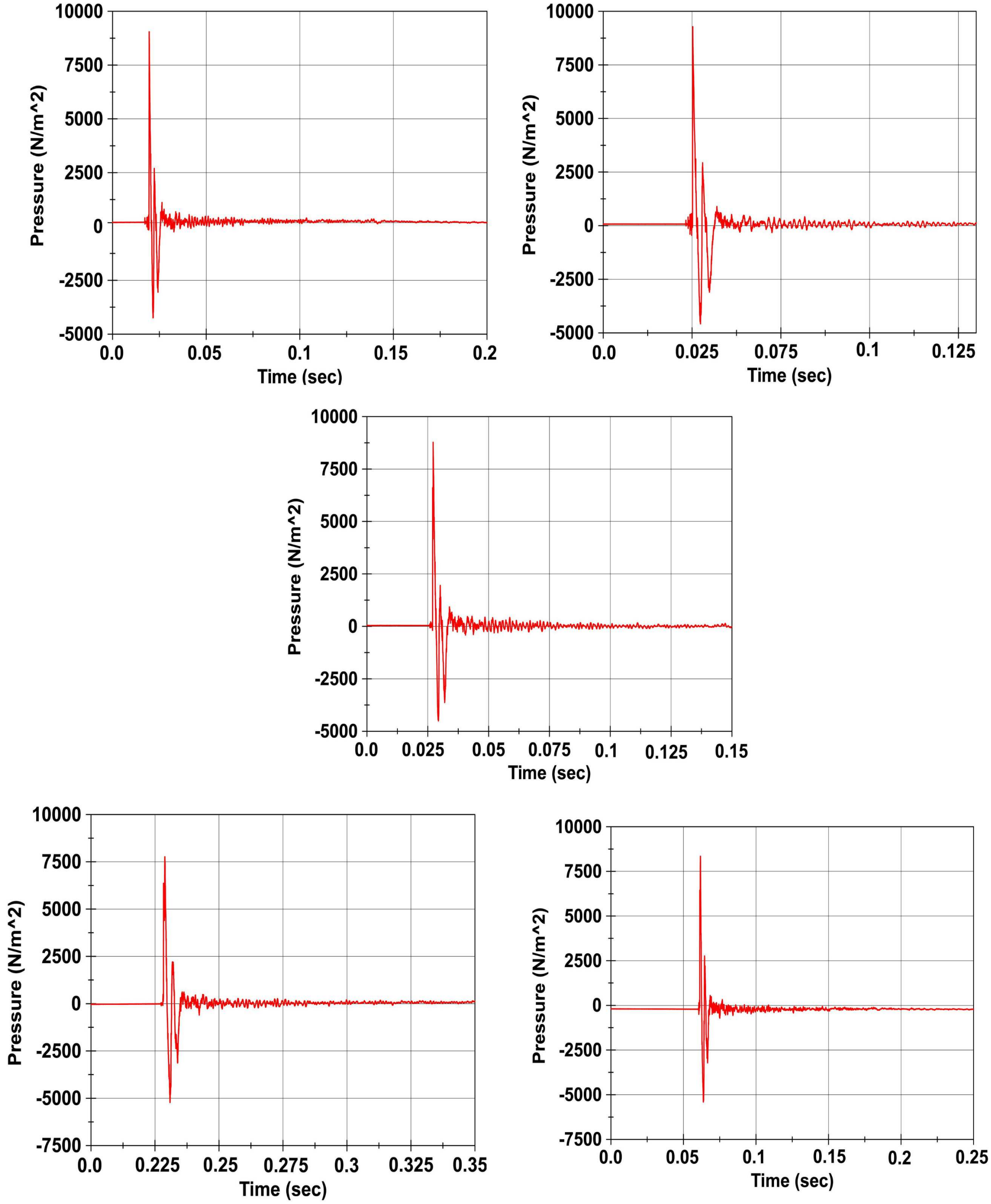

Figure 5.19 Pressure-time profile of blast wave of probe 1.

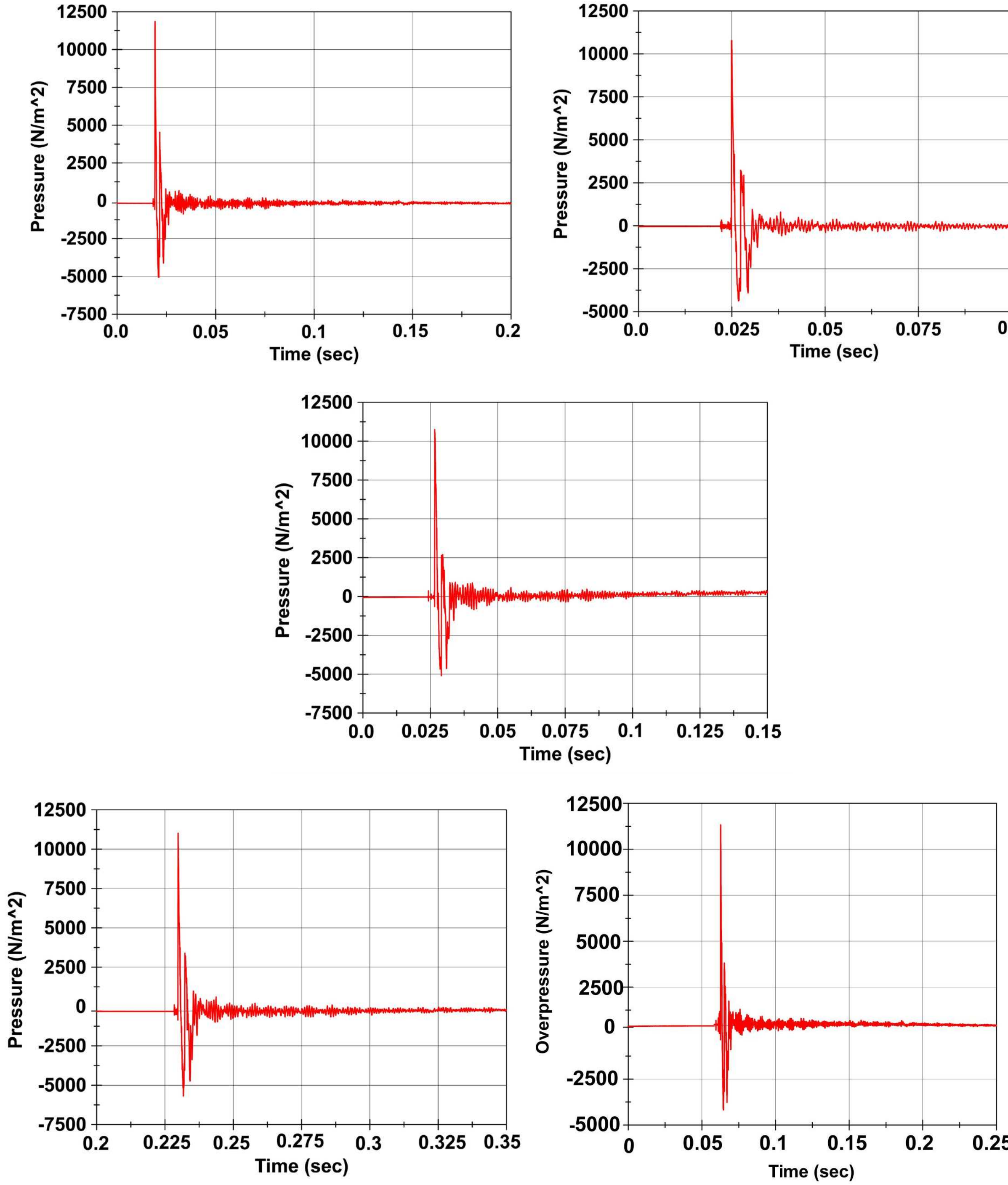

Figure 5.20 Pressure-time profile of blast wave of probe 2.

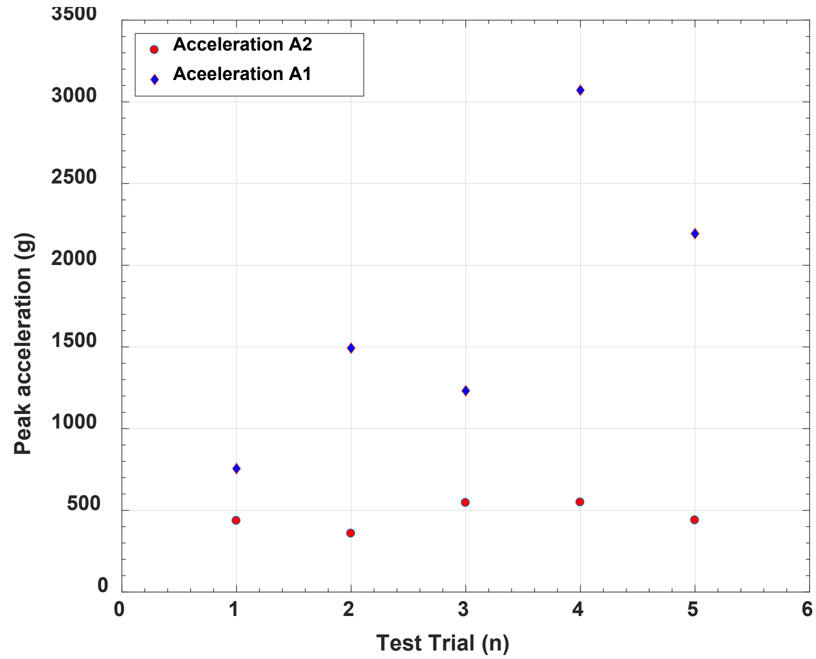

Figure 5.21 Peak acceleration of OSB wall.

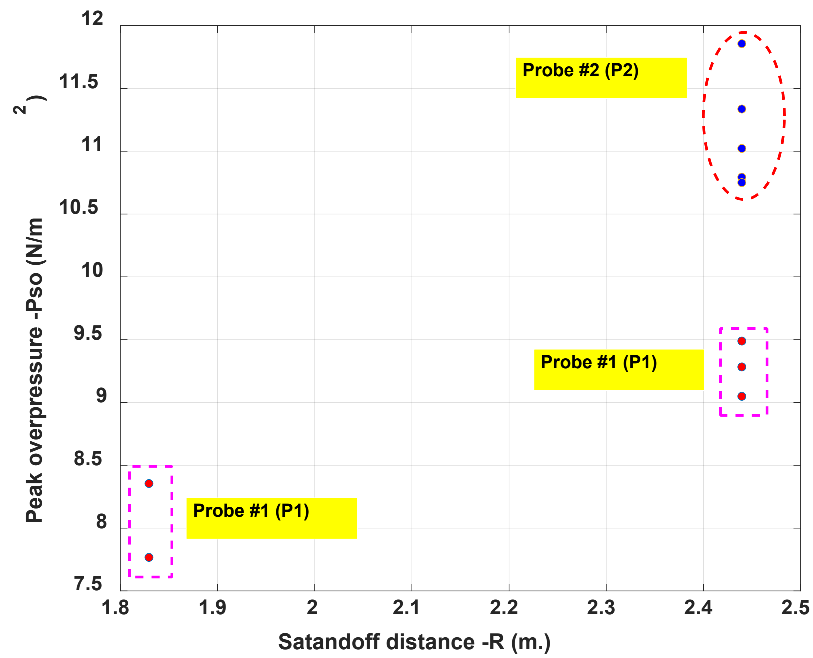

Figure 5.22 Measurements of peak overpressure-distance.

Table 5.8 Peak air- blast pressure of OSB wall test.

Probe #	Distance (m)	Charge weight (gm)	Peak pressure (mean)-(kPa)	Decrease (%)
P1 (behind wall)	2.44	9.96	9.27	18.24
P2 (off wall)	2.44	9.96	11.13	

5.7.2 Validation of OSB test results

The experimental results were compared to the finite element model results using ABAQUS/Explicit software ver. 6.14. Three-dimensional dynamic finite element model of 60-centimeter wide, 2.44-meter height and 1.0-centimeter thick of OSB wall is considered. The geometry of this model is shown in Figure 5.16. The finite element model details were explained in section 5.2. The mechanical properties of OSB sheet are listed in Table 5.1, and it was assumed to be orthotropic. The calculated acceleration from the numerical analysis is shown in Figure 5.23. The measured peak acceleration for the wall is in an excellent agreement with ConWep predictions within ABAQUS as shown in Table 5.9.

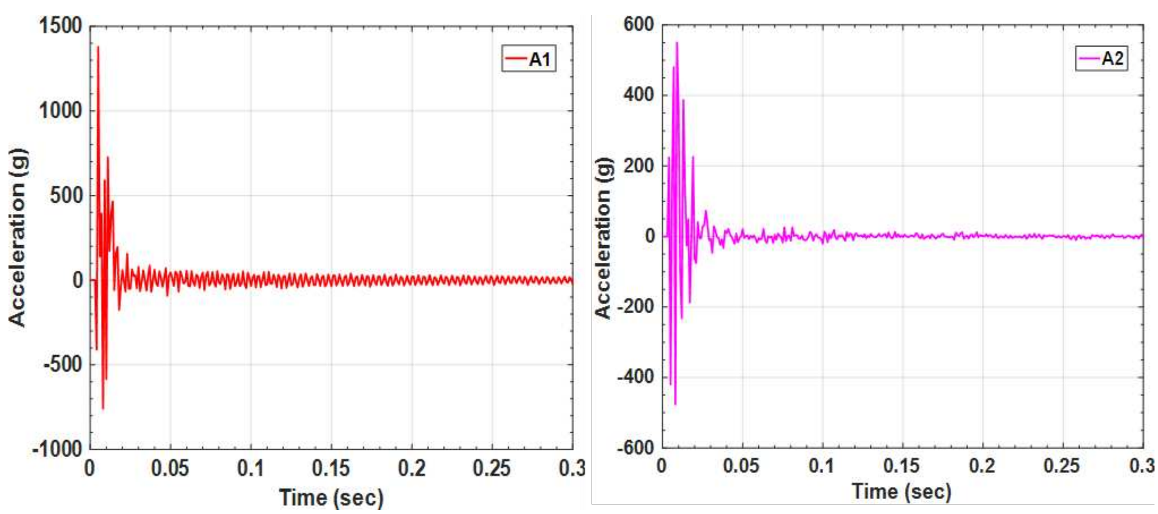

Figure 5.23 Calculated acceleration from numerical analysis of OSB wall.

Table 5.9 Comparison of acceleration response between test and numerical results.

Distance (m)	TNT (gm)	Peak acceleration (g) ABAQUS	Peak acceleration (g) test (avg.)	Diff. (%)
1.52	9.96	1377.9	1748.80	23.72
1.52	9.96	550.46	465.18	16.80

5.8 Large-Scale Test of Oriented Strand Board (OSB) Wall

The second OSB wall was tested in November 2017. This blast field test was conducted at Maxwell Ranch site. The wall was fixed to a wood frame as in the case of the small-scale test (see Figure 5.16). All fabrications associate with the specimen were made at Engineering Research Center (ERC) - Structural Laboratory of Colorado State University. The wall was fixed to the ground by six 14"x26" sandbags, weight 23-kilograms, which are usually used for flood control and military fortification. The steel stands were supported by five sandbags. Two sizes of TNT round demolition charges, 0.15, and 0.34-kilogram were used. All handling and set up of explosive charge were done by the CSU explosives team. Setting of the ICP® shock accelerometers and ICP® pencil pressure probes were the same as in the small-scale test.

5.8.1 Free-Air Blast Pressure Measurements Test

Pressure-time profile of generated blast wave was recorded by two ICP® pencil pressure probes (without wall). Four explosive shots were made to measure the air-blast pressure. The free-air blast test setup is shown in Figure 5.24. Table 5.10 shows the free-air blast pressure and Figures 5.25, and 5.26 show pressure-time profiles of the generated blast shock wave of the two ICP® pencil probes (P1, and P2), respectively. All plots were typical and identical to standard charts (Kingery and Bulmash,1984). Figure

5.27 shows good agreement between the measured free-air blast pressure and the Kingery-Bulmash measurements of a spherical wave of TNT charges in free-air bursts (UFC3-340-02, 2008).

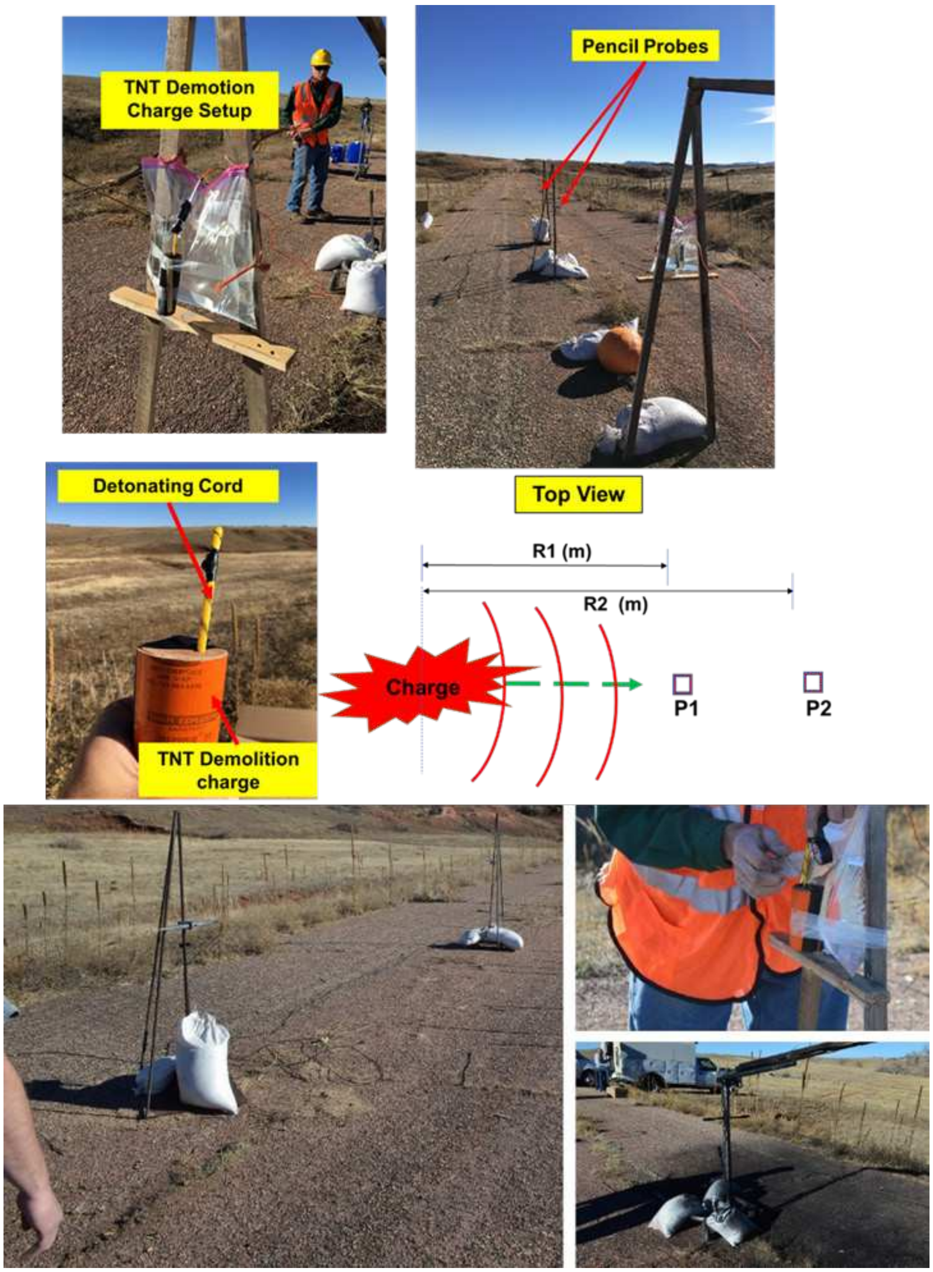

Figure 5.24 Free- air blast test setup.

Table 5.10 Measured peaks air-blast pressure.

Probe	Distance - R1, R2 (m)	TNT weight (kg)	Peak Pressure (kPa)
P1	5.66	0.15	12.89
P1	5.66	0.15	12.31
P1	9.0	0.34	14.12
P1	8.0	0.34	17.84
P2	8.2	0.15	8.71
P2	3.35	0.15	19.46
P2	3.29	0.34	38.47
P2	2.44	0.34	64.97

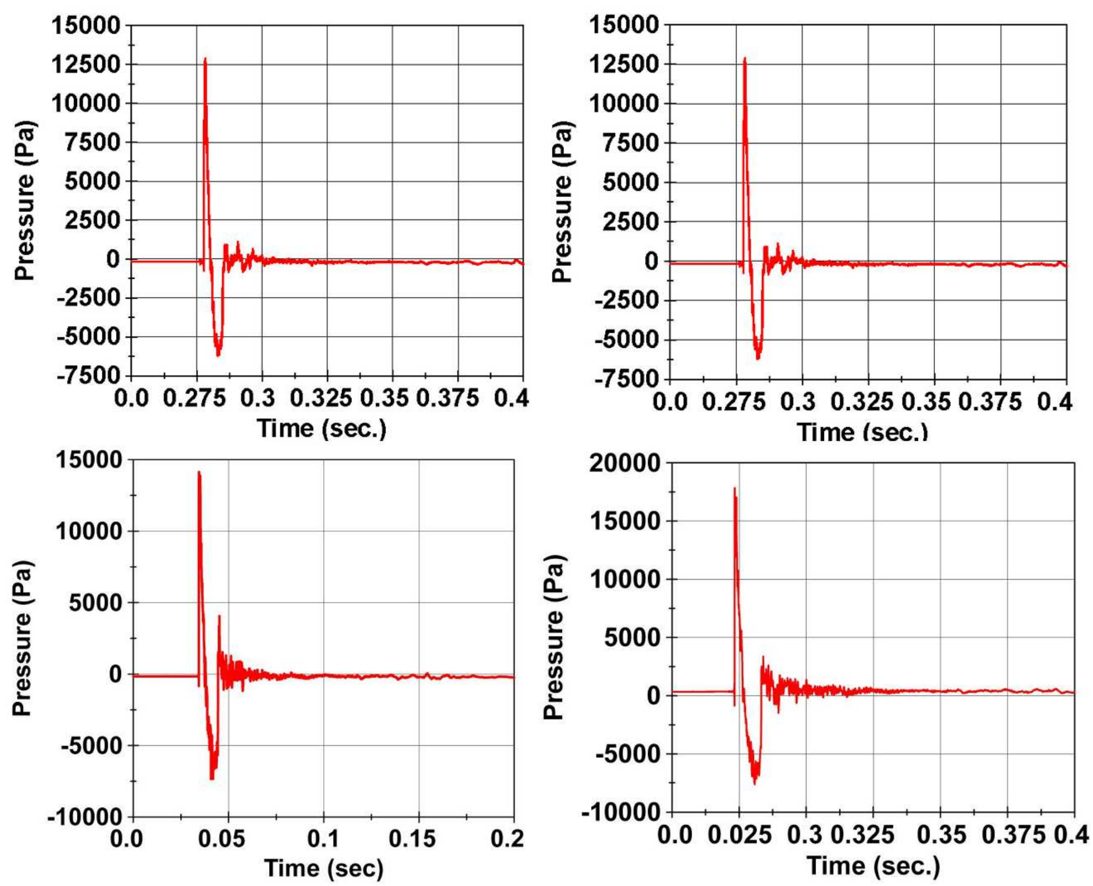

Figure 5.25 Measured pressure-time profile of blast shock wave- Probe 1.

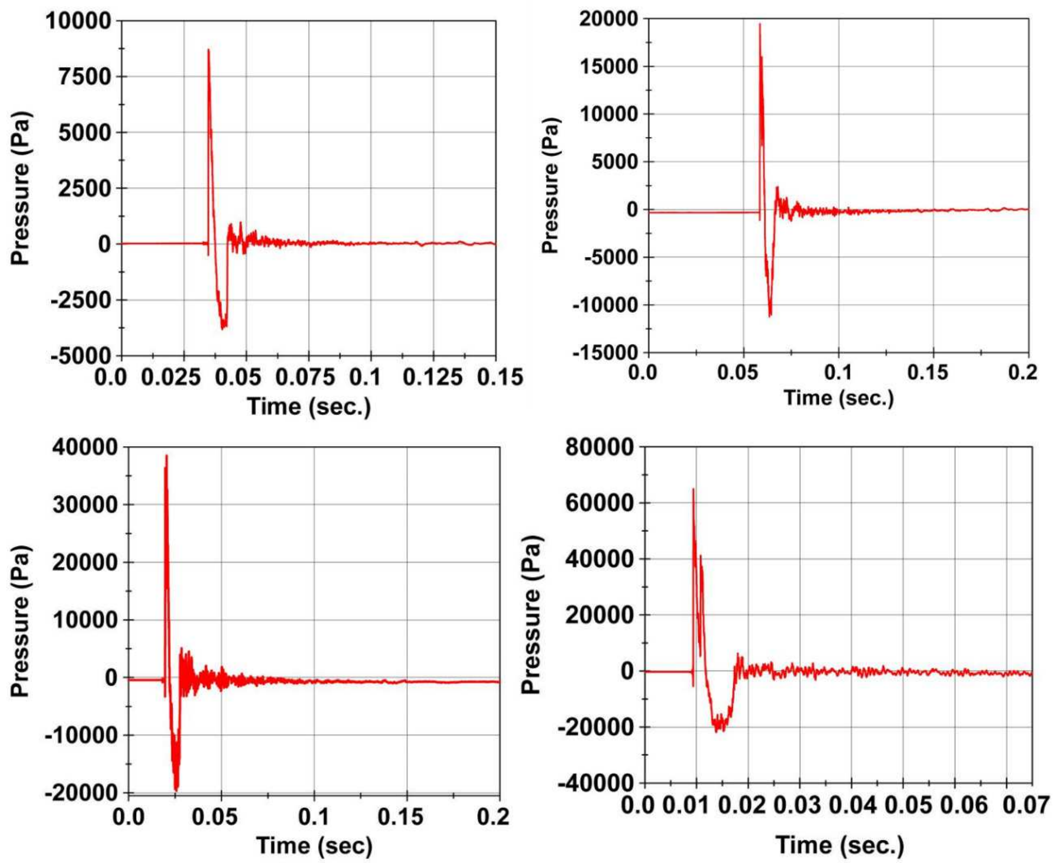

.

Figure 5.26 Measured pressure-time profile of blast shock wave- Probe 2.

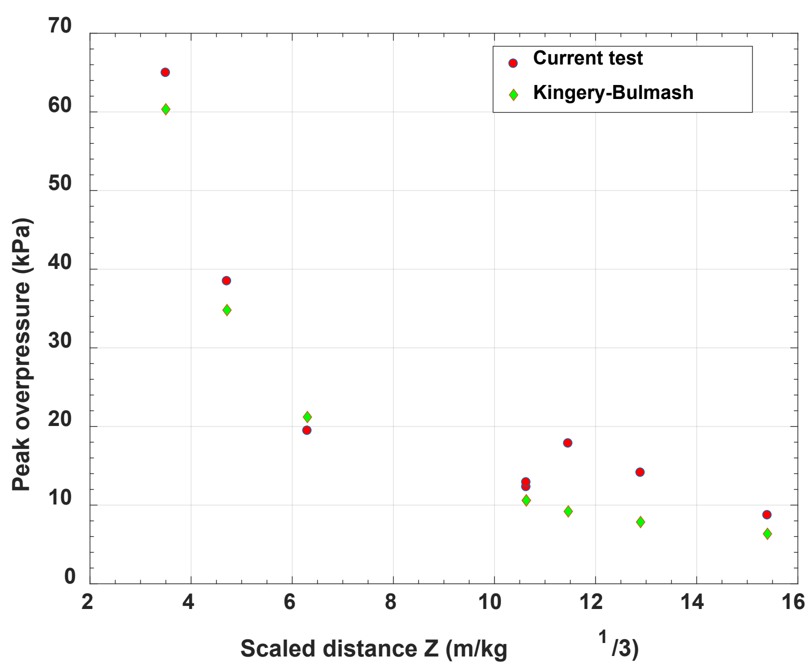

Figure 5.27 Measured and Kingery-Bulmash peak overpressure measurements.

5.8.2 Response of OSB Wall under Blast Loading

The response of the OSB wall was examined under blast loading in free-air. The standoff distance between the TNT charge and the wall was 3.0-meter. Two charges were 0.15-kilogram,and 0.34-kilogram and were detonated by Colorado State University (CSU) explosive experts. The charge is the same as in the free-air blast pressure test. Shock acceleration and free-air blast pressure behind the wall were measured. Three trials were performed, then the instruments were removed from behind the wall and destructive tests conducted using 0.34-kilogram of TNT charge placed right in front of the wall. The test setup is shown in Figure 5.28. Figures 5.29, and 5.30 show the pressure-time profiles of the generated blast shock wave of the two ICP® pencil probes (P1, and P2), respectively.

Figure 5.28 OSB wall blast test setup.

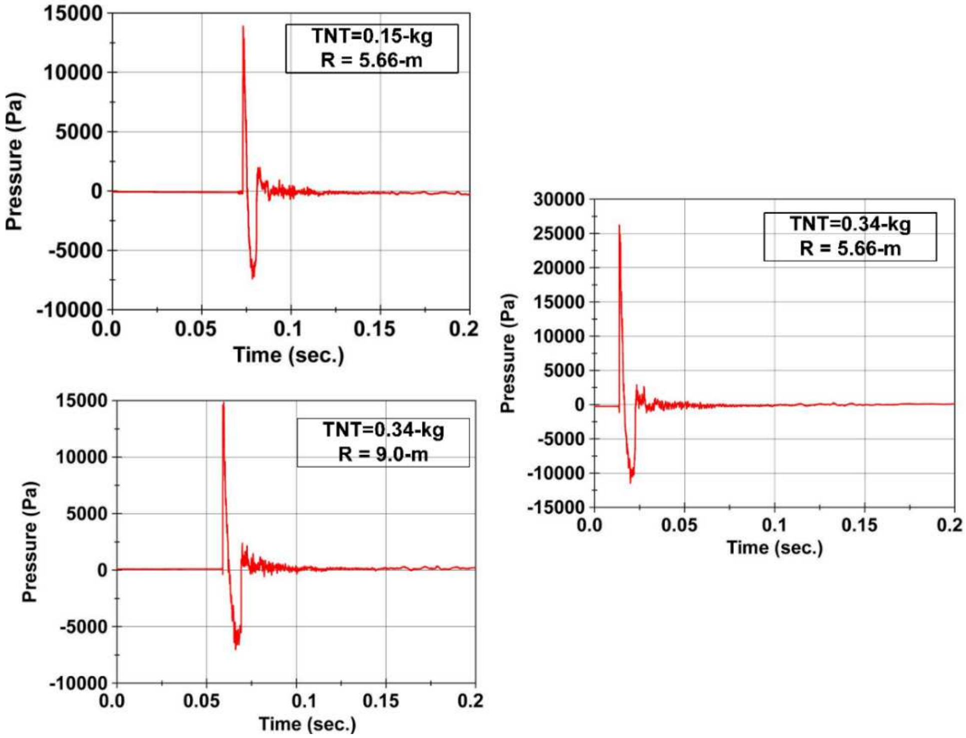

Figure 5. 29 Measured pressure-time profile of blast shock wave behind OSB wall-Probe 1.

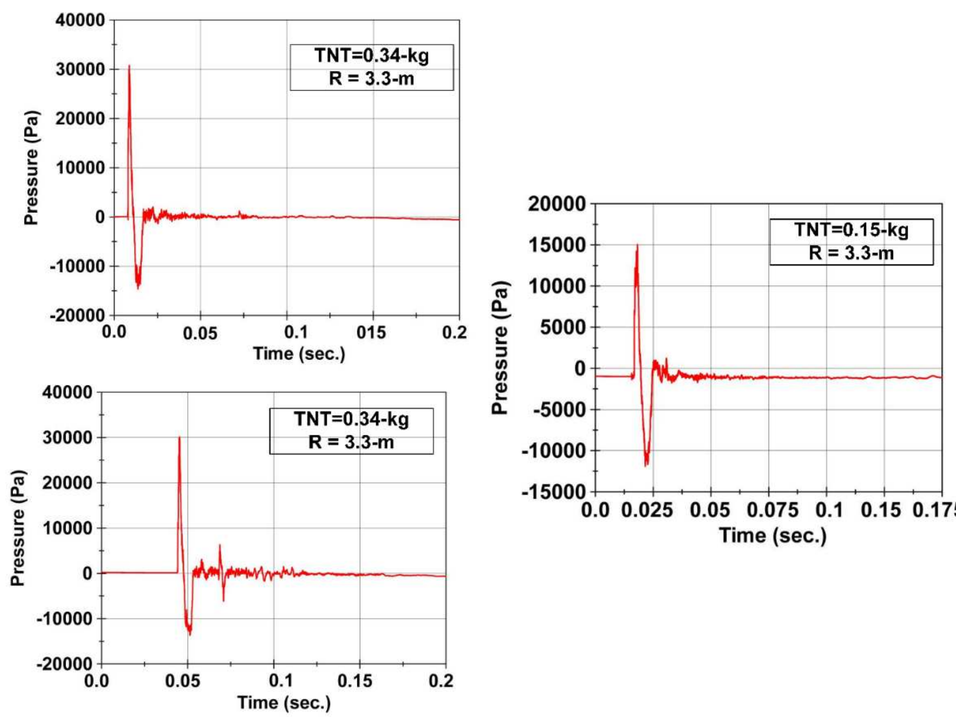

Figure 5.30 Measured pressure-time profile of blast shock wave behind OSB wall-Probe 2.

The measurements of the air-blast pressure distribution behind the OSB wall gave a clear idea about the efficiency of simple blast walls in blocking and reducing a threat from high-explosives bursts. For the current test, the presence of a thin sheet of OSB wall reduced the blast pressure by 22 percent for probes positioned just behind the wall. This type of wall could help prevent injuries/casualties from shrapnel/debris in several attack scenarios. The experimental results were verified with numerical model results of ABAQUS/Explicit software. Figure 5.31 shows numerical model details of the OSB wall.

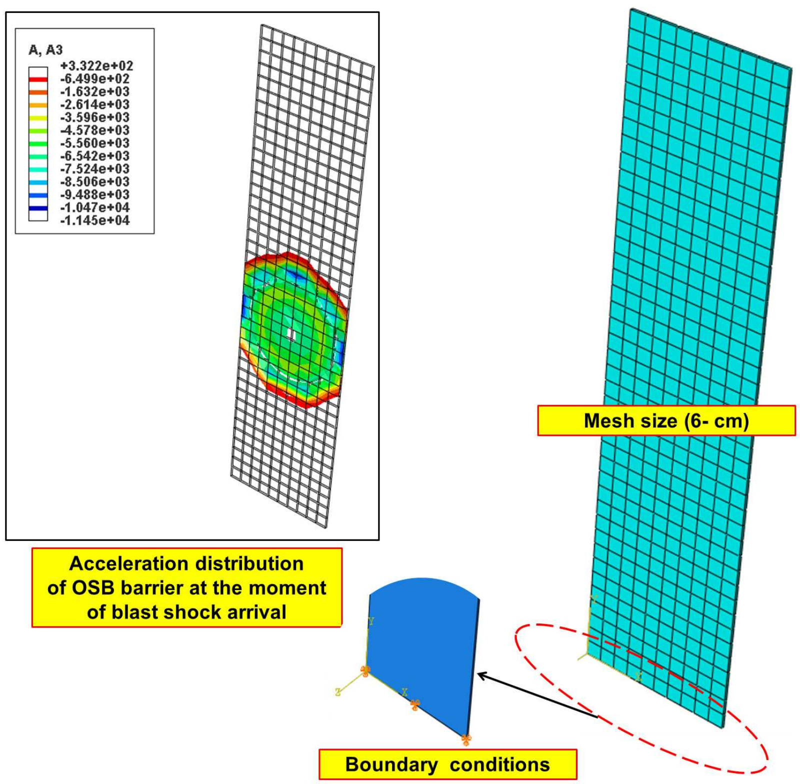

Figure 5.31 Mesh, boundary condition and acceleration distribution of OSB wall.

The numerical and measured time-histories of out-of-plane accelerometer A1 (at the center of the OSB wall), and A2 (at the top corner of the OSB wall) are shown in Figure 5.32 a, b, c, d, and 5.33 a, b, c, d, e, and f, respectively. Summary of the peak accelerations is listed in Table 5.11. Good agreement, in terms of the acceleration peaks, between the measured and numerically computed accelerations is seen. The peak of shock acceleration at the center of the wall is larger by 60 percent than its value at the corner. The peak acceleration increased by 50 percent when the size of the charge increased by 75 percent.

Table 5.11 Measured and calculated peaks of acceleration of OSB wall.

Accel. #	Distance (m)	TNT (kg)	Peak acceleration (Numerical)-(g)	Peak acceleration (Test)-(g)	Difference (%)
A1	3.0	0.15	827.14	791.26	4.48
A2	3.0	0.15	515.21	430.53	17.91
A1	3.0	0.34	1105.17	1321.90 (Avg.)	17.86
A2	3.0	0.34	598.48	689.61(Avg.)	14.15

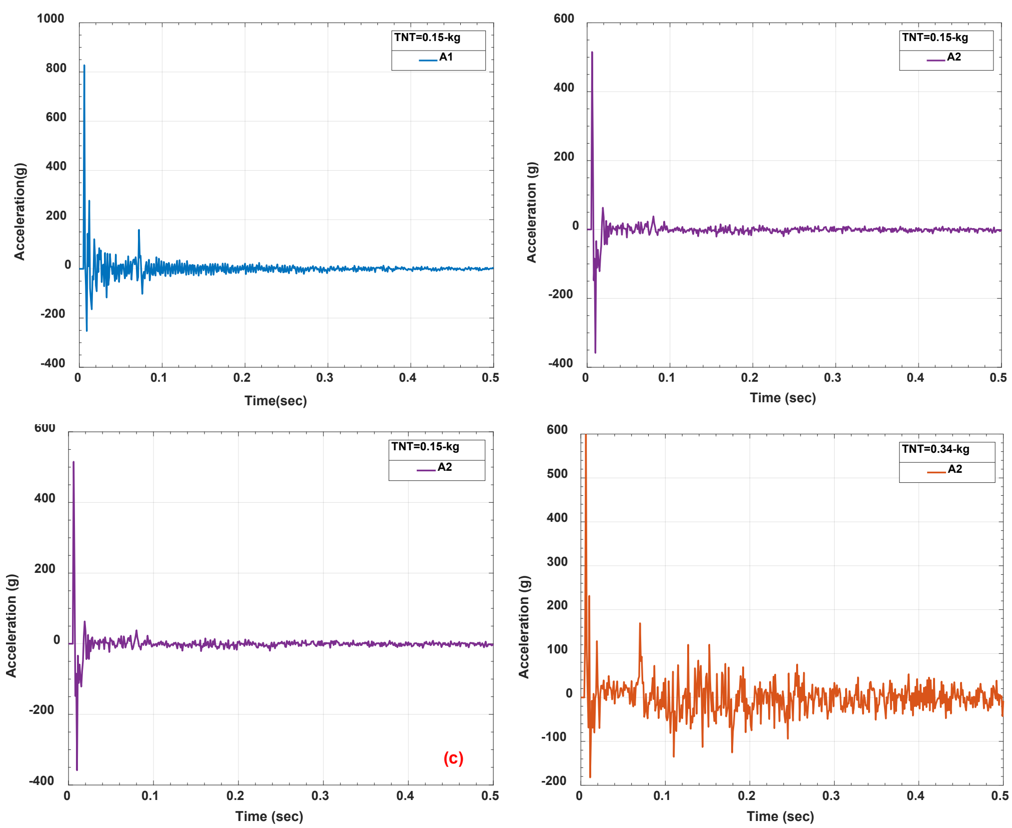

Figure 5.32 Numerical results of out-of-plane acceleration of OSB wall.

The measured peak acceleration of the wall is in good agreement with the ConWep predictions within ABAQUS. The recorded acceleration signal distorted slightly due to loss of connection between the wall and the wooden frame because of the exposure to the blast shock wave multiple times (see Figure 5.33, e). Figure 5.34 shows the damage to the OSB wall from placing 0.34-kilogram of TNT just in front of it. The shrapnel found at 100-meter from the location of the wall and almost nothing left from the wall.

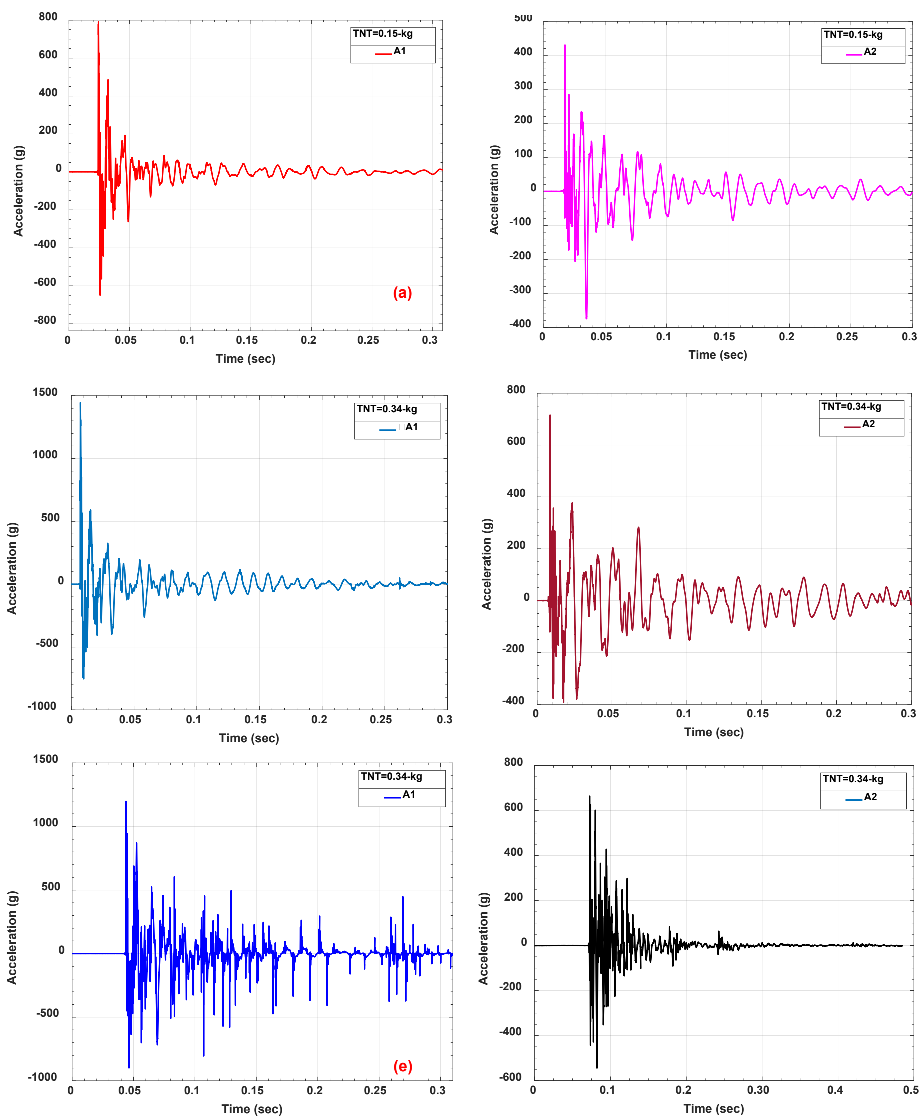

Figure 5.33 Measured-out-of-plane acceleration of OSB wall.

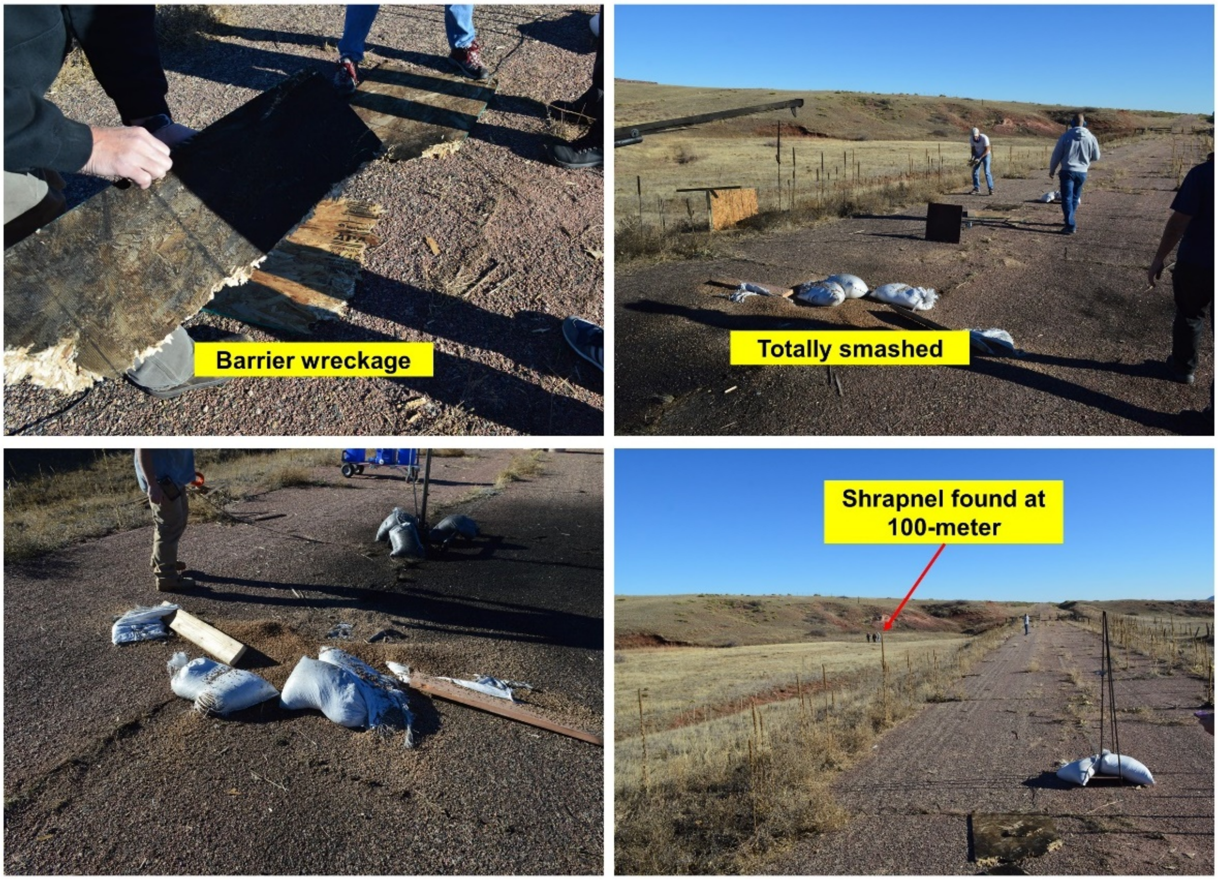

Figure 5.34 OSB wall collapse.

5.9 Blast Shock Wave Energy Distribution Test

Free-air blast test was conducted in December 2017 at the CSU blast field-Laporte site to evaluate the air-blast pressure differentiation in front and back side of the charge. The main goal was to obtain an idea on the distribution of blast shock wave pressure that represents having suicide vest attack scenario (non-symmetric charge). The DETASHEET® flexible explosive charge of C1 (5-cm x 7.63-cm) was used along with 60-cm of detonating cord. The equivalent TNT mass of this charge is equal to 9.96-grams. The test setup is shown in Figure 5.35.

From the recorded pressure measurements, the peak overpressure in the front direction of blast shock is double its value in the opposite direction as shown in Figure 5.36. Good agreement with the Kingery-Bulmash measurements of peak overpressure is noted, considering the nature of the charge (see Figure 5.37). According to the test measurements, the distribution of blast shock wave energy is not even in all directions. This can explain why some victims have survived from explosion incidents even though they were at close range from the source of the explosion, while serious casualties at far distances from explosion source were recorded.

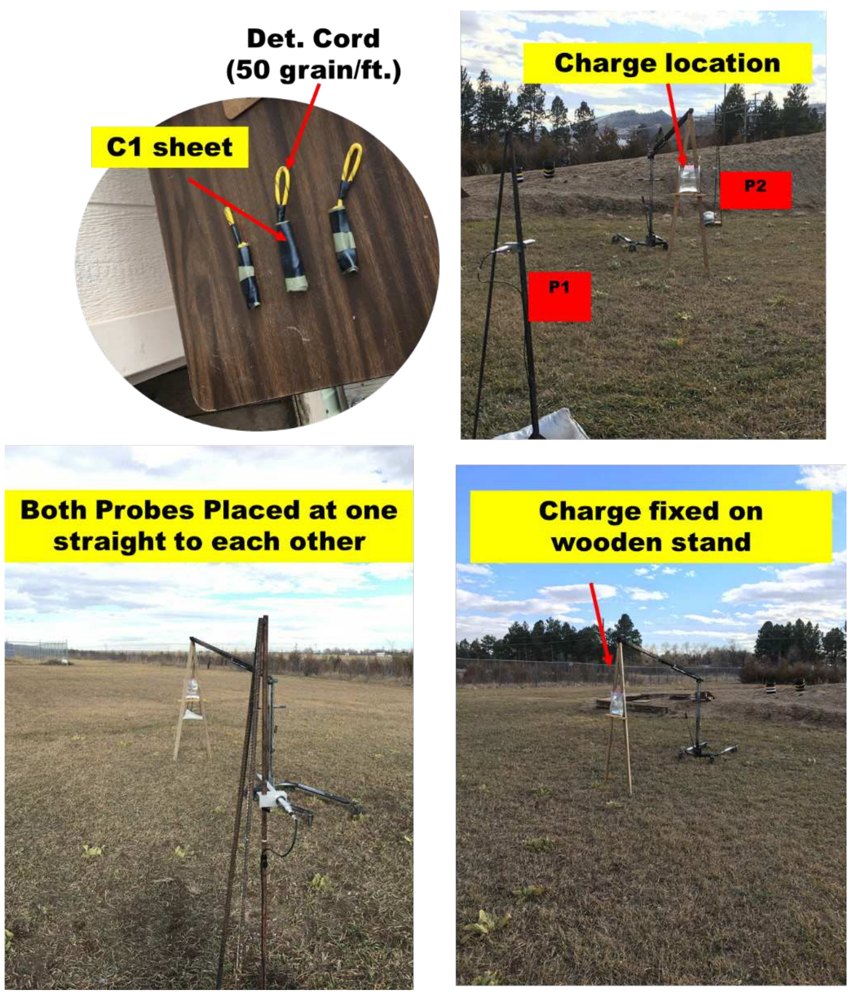

Figure 5.35 Blast shock wave pressure distribution test setup.

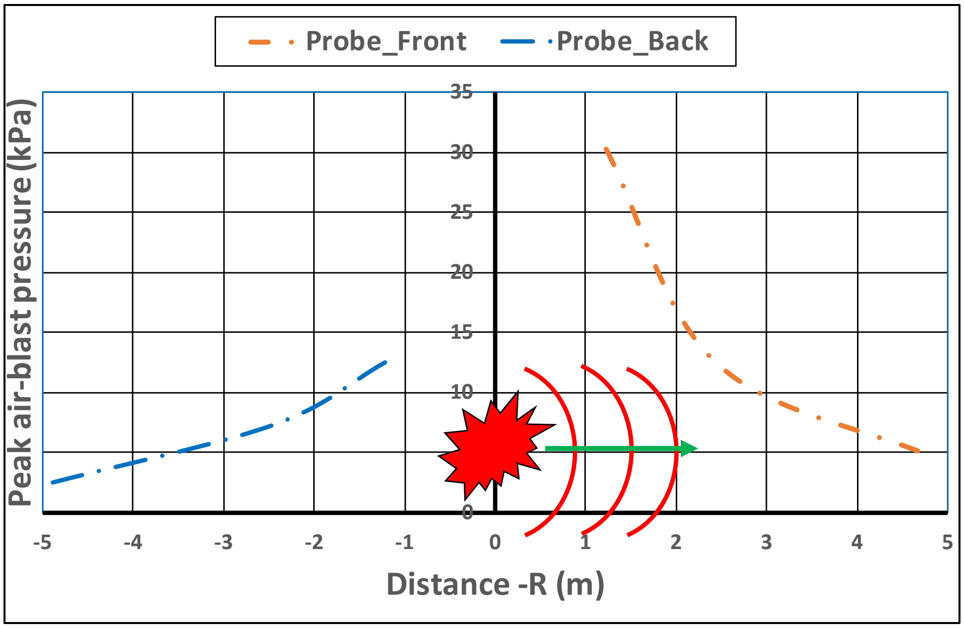

Figure 5.36 Measured Peak overpressure.

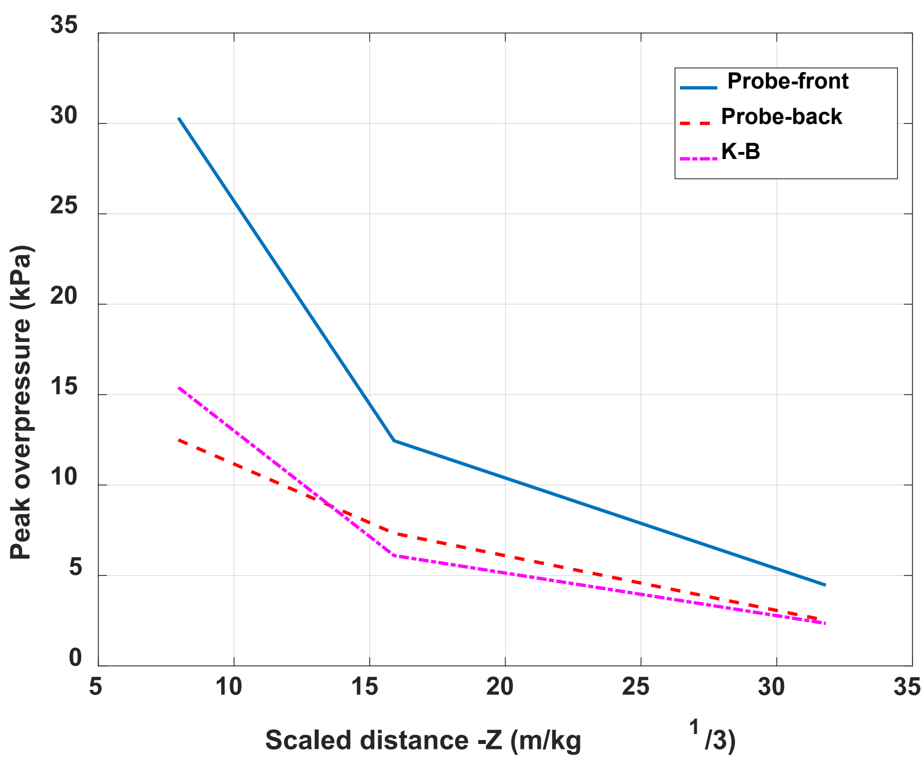

Figure 5.37 Measured peak overpressure versus Kingery-Bulmash measurements.

5.10 Blast Shock Wave Effect on Eardrum-Experimental Study

5.10.1 Introduction and Background

Exposure to blast shock wave directly without protection could lead to serious injuries to organs and tissues. Information about the direct effect of air-blast pressure on the human body is limited and not often available due to uncertainties in the exact charge weight and safe distance from the source of the explosion (Richmond, Yelverton, & Fletcher, 1986). The direct effects of the blast shock wave are available from animal's tissue tests (Richmond et al., 1986). These effects have been investigated on sheep tissues for three categories of blast duration: short, intermediate, and long (Richmond, Damon, Fletcher, Bowen, & White, 1968). Detailed work on human blast injuries from exposure to 1.6-kilograms of explosive charge confirmed that the adopted criteria of animal tissue test is accurate and valid (Hamit, Bulluck, Frumson, & Moncrief, 1965). Ear and eye can be subjected to high pressure from an explosion causing severe injuries.

Eardrum rupture is one of the main injuries due to blast shock wave and could lead to temporary or permanent hearing loss (Choi, 2012). The ear is an organ transduces a sound wave to hearing nerve. The eardrum has a sensitive membrane and high level of pressure/loud sound can cause a tear in the eardrum. The internal view of the tympanic cavity is shown in Figure 5.38. The blast shock wave impacts the sensitivity of the ear to low tones (10-30 dB), as well as high tones (40-80 dB) (Hirsch, 1968). The threshold of rupturing eardrum due to blast shock wave is 34.5 kPa (5 psi), while 103.4 kPa (15 psi) level of pressure increases the percentage to 50 percent (UFC3-340-02, 2008). Several clinics have reported victims with temporary loss in hearing for hours or weeks from experiencing explosion incidents (American College of Emergency Physician, 2017). The victims required medical treatment for long and/ or short periods ("Understand blast Injury", 2018).

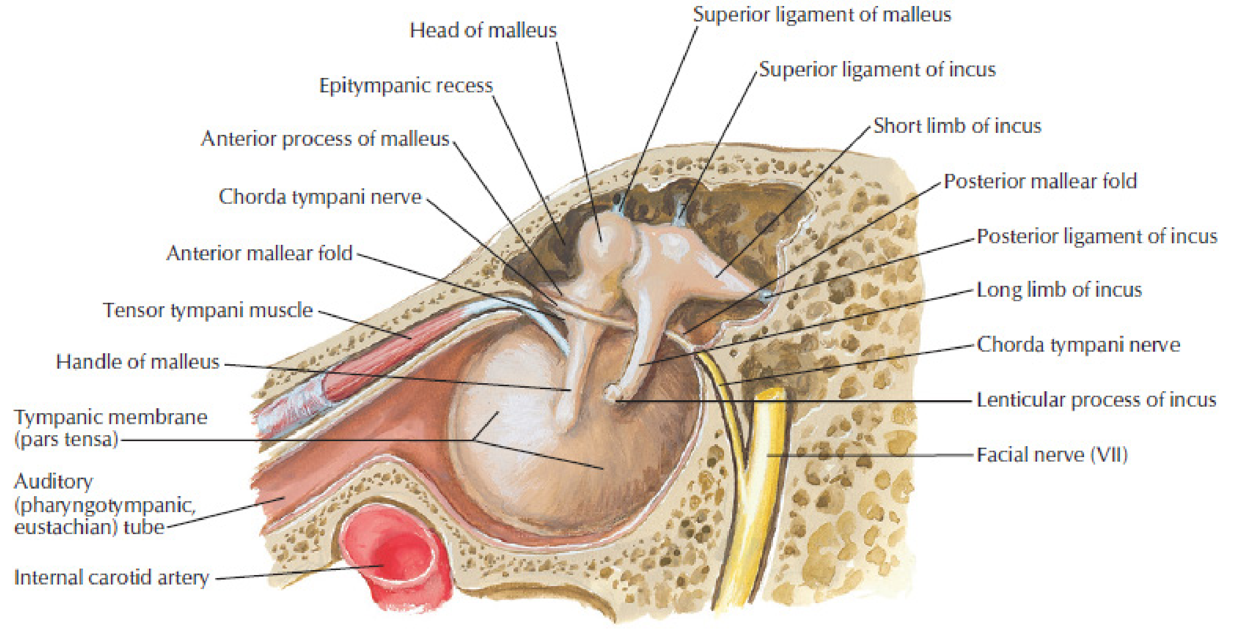

Figure 5.38 Internal view of the tympanic cavity (Frank,2014).

There is a relationship between the maximum pressure and impulse, and the probability of eardrum rupture. This relationship is listed in Table 2.1 and presented graphically in Figure 5.39 (UFC 3-340-02,2008). Primary and secondary blast injury recorded by clinics due to the blast shock wave. The primary ear injuries resulted from peak overpressure and visual inspection in some cases is enough to evaluate the harm, while extensive and deep examinations are required to check the rupture of the eardrum (American College of Emergency Physician, 2017). In this study, eardrum samples of sheep were tested to evaluate the damage level of the eardrum from being subjected to blast shock wave generated from high-explosive detonation.

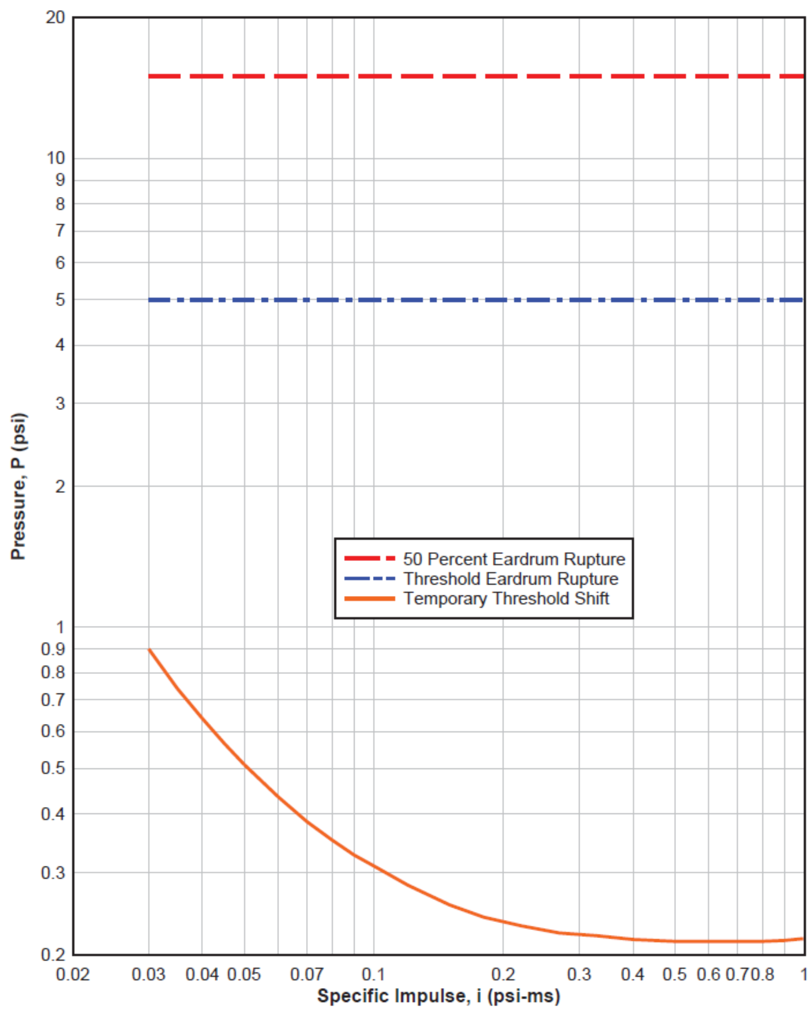

Figure 5.39 Pressure-impulse curves of eardrum rupture (UFC3-340-02, 2008).

5.10.2 Experimental Test of Animal Tissue

The framework of the animal tissue test included six trials with different standoff distances. The main goal was to evaluate the damage to the eardrum of the sheep. Pressure probe #3 was used to examine the air-blast pressure differentiation of the measurements. The first two trial tests were to measure air-blast pressure generated from blast cap at a certain distance from the source of the explosion as shown in Figure 5.40.

The measured air-blast pressure of the three pressure probes (P1, P2, and P3) are shown in Figure 5.41.

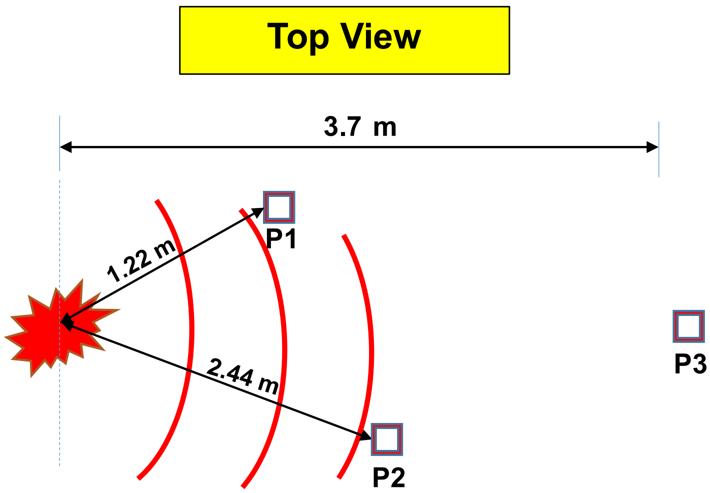

Figure 5.40 Blast cap test setup.

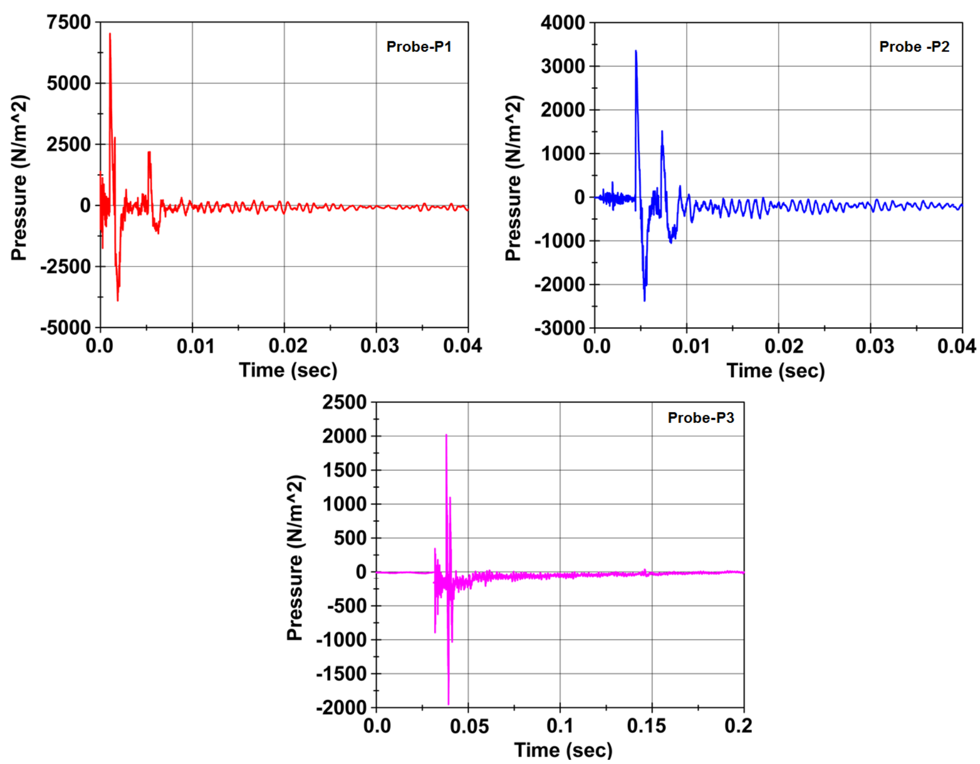

Figure 5.41 Measured pressure-time profile of blast shock wave generated from a blasting cap.

Five Rambouillet-Columbia sheep head samples were provided by the College of Veterinary Medicine & Biomedical Sciences at Colorado State University (CSU) were used in this test. These heads were subjected to air-blast pressure with either right or left ear facing the direct blast shock wave as shown in Figure 5.42, generated from the detonation of DETASHEET® flexible explosive charge of C1 (5-cm x7.6-cm) along with 30-cm of detonating cord. This charge is equivalent to 3.3-grams of TNT. The sheep heads were positioned to ensure that the auricle (Pinna) was subjected directly to blast shock wave.

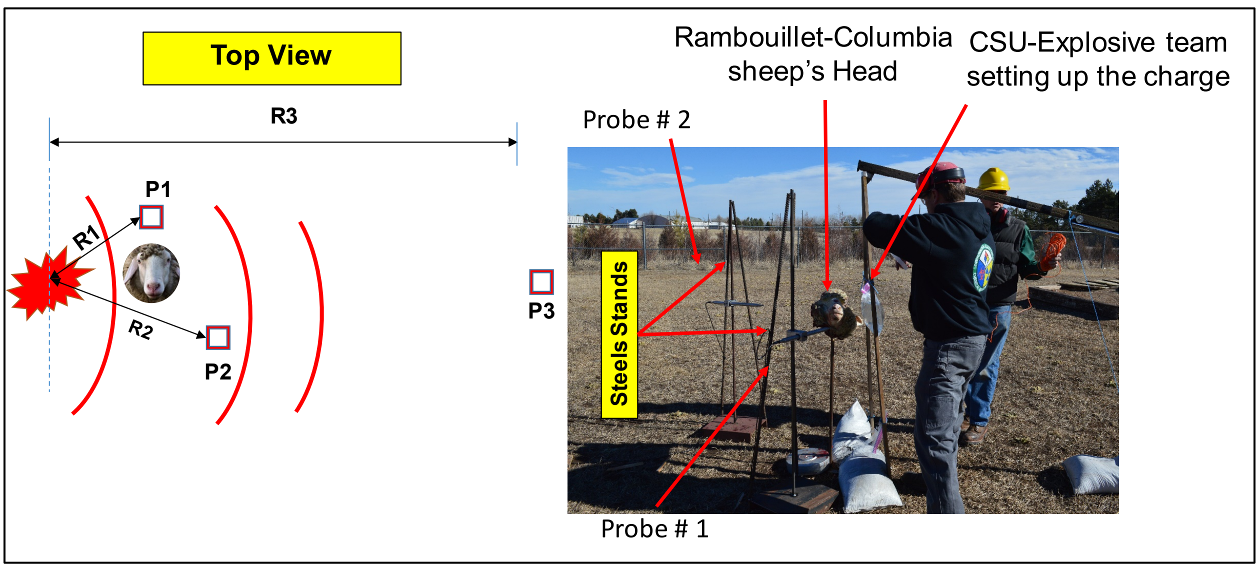

Figure 5.42 Animal tissue blast test setup.

The measured air-blast pressure of the probes (P1, P2, and P3) of the five trials are shown in Figures 5.43, 5.44, 5.45, 5.46, and 5.47, respectively. These air-blast pressure measurements were taken at the tip of the pencil probes and the pressure values were very close to applied blast pressure on the animal tissue.

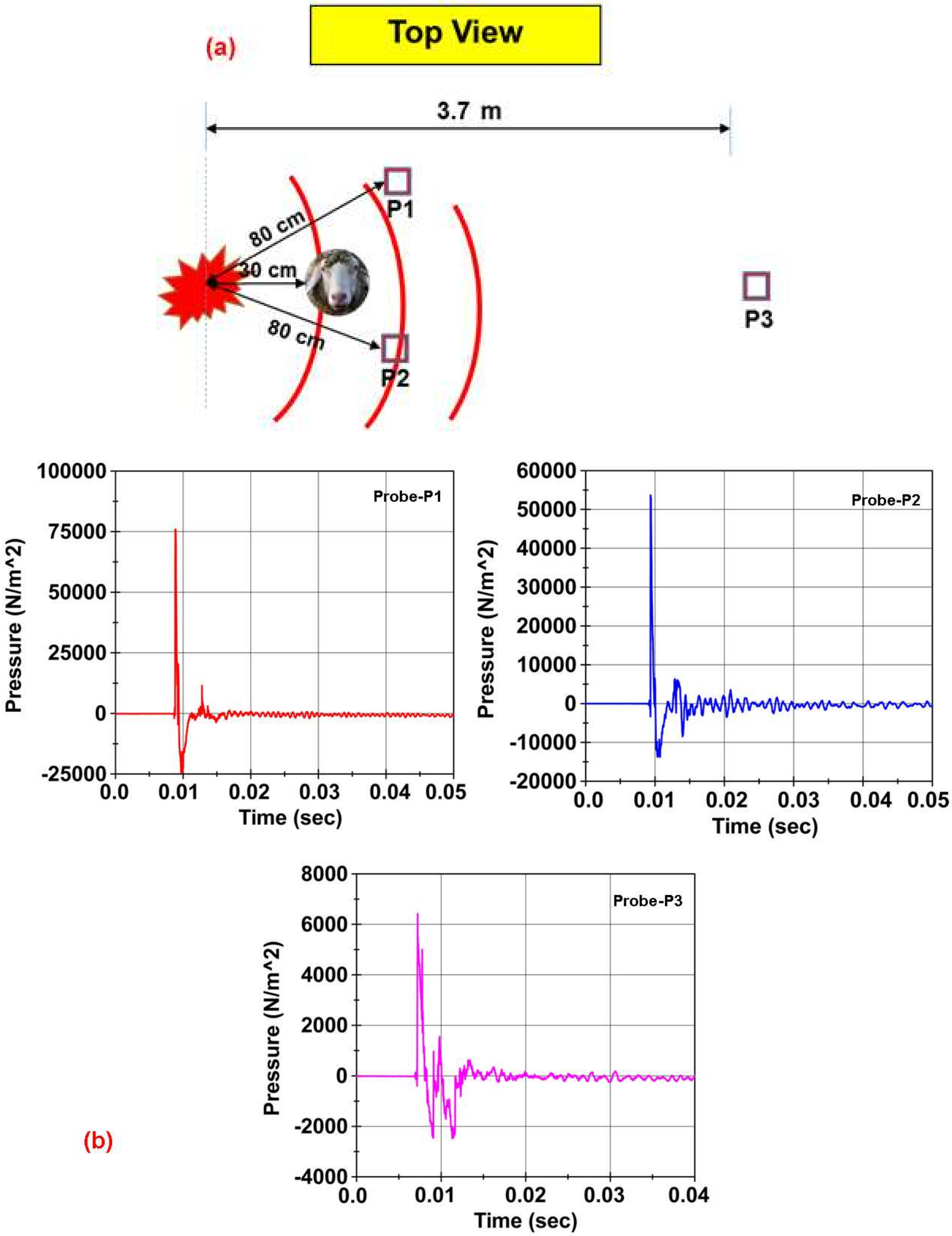

Figure 5.43 a. Animal tissue test setup b. measured blast pressure-time profile-Trial #1.

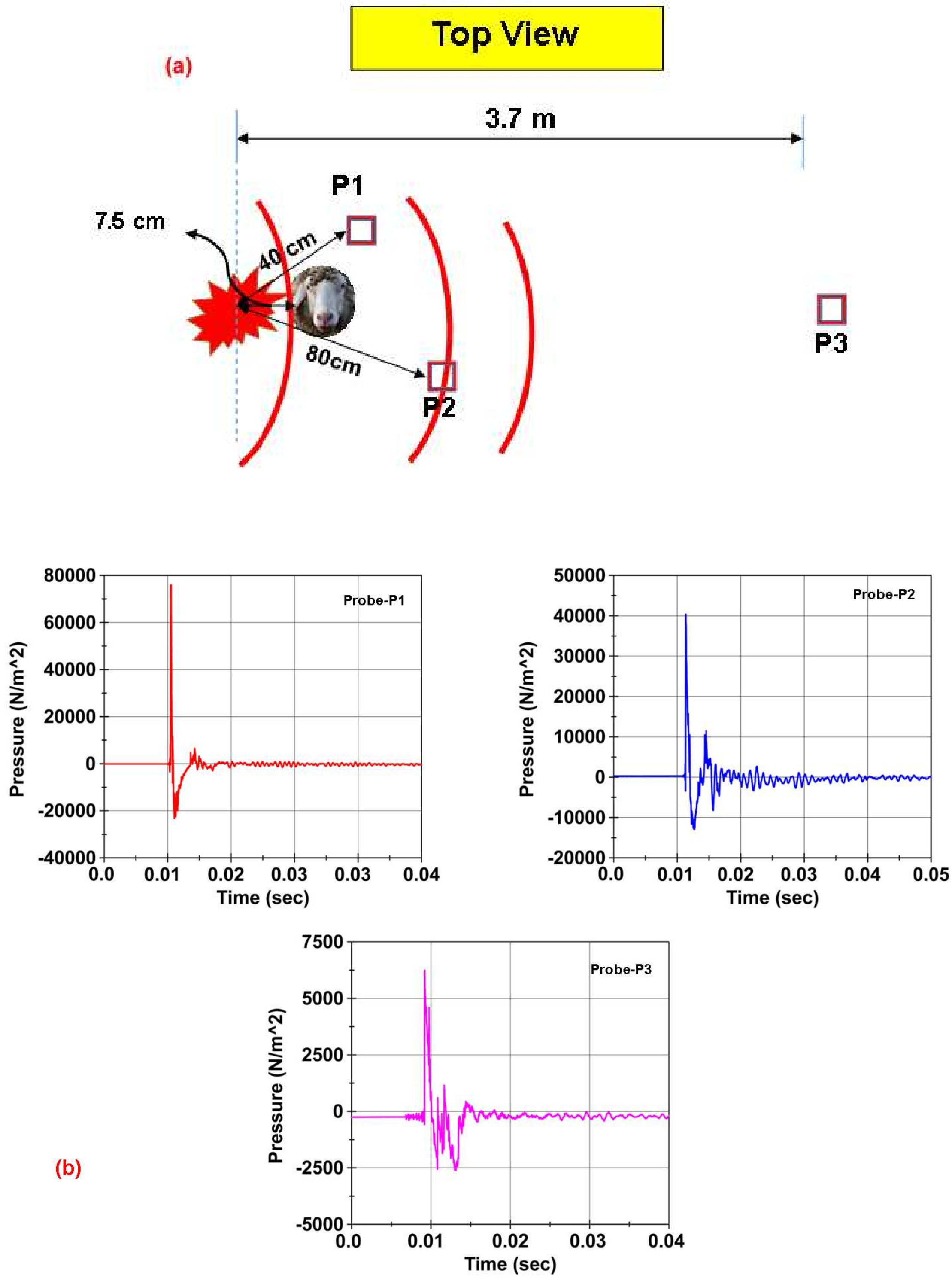

Figure 5.44 a. Animal tissue test setup b. measured blast pressure-time profile-Trial #2.

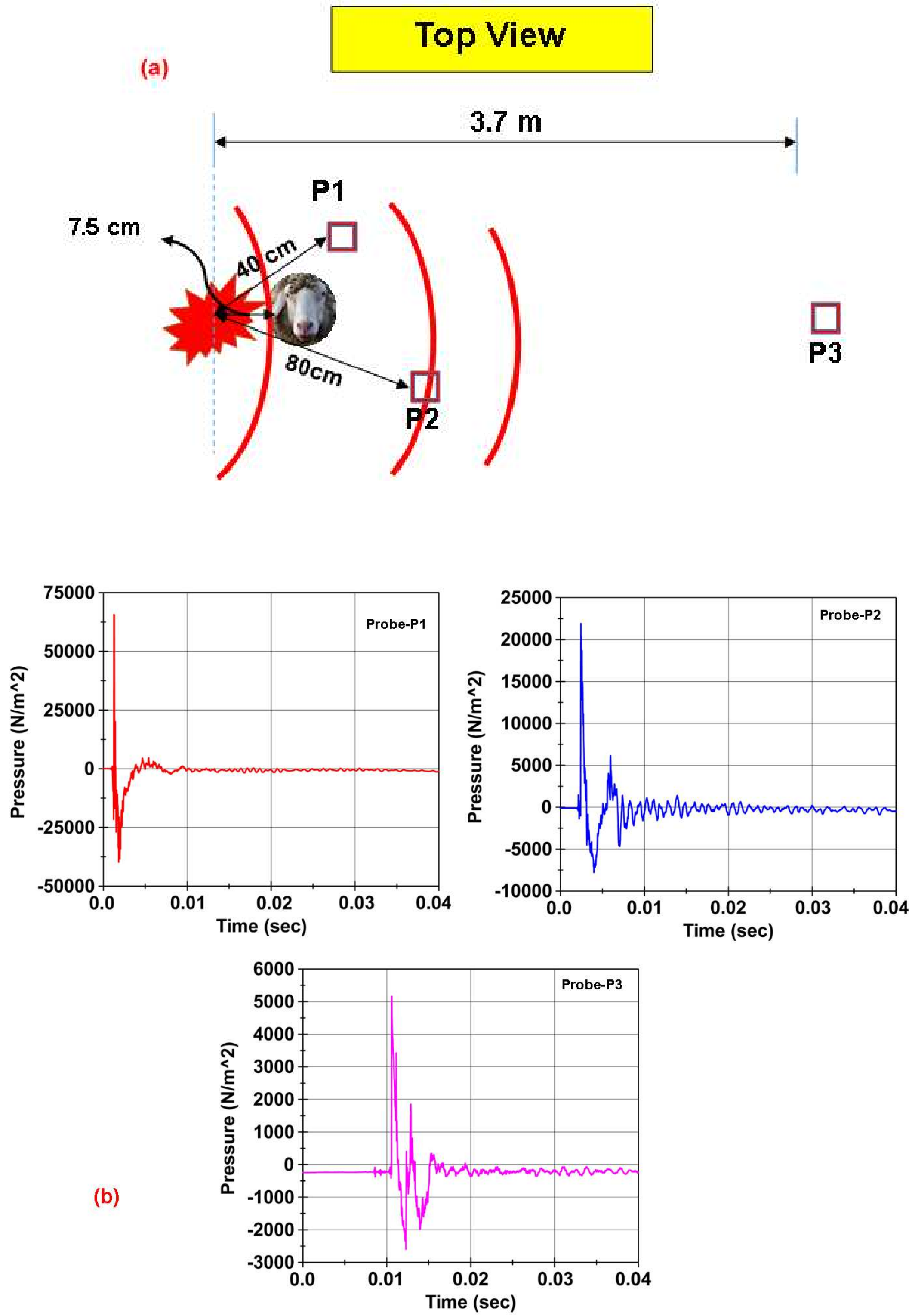

Figure 5.45 a. Animal tissue test setup b. measured blast pressure-time profile-Trial #3.

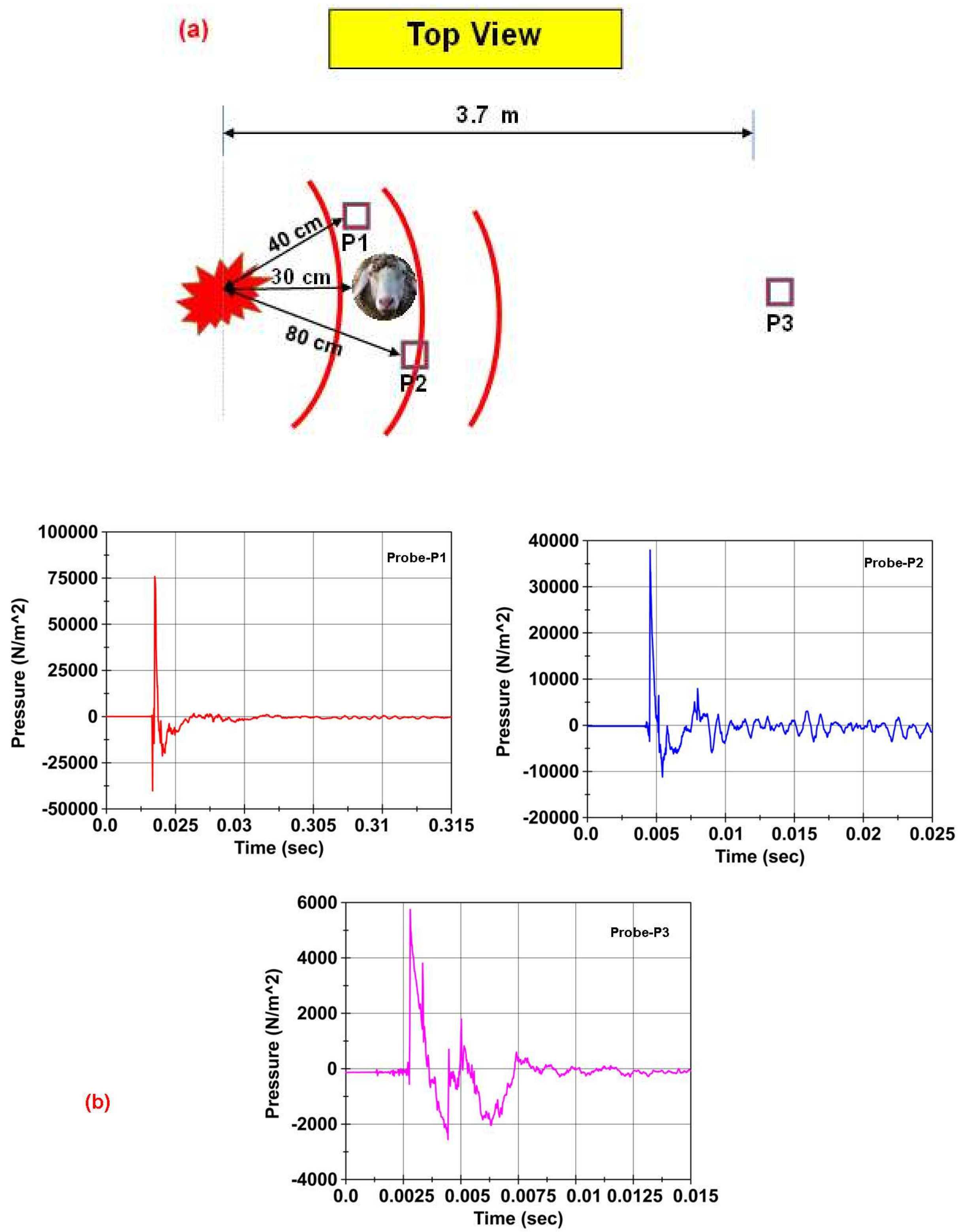

Figure 5.46 a. Animal tissue test setup b. measured blast pressure-time profile-Trial #4.

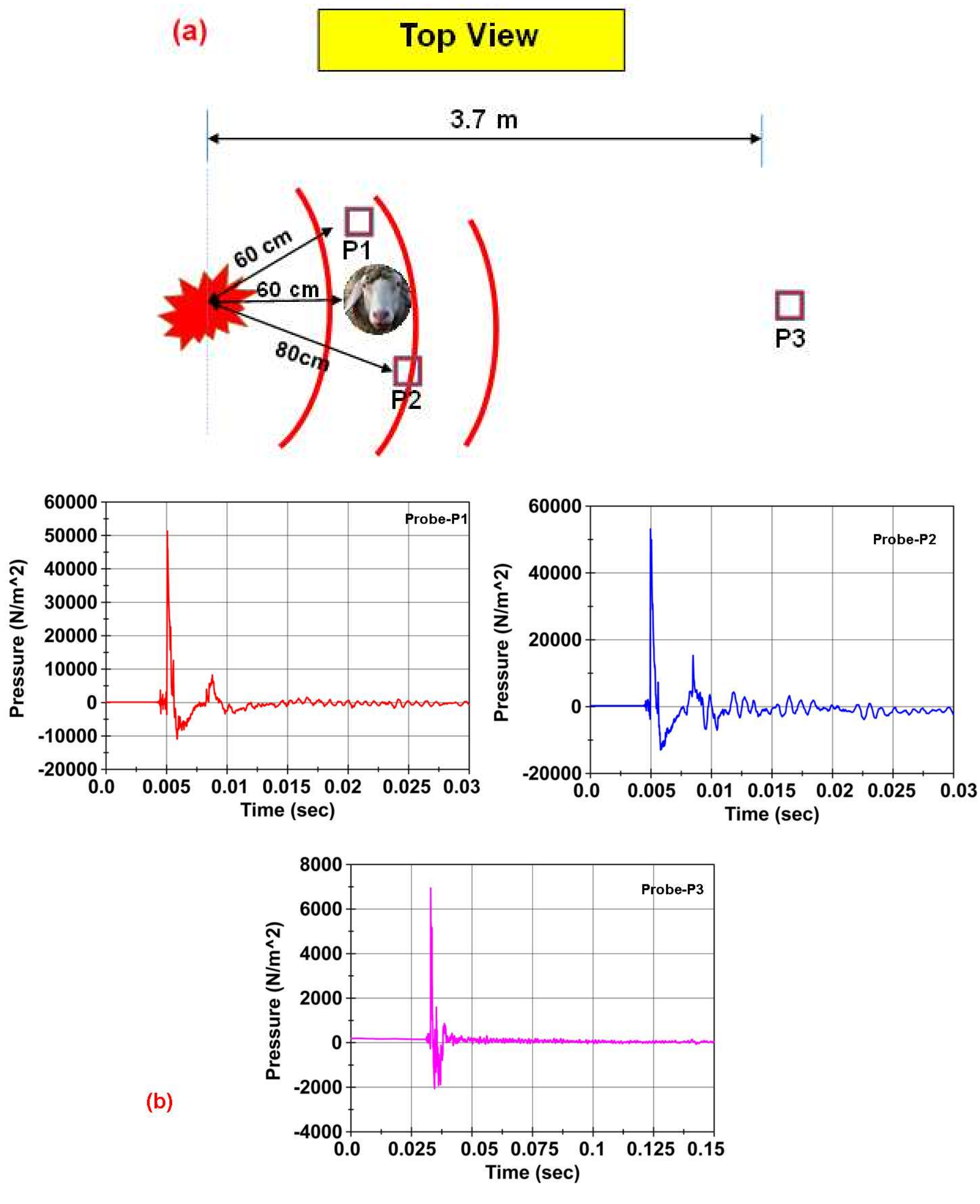

Figure 5.47 a. Animal tissue test setup. b. measured blast pressure-time profile-Trial #5

5.10.3 Dissecting procedure of the eardrum

Previous studies found large similarity between sheep and human ears structure except for the size of the human ear is smaller (Seibel, Lavinsky, & Irion,2006). Dissecting ears is unusual since it requires declassification of part of the skull bone. The procedure of dissecting started by cutting through the skull bone and removing part of the external ear to reach the tympanic membrane (eardrum) using an electrical band saw. The removing of the skull bone required a heavy-duty band saw, which was not available at the Orthopaedic Bioengineering Research Laboratory (OBRL). The specimens were dissected at the Veterinary and Teaching Hospital of Colorado State University (CSU). Thereafter, the specimens were moved back to OBRL lab to remove undesired tissues/bone around the ears and imaging them by micro-CT scanner as shown in Figure 5.48, a. The left and right ear samples were ready for micro-CT scanner as shown in Figure 5.48 b, and c.

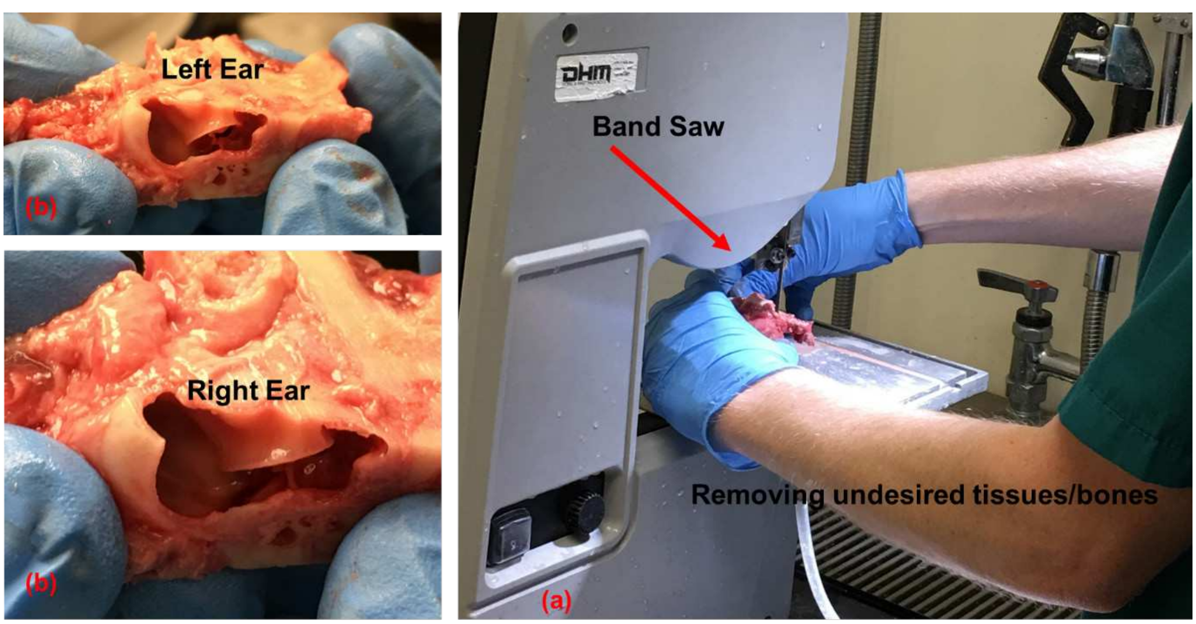

Figure 5.48 a. Removing undesired tissue. b. left ear c. right ear.

According to the way in which the head of the sheep was positioned in the tests, in some test attempts, the right ear was exposed directly to blast shock wave, while the one on the left side was not and vice versa. The effects of the blast shock wave on tested sheep heads were based on the level of pressure which is also related to charge mass and the distance to the explosion source. From visual inspection, it can be seen that the ear cartilage was totally burned, and an extensive section of skin was completely torn off the underlying tissue as shown in Figure 5.49 a. Figure 5.49, b, shows rupture and inflation of the eye globe. Due to challenges in investigating the damage of the eyes under blast shock wave, the current study was focused on eardrum rupture. These injuries of animal tissues can give a clear view about the expected casualties/injuries to the victims who may be subjected to a severe blast shock wave. The fixation process included placing the ear specimens in formalin solution to preserve eardrums tissues permanently in a life state condition as possible.

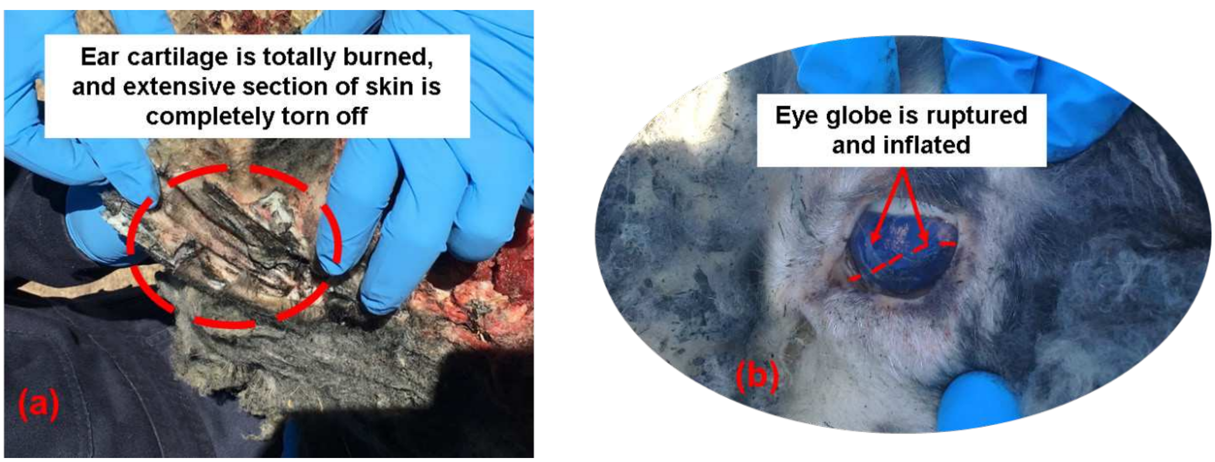

Figure 5.49 Visual inspections results a. Ear cartilage injury. b. Eye globe injury.

The dissecting was performed to delineate the damaged and undamaged eardrums using micro-CT 80 Scanco® scanner as shown in Figure 5.50. This instrument was used as a tool to measure, visualize and quantify the structure of the eardrums. The specimen was fitted inside the holder to prevent holder damage and get accurate measurements. The micro-CT scanner can perform three and two-dimensional tomographic assessment for different regular and irregular geometric shapes of specimens. The system specifications are shown in Table 5.12.

Figure 5.50 Micro-CT 80 Scanco® scanner (*Palaeo-electronica Electronica* ,2018).

Table 5.12 System specifications of the micro-CT 80 Scanco Medical.

Specifications	Range
Peak energy	30-80 kVp
Max. scan diameter	36.9 mm
Max. scan length/height	80 mm
Automatic sample changer option	Up to 10 holders
Resolution (Norm./10%MTF)	3-72 μm / < 8 μm
Minimal scan time per stack	2 min
Image matrix	512 x 512 – 4096 - 4096

The computed tomography (CT) can represent a view of a cross-section through the eardrum specimens. As other normal (medical) x-ray, denser materials (tissue/bone) absorb more x-rays than soft tissue. Measurement of densities is just used for 3-D x-ray. The scanned images of the micro-CT scanner of the left ear are shown in Figure 5.51, a. The density measurement is shown in Figure 5.51, b. For instance, from the computed tomography images, the eardrum on the left side survived after being exposed to the blast shock wave. This decision was also made based on visual inspection.

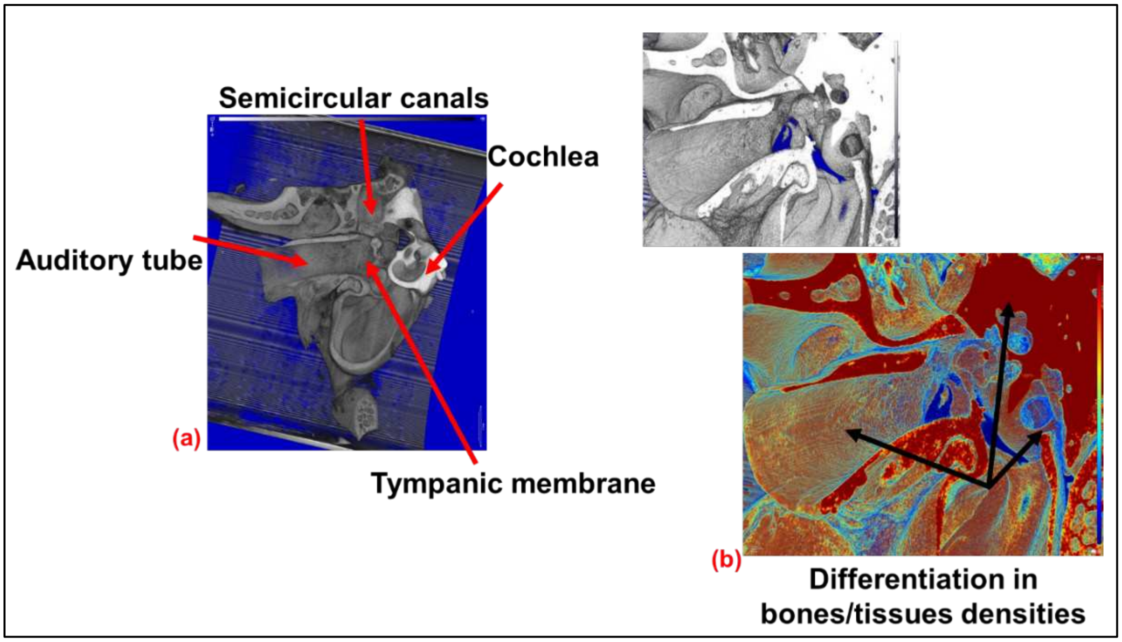

Figure 5.51 a. Micro-CT image of the left eardrum. b. density measurement of the eardrum.

According to the blast pressure measurements, the sheep eardrums was subjected to a maximum blast pressure of 75.9 kPa (11 psi). This means that the threshold for eardrum rupture was already surpassed and a 50 percent probability of eardrum rupture is expected (see Table 2.1). Three eardrums on the right side were ruptured, while only two samples on the left side were ruptured. There was uncertainty about the applied pressure on the ears on the opposite side of the blast wave direction. The summary of the tested ear samples results showed the main variables are the peak overpressure and the position to the blast shock wave as shown in Table 5.13. Moreover, the results of the micro-CT images showed the structure of the eardrum is totally ruptured as shown in Figure 5.52 and Figure 5.53. The probability of temporary hearing loss injury could take place at a level of pressure less than the threshold (see Figure 5.39), which can be considered the starting point of eardrum rupture (UFC 3-340-02).

Table 5.13 Summary of the eardrums condition.

Test Trial	Ear labels	Probe1 Pso (kPa)	Probe 2 Pso (kPa)	Ear condition
1	1L	75.9	53.67	Ruptured
	1R			Intact
2	3L	75.9	40.4	Ruptured
	3R			Ruptured
3	2L	65.72	21.9	Intact
	2R			Intact
4	4L	75.9	37.94	Intact
	4R			Ruptured
5	5L	51.27	53.17	Intact
	5R			Ruptured

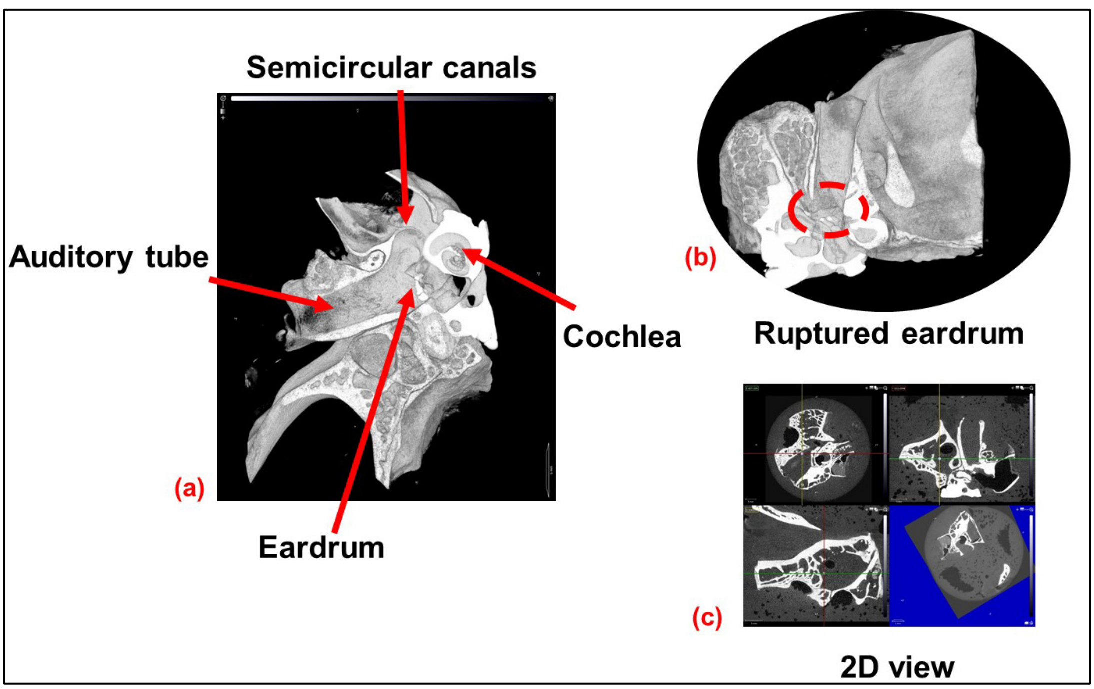

Figure 5.52 a. Micro-CT image of right eardrum. b. Ruptured eardrum. c. 2D view.

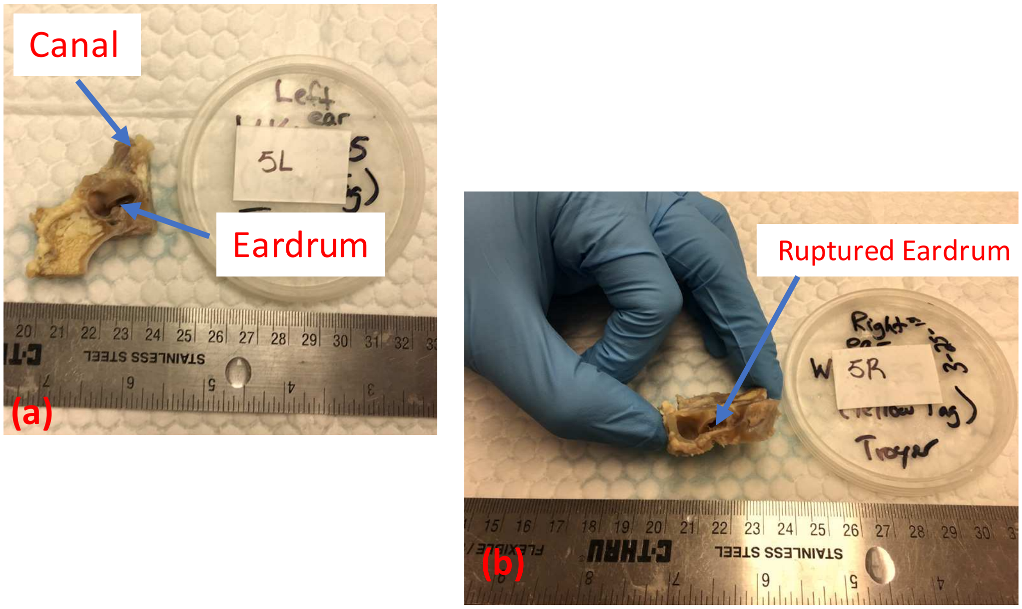

Figure 5.53 a. Intact left eardrum b. ruptured right eardrum.

5.11 Large-Scale Test of WSaW Blast Wall

5.11.1 WSaW Wall Construction and Test Setup

The large-scale blast field test was conducted in September 2018 at Maxwell Ranch site. The construction of the WSaW wall was done at the Engineering Research Center (ERC) - Structural Laboratory of Colorado State University, then it hauled to the blast test field. Due to a limitation in constructing a foundation at the site of the test, the wall is connected to the ground by a steel rigid connection system. The wooden frame of the WSaW was connected to a steel plate from the right and left sides thorough four stainless steel bolt grade 5 (medium carbon steel). The steel plate was welded to an angel, which was fixed to the ground using 16 rebars (#4). This system provided high stability to the wall and represented a fixed boundary condition of the bottom side as shown in Figure 5.54.

Setting up the WSaW wall at the test site included assigning the appropriate location for the wall so that the explosive charges can be set up, determine the pressure positions/distances around the wall, and extending the sensors cables. Thereafter, the team started pouring the sand inside the wall, mounting accelerometers, installing probes, wiring the instruments, and setting up the explosive charge. Figure 5.55 shows the steps taken by the research team.

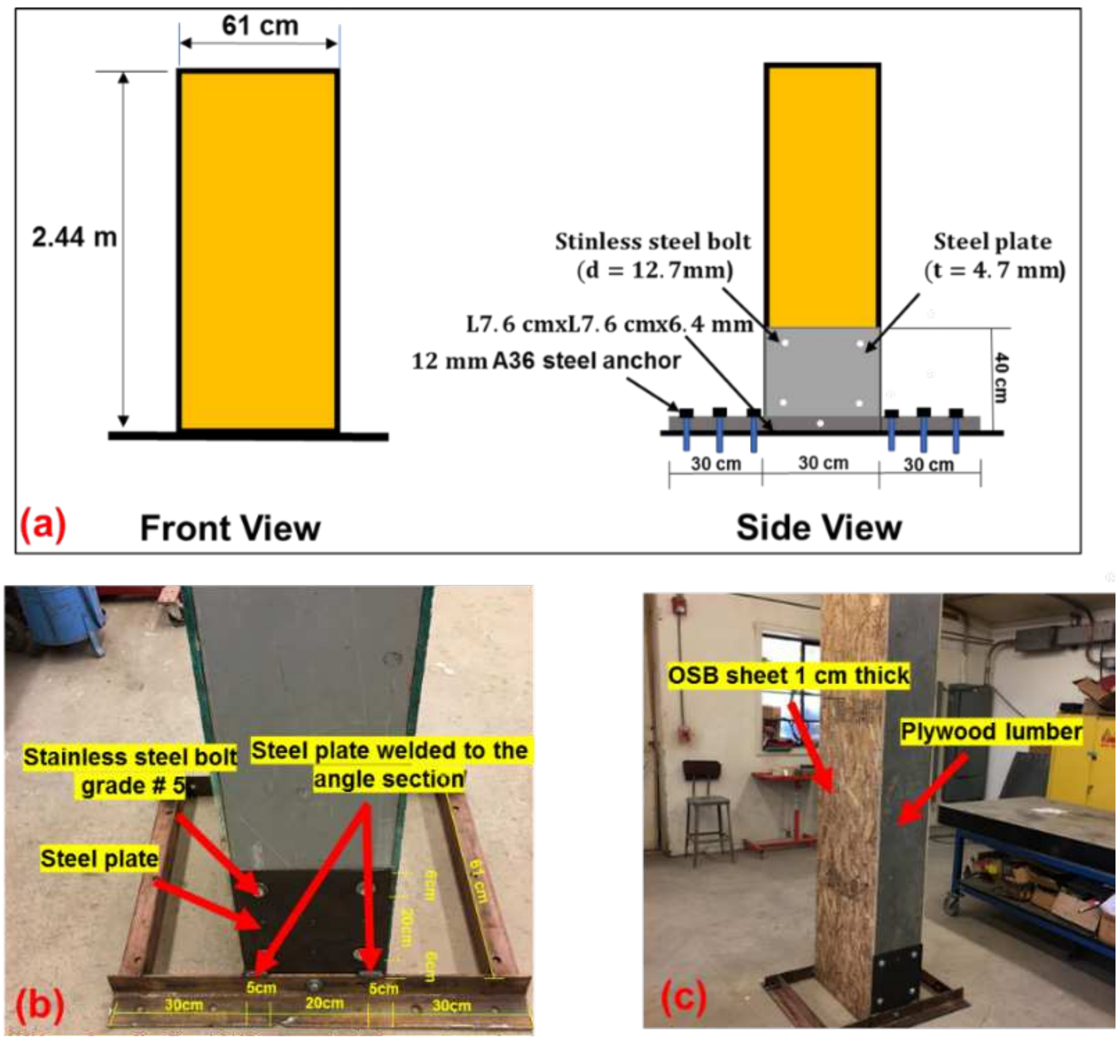

Figure 5.54 a. Schematic sketch of the WSaW wall b. connection system details. WSaW wooden frame.

Figure 5.55 WSaW blast wall test setup.

5.11.2 Particles Distribution and Classification of Sand

The used sample of sand was taken from a stock of sand outside of the ERC, then packed in sandbags (23 kg. capacity), and moved to the test field. Mechanical sieve analysis of the used sand was conducted at the geotechnical lab of the Civil and Environmental Engineering Department. The sieve analysis was performed according to the ASTM D-422 standard. The unit weight and moisture content of the sample were also determined. The aim from the analysis was to determine the particle size distribution. The particles distribution curve of the sand is shown in Figure 5.56. The unit weight of the sample was 1700 kg/m^3 and the sample was dry since the measured moisture content was 0.27%. From the sieve analysis results, the sand sample can be classified as well-graded sand (SW). The sample can also be classified as coarse sand since the fineness modulus was 3.6, which typically ranges from 2-4 for fine sand.

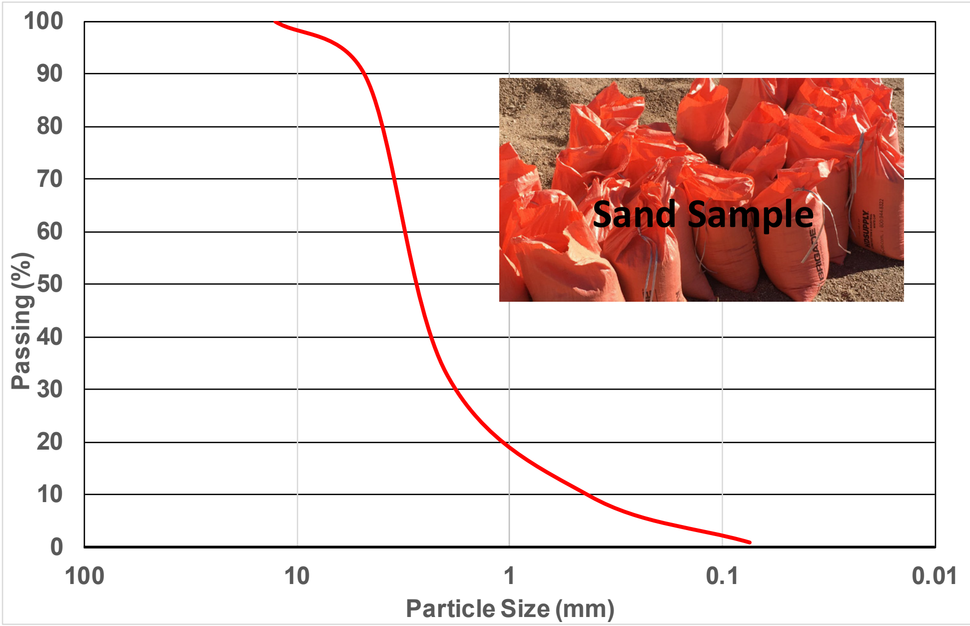

Figure 5.56 Particle distribution curve of sand sample.

5.11.3 Free-Air Blast Pressure Measurements

Free-air blast pressure was measured under blast shock wave generated from TNT charge detonation. The standoff distance between the TNT charge and the wall were 1.22,2.44 and 3.96-meter. Two TNT charges were used, 0.226, and 0.34-kilogram by Colorado State University (CSU) explosive experts. Air- blast pressure of generated blast shock wave is recorded by two ICP® pencil pressure probes (without wall). The detonation of the TNT charge presented typical blast phenomena in free air. The blast phenomena are illustrated in Figure 5.57 from start to finish.

The measurements of free-air blast pressure showed good agreement with Kingery-Bulmash model (UFC 3-340-02,2008), considering open space test affecting factors on the probes readings. The two probes (P1, P4) were moved to different standoff distances from the explosive charge to measure the air-blast pressure in open space, while probe P2 and P3 stayed at the same positions behind the wall to examine the reduction in the recorded air-blast pressure from the existence of WSaW blast wall. The measured peak overpressure versus the Kingery-Bulmash measurements in free air in terms of scaled distance is shown in Figure 5.58. It is noticed there were some variation between the recorded air blast pressure and the reference values from Kingery-Bulmash model especially for the measurements located in the scaled distance range (2.41 ≤ Z ≤ 4.44). Another important blast wave parameter was estimated and compared to the Kingery-Bulmash empirical model is the time of arrival (Ta). Figure 5.59 shows a comparison between the estimated values from the numerical analysis and the published values (UFC 3-340-02,2008).

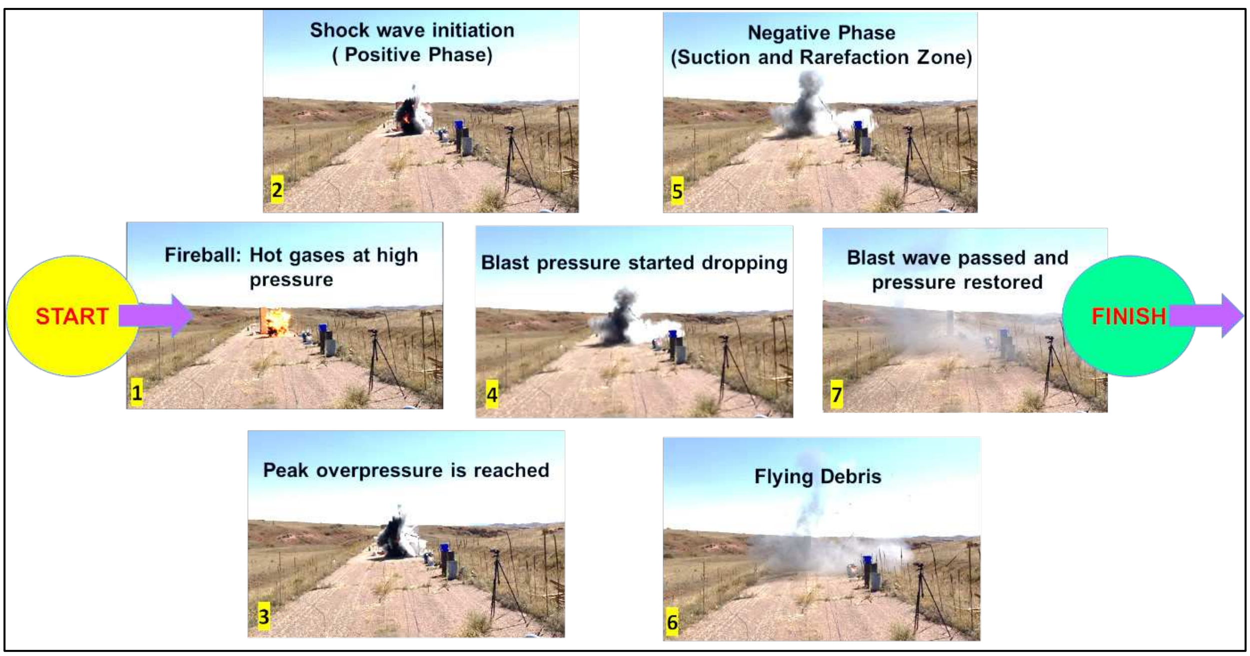

Figure 5.57 Blast wave phenomena in free air as recorded in the current Test.

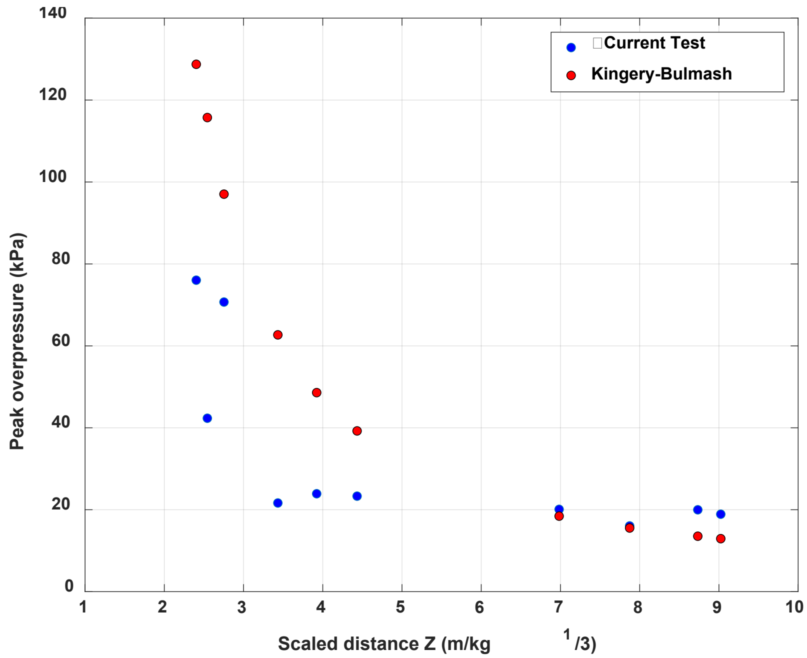

Figure 5.58 Measured peak overpressure versus Kingery-Bulmash measurements.

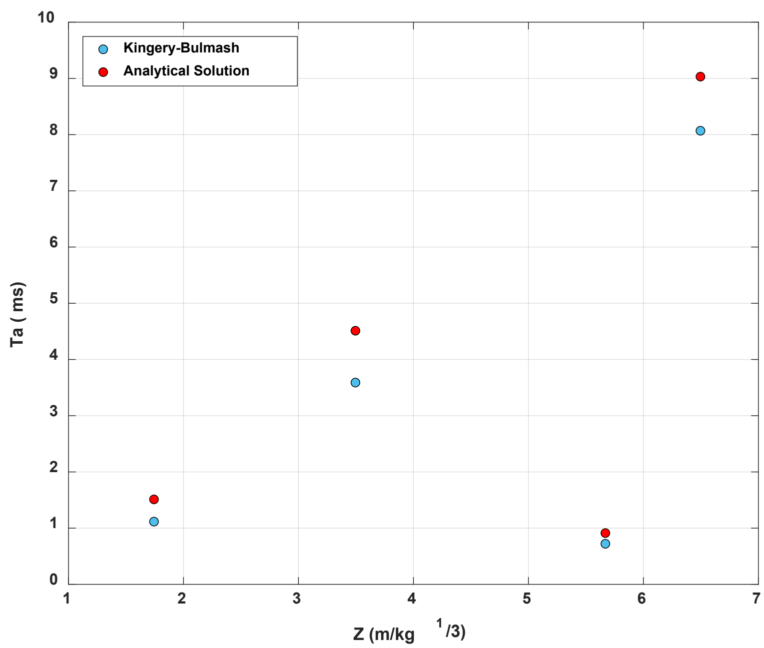

Figure 5.59 Estimated time of arrival versus Kingery-Bulmash measurements.

The measurements of the recorded air-blast pressure presented the following conclusion:

- Probe P2 which was placed at 4.88-m from the charge and 60-centimeter behind the wall almost did not read any significant air blast pressure. This is indicative of the efficiency of the WSaW blast wall in mitigating the energy of the blast shock wave.
- Due to insufficient width of the tested WSaW wall, the incident shock wave reflected and passed around the wall leading higher air-blast pressure being recorded by probes P3. The recorded air blast pressure by Probe P4 was higher than the incident shock wave pressure in free air. This could be from the magnification of blast pressure due to reflection phenomenon of the incident shock wave. The reduction (ϕ) in free air-blast pressure due to the presence of the WSaW wall is illustrated in Table 5.14.

Table 5.14 Reduction in air-blast pressure due to existing of WSaW wall.

Probe #	Z ($m/kg^{1/3}$)	Pso (Free air) (kPa)	Pso (behind wall) (kPa)	ϕ (%)
2	6.99	18.3	0.022	99.88
	6.99	18.3	0.44	97.6
	6.99	18.3	0.234	98.72
	8.01	15.0	0.1	99.33
	8.01	15.0	0.06	99.6
	8.01	15.0	1.1	92.7
	8.01	15.0	0.06	99.6
Probe #	Z ($m/kg^{1/3}$)	Pso (Free air) (kPa)	Pso (behind wall) (kPa)	ϕ (%)
3	7.88	15.4	14.92	3.12
	7.88	15.4	13.83	10.2
	7.88	15.4	14.41	6.43
	7.88	15.4	10.6	36.92
	9.03	12.8	31.3	-
Probe #	Z ($m/kg^{1/3}$)	Pso (Free air) (kPa)	Pso (behind wall) (kPa)	ϕ (%)
4	8.74	13.4	19.85	-
	10.01	11.4	34.22	-
	3.44	62.55	21.51	65.61

- It was noticed that there was a variation in the recorded air-blast pressure. For instance, Probes P1, P3, and P4 recorded different level of pressure in some test trials despite placing at same standoff distances from the source of the detonation as shown in Figure 5.60, Furthermore, there was clipping in the recorded signal, which could be related to different affecting factors such as thermal effect on unprotected sensors' cables.

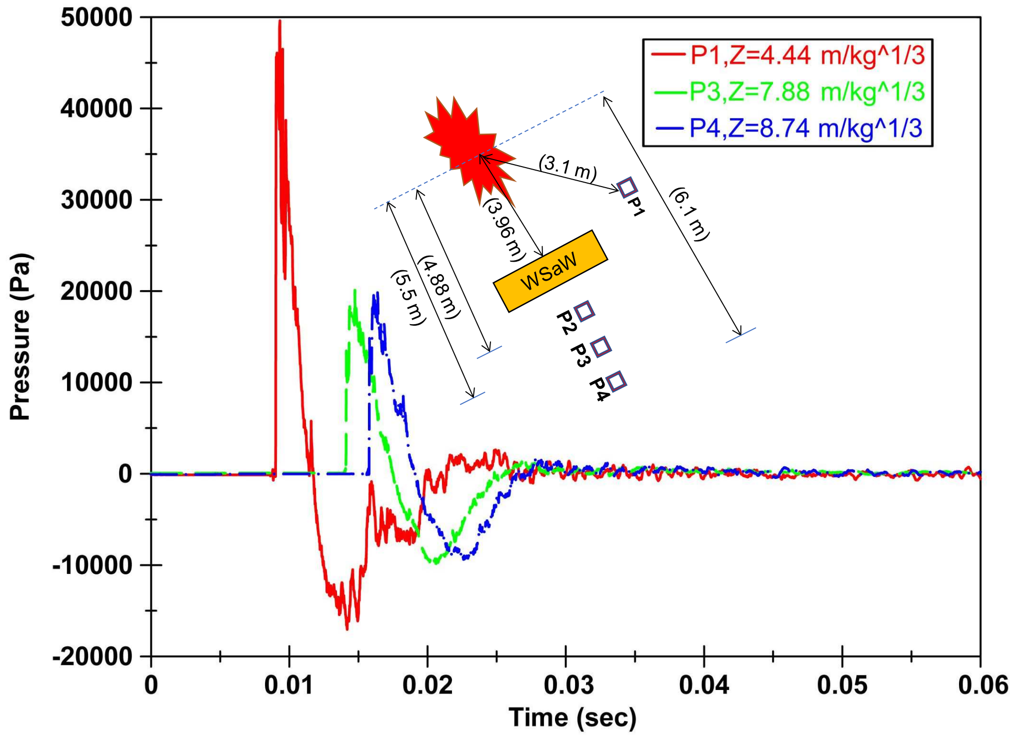

Figure 5.60 Pressure-time profile of probe P1, P3, and P4.

- The effect of the height-to-width ratio of the wall on the efficiency of absorbing the blast shock wave energy was clearly noticed from the test results. In this study, the current WSaW blast wall width was restricted due to logistical factors related to conducting the test and for comparison purposes with the OSB blast wall results.

5.11.4 Measurement of the WSaW Blast Wall Response

The response of the WSaW wall was investigated by measuring the shock acceleration. Two accelerometers were mounted on the back face-sheet of the WSaW wall. Accelerometer A1 was positioned at the center of the wall (1.22-meter above the ground), and Accelerometer A2 was placed at the top left corner of the wall. The time-history of shock acceleration recorded by acetometers A1 and A2 are shown in Figure 5.61, and 5.62, respectively

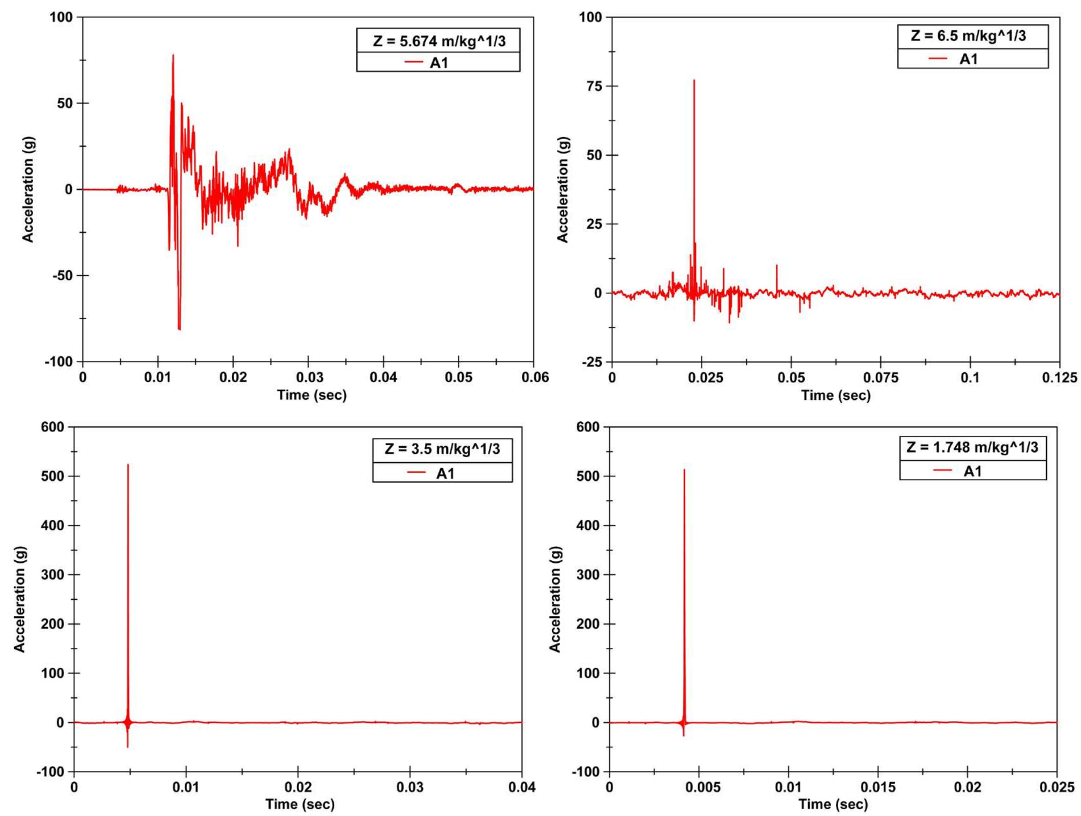

Figure 5.61 Time-histories of recorded shock acceleration of WSaW blast wall of Accelerometer A1.

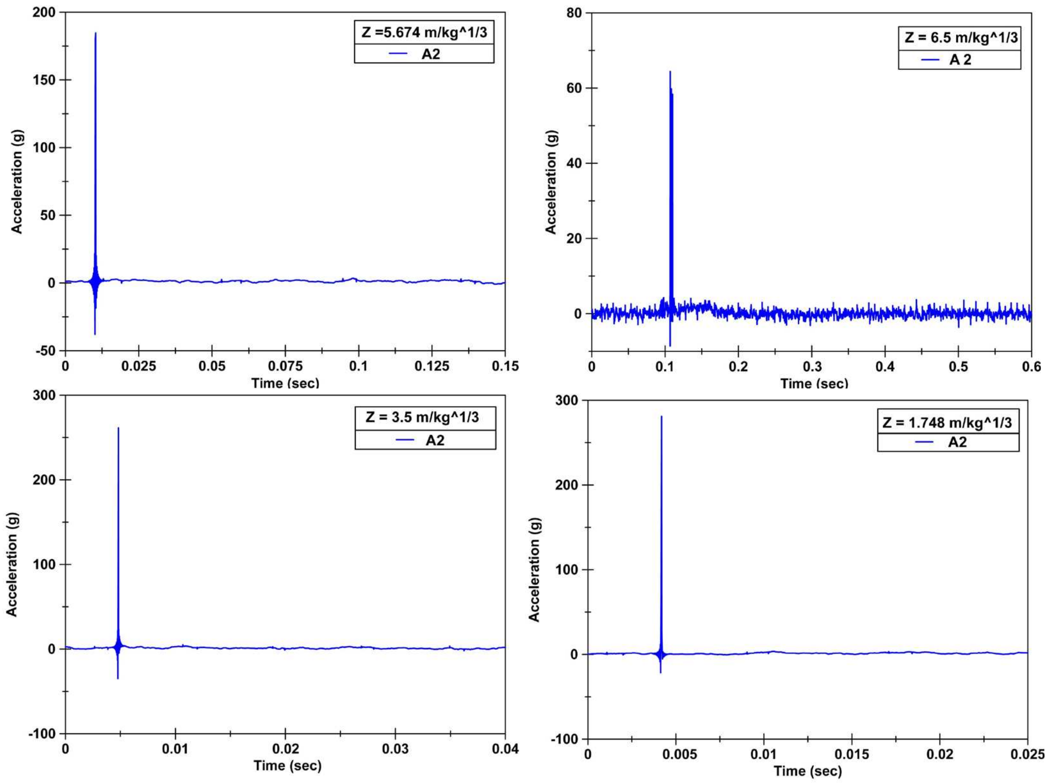

Figure 5.62 Time – histories of recorded shock acceleration of WSaW blast wall of Accelerometer A2.

The results show that the acceleration at the back center of the WSaW wall is higher than its value at the top corner by 60 percent on average due to the high intensity of blast shock wave for the same scaled distances. The results of the WSaW blast wall test were verified and validated with the analytical solution of three–dimensional dynamic finite element method (3-D FEM) using ABAQUS® software. The time-history profile of out-of-plane acceleration from the numerical analysis of WSaW blast wall are shown in Figure 5.63, and 5.64, respectively. The Measured peak acceleration of the wall showed a good agreement with ConWep predictions within ABAQUS as illustrated in Figure 5.65. For instance, the difference between the measured and computed shock accelerations is 37.78 percent at the center of the wall, and 30.47 at the top corner of the wall for Z = 1.748 m/kg$^{1/3}$ as shown in Table 5.15.

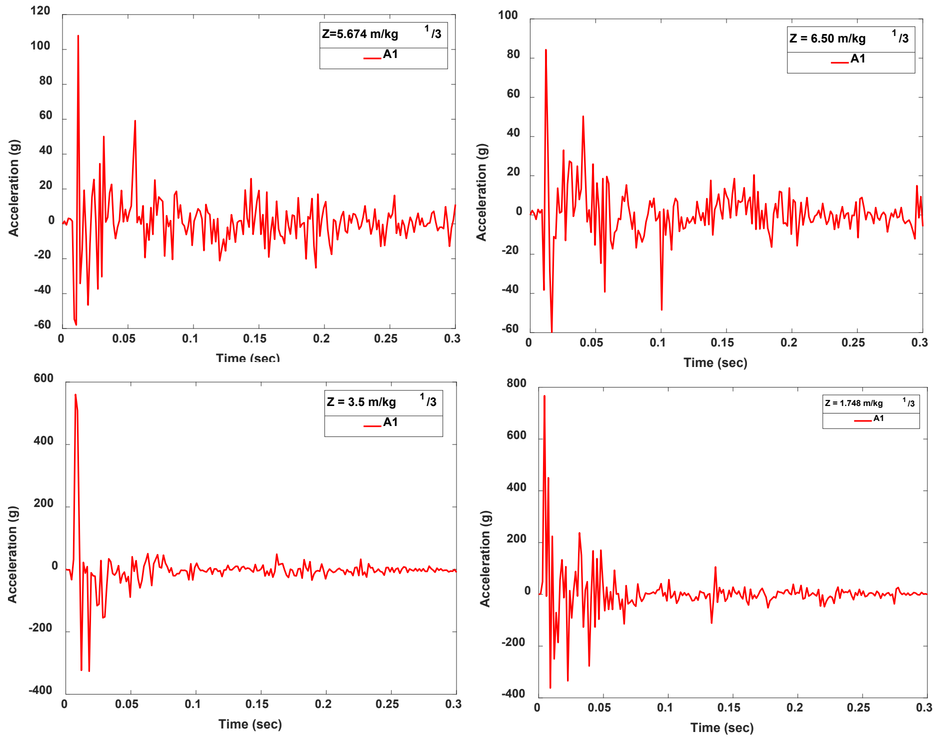

Figure 5.63 Numerical results of out-of-plane acceleration at back center of WSaW blast wall.

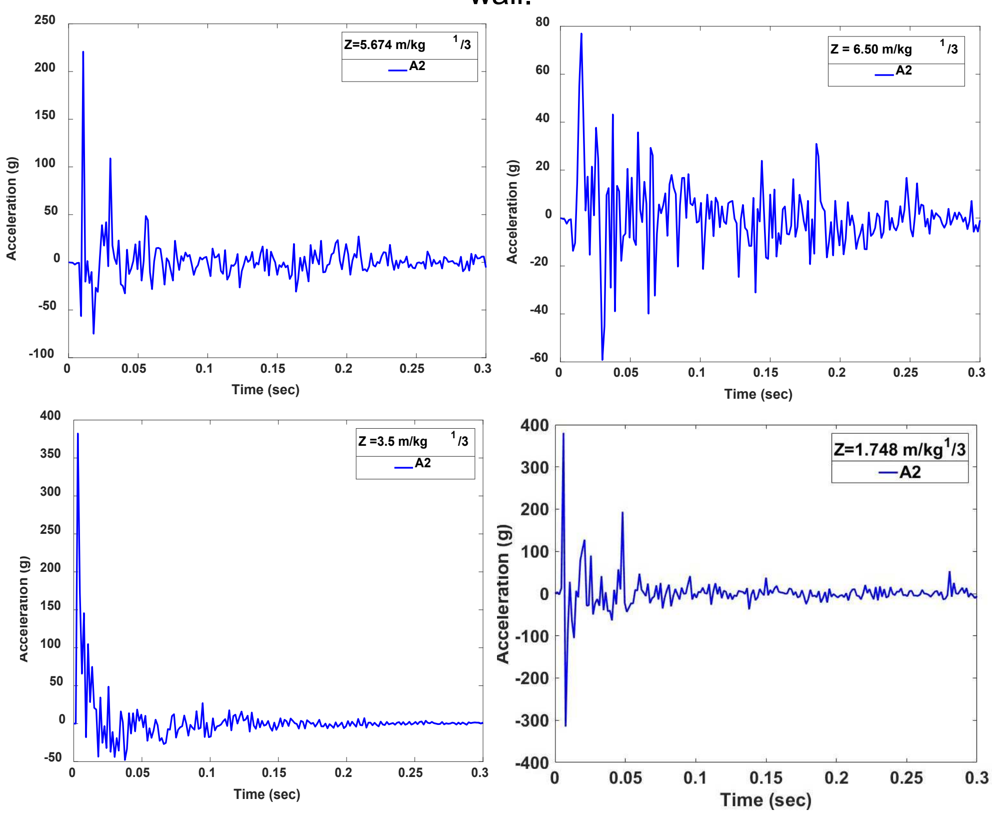

Figure 5.64 Numerical results of out-of-plane acceleration at back top corner of WSaW blast wall.

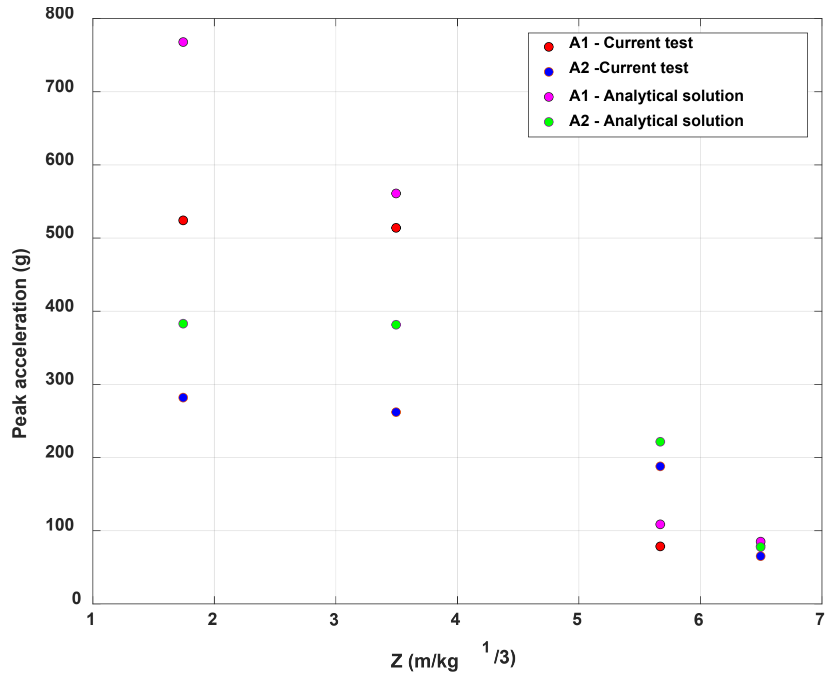

Figure 5.65 Comparison of peak shock accelerations.

Table 5.15 Measured and computed peak of acceleration of the WSaW wall.

Z (m/kg$^{1/3}$)	A1 (Test) (kPa)	A1 (FE) (kPa)	Diff. (%)	A2 (Test) (kPa)	A2 (FE) *(kPa)*	Diff. (%)
1.748	523.44	767.17	37.78	281.16	382.23	30.47
3.5	513.22	560.23	8.76	261.3	380.77	37.21
5.674	77.8	107.95	32.46	187.2	220.83	16.48
6.5	77.72	84.3	8.12	64.43	76.95	17.71

5.12 Summary and Conclusion

In this chapter, the open space blast tests and the numerical analysis results of the OSB and WSaW blast walls were summarized. Furthermore, free-air blast tests measurement and animal tissue tests were explained. Trials and small-scale tests were conducted to check the configuration of the DAQ system and the sensors. The distribution of free-air blast measurements was investigated and compared to the reference values of the H-Kingery-Bulmash measurements.

Two blast field tests were conducted to measure free-air blast in free air and check the efficiency of a thin OSB sheet in blocking blast shock waves. In the first test, small explosive weights were used due to site constraints while larger charges were used in the second test. The OSB blast wall showed good capability in resisting the blast shock wave in both tests, therefore, this study is recommending this type of a thin blast wall to be made using readily available materials to prevent injuries/casualties from flying shrapnel/debris in several attacks scenarios. This is supporting the main idea behind conducting the current study. *That is - It is not necessary to have high-tech sophisticated blast wall system to mitigate blast loading.*

In conjunction with blast wall tests, sheep eardrums were tested to determine the intensity level of the blast shock wave at which the eardrum could rupture. The reason behind selecting the sheep eardrum is due to similarity with the human eardrum structure. The results of blast pressure measurements and considered approach to examine the level of eardrum damage were explained. The ear samples status was evaluated using visual inspection and micro-CT images. According to the blast pressure measurements, the sheep eardrums was subjected to a maximum blast pressure of 75.9 kPa (11 psi). This means that the threshold for eardrum rupture was already surpassed and a 50 percent probability of eardrum rupture is expected. Three eardrums on the right side were ruptured, while only two samples on the left side were ruptured.

The last test of the experimental program was the large-scale of WSaW blast wall test. The WSaW blast wall was subjected to different size of TNT charges at different standoff distances several times and it showed a good capability in mitigating the blast shock wave. In this test, two sizes of TNT charges were used, 0.226, and 0.34 kilogram which were placed at different standoff distances from the wall. The WSaW absorbed the blast shock wave effectively for the probe placed 60-centimeters behind it. The other pressure probes readings did not show a significant reduction in the blast shock wave energy. This is logical due to insufficient width of the tested wall. Several trials were implemented, and the wall remained intact without fracture sign till the last trial when the connection between the OSB sheet and the side plywood sheet lost.

In compression to the OSB blast wall performance, WSaW wall had higher contribution in mitigating the blast shock wave energy since the reduction in peak overpressure was almost 100 percent for the probe positioned just behind it. The test results were validated with analytical solution of 3-D dynamic finite element analysis.

According to the results of the conducted test in this study, the use of WSaW blast wall is recommended to reduce casualties and losses to properties in different blast scenarios. A full realization of these walls will have to be case-specific and will require a more integrated study in which the efficiency of the wall is assessed based on the height-to-width ratio, and thickness. Architecture design modifications are required for different site conditions.

Chapter 6. Probabilistic Analysis of Single-Degree of Freedom System

6.1 Introduction and Background

Reliable and efficient structural failure criteria to predict the failure limit of variety of structures should be available to engineers. These criteria should be represented probabilistically to account for randomness in load and resistance. Performance-based design is a well-known approach for structures under natural hazards such as earthquake, wind, and fire (Olmati, Petrina, & Gkoumas, 2014). While indeed the probability of having explosive incidents is relatively low as stated in the published literature (Ellingwood, 2006), such probability will depend on the location of interest. Consequently, structures performance needs to be investigated under expected threats scenarios.

The performance-based blast design was determined initially based on deterministic parameters of structures when subjected to blast events (Ding et al., 2017; Olmati et al., 2014). This determination does not reflect the reality of failure mechanisms of structures because of the uncertainty and variation in load characteristics and structural properties. In this study, fragility functions, describing the probability of failure under increasing intensity of blast loads, were determined using a simplified/equivalent single-degree-of-freedom system (SDOF) model of the WSaW blast wall. he response of SDOF system was calculated to represent the horizontal displacement measured at the back center of the WSaW wall. The framework of the of the probabilistic analysis was established based on a specified probability density function and conditional limit state to predict the probability of failure of the system.

6.2 Determination of Blast Loading Model

Detonation from a high-explosive charge generates a strong shock wave that lasts for micro-second. In this study, burst in free-air from suicide vest was considered as it is the most followed technique by terrorists. Blast time-pressure profile was represented by an equivalent triangular pulse force function (Stewart & Netherton, 2008; Ding et al., 2017; Rong, & Li, 2007). The equivalent pressure includes the positive phase of the typical blast wave pressure history in free-air (see Figure 3.8). The negative phase is neglected in most design approaches since it does not have strong contribution to response, unless ultra-low cycle fatigue is of interest, compared to the positive phase. The impulse force takes triangular shape rising instantaneously from time equal to zero to peak value (F_o) and decreasing linearly to zero at time of (t_d).

6.3 Structural Response to Idealized Blast Forcing

6.3.1 Introduction

Due to low contribution of higher modes in the response of structure under blast load, available design procedures of simplified spring-mass systems can provide an accurate estimation to calculate system response along with reducing the time and cost of analysis (Williamson et al.,2010; Conrath et al.,1999). Furthermore, considering that a complex model does not give a warranty to provide higher accuracy since blast load parameters uncertainties exist (Williamson, 2010; Biggs, 1964). The results of simplified elastic single-degree-of-freedom (SDOF) systems have been published and presented graphically in the standards and design codes for different shapes of pulse loading for different blast-resistant design systems (Williamson et al.,2010). For instance, SDOF system was considered in the US Army TM5-1300 technical manual extensively for several blast-resistant design systems.

In the current study, an equivalent spring-mass system was considered to represent the response of WSaW blast wall under blast loading to estimate the probability of failure. The system was assumed to be at rest and damping is ignored since the blast load reaches the peak value at very short duration before the structure response finishes one cycle (Biggs, 1964).

6.3.2 Failure Prediction and Structural Response of WSaW Blast Wall

The WSaW composite blast wall was modeled using ABAQUS/Explicit software ver. 6.14. Geometrical dimensions of the WSaW model are 1.83-meter (6-feet) height and 1.22-meter (4-feet) width as shown in Figure 6.1. The wall is assumed to be anchored 60-centimeters into the ground, and the construction details of the wall are shown in Figure 6.2. The mechanical properties of OSB sheet are listed in Table 5.1 and It is assumed to be orthotropic. Drucker-Prager plasticity model (Drucker & Prager, 1952), is considered to simulate sliding motions between sand grains. This plasticity model is available in ABAQUS software materials library. The mechanical properties and Drucker-Prager plasticity model parameters are listed in Table 6.1 (Goel et al., 2012).

Table 6.1 Mechanical properties and Drucker-Prager parameters (Goel at al., 2012).

Quantity	Symbol	Values
Density (kg/m^3)	ρ	1800
Modulus of elasticity (MPa)	E	50
Poisson’s ratio	ν	0.3
Drucker-Prager Plasticity model	σ_y = 100 kPa, Ψ = 10º, ϕ = 30º, K= 0.8	

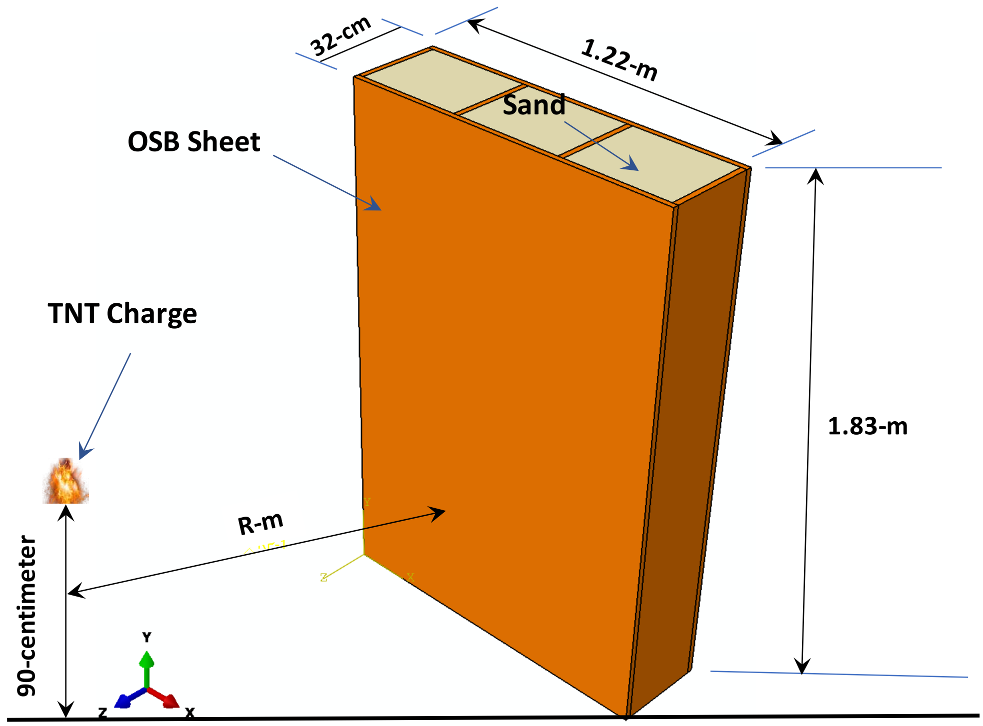

Figure 6.1 WSaW Blast Wall model.

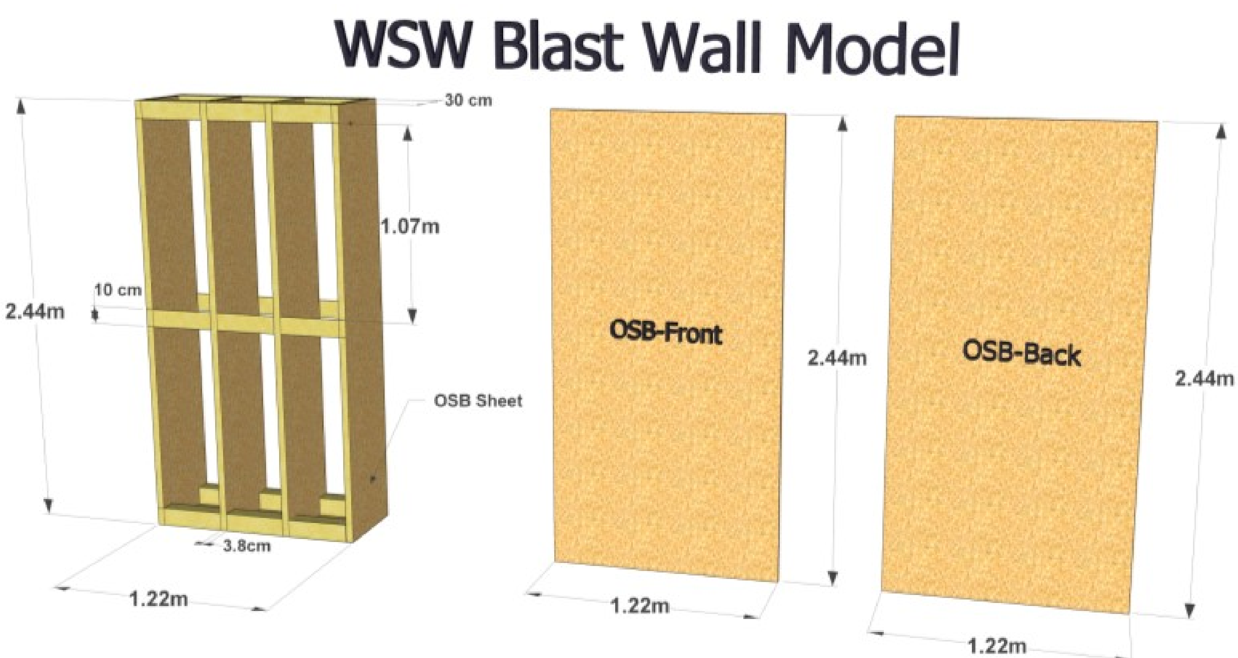

Figure 6.2 WSaW blast wall design details.

The modeling approach is the same as have been done in the previous chapter. The Interaction between all parts of the wall was accounted for using general contact algorithm. Surface-to-surface contact was defined, based on master-slave type. The total time of load application was 0.01-second for a typical blast loading, with time-step size 3.69029e-6-second. The TNT charge was placed at 90-centimeters above the ground level and different standoff distances were considered to examine the performance of the wall. In-plane stress components (σ_x, σ_y, and σ_{xy}) of the WSaW model were computed numerically. The interaction equation of the von Mises invariant failure criterion was used to predict the failure index. The calculated failure index (I_F) versus scaled distance (Z) index is listed in Table 6.2.

Table 6.2 Failure index of the WSaW blast wall.

Scaled distance-Z ($m/kg^{1/3}$)	Failure Index (I_F)
0.22	1.70
0.25	1.10
0.44	0.40
0.50	0.33
0.66	0.22
0.75	0.21
1.00	0.03
1.5	0.02

The analysis results showed that the WSaW wall can resist blast shock wave generated from high-explosive charges without fracture if the scaled distance Z ≥ 0.44-$m/kg^{1/3}$. Any scaled distance less than this range leads to failure of the structure. Failure index versus scaled distance is shown in Figure 6.3. The response of WSaW wall decreased as the scaled distance increased. For example, peak out-of-plane deformation of the WSaW wall was reduced by 50 percent when the scaled distance increased from 0.5 to 1.0 $m/kg^{1/3}$ as shown in Figure 6.4. Moreover, peak incident surface shock wave pressure decreased by 90 percent for the same increase range of scaled distance as shown in Figure 6.5. Time history analysis of incident shock wave pressure is shown in Figure 6.6. The conditional statement in the probabilistic analysis framework is considered according to the von Mises invariant failure criterion.

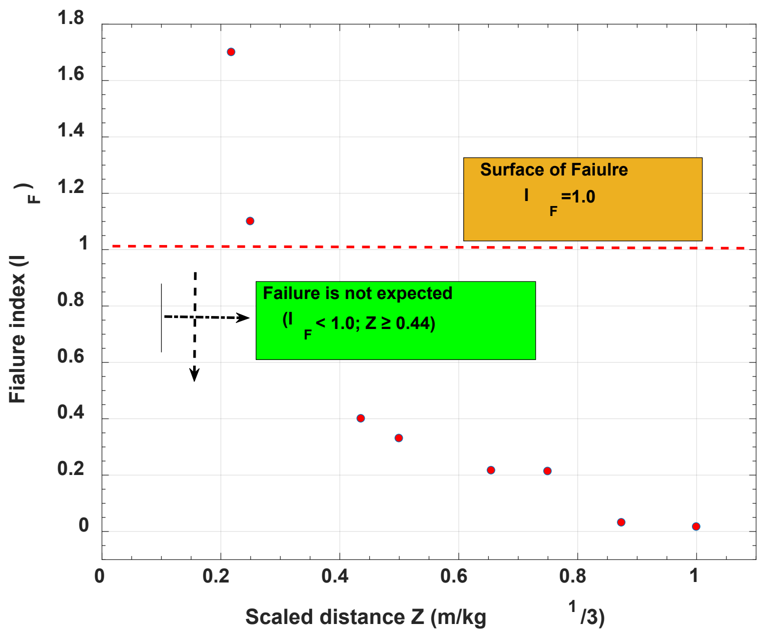

Figure 6.3 Failure surface of WSaW blast wall.

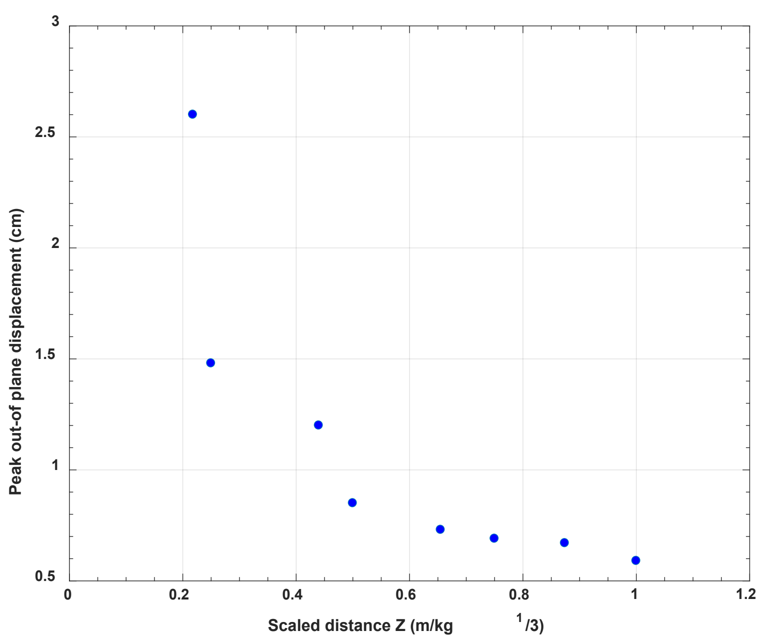

Figure 6.4 Peak out-of-plane displacement of WSaW wall.

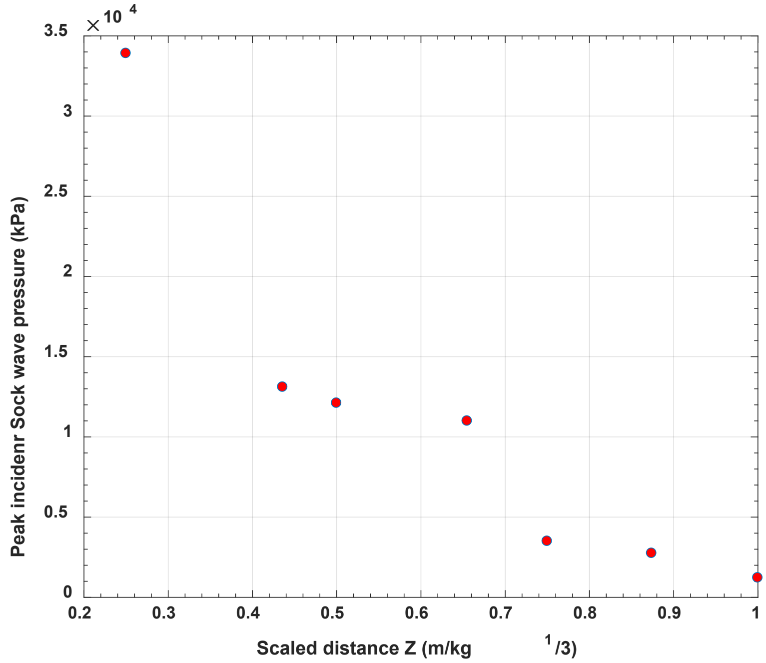

Figure 6.5 Peak incident shock wave pressure of WSaW wall.

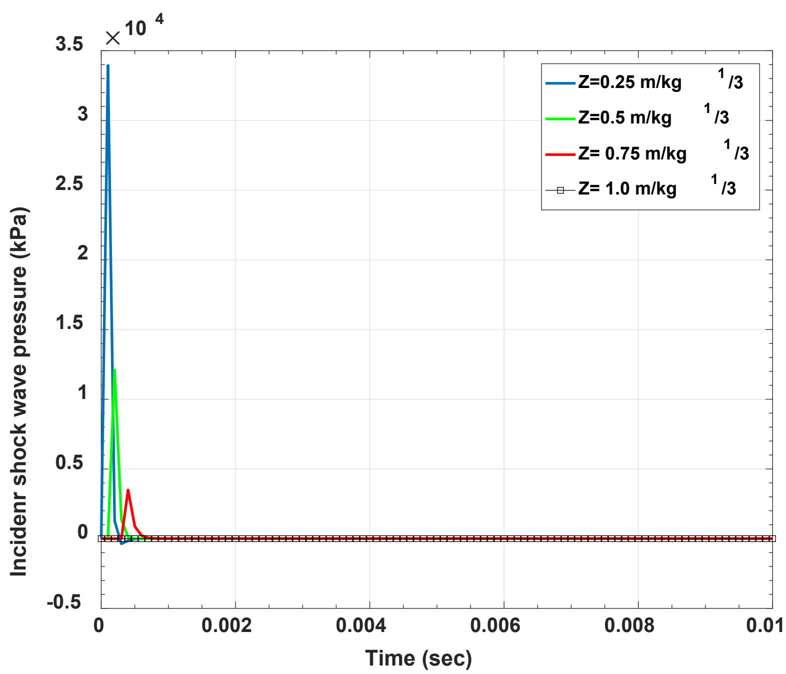

Figure 6.6 Incident shock wave pressure time histories.

6.3.3 Response of SDOF System under Triangular Impulse Force

The response of the considered blast wall (WSaW) was estimated based on an equivalent spring-mass system. Damping was neglected since it does not have impact on the response of the system under blast loading.

The equation of motion for the undamped system:

$$m\ddot{u}(t) + ku(t) = F(t) \qquad (6.1)$$

Where, *m* is mass; $\ddot{u}$ is the acceleration; *k*; is the stiffness of the system; *u*, is the displacement, and *F(t)* = $F_O\left(1 - \frac{t}{t_d}\right)$. The complete solution of the equation of motion is as follows:

$$u(t) = A.\sin w(t) + B.\cos w(t) + \frac{F_o}{k}\left(1 - \frac{t}{t_d}\right) \qquad (6.2)$$

By considering initial conditions, u (0) =0; and $\dot{u}(0) = 0$, the general solution is:

$$u(t) = \frac{F_o}{k}\left(\frac{sinw\ (t)}{wt_d} - cosw(t) - \frac{t}{t_d} + 1\right) \qquad (0 \le t \le t_d) \qquad (6.3)$$

$$\dot{u}(t) = w.sin(t) - \frac{1}{t_d} - \frac{cosw(t)}{t_d} \qquad (0 \le t \le t_d) \qquad (6.4)$$

The response of undamped SDOF system subjected to triangular impulse is shown in Figure 6.7. Where DLF, is the dynamic load factor and can be found from the following equation:

$$DLF = \left(\frac{sinw(t)}{w.t_d} - cosw(t) - \frac{t}{t_d} + 1\right) \qquad (0 \le t \le t_d) \qquad (6.5)$$

The dynamic load factor is the ratio of maximum dynamic displacement to the maximum static displacement, written as $DLF = \frac{u_{max.dyn.}}{u_{max.st}}$.

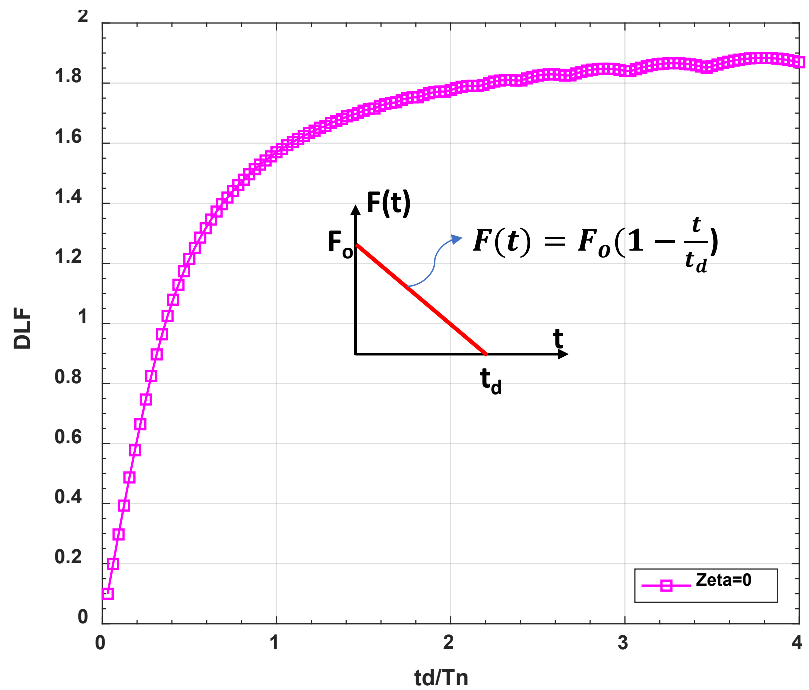

Figure 6.7 Response spectra of the triangular pulse shape.

The response of the system was estimated based on (t_d/T_n) ratio for three categories as follows:

- If $t_d >> T_n$, then the structure response will reach the maximum value before the blast load starts to decay (Mays & Smith, 1995). In this case, the blast load is called quasi-static loading. Blast load generated from a nuclear explosion is a perfect example of this case (Hetherington & Smith, 2011).
- If $t_d << T_n$, then the blast wave will vanish before the structure shows any response. In this case, blast loading can be described as an impulsive loading (Mays & Smith, 1995; Hetherington & Smith, 2011).
- If $t_d = T_n$, obtaining the response will require the equation of motion to be solved for impulsive and quasi-static loadings to determine the dynamic pressure (Hetherington & Smith, 2011).

6.4 Probabilistic Analysis of SDOF System

6.4.1 Review of Literature

Several studies have considered probabilistic analysis of an equivalent SDOF system subjected to blast load (Stewart & Netherton, 2008; Olmati et al., 2014; Netherton & Stewart,2010; Olmati et al.,2015; Ding et al.,2017). The studies stated that blast wave parameters and structural properties evaluated using deterministic mathematical approaches do not represent the stochastic variation in demand and capacity. Probabilistic analysis models provide a distribution of the possible probability of failure based on a conditional limit state of failure and randomness in structural properties and load parameters.

Rong and Li (2007), conducted a probabilistic analysis to evaluate the elastic response of reinforced concrete flexural members subjected to blast load. The study used Monte Carlo simulations to vary the random parameters. Simplified equivalent SDOF system was considered due to the complex behavior of concrete structural members under blast loading. Two non-dimensional indices were considered to identify the differences between simplified system and RC flexural members. The probabilistic response was estimated according to two different types of uncertainties, PDF, and CDF. Different support conditions were assumed to calculate the response of the system to the blast loading. The simplified approach of nonlinear dynamic analysis of SDOF results showed good agreement with probabilistic nonlinear finite element analysis.

Stewart and Netherton (2008), carried out a probabilistic risk assessment study (PRA) of simplified glazing system. Uncertainties in blast load, glazing system response, and damage index were considered to construct the fragilities. Two types of glass were considered: annealed and toughened, which were subjected to a range of explosive charges weights at different standoff distances. The framework of the risk analysis included three levels: Fragility curves, the probability of failure against specific risk scenario, and the probability of failure predicted from the accumulation of multiple threat scenarios. Moreover, the study developed blast reliability curves (BRCs) for a range of explosive weights and standoff distances. The study showed how the predicted failure probability along with risk-based decision criteria can be used to construct an optimizing analysis of risk attenuation strategies.

Uncertainty and variability of blast wave parameters from two threat scenarios were investigated (Netherton & Stewart, 2010). These are military Collateral Damage Estimation (CDE) (Military threat scenario), and Vehicle-Borne Improvised Explosive Device (VBIED) scenarios (adopted by terrorists). The explosive charge for CDE scenario is Tritonal, while it is home-made ANFO for VBIED scenario. The probabilistic blast model considered the variability in explosive weight (W), standoff distance (R), air-blast pressure (P_a), and air temperature (T_a). The authors provided a literature review of previous works of statistical analysis of blast load parameters.

It was found that the median of the suggested design range of the peak reflected pressure (P_r), reflecting the probability distribution in the TM5-1300 technical code, is higher by 40 percent with a probability of failure 4 to 23 percent. This can lead to conservative design of structures. A comparison was conducted between ConWep and TM5-1300 blast codes design limits and the probability of failure distribution of blast loading to examine the “conservatism level” of the design load.

Olmati et al., (2014), conducted fragility analysis to estimate the performance-based design of precast concrete cladding wall panels system subjected to vehicle- Borne Improvised Explosive Device (VBIED) scenario. The study stated fragility analysis has been heavily used to investigate the performance-based design for structures subjected to natural-hazards. The blast wave parameters: Peak overpressure (P_{so}), Scaled distance (Z), and Impulse (i_{so}) calculated using empirical formulas, and an equivalent single-degree-of-freedom system was assumed to represent the prototype system. The study considered Monte Carlo simulation method to predict the probability of exceedance based on conditional and unconditional approaches.

The FCs calculated for each component damage level (CDL) algorithm in MATLAB®. The authors suggested conducting probabilistic analysis for advanced systems using suitable approaches with the current element-based approach outcomes.

Ding et al., (2017), investigated the probability of failure of ten-story steel frame subjected to blast loading from a detonation of Vehicle-Borne Improvised Explosives (VBIED). The damage level of structural elements was evaluated for an equivalent single-degree-of-freedom system, then, for post-failure of steel frame structure. The system-level and structural-components damage levels were considered in the probabilistic framework. The probability of failure was calculated based on subset simulation (SS) with Markov Chain Monte Carlo (MCMC) simulation method. This algorithm provided higher accuracy than the direct Monte Carlo simulation method. The probabilistic framework clarified an effective approach to determine the most important parameters in designing structure to mitigate blast loading.

6.4.2 Monte Carlo Simulation Method

Monte Carlo simulation method is the most considered method by engineers to predict the probability of failure of structural systems based on random sampling of stochastic variables (Memari,2016;Ding et al.,2017). Failure is indicated once the conditional limit state of the deterministic analysis is passed. Accordingly, if an uncertain parameter (θ^i), is estimated to be in the failure zone, then the failure indicator, $I_F = 1$, otherwise $I_F = 0$. The probability of failure can be defined as the ratio between the summation number of samples exceeding a failure limit state to the total number of samples as shown in Equation 6.6 (Ding et al., 2017).

$$P_F = \frac{\sum_{i=1}^{N} I_F(\theta^i)}{N} \qquad (6.6)$$

Where,

P_F, Probability of failure.

I_F, indicator failure statement.

θ^i, uncertain parameters.

N, sample size.

6.4.3 Equivalent SDOF System Response of WSaW Blast Wall

Simplified equivalent single-degree-of-freedom system (SDOF) of WSaW blast wall was considered as shown in Figure 6.8. The blast wave parameters were calculated from design free-air blast charts (UFC 3-340-02, 2008) for a reasonable range of scaled distances. The system is assumed to be at rest and stay in the elastic region while applied load in effect.

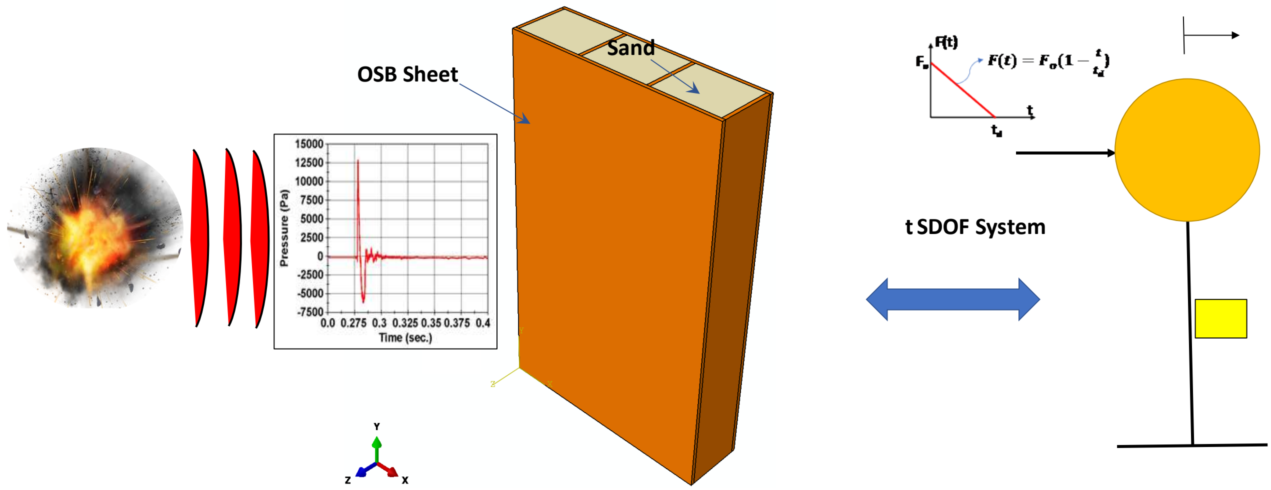

Figure 6.8 Equivalent SDOF system of WSaW blast wall.

The response of considered SDOF system was calculated using MATLAB® code, and the equation of motion was solved using Duhamel integral technique as shown in Equation 6.7 (Rajasekaran, 2009).

$$u(t) = \frac{F_o}{mw_n}\int_0^t (1-\frac{\tau}{t_d}).\, sinw_n(t-\tau)\,.\,d\tau \qquad (6.7)$$

Where, F_o, peak of the applied load; m, mass of the system; w_n, natural frequency of the system; t, time; τ, small increment of the time.

The calculated response of the SDOF system was compared to the finite element model response results measured at the center of the back face-sheet of WSaW blast wall. The results of SDOF model showed good agreement with the finite element analysis results as shown in Figure 6.9. For instance, the peak of dynamic displacement was off by 20 percent and the differences in the natural period of motion was 25 percent for Z= 1.0 m/kg$^{1/3}$. This is considered acceptable, given the simplicity of the SDOF model and its superior computational efficiency over the 3D finite element model.

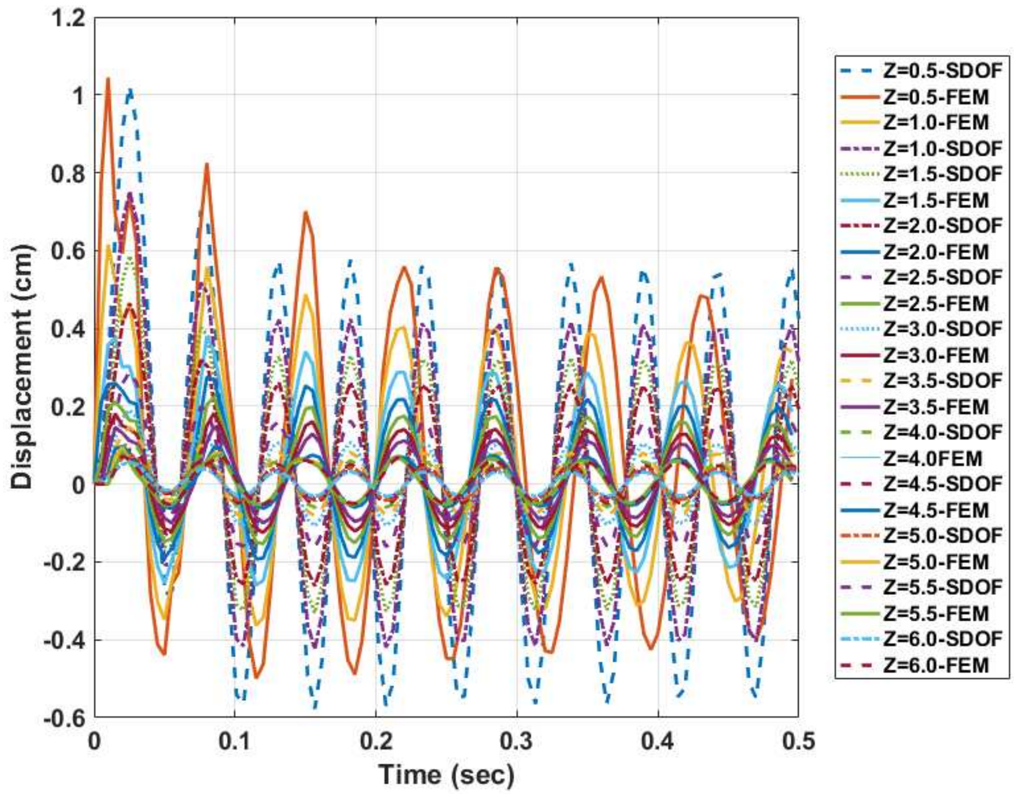

Figure 6.9 Comparison between SDOF and finite element analysis results.

The calculated peak response of the spring-mass system was modified and adjusted according to the numerical results of the finite element method. The modified response factor (MRF) was calculated as shown in Equation 6.8. The MRF factor was applied in probabilistic analysis algorithm to adjust the response of SDOF system to improve the accuracy and reduce the error in the predicted FCs. The MRF factor computed for a range of scale distances (Z) as shown in Table 6.3.

$$MRF = \frac{U_{FEM}}{U_{SDF}} \qquad (6.8)$$

Where, *MRF i*s the Modified Response Factor; U_{FEM} is the calculated peak response from FE; U_{SDF} is the calculated peak response from SDOF system.

Table 6.3 MRF factors in terms of scaled distance.

Scaled distance Z (m/kg$^{1/3}$)	U3 _max (SDOF) (cm)	U3_max (FEM) (cm)	MRF factor
0.5	1.02	1.04	1.02
1.0	0.753	0.615	0.817
1.5	0.586	0.38	0.648
2.0	0.464	0.275	0.6
2.5	0.288	0.224	0.78
3.0	0.19	0.182	0.96
3.5	0.146	0.148	1.01
4.0	0.106	0.118	1.1
4.5	0.09	0.097	1.11
5.0	0.075	0.095	1.26
5.5	0.063	0.084	1.33
6.0	0.057	0.074	1.30

6.4.4 Fragility Analysis

Fragility analysis is a statistical tool representing the cumulative probability of structural failure exceeding a specified damage limit state. The fragility analysis is well known and developed for predicting the probability of failure for structures subjected to natural hazards (Olmati et al.,2014). In this study, fragility analysis was considered using Monte Carlo simulation method for an equivalent SDOF of a WSaW blast wall. The uncertainty parameters include equivalent TNT weight and modulus of elasticity. The probability of failure was established based on the following conditional failure relation shown in Equation 6.9 (Stewart & Netherton, 2008):

$$P_f \mid \theta_{ij} = \sum_{s=0}^{\infty} P_r[G(X) < 0 \mid S = s]\, P_r[S = s] \qquad (6.9)$$

Where, P_f is the probability of failure; *θij* is the threat scenario (i: explosive mass; j, standoff distance); *G(x)* is the limit state function; P_r [S=s] is the probability density of uncertainty parameter; *N* is the sample size

The variability and uncertainty include attack scenario, blast wave parameters: standoff distance (R), and explosive charge weight (W) (Stewart & Netherton,2008). In the current study, the blast load was applied using idealized blast forcing function (see Equation 6.1), and this approximation function could lead to a percentage of error to the model (Stewart & Netherton, 2008). This error has been estimated to be in acceptable range (COV=0.01) in the case of free-air blast burst (Lofton & Meyers, 2001). The bias for confined explosions is expected to be higher and a reliability study is required to predict it (Twisdale, Sues, Lavelle, & 1994; Stewart & Netherton, 2008). The probabilistic analysis of the structural systems subjected to blast load comprises the uncertainties of TNT weight and structural parameters. The blast loading parameters were calculated for a range of scaled distances, Z ($m/kg^{1/3}$), and the peak pressure was estimated from the Kingery-Bulmash chart (UFC 3-340-02, 2008) assuming spherical wave that is normally reflected from the targeted surface (see Figure 3.13). Wave-wave interaction was not included in blast load-model since it is not expected for free-air blast configuration.

6.5 Probability of Exceedance of SDOF System

The response of SDOF system was calculated to represent the horizontal displacement measured at the back center of the WSaW wall. The uncertainty in modulus of elasticity of the OSB material and variation in the equivalent TNT weight were represented by the normal distribution of probability density function as shown in Figure 6.10, and 6.11, respectively. This assumption was based on the provided data in FEMA 453 (2006), for a suicide vest threat scenario (see Figure 6.12). The summary of statistical data for modulus of elasticity of OSB and equivalent TNT charge weight are shown In Table 6.4.

Table 6.4 Statistical data for the current probabilistic analysis.

Symbol	Description	Mean	COV	Std. error	Distribution
E (OSB) (Suzuki,2000)	Modulus of elasticity	5(GPa)	0.9	0.0002	Normal
W	Explosive mass	9 (kg)	0.2	0.006	Normal

The failure limit state was calculated according to the von Mises invariant failure criterion (see sections 3.10, & 6.4.3). This limit state was used as a conditional statement in the framework of the probabilistic analysis. The fragility analysis was conducted using MATLAB® to evaluate the performance of the considered system as shown in Figure 6.13.

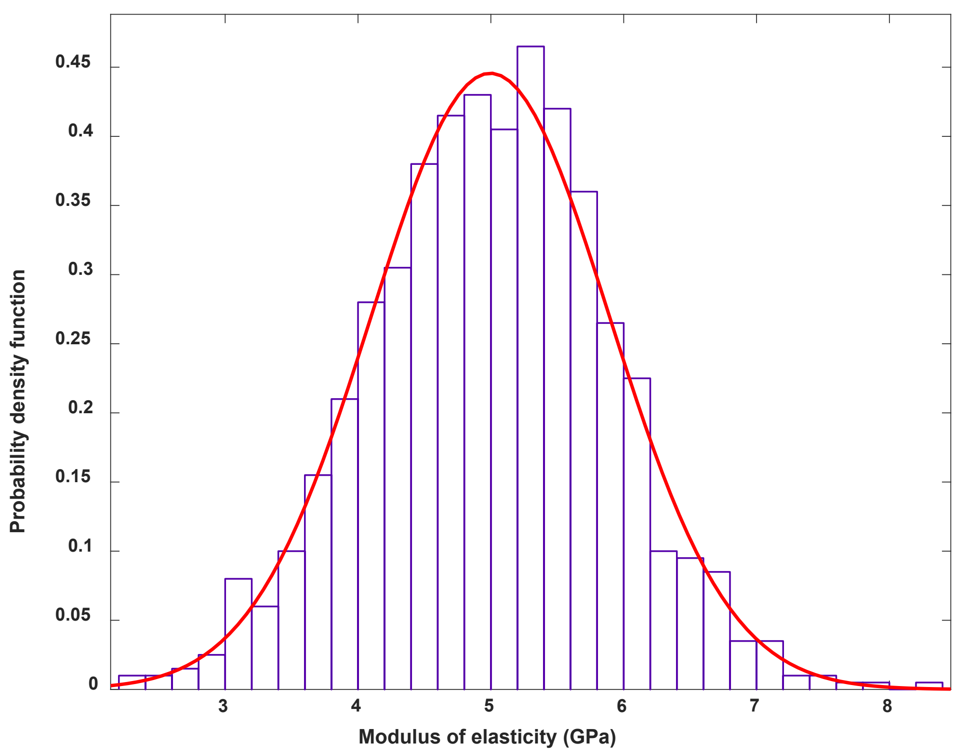

Figure 6.10 The probability distribution function of the modulus of elasticity for OSB.

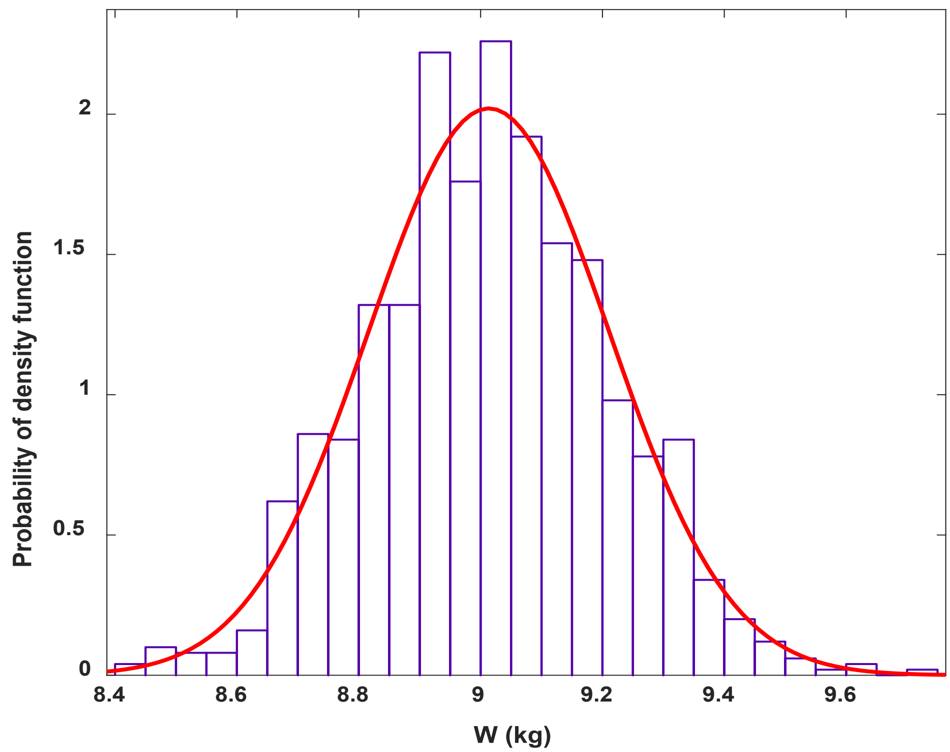

Figure 6.11 The probability distribution function of the equivalent TNT weight.

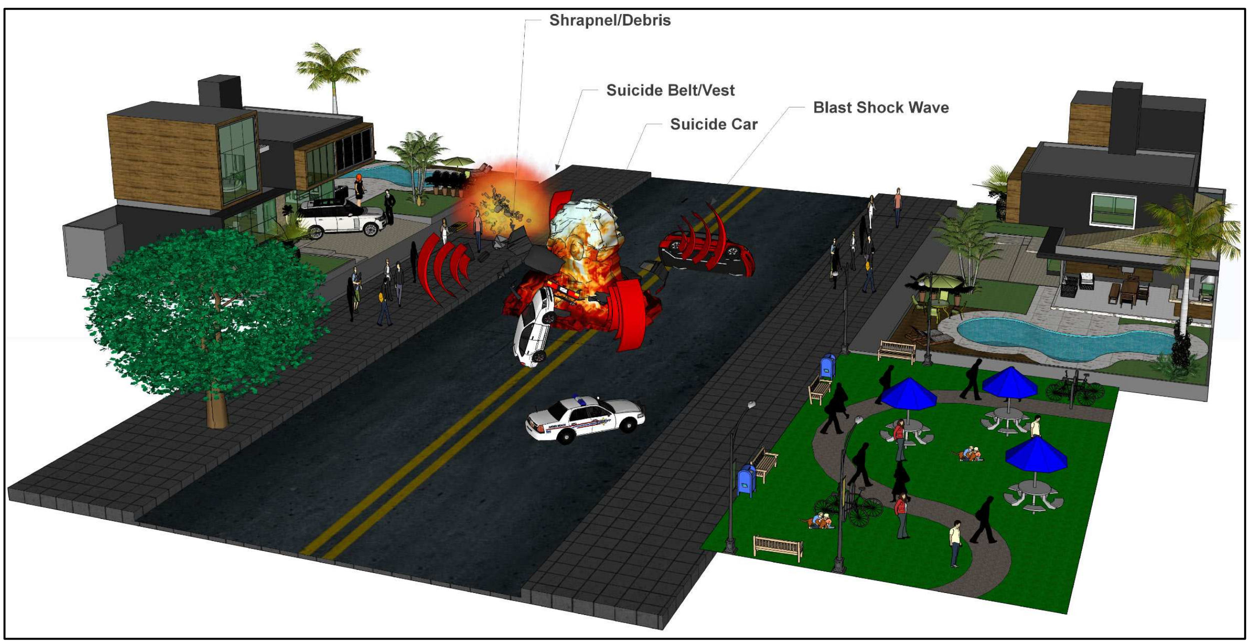

Figure 6.12 Followed Terrorists Attacks scenarios.

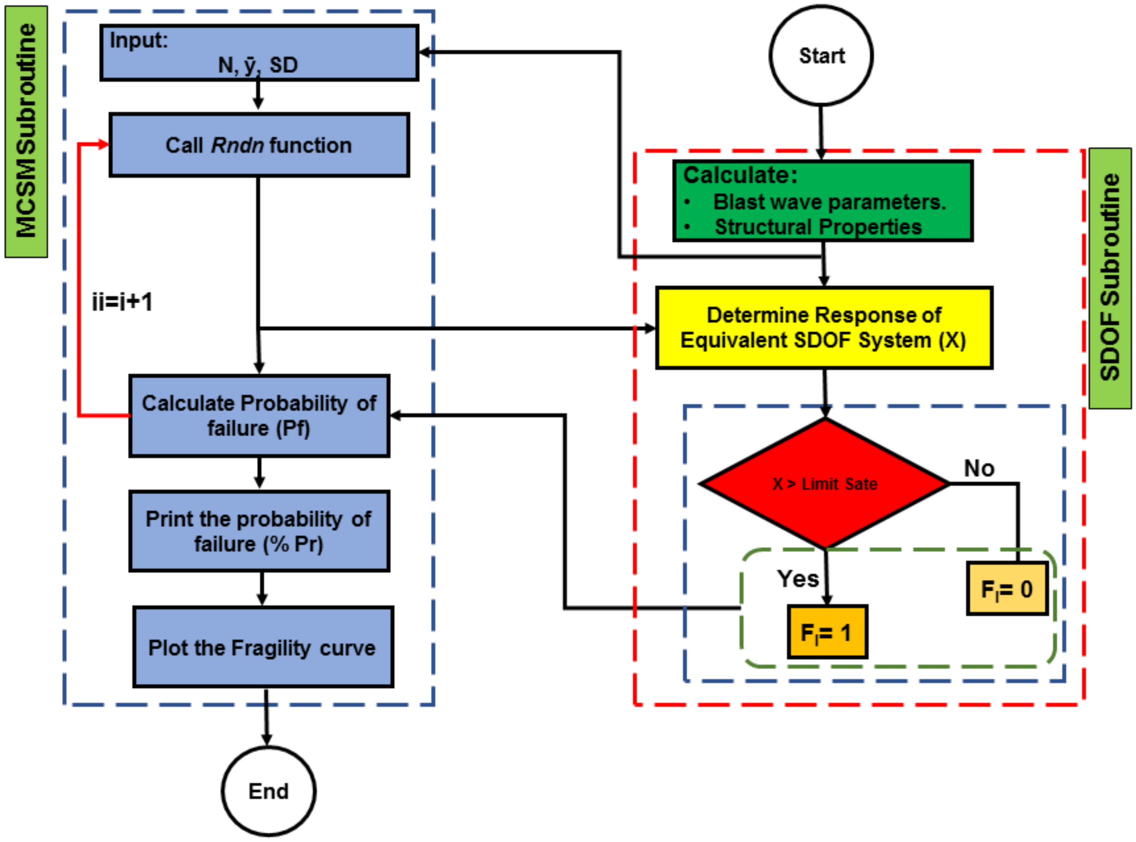

Figure 6.13 Flowchart of fragility analysis.

The probability of exceedance of an equivalent SDOF system of a WSaW blast wall was estimated for a realistic range of scaled distance (Z). The fragility curve was modified according to the adjusted peak response as shown in Figure 6.14. It is seen that the probability of failure decreases when the scaled distance increases as expected. It is also noted that the increase of the scaled distance from 2.0-4.0 m/kg$^{1/3}$, reduced the probability of failure by 28 percent. Moreover, the probability of failure dropped significantly when the scaled distance was equal to or larger than 5.5 m/kg$^{1/3}$ and failure would not occur if the scaled distance exceeded this value.

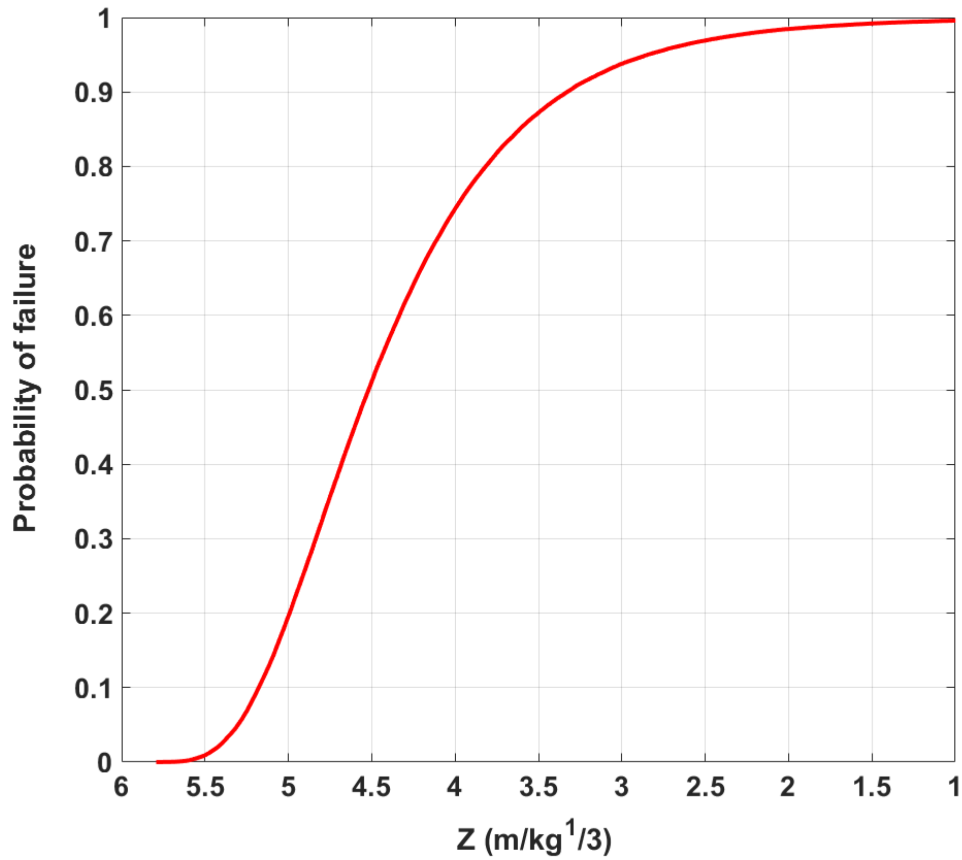

Figure 6.14 The probability of exceedance of equivalent SDOF system of WSaW wall.

In comparison between the probability of exceedance based on the SDOF response solution, and the probability of failure results based on the adjusted response of the equivalent SDOF system (see Table 6.3), the following conclusion can be summarized (see Figure 6.15).

- The probability of failure (P_f) is increased for $0.5 \leq Z \leq 2.5$.
- The probability of failure (P_f) is almost the same for $3.0 \leq Z \leq 4.5$.
- For $5.0 \leq Z \leq 6.5$, the probability of failure (P_f) is decreased.

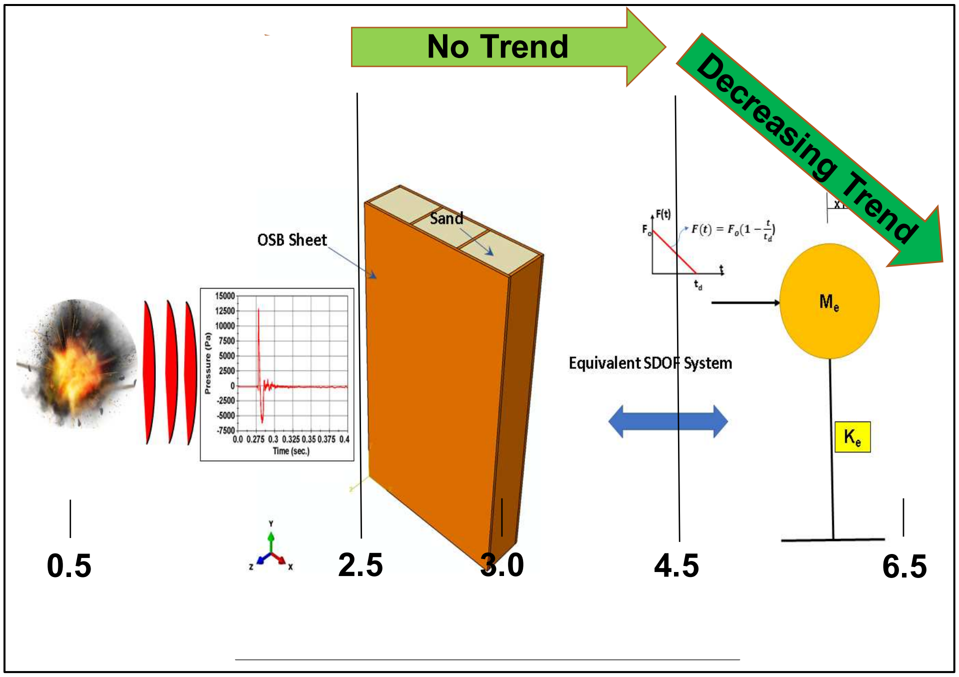

Figure 6.15 the probability of failure trend based on the adjusted response of the equivalent SDOF system in terms of scaled distance.

Fragility curves were also estimated based on the variability in the equivalent TNT weight for a suicide vest threat scenario placed at three standoff distances (R= 1m, 4m, & 8m) as shown in Figure 6.16 a, b, and c, respectively. It is noticed that the probability of failure decreased as the standoff distance increased (R). For example, the probability of failure is 74 percent from placing 1.0-kilogram of TNT at 1.0-meter in front of the wall, while the probability of failure dropped to 28 percent by placing the same TNT weight at 4.0-meter, and to 4.0 percent by placing it at 8.0-meter. Furthermore, Figure 6.16, a, shows that the probability of failure increases by 25 percent when the weight of TNT increased from 1.0 to 2.0 kilograms. It is noted that the fragility curve for R= 1.0-meter, increases sharply while it increases gradually when R= 4.0, and 8.0-meter due to the high intensity of blast shock wave.

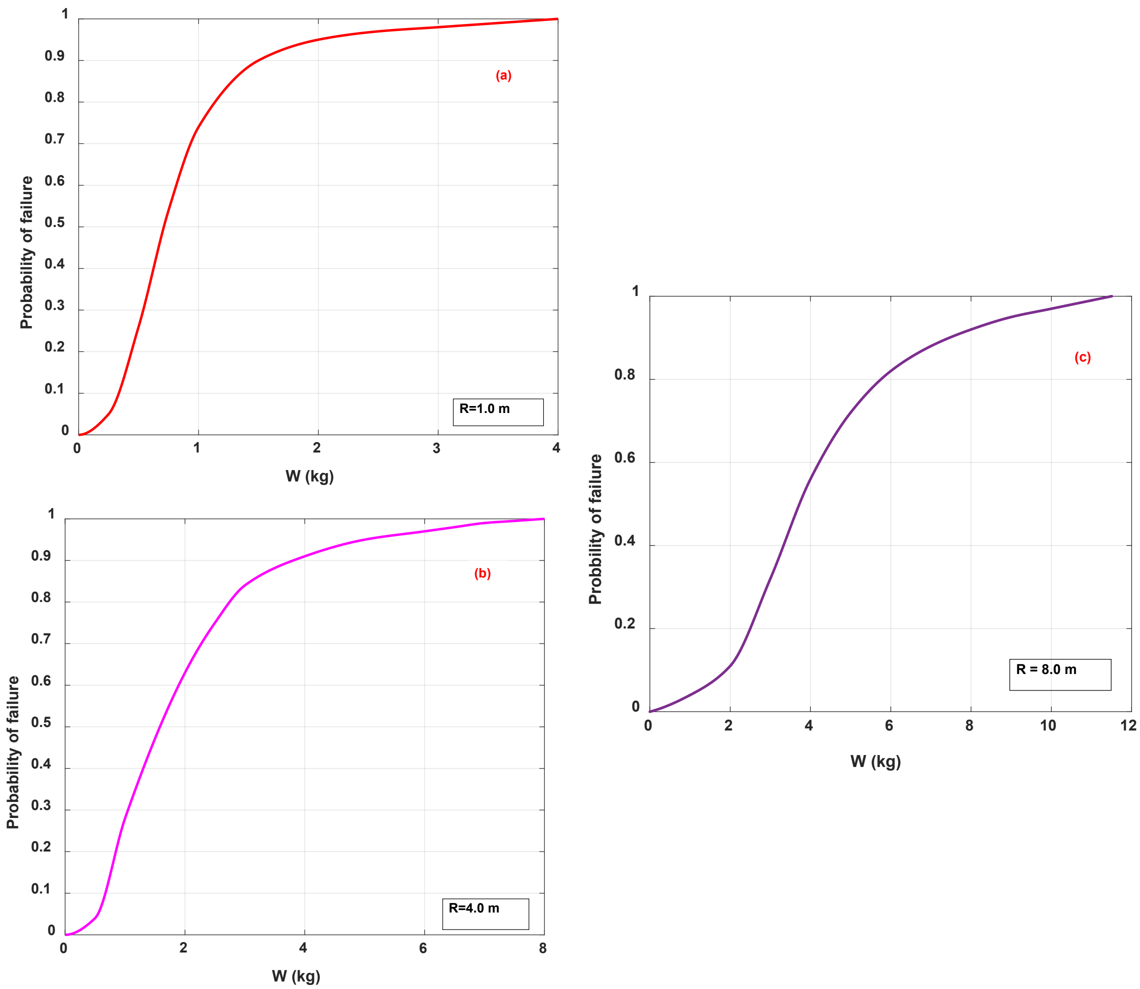

Figure 6.16 The probability of exceedance of equivalent SDOF system of WSaW wall for given standoff distances and equivalent TN weight. a. R=1-meter.b. R=4-meter. c. R=8-meter.

6.6 Summary

In this study, a probabilistic analysis of an equivalent SDOF system for a WSaW blast wall was conducted to estimate the FCs of the system under free-air blast load. The analysis framework was developed to probabilistically evaluate the performance of the proposed blast wall in the presence of uncertainties in structural properties and blast load parameters. The FCs were estimated using direct Monte Carlo simulation method.

The response of the SDOF system was calculated to represent the horizontal displacement measured at the back center of the WSaW wall. The structural properties variation can affect the resistance of the system while the load in effect. Therefore, the fragility curve is predicted according to the probability density of uncertainty of the modulus of elasticity of OSB material. The probability of failure was presented for a range of scaled distances (Z). It was seen that the probability of failure decreases when scaled distance increases. It was noticed that increase the scaled distance from 2.0-4.0 m/kg$^{1/3}$, reduced the probability of failure by 28 percent. Furthermore, the probability of failure is dropped significantly when scaled distance equal or larger than 5.5 m/kg$^{1/3}$. Failure is not predicted beyond the scaled distance exceeding 5.5 m/kg$^{1/3}$.

The FCs were also estimated based on the variability in the equivalent TNT weight for a suicide vest threat scenario. It is noticed that the probability of failure decreased when the standoff distance increased (R). For example, the probability of failure was 74 percent from placing 1.0-kilogram of TNT at 1.0-meter in front of the wall, while the probability of failure is dropped to 28.0 percent by placing same TNT weight at 4.0-meter, and to 4.0 percent by placing it at 8.0-meter. It was noticed that the fragility curve for R = 1.0-m, increased sharply while it increased gradually when R= 4.0-m, and 8.0-m due to the high intensity of blast shock wave.

Chapter 7. Conclusions and Future Works

7.1 Summary and Outlines of Current Study

The main goal behind terrorist attacks is to increase number of victims to give the event more power globally. Therefore, adopting reliable blast mitigation approaches to reduce number of victims is required. Simple protection strategies from explosions have been used for military purposes and temporary fortifications in the last century. This research was focused on considering simple blast wall systems to mitigate blast loading in free-air to be used in urban areas. Simple blast wall systems made of readily available materials could mitigate blast loading and provide the required level of protection in several attacks scenarios. The current study was tried to suggest simple, cheap, fast and easy to construct and maintain blast wall system. The goal was to simulate the suicide attacks scenarios especially in the Middle East and developing countries due to the increase in explosion events in the last ten years. Since mitigating blast loading without partial collapse is not required in most structural systems, the OSB and WSaW blast walls were considered as examples composed of readily available materials. This approach has been discussed and approved through the experimental program measurements and numerical analysis results. The study found the considered blast walls have a good capability to resist blast loading and provide the required level of protection for specified TNT charges and standoff distances.

The animal tissue test was implemented to evaluate the effect of the blast shock wave on sheep eardrum due similarity with human auditory system. Five ear samples were dissected and imaged to examine the eardrum rupture. The test results clarified blast shock wave can lead to hearing loss through short or long-term effect.

A Probabilistic analysis was performed for an equivalent SDOF system of WSaW blast wall to estimate the FCs using Monte Carlo simulation method. The suggested framework of the probabilistic analysis was developed to study the performance of the proposed blast wall according to the uncertainties in structural properties and blast load parameters. The FCs were also estimated based on the variability in the equivalent TNT weight of a suicide vest threat scenario.

The following conclusions were summarized according to the current literature, experiments, and numerical analysis results:

7.2 Blast Wall Systems-Limitations and features

7.2.1 High-Tech Blast-Resistant Wall Systems

The current trend of designing blast-resistant wall systems is:

- Considering multi-layer systems composed of parent structure made of high ductile materials and low density (high compressible) core structure (High-tech Systems)
- The function of the front-face sheet is to reflect/absorb most of blast shock wave energy, while the core structure task is to absorb the rest of passing wave energy through front face sheet.
- The occurrence of permanent deformation in the core structure considers failure to the system.

- Applications of such systems are limited and related to the important of the structure when permanent deformation is not permissible due to design considerations.
- These blast-resistant wall systems can mitigate blast shock wave effectively, but with the increase of the cost.

7.2.2 Simple Blast-Resistant Wall systems

In this study, simple blast wall systems were considered as an effective alternative. Features of considering this type of blast wall systems can be summarized as follows:

- It is not applicable in the Middle East and most developing countries to use high-tech blast wall systems due to a lack of funds and construction technology.
- Simple blast walls are inexpensive, fast and easy to construct and maintain.
- In general, mass of the structure is playing the main role to absorb blast shock wave energy. Compare to high-tech systems this is very useful and an effective alternative to mitigate blast loading. For example, in case of WSaW wall sand mass has a significant contribution to improve the system efficiency to mitigating the blast loading. Moreover, sand is not producing any shrapnel, therefore, injuries from flying fragments are not expected.
- Partial collapse could be expected, and structural integrity assessment is not applied, since the required level of protection behind/around blast wall is already provided.

- Additional integrated studies are required to suggest and investigate the performance of different types of simple blast wall systems for different site conditions.
- This type of blast-resistant wall systems still cannot be used in urban areas and architecture design modifications need to be considered before it becomes applicable to implement in such areas.
- Most funds have been assigned to the military departments. Therefore, efforts should be made to encourage construction companies to support the new applications of the simple blast wall systems.

7.3 Experimental Test Results and Numerical Analysis Validation of Simple Wall Systems

The present study is unfunded project with a lot of volunteer efforts and donated materials. Therefore, there were some limitations in number and scale of implemented tests and availability of required equipment. The literature on the distribution of air pressure and the response of simple blast walls are limited and rarely published. In this study, several trial tests, small, and large-scale tests were implemented to measure free-air blast pressure and simple blast walls response. Two trial tests were conducted to check the configuration of DAQ system and the connection of ICP® pencil probes and shock accelerometers. Next, open space blast tests were conducted to measure free-air blast pressure and efficiency of OSB and WSaW blast walls in mitigating blast shock wave. Several TNT charges were placed at different standoff distances in front of the tested wall. Free-air blast pressure was measured at different positions behind/around the wall and measurements were compared to the standards. The animal tissue test was implemented in conjunction with OSB and WSaW tests to evaluate the effect of the blast shock wave on sheep eardrum. The tested eardrum samples were inspected visually then scanned by micro-CT scanner to check the eardrum rupture after blast tests.

7.3.1 Free-Air Blast Test of OSB Blast Wall

- The generated blast shock wave from low-explosive charges was low and not propagated evenly in all directions due to charge shape (small-scale test)
- The measured blast wave pressure-time profiles were consistent with typical standard charts.
- Free-air blast measurements showed a good agreement with Kingery-Bulmash charts of a spherical wave of TNT charges in free-air.
- Free-air blast measurements showed peak overpressure in the front direction of blast shock is almost double its value in opposite direction.
- Blast pressure measurements of the large-scale test were very consistent.
- The OSB blast wall reduced the blast pressure 20 percent for the probe positioned behind the wall.
- Measured peak accelerations for the wall were in excellent agreement with ConWep predictions within ABAQUS.
- Peak shock acceleration of OSB wall at the center of the wall was 60 percent higher than its value at the top corner because of the high-intensity shock wave.

- This study recommended using this type of thin blast wall made of readily available materials to prevent injuries/causalities from flying shrapnel/debris.

7.3.2 Free-Air Blast Test of WSaW Wall

- The measured pressure-time curves are typical and consistent with standards plots of burst in free-air.
- A good agreement with Kingery-Bulmash model measurements of peak overpressure was noticed.
- Due to the thermal effect on the unprotected sensor cables, some variation in the probe measurements were noticed.
- Blast shock wave energy is significantly mitigated by the WSaW blast wall according to recorded air-blast pressure by the probe positioned just behind the wall.
- Measured peak shock acceleration showed a good agreement with analytical solution values.
- Peak shock acceleration in the back center of the WSaW blast wall was 60 percent higher than its value at the top corner. This was also confirmed from outcomes of OSB blast wall test.
- It was noticed from the failure mechanism that WSaW blast wall is not producing any debris.
- According to the current study results, it is recommended to use WSaW blast wall to reduce casualties and losses in properties in different attack scenarios.

7.3.3 Blast Shock Wave Effect on the Eardrum-Experimental study

Five Rambouillet-Columbia sheep heads samples were used in this test. These heads subjected to blast shock wave generated from the detonation of DETASHEET® flexible explosive charge of C1 (5-cm x 7.6-cm), and 30-cm of detonating cord. This charge is equivalent to 3.3-grams of TNT. The results of the dissected and inspected samples after the analysis can be summarized as follows:

- Dissecting eardrums is a challenge since it needs to declassify part of the skull bone. Furthermore, identifying the rupture is hard and need to be done carefully using a combination of visual inspections and advanced scanning techniques.
- The sheep heads placed on a steel stand, either the right-side or left side ear facing the blast shock wave directly.
- From visual inspection, it can be seen that the ear cartilage was totally burned, and an extensive section of skin was completely torn off the underlying.
- The threshold of eardrum rupture was passed from the measured blast pressure, and 50 percent portability of eardrum rupture is expected for the right eardrum.
- Three eardrum samples on the right side were ruptured while only two samples on the left side were ruptured due to blast shock wave effects.
- Temporary hearing loss could occur at a pressure level less than the threshold in several cases. This can be considered as a starting point of eardrum rupture.

7.4 Numerical Analysis Results and Validation of Test Results

7.4.1 Failure Prediction Analysis of OSB Blast Wall

- The von Mises invariant failure criterion was used to estimate the failure index of OSB. The results of the analysis showed that OSB wall can resist a blast shock wave generated from high-explosive charges without fracture if the scaled $Z \geq 1.5$ m/kg$^{1/3}$.
- Peak out-of-plane deformation of OSB wall reduced by 76 percent when scaled distance increased from 1.0 to 2.0 m/kg$^{1/3}$.
- Peak incident surface shock wave pressure decreased by 53 percent when scaled distance increased from 1.0 to 2.0 m/kg$^{1/3}$.

7.4.2 Failure Prediction Analysis of WSaW Blast Wall

- The results of the analysis based on von Mises invariant failure criterion showed that WSaW wall can resist a blast shock wave generated from high-explosive charges without fracture if the scaled $Z \geq 0.44$ m/kg$^{1/3}$.
- The peak of out-of-plane deformation was measured at the back-face center of the WSaW wall
- Peak out-of-plane deformation of WSaW wall reduced by 50 percent when the scaled distance increased from 0.5 to 1.0 m/kg$^{1/3}$.
- Peak incident surface shock wave pressure decreased by 90 percent when scaled distance increased from 0.5 to 1.0 m/kg$^{1/3}$.
- The calculated failure index of WSaW wall was used as a conditional statement in the probabilistic analysis framework.

7.5 Probabilistic Analysis of SDOF system

This study performed a probabilistic analysis of an equivalent SDOF system of WSaW blast wall to estimate the FCs of the system under blast loading. The suggested framework of the probabilistic analysis was developed to study the performance of the proposed blast wall according to the uncertainties in the structural properties and blast load parameters. The FCs were estimated using Monte Carlo simulation method. This method has been widely employed by engineers to investigate the performance of structural systems. Simplified equivalent SDOF of WSaW blast wall was considered. The response of SDOF system was calculated to represent the horizontal displacement at the back-face center of WSaW wall. The following conclusion was summarized according to the probabilistic analysis results:

- The probability of failure was presented for a range of scaled distances (Z). It was seen that the probability of failure decreases when scaled distance increases.
- It was noticed the probability of failure decreased by 28 percent when scaled distance increased from 2.0 to 4.0 m/kg$^{1/3}$
- The probability of failure is dropped significantly when scaled distance equal or larger than 5.5 m/kg$^{1/3}$.
- Failure was not predicted when the scaled distance exceeded 5.5 m/kg$^{1/3}$.
- The FCs were estimated based on the variability in the equivalent TNT weight for a suicide vest threat scenario. It was noticed the probability of failure

increased when the equivalent TNT weight increased for specific standoff distance.

- The fragility curve increased sharply when a TNT charge was placed at 1-m from the target because of the high intensity blast shock wave.
- The probability of failure was 74 percent from placing 1-kg at 1-m from the targeted structure, while the probability of failure was dropped to 28 percent by placing the same TNT mass at 4-m, and to 4 percent by placing it at 8-m.
- The probability of failure increased by 25 percent when the weight of TNT (R=1-m) increased from 1 to 2 kg.

7.6 Recommendation for Future Works

The present work discussed and highlighted the worldwide social impact and economic losses due to the suicide attacks. The study clarified there is a research gap in considering simple blast walls made of available ready materials to mitigate blast loading. The performance of simple blast wall systems in attenuating the hazard of explosions from high-explosive detonation was investigated experimentally and numerically. This is can be considered as a first step to adopt such type of blast walls for non-military applications. Therefore, future studies can focus on the following trends:

- The current study focused on free-air blast distribution from high-explosive burst and structural response of simple blast wall systems. These type of blast walls are not applicable to be installed in city centers without considering architecture design modifications. It is recommended to establish integrated studies to investigate these design modifications.

- Sand and wood were used in the present study. Considering different readily available materials are recommended since the performance of different materials have not been investigated to reduce the hazard of explosions.
- Lagrangian element and ConWep blast loading model were considered in the current study. It is suggested for complex geometry structures to use different elements and blast loading model especially when ConWep is not a suitable choice.
- Thermal effects did not consider in the current study. Future studies can investigate these effects.
- By considering the output of probabilistic analysis, it is recommended to run a risk-cost-benefit analysis for the current model.
- It is suggested to run an optimization study for different thicknesses and height-to-width ratio since these were constant in the current study.
- Conducting a comparison study between simplified SDOF and Multi-degree-of-freedom (MDOF) systems probabilistic analysis results is suggested to estimate the accuracy of the simplified approach.

This study recommends WSaW blast wall to reduce casualties and losses in properties in different attack scenarios. It is important to draw the attention of researchers and designers to start investigating the performance of other simple blast walls made of other low-tech materials since it is an urgent need in most areas threatened by terrorism.

References

Aashto, L. (1998). Bridge design specifications: American Association of State Highway and Transportation Officials, Washington, DC.

Abaqus, V. (2014). 6.14 Documentation. *Dassault Systemes Simulia Corporation*.

Baker, W. E., Cox, P. A., Kulesz, J. J., Strehlow, R. A., & Westine, P. S. (2012). *Explosion hazards and evaluation* (Vol. 5): Elsevier.

Baker, W. E., Kulesz, J. J., Westine, P. S., Cox, P. A., & Wilbeck, J. S. (1981). *A manual for the prediction of blast and fragment loadings on structures*.

Bangash, M. Y. H. (1993). *Impact and explosion: analysis and design*: Blackwell.

Beyer, M. E. (1986). *Blast loads behind vertical walls*.

Bhattacharjee, Y. (2008). Shell Shock Revisited: Solving the Puzzle of Blast Trauma. *Science, 319*(5862), 406.

Biggs, J. M., & Testa, B. (1964). *Introduction to structural dynamics* (Vol. 3): McGraw-Hill New York.

Bogosian, D., Ferritto, J., & Shi, Y. (2002). *Measuring uncertainty and conservatism in simplified blast models*.

Boyd, S. D. (2000). *Acceleration of a plate subject to explosive blast loading-trial results*.

Brode, H. L. (1955). Numerical solutions of spherical blast waves. *Journal of Applied physics, 26*(6), 766-775.

Brown, M. D., & Loewe, A. S. (2003). Reference manual to mitigate potential terrorist attacks against buildings. *USA, FEMA*, 4-19.

Budziak, M. P., & Garbowski, T. (2014). Failure Assessment of Steel-Concrete Composite Column Under Blast Loading. *Engineering Transactions, 62*(1), 61-84.

Center for Substance Abuse, T. (2014). Trauma-Informed Care in Behavioral Health Services.

Chesney, M., Reshetar, G., & Karaman, M. (2011). The impact of terrorism on financial markets: An empirical study. *Journal of Banking & Finance, 35*(2), 253-267.

Conrath, E. J. (1999). *Structural design for physical security: State of the practice*.

Courtney, E., Courtney, A., & Courtney, M. (2015). A $55 Shock Tube for Simulated Blast Waves. *arXiv preprint arXiv:1502.06112*.

Cowper, G. R., & Symonds, P. S. (1957). *Strain-hardening and strain-rate effects in the impact loading of cantilever beams*.

Cranz, C. Lehrbuch der Ballistic. 1926. *Textbook of ballistics*.

Crawford, J. E., & Lan, S. (2006). *Blast wall design and testing*.

Cullis, I. G. (2001). Blast waves and how they interact with structures. *Journal of the Royal Army Medical Corps, 147*(1), 16-26.

Curley, K. C., Leggieri, M., Jaffee, C. M. S., & Moore, D. F. (2011). Opening editorial, international state of the science meeting on non-impact blast-induced mild traumatic brain injury. *Neuroimage, 54*, S14-S20.

Deschambault, E. J., & Zehrt Jr, W. H. (2010). *Comparison of US Blast Design Guidance Documents*.

Design, S. S. S. (1977). Analysis Handbook. *US Army Corps of Engineers, Huntsville Division (November 1977) HNDM-1110-1-2*.

Dharmasena, K. P., Wadley, H. N., Xue, Z., & Hutchinson, J. W. (2008). Mechanical response of metallic honeycomb sandwich panel structures to high-intensity dynamic loading. *International Journal of Impact Engineering, 35(9), 1063-1074.*

Ding, Y., Song, X., & Zhu, H.-T. (2017). Probabilistic progressive collapse analysis of steel frame structures against blast loads. *Engineering Structures, 147*, 679-691.

DoD, U. S. (2008). Structures to resist the effects of accidental explosions. *Unified Facilities Criteria, United States of America, Department of Defense, Washington, DC, Document No. UFC*, 3-340.

Drucker, D. C., & Prager, W. (1952). Soil mechanics and plastic analysis or limit design.

Quarterly of applied mathematics, 10(2), 157-165.

Dusenberry, D. O. (2010). *Handbook for blast resistant design of buildings*: John Wiley & Sons.

Dvorak, G., & Bahei-El-Din, Y. (2005). Enhancement of blast resistance of sandwich plates. *Sandwich Structures 7: Advancing with Sandwich Structures and Materials*, 107-116. Springer, Dordrecht.

Ellingwood, B. R. (2006). Mitigating risk from abnormal loads and progressive collapse. *Journal of Performance of Constructed Facilities, 20*(4), 315-323.

Fatt, M. S. H., Gao, Y., & Sirivolu, D. (2013). Foam-core, curved composite sandwich panels under blast. *Journal of Sandwich Structures & Materials, 15*(3), 261-291.

Geckle, L., & Lee, R. (2004). *Soldier perceptions of deployment environmental exposures*. In Albuquerque:NM:Force Health Protection Conference.

Gilbert, F. K., & Kenneth, J. G. (1985). Explosive shocks in air. *2nd Sub edition*.

Goel, M. D. (2015). Blast: Characteristics, Loading and Computation—An Overview *Advances in Structural Engineering* (pp. 417-434): Springer.

Goel, M. D., Chakraborty, T., & Matsagar, V. A. (2012). Dynamic response of steel-sand composite stiffened plates under impulsive loading. *Journal of Battlefield Technology, 15*(3), 7.

Goel, M. D., & Matsagar, V. A. (2013). Blast-resistant design of structures. *Practice Periodical on Structural Design and Construction, 19*(2), 04014007.

Goel, M. D., Matsagar, V. A., & Gupta, A. K. (2014). Blast resistance of stiffened sandwich panels with closed-cell aluminum foam. *Latin American Journal of Solids and Structures, 11*(13), 2497-2515.

Goel, M. D., Matsagar, V. A., Gupta, A. K., & Marburg, S. (2012). An abridged review of blast wave parameters. *Defence Science Journal, 62*(5), 300-306.

Greenwald, A. L. (2010). Trends in Terrorist Activity and Dynamics in Diyala province, Iraq, during the Iraqi Governmental Transition, 2004-2006. *Perspectives on Terrorism, 4*(1).

Gupta, R. K., & Przekwas, A. (2013). Mathematical models of blast-induced TBI: current status, challenges, and prospects. *Frontiers in neurology, 4*, 59.

Guzas, E. L., & Earls, C. J. (2010). Air blast load generation for simulating structural response. *Steel Compos. Struct, 10*(5), 429-455.

Ha, J.-H., Yi, N.-H., Choi, J.-K., & Kim, J.-H. J. (2011). Experimental study on hybrid CFRP-PU strengthening effect on RC panels under blast loading. *Composite Structures, 93*(8), 2070-2082.

Hallquist, J. O., & Manual, L. S. D. T. (1998). Livermore Software Technology Corporation. *Livermore, Ca*.

Hammond, L., & Saunders, D. (1997). The applicability of scaling laws to underwater shock tests.

Harris, H. G., & Sabnis, G. (1999). *Structural modeling and experimental techniques*: CRC press.

Henrych, J., & Major, R. (1979). *The dynamics of explosion and its use*: Elsevier Amsterdam.

Hinaman, E. (2006). Safe Rooms and Shelters-Protecting People Against Terrorist Attacks. *Risk Management Series, Federal Emergency Management Agency, USA*.

Hopkinson, B. (1915). British ordnance board minutes. *Rep, 13565*.

Hryciów, Z., Borkowski, W., Rybak, P., & Wysocki, Z. (2014). Influence of the shape of the explosive charge on blast profile. *Journal of KONES, 21*.

Hua, Y., Akula, P. K., & Gu, L. (2014). Experimental and numerical investigation of carbon fiber sandwich panels subjected to blast loading. *Composites Part B: Engineering, 56*, 456-463.

Hyde, D. W. (1991). Conventional weapons program (ConWep). *US Army Waterways Experimental Station, Vicksburg, MS, USA*.

Institute for Economics and, P. (2014). *Global Terrorism Index 2014: Measuring and Understanding the Impact of Terrorism*.

Institute of Medicine. Committee on Gulf War and Health: Long-Term Effects of Blast, E.

(2014). *Gulf War and Health: Long-term Effects of Blast Exposures*.

Iqbal, J. (2008). Effects of an External Explosion on a concrete Structure.

Jablonski, J., Carlucci, P., Thyagarajan, R., Nandi, B., & Arata, J. (2013). *Simulating Underbelly Blast Events using Abaqus/Explicit-CEL*.

Jankowiak, T., & Lodygowski, T. (2005). Identification of parameters of concrete damage plasticity constitutive model. *Foundations of civil and environmental engineering, 6*(1), 53-69.

Johnson, G. R., & Cook, W. H. (1983). *A constitutive model and data for metals subjected to large strains, high strain rates and high temperatures*.

Karlos, V., & Solomos, G. (2013). Calculation of blast loads for application to structural components. *Luxembourg: Publications Office of the European Union*.

Karlos, V., Solomos, G., & Larcher, M. (2016). Analysis of the blast wave decay coefficient using the Kingery–Bulmash data. *International Journal of Protective Structures, 7*(3), 409-429.

Khan, A., & Estrada, M. A. R. (2016). The effects of terrorism on economic performance: the case of Islamic State in Iraq and Syria (ISIS). *Quality & Quantity, 50*(4), 1645-1661.

Kinney, G. F., & Graham, K. J. Explosive Shocks in Air, 1962. *Mac Millan, London*.

Kinney, G. F., & Graham, K. J. (1985). The Scaling Law *Explosive Shocks in Air* (pp. 107-118): Springer.

Kinney, G. F., & Graham, K. J. (2013). *Explosive shocks in air*: Springer Science & Business Media.

Koccaz, Z., Sutcu, F., & Torunbalci, N. (2008). *Architectural and structural design for blast resistant buildings*.

LaFree, G., & Dugan, L. (2006). Global terrorism database, 1970–1997. *Computer file]. ICPSR04586-v1. College Park, MD: University of Maryland [producer]*.

Lahiri, S. K., & Ho, L. (2011). *Simulation of rapid structural failure due to blast loads from conventional weapons (CONWEP)*.

Langdon, G. S., Karagiozova, D., Theobald, M. D., Nurick, G. N., Lu, G., & Merrett, R. P.

(2010). Fracture of aluminium foam core sacrificial cladding subjected to air-blast. loading. *International Journal of Impact Engineering, 37*(6), 638-651.

Lee, D. K., & O'Toole, B. J. (2004). *Energy absorbing sandwich structures under blast loading*.

Levy, B. S., & Sidel, V. W. (2013). Adverse health consequences of the Iraq War. *The Lancet, 381*(9870), 949-958.

Liu, X., Tian, X., Lu, T. J., Zhou, D., & Liang, B. (2012). Blast resistance of sandwich-walled hollow cylinders with graded metallic foam cores. *Composite Structures, 94*(8), 2485-2493.

Lofton, S. C., & Meyers, G. E. (2001). Preliminary Validation of Computer Programs for Prediction of Glazing Response to Explosive Airblast *Structures 2001: A Structural Engineering Odyssey* (pp. 1-8).

Makhutov, N. A., Petrov, V. P., & Reznikov, D. O. (2009). *Characteristics of Technological Terrorism Scenarios and Impact Factors*.

Matsagar, V. A. (2016). Comparative performance of composite sandwich panels and non-composite panels under blast loading. *Materials and Structures, 49*(1-2), 611-629.

Mays, G., Smith, P. D., & Smith, P. D. (Eds.). *Blast effects on buildings: Design of buildings to optimize resistance to blast loading*: Thomas Telford.

Memari, M. (2016). Performance of steel structures subjected to fire following earthquake.

Miller, D., Pan, H., Nance, R., Shirley, A., & Cogar, J. (2010). *A coupled Eulerian/Lagrangian simulation of blast dynamics*.

Mills, C. A. (1987). *The design of concrete structure to resist explosions and weapon effects*.

Mlakar, P. F., & Barker, D. (2010). 6 Blast Phenomena. *Handbook for Blast-Resistant Design of Buildings*, 161.

Netherton, M. D., & Stewart, M. G. (2010). Blast load variability and accuracy of blast load prediction models. *International Journal of Protective Structures, 1*(4), 543-570.

Ngo, T., Mendis, P., Gupta, A., & Ramsay, J. (2007). Blast loading and blast effects on structures–an overview. *Electronic Journal of Structural Engineering, 7*, 76-91.

Low, H. Y., & Hao, H. (2001). Reliability analysis of reinforced concrete slabs under explosive loading. *Structural safety*, *23*(2), 157-178.

Olmati, P. (2013). *Monte Carlo analysis for the blast resistance design and assessment of a reinforced concrete wall*.

Olmati, P., Petrini, F., & Gkoumas, K. (2014). Fragility analysis for the Performance-Based Design of cladding wall panels subjected to blast load. *Engineering Structures, 78*, 112-120.

Olmati, P., Trasborg, P., Naito, C., & Bontempi, F. (2015). Blast resistant design of precast reinforced concrete walls for strategic infrastructures under uncertainty. *International Journal of Critical Infrastructures, 11*(3), 197-212.

Pedahzur, A. (2005). *Suicide terrorism*: Polity.

Rajasekaran, S. (2009). *Structural dynamics of earthquake engineering: theory and application using MATHEMATICA and MATLAB*: Elsevier.

Razaqpur, A. G., Campidelli, M., Foo, S., Hao, H., & Li, Z. X. (2012). *Experimental versus analytical response of structures to blast loads*: Taylor and Francis Group, London.

Remennikov, A. M., & Rose, T. A. (2005). Modelling blast loads on buildings in complex city geometries. *Computers & Structures, 83*(27), 2197-2205.

Ritz, M. W., Hensley, R. G., & Whitmire, J. C. (2004). *The Homeland Security Papers: Stemming the Tide of Terror*: USAF Counterproliferation Center.

Rong, H.-C., & Li, B. (2007). Probabilistic response evaluation for RC flexural members subjected to blast loadings. *Structural Safety, 29*(2), 146-163.

Rose, T. A., Smith, P. D., & Mays, G. C. (1995). The effectiveness of walls designed for the protection of structures against airblast from high explosives. *Proceedings of the Institution of Civil Engineers. Structures and buildings, 110*(1), 78-85.

Rose, T. A., Smith, P. D., & Mays, G. C. (1997). Design charts relating to protection of structures against airblast from high explosives. *Proceedings of the Institution of Civil Engineers. Structures and buildings, 122*(2), 186-192.

Rose, T. A., Smith, P. D., & Mays, G. C. (1998). Protection of structures against airblast using walls of limited robustness. *Proceedings of the Institution of Civil Engineers. Structures and buildings, 128*(2), 167-176.

Schmidt, J. A. (2003). Structural design for external terrorist bomb attacks. *Structure, 3*, 21-23.

Schweitzer, E. G. (2009). *Countering Terrorism: Biological Agents, Transportation Networks, and Energy Systems*.

Shin, J. (2014). Air-blast effects on civil structures.

Shin, J., Whittaker, A. S., & Cormie, D. (2015). Incident and normally reflected overpressure and impulse for detonations of spherical high explosives in free air. *Journal of Structural Engineering, 141*(12), 04015057.

Siba, F. (2014). Near-field explosion effects on reinforced concrete columns: An experimental investigation.

Slotnick, J. A. (2010). *Explosive threats and target hardening understanding explosive forces, it's impact on infrastructure and the human body*.

Smilowitz, R. (2008). Designing buildings to resist explosive threats. *Whole Building Design Guide*, 18-21.

Smith, H. D., Clark, R. W., & Mayor, R. P. (1963). *Evaluation of Model Techniques for the Investigation of Structural Response to Blast Loads*.

Smith, P. D., & Hetherington, J. G. (1994). *Blast and ballistic loading of structures*: Digital Press.

Stewart, C., & Center, S. (2009). Blast Injuries" True Weapons of Mass Destruction". *Work, 918*, 660-2828.

Stewart, M. G., & Netherton, M. D. (2008). Security risks and probabilistic risk assessment of glazing subject to explosive blast loading. *Reliability Engineering & System Safety, 93*(4), 627-638.

Sweden, C. (2008). Shell shock revisited: solving the puzzle of blast trauma.

Trasborg, P., Olmati, P., & Naito, C. INCREASING THE DUCTILITY OF REINFORCED CONCRETE PANELS TO IMPROVE BLAST RESPONSE.

Twisdale, L. A., Sues, R. H., & Lavelle, F. M. (1994). Reliability-based design methods for protective structures. *Structural Safety, 15*(1-2), 17-33.

United States, A. (1969). *Structures to resist the effects of accidental explosions*: US Government Printing Office.

Wadley, H. N. G., Dharmasena, K. P., He, M., McMeeking, R. M., Evans, A. G., Bui-Thanh, T., & Radovitzky, R. (2010). An active concept for limiting injuries caused by air blasts. *International Journal of Impact Engineering, 37*(3), 317-323.

Wang, Y., Liew, J. Y. R., & Lee, S. C. (2015). Theoretical models for axially restrained steel-concrete-steel sandwich panels under blast loading. *International Journal of Impact Engineering, 76*, 221-231.

Williamson, E. B. (2010). *Blast-resistant highway bridges: Design and detailing guidelines* (Vol. 645): Transportation Research Board.

Yandzio, E., & Gough, M. (1999). *Protection of buildings against explosions*: Steel Construction Institute UK.

Yazici, M., Wright, J., Bertin, D., & Shukla, A. (2014). Experimental and numerical study of foam filled corrugated core steel sandwich structures subjected to blast loading. *Composite Structures, 110*, 98-109.

Yazici, M., Wright, J., Bertin, D., & Shukla, A. (2015). Preferentially filled foam core corrugated steel sandwich structures for improved blast performance. *Journal of Applied Mechanics, 82*(6), 061005.

Yuen, S. C. K., & Nurick, G. N. (2014). The Use of Tubular Structures as Cores for Sandwich Panels Subjected to Dynamic and Blast Loading: A Current "State of the Art" *Blast Mitigation* (pp. 229-248): Springer.

Yusof, M. A., Nor, N. M., Ismail, A., Sohaimy, R., Daud, N. G. N., Peng, N. C., Zain, M. (2011). *Measurement of field blast testing data using high speed data acquisition system for steel fiber reinforced concrete*.

Zhang, B., Wu, Q., Wang, L., & Han, G. (2005). The Influence of in-plane Density Variation on Engineering Properties of Oriented Strandboard: a Finite Element Simulation. *Proceedings of McMat2005*.